

# **RCA REVIEW**

*a technical journal*

**RADIO AND ELECTRONICS  
RESEARCH • ENGINEERING**

**VOLUME XX**

**DECEMBER 1959**

**NO. 4**

RADIO CORPORATION OF AMERICA

DAVID SARNOFF, *Chairman of the Board*

FRANK M. FOLSOM, *Chairman of the Executive Committee*

JOHN L. BURNS, *President*

E. W. ENGSTROM, *Senior Executive Vice-President*

DOUGLAS H. EWING, *Vice-President, Research and Engineering*

JOHN Q. CANNON, *Secretary*

ERNEST B. GORIN, *Vice-President and Treasurer*

---

RCA LABORATORIES

J. HILLIER, *Vice-President*

---

RCA REVIEW

C. C. FOSTER, *Manager*

R. F. CIAFONE, *Administrator*

PRINTED IN U.S.A.

RCA REVIEW, published quarterly in March, June, September, and December by RCA Laboratories, Radio Corporation of America, Princeton, New Jersey. Entered as second class matter July 3, 1950 under the Act of March 3, 1879. Second-class postage paid at Princeton, New Jersey, and at additional mailing offices. Subscription price in the United States and Canada; one year \$2.00, two years \$3.50, three years \$4.50; in other countries: one year \$2.40, two years \$4.30, three years \$5.70. Single copies in the United States, \$.75; in other countries, \$.85.



# RCA REVIEW

## BOARD OF EDITORS

*Chairman*

R. S. HOLMES  
*RCA Laboratories*

E. I. ANDERSON  
*RCA Victor Home Instruments*

A. A. BARCO  
*RCA Laboratories*

G. L. BEERS  
*Radio Corporation of America*

G. H. BROWN  
*Radio Corporation of America*

I. F. BYRNES  
*Industrial Electronic Products*

O. E. DUNLAP, JR.  
*Radio Corporation of America*

E. W. ENGSTROM  
*Radio Corporation of America*

D. H. EWING  
*Radio Corporation of America*

A. N. GOLDSMITH  
*Consulting Engineer, RCA*

A. L. HAMMERSCHMIDT  
*National Broadcasting Company, Inc.*

J. HILLIER  
*RCA Laboratories*

D. D. HOLMES  
*RCA Laboratories*

E. A. LAPORT  
*Radio Corporation of America*

H. W. LEVERENZ  
*RCA Laboratories*

G. F. MAEDEL  
*RCA Institutes, Inc.*

H. F. OLSON  
*RCA Laboratories*

R. W. PETER  
*RCA Laboratories*

D. S. RAU  
*RCA Communications, Inc.*

D. F. SCHMIT  
*Radio Corporation of America*

G. R. SHAW  
*Electron Tube Division*

L. A. SHOTLIFF  
*RCA International Division*

S. STERNBERG  
*Astro-Electronic Products Division*

W. M. WEBSTER  
*RCA Laboratories*

I. WOLFF  
*RCA Laboratories*

*Secretary*

C. C. FOSTER  
*RCA Laboratories*

---

## REPUBLICATION AND TRANSLATION

Original papers published herein may be referenced or abstracted without further authorization provided proper notation concerning authors and source is included. All rights of republication, including translation into foreign languages, are reserved by RCA Review. Requests for republication and translation privileges should be addressed to *The Manager*.

## FOREWORD

THIS ISSUE of *RCA Review* is devoted to basic research on three related phenomena observed in certain insulator and semiconductor materials—luminescence, photoconductivity and space-charge current flow—and to device research work based upon these three phenomena. Major advances during the past two or three years both in the basic understanding of these phenomena and in their application to useful novel devices promise to open entirely new areas for electronics in the near future.

Luminescence or “light generation” has entered a new era with “electroluminescence.” During the past few years, electroluminescence has shown a dramatically steep and continued rise to importance, while increases in the efficiency of conventional means of converting electricity into light, including cathodoluminescent phosphors for color television, have been relatively small. Luminous panels of various shapes and colors are beginning to appear on the market for many special lighting applications. It is conceivable that, ultimately, greatly improved electroluminescent panels may even become practicable for general lighting.

In the field of photoconductors, the theoretical possibility of large increases in performance has recently been demonstrated by A. Rose and co-workers. During the past year, photoconducting crystals with about two orders of magnitude higher performance factors have been grown. It can be assumed that these spectacular advances, presently achieved in selected crystals only, may ultimately be duplicated in powders and sintered layers, which are of great importance for most photoconductor devices. During the past decade similar, though little publicized, advances have been made with infrared photoconductors, both in increasing absolute sensitivity and in extending it toward longer wavelengths. Finally, space-charge-limited current flow, well known in vacuum tubes, has recently been measured in insulators, and the first solid-state analog to the vacuum triode has been demonstrated.

Initially considered mainly as an aspect of and possibly limiting factor in photoconductivity, space-charge current flow is now being put to use on its own merits. A whole new class of "insulator devices" with interesting characteristics, such as extremely high input impedance, may be added in the near future to the vacuum, gas tube, and semiconductor devices.

Well known and established applications of photoconductivity and luminescence, such as photocells, Electrofax and Xerography, Vidicon pickup, and television reproducer tubes, are being joined by novel, far more sophisticated devices. Light and x-ray amplifiers, information storage panels, and optoelectronic computer elements are presently objectives of research studies in many laboratories. They are examples of the trend to integrate intimately different electronically active solids having complementary functions into new compact components and devices.

As scientific tools for investigating basic characteristics of solids, luminescence, photoconductivity, and space-charge current flow acquire a steadily growing importance. Applicable to the study of semiconductors as well as insulators, they can provide information on the energy-level structure of a material which is necessary for an understanding of its electronic behavior.

Luminescence is probably the longest known electronic solid-state phenomenon. Descriptions of studies of luminescence go back to the 16th century, but even today its complex mechanisms are generally very little understood. Photoconductivity is only about one century old, observed for the first time in selenium by W. Smith in 1873. Its basic physics, however, is much better known, though more in phenomenological than in quantum mechanical terms. Semiconduction is the youngest phenomenon studied in solid matter, but, without any doubt, its theory is best understood, well founded on "first principles," and verified by extensive experimental data.

This astonishing reverse relationship between discovery and understanding of these phenomena must be attributed to nature itself. It is said that every additional electron volt of energy gap in the material multiplies by an order of magnitude the number of, and interrelations between, possible crystal defects. Semiconductors are distributed about an average band gap of about 1 ev, visible photoconductors, roughly about 2 ev, and phosphors about 3 ev, and the complexity of observed phenomena indeed seems to increase accordingly.

For the chemist and metallurgist the difficulties grow exponentially when trying to prepare a photoconductor with semiconductor purity, or pure enough to approximate the theoretical physicist's simplified

models. Conversely, the theorist is hard put to include all the needed defects in his model to make it realistic. In addition, the difficulties increase greatly when one progresses from elemental materials (such as germanium and silicon) to compounds (such as cadmium sulfide or gallium arsenide). Had nature provided an elemental insulator with a bandgap between 2 and 3 ev amenable to purification and perfection equal to modern germanium, I venture to say that this *RCA Review* issue on luminescence and photoconductivity would have been written quite a few years earlier.

RCA Laboratories  
Princeton, N. J.

ROLF W. PETER  
Director Physical and Chemical Research Laboratory

# ELECTROLUMINESCENCE OF POLYCRYSTALLITES\*

BY

SIMON LARACH AND ROSS E. SHRADER

RCA Laboratories,  
Princeton, N.J.

*Summary*—The important aspects of luminescence and of electroluminescence are discussed, including incandescence, differences between electroluminescence and other types of luminescence, designing electroluminescent materials to emit in any desired (visible) spectral range, nature of the energy-absorbing layer, and various electrical and optical aspects of the electroluminescence from polycrystallites.

## INTRODUCTION

ELECTROLUMINESCENCE is a fairly recent phenomenon when viewed as part of the developing picture in luminescence, and can be classified as one of the types of luminescence. This paper (1) summarizes some of the important aspects in the history of luminescence, (2) develops the concepts of luminescence, and (3) discusses some aspects of electroluminescence.

## HISTORICAL ASPECTS

Three hundred and fifty-six years ago, in 1603, Cascariolo<sup>1</sup> carried out the first known synthesis of a luminescent material. Cascariolo had found some unusual stones (which we now know to have been barium sulfate) which he heated with coal ( $\text{BaSO}_4 + 2\text{C} \rightarrow \text{BaS} + 2\text{CO}_2$ ). Cascariolo then noted a feeble blue glow being emitted from the material at night, and named his material *lapis solaris* (sun stone).

More than a century elapsed before J. Canton, in 1768, obtained a brighter luminescing material by heating ground oyster shell (calcium carbonate) with sulfur ( $2\text{CaCO}_3 + 3\text{S} \rightarrow 2\text{CaS} + 2\text{CO}_2 + \text{SO}_2$ ); in 1866, T. Sidot heated zinc oxide with hydrogen sulfide ( $\text{ZnO} + \text{H}_2\text{S} \rightarrow \text{ZnS} + \text{H}_2\text{O}$ ), and obtained the first green-emitting zinc sulfide luminescent material. It was not until 1886 that A. Verneuil proved that Canton's material only luminesced when a trace of bismuth was present, and that a trace of copper was essential in Sidot's material.

\* Manuscript received October 22, 1959.

<sup>1</sup> For detailed discussions of the early history of luminescence, see *A History of Luminescence*, by E. N. Harvey, American Philosophical Society, Philadelphia, 1957.

The word *luminescenz* (luminescence) was first used by E. Wiedemann in 1888, for "all those phenomena of light which are not solely conditioned by the rise in temperature," and *luminescence* has been defined recently<sup>2</sup> as a "process whereby matter generates nonthermal radiation which is characteristic of the particular luminescent material."

#### INCANDESCENCE AND LUMINESCENCE

##### *Incandescence*

Light emission due to the temperature of a source is called *incandescence*. The radiation of most incandescent solids approximates that of a black body, for which there will be more total flux than that obtainable from any other source operating at the same temperature. For black-body radiation, Planck's Law applies;

$$W_J = C_1 \frac{\lambda^{-5}}{\exp\left(\frac{C_2}{\lambda T}\right) - 1}, \quad (1)$$

where  $W_J$  = radiated watts per  $\text{cm}^2$  of surface per micron, at wavelength  $\lambda$ ,

$\lambda$  = wavelength (microns),

$T$  = temperature of the black body in degrees Kelvin,

$C_1 = 3.738 \times 10^{-5}$  erg  $\text{cm}^2$   $\text{sec}^{-1}$ ,

$C_2 = 1.438$  cm degree.

With increasing temperature, the peak wavelength of emission is shifted to shorter wavelengths. The value of the peak wavelength (in microns) can be obtained from Wien's Displacement Law

$$\lambda_{pk} = 2.9 \times 10^3 T^{-1}. \quad (2)$$

By integrating  $W_J$  of Equation (1) for values of  $\lambda$  from zero to infinity, we obtain the Stefan-Boltzmann Law—the total radiant power per unit area of a black body varies as the fourth power of the temperature;

$$W = cT^4 \text{ (watts cm}^{-2}\text{)}, \quad (3)$$

where  $c = 5.672 \times 10^{-5}$  erg  $\text{cm}^{-2}$   $\text{deg}^{-4}$   $\text{sec}^{-1}$ .

<sup>2</sup>H. W. Leverenz, *An Introduction to Luminescence of Solids*, John Wiley & Sons, New York, N. Y., 1950.

### Luminescence

While incandescence emission is the result of a statistically averaged effect over all atoms of the source, the nature of *luminescence* emission is determined by the physico-chemical character of discrete volumes or elements. In the case of solids, these can be less than one per cent of the total volume. Thus, in luminescence, the basic time constant involved in transient responses is primarily determined by the luminescent center rather than by the bulk of the containing material,\* whereas in incandescence, the basic time constant for transient effects is determined by the thermal inertia of the source.

In luminescence emission, if  $P_R$  is the probability of radiative transitions,  $P_N$  is the probability of nonradiative transitions, and  $\eta$  is the luminescence-emission efficiency, then

$$\eta = \frac{P_R}{P_R + P_N}. \quad (4)$$

Assuming that  $P_R$  is essentially independent of temperature, and that  $P_N = K \exp(-E/kT)$ ,

$$\eta = \frac{1}{1 + a \exp\{-E/kT\}}. \quad (5)$$

This expression fits remarkably well many of the efficiency-versus-temperature curves of many luminescent materials.

### TYPES OF LUMINESCENCE

Luminescence involves the absorption of energy, excitation, and the emission of radiant energy.† Luminescence can thus be classified by the type of excitation required to excite the luminescence.

#### Photoluminescence

Excitation is by photons of higher energy than the emitted (luminescence) photons. A common example of photoluminescence is the fluorescent lamp, in which ultraviolet photons are used to excite a photoluminescent material to emit in a specific spectral range.

---

\* The average duration time of the excited state in light emission from excited monatomic gases at low pressure is of the order of  $10^{-8}$  second. *Fluorescence* is the term which has been adopted for light emission processes capable of this speed of response. The emission of light from slower processes as in liquids and solids is sometimes referred to as *phosphorescence*. This latter term is also applied to the emission which is detectable after removal of the source of excitation.

† For the purposes of this paper, luminescence will be taken as occurring over the electromagnetic energy range of 0.2 to 2.0 microns.

*Chemiluminescence*

Excitation energy is obtained from a chemical reaction, as, for example, the chemiluminescence from 3-aminophthalhydrazide.<sup>3</sup> Bioluminescence, as occurring, for example, in fireflies, can be considered as a form of chemiluminescence.

*Cathodoluminescence*

Excitation of solids to luminescence is effected by the direct impact of electrons. Excitation energies vary from a fraction of an electron volt to millions of electron volts.

*Electroluminescence*

Electroluminescence can be defined as the process whereby, on excitation by an electric field, nonthermal radiation is generated which is characteristic of the material.

In 1920, Gudden and Pohl<sup>4</sup> observed that the photoluminescence decay of a ZnS:Cu phosphor\* was affected by the application of an electric field.† Lossev<sup>5</sup> (1923) obtained luminescence by applying electrodes and a field to silicon carbide, and in 1936 Destriau<sup>6</sup> reported that a microcrystalline powder in an insulating surround could be excited to luminescence by the application of an electric field. During this last decade, vastly increased research in electroluminescence has resulted in large numbers of publications, as summarized in several review articles.<sup>7</sup>

---

<sup>3</sup> E. H. Huntress, L. Harris, A. S. Parker, and L. N. Stanley, "The Preparation of 3-Aminophthalhydrazide for Use in the Demonstration of Chemiluminescence," *Jour. Amer. Chem. Soc.*, Vol. 56, p. 241, January, 1934.

<sup>4</sup> B. Gudden and R. W. Pohl, "Enhancement of Phosphorescence by Electric Fields," *Zeit. f. Physik*, Vol. 2, p. 192, 1920.

\* The chemical phosphor nomenclature used in this article conforms to the convention of stating the host crystal, which is set off by a colon from the impurity additives. Figures preceding a chemical symbol denote mole-percent, whereas figures in parenthesis, after a chemical symbol, denote percent-by-weight.

† The phenomenon of modifying photoluminescence by the application of an electric field is now known as *electrophotoluminescence*.

<sup>5</sup> O. W. Lossev, "Luminous Carborundum Detector and Detection Effect and Oscillations with Crystals," *Phil. Mag.*, Vol. 6, p. 1024, November, 1928.

<sup>6</sup> G. Destriau, "Experimental Studies on the Action of an Electric Field on Phosphorescent Sulfide," *Jour. de Chem. Phys.*, Vol. 33, p. 620, 1936.

<sup>7</sup> D. W. G. Ballentyne, "The Phenomenon of Electroluminescence and Its Application in the Electronics Industry," *Marconi Review*, Vol. 19, No. 123, p. 160, 1956; G. Destriau and H. F. Ivey, "Electroluminescence and Related Topics," *Proc. I.R.E.*, Vol. 43, p. 1911, December, 1955. Many additional references on various aspects of electroluminescence can be found in the article by H. F. Ivey, "Bibliography on Electroluminescence and Related Topics," *Trans. I.R.E. PGED*, p. 203, April, 1959.

## ELECTROLUMINESCENT MATERIALS

Electroluminescent materials have been described by several workers in the field. Destriau<sup>8</sup> originally discussed mixtures of zinc sulfide and zinc oxide, with relatively large amounts of copper activator. Similar materials have been described with the inclusion of lead,<sup>9</sup> as well as other preparative methods.<sup>10,11</sup> Electroluminescence from zinc sulfoselenide phosphors has also been reported,<sup>12</sup> and a systematic survey of this system has been published.<sup>13</sup>

It is noteworthy that, with few exceptions, polycrystalline materials of the zinc sulfide type are the major phosphors which have appreciable emission intensity under field excitation. Thus, zinc sulfide, or solid solutions of Zn(S:Se:Te), are used as the *host crystal*, copper is used as the *activator* (or acceptor) impurity, and a halide, or trivalent cation, as the *charge-compensator* (or donor impurity).

Thus, electroluminescent phosphors would seem to be identical with many of their non-electroluminescent counterparts, except for the major difference of their ability to absorb and utilize energy from the exciting field. Design of electroluminescent materials therefore involves maximizing (1) the efficiency of energy utilization from the field and (2) the efficiency of energy conversion to radiative transitions; and minimizing (1) competing dissipative processes for the field energy and (2) nonradiative energy conversion.

Generally, electroluminescent sulfide microcrystalline phosphors require, in addition to the host crystal, volume copper, volume charge-compensator, and an energy-absorbing layer, possibly consisting of an inter-diffused copper-zinc sulfide region.<sup>14</sup>

---

<sup>8</sup> G. Destriau, "The New Phenomenon of Electrophotoluminescence and Its Possibilities for Investigation of Crystal Lattices," *Philos. Mag.*, Vol. 38, p. 700, October, 1947.

<sup>9</sup> H. H. Homer, R. M. Rulon, and K. H. Butler, "Electroluminescent Zinc Sulfide Phosphors," *Jour. Electrochem. Soc.*, Vol. 100, p. 566, December, 1953.

<sup>10</sup> P. Zalm, G. Diemer, and H. A. Klasens, "Electroluminescent ZnS Phosphors," *Philips Research Reports*, Vol. 9, p. 81, April, 1954.

<sup>11</sup> H. C. Froelich, "Electroluminescent Zinc Sulfide Phosphor," U. S. Patent 2,660,560, 1953.

<sup>12</sup> E. Krautz, "Über das Verhalten von Phosphoren und Photoleitern in hohen elektrischen Feldern," *Zeit. f. Naturf.*, Vol. 4a, Heft 4, 1949; S. Roberts, "Field Strength and Temperature Studies of Electroluminescent Powders in Dielectric Media," *Jour. Opt. Soc. Amer.*, Vol. 42, p. 850, November, 1952; J. S. Prener, U. S. Patent 2,731,423; A. Fischer, "Zur Elektrolumineszenz der Halbleiterphosphore," *Zeit. f. Naturf.*, Vol. 8a, Heft 11, p. 756, 1953; P. Zalm, "Electroluminescence of ZnS Type Phosphors," *Philips Research Reports*, Vol. 11, p. 353, 1956.

<sup>13</sup> I. J. Hegyi, S. Larach, and R. E. Shrader, "Electroluminescence of Zinc Sulfoselenide Phosphors with Copper Activator and Halide Coactivator," *Jour. Electrochem. Soc.*, Vol. 104, p. 717, December, 1957.

<sup>14</sup> S. Larach and R. E. Shrader, "Chemical Evidence for a Barrier in Electroluminescent ZnS," *Jour. Phys. Chem. Solids*, Vol. 3, p. 159, 1957.

## DESIGN OF ELECTROLUMINESCENT PHOSPHORS

Electroluminescent phosphors may be synthesized to emit in any desired region of the visible portion of the spectrum. This is accomplished by adjusting the composition of a given zinc inter-chalcogenide to yield the proper band gap. Incorporation of donors and acceptors, and provision of an energy-absorbing layer then yields an electroluminescent phosphor with desired spectral emission.

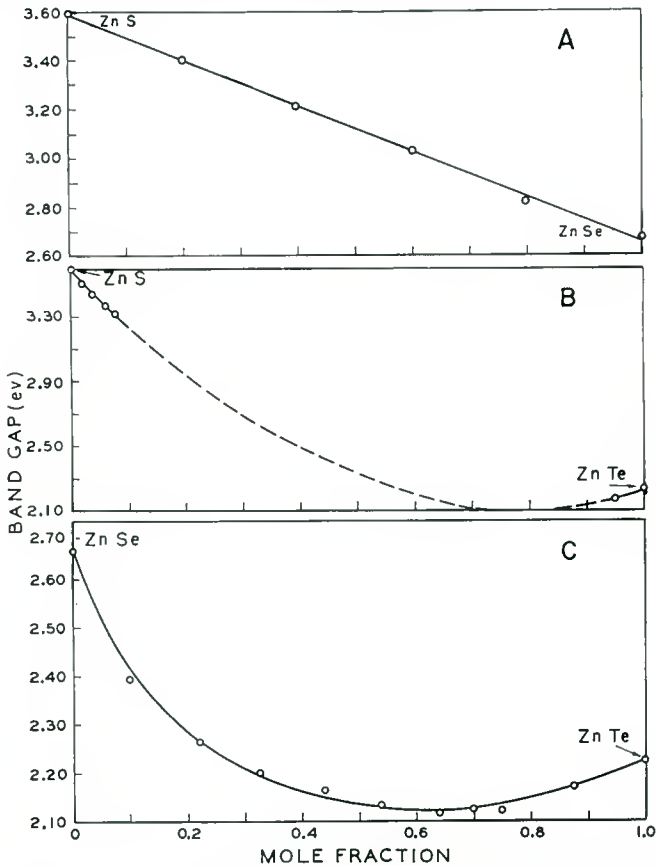


Fig. 1—Band gap as a function of composition for the systems Zn(S:Se), Zn(S:Te) and Zn(Se:Te).

#### Zinc Sulfo-Selenide Phosphors

The zinc sulfo-selenide system has a linear variation of band gap with composition,<sup>15</sup> as is shown in Figure 1. Materials from this

<sup>15</sup> S. Larach, R. E. Shrader, and C. F. Stocker, "Anomalous Variation of Band Gap with Composition in Zinc Sulfo- and Seleno-Tellurides," *Phys. Rev.*, Vol. 108, p. 587, November, 1957.

system can therefore be synthesized to emit from the blue to the red region of the spectrum.

Figure 2 shows the effect on the spectral distribution of the electroluminescence emission of varying the sulfur-to-selenium ratio in solid solutions of ZnS:ZnSe, activated with copper, and various halides

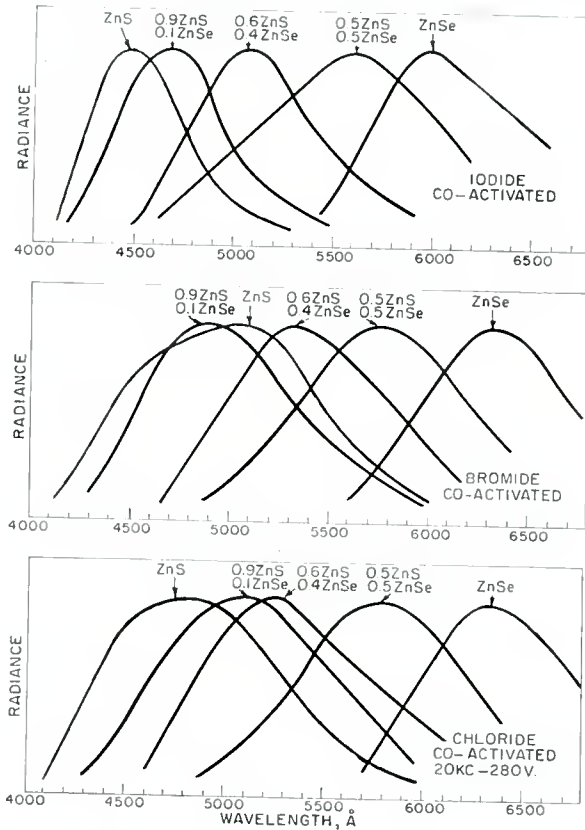


Fig. 2—Spectral distribution curves of the electroluminescence of Zn(S:Se)Cu with varying S:Se ratios, coactivated with chloride, bromide or iodide. (The S:Se ratios refer to compositions before firing.)

as co-activators. Solid solutions of the systems (ZnSe: CdSe) and (ZnSe: ZnTe) can be utilized to obtain electroluminescence emissions with peak wavelengths up to, or beyond, 7000 Å, within the composition limits indicated.

#### The Halide Effect

The preparation of zinc sulfide phosphors in the presence of halide has long been known.<sup>2</sup> The effect of the halide has been described as

(1) a "flux" to aid in recrystallization, thus affecting particle growth; (2) actual incorporation of the halide into the lattice;<sup>16</sup> (3) charge-compensating role;<sup>17</sup> (4) a donor-type of impurity;<sup>18,19</sup> and (5) lattice-perturbing agents.<sup>20</sup>

In the past, the particular type of halide used was not considered important. It has been shown<sup>21</sup> that, while the *cathodoluminescence* of ZnS:Cu prepared with chloride, bromide, or iodide is mainly in the blue with traces of green for the materials prepared with bromide and chloride, the *photoluminescence* of these phosphors, as shown in Fig-

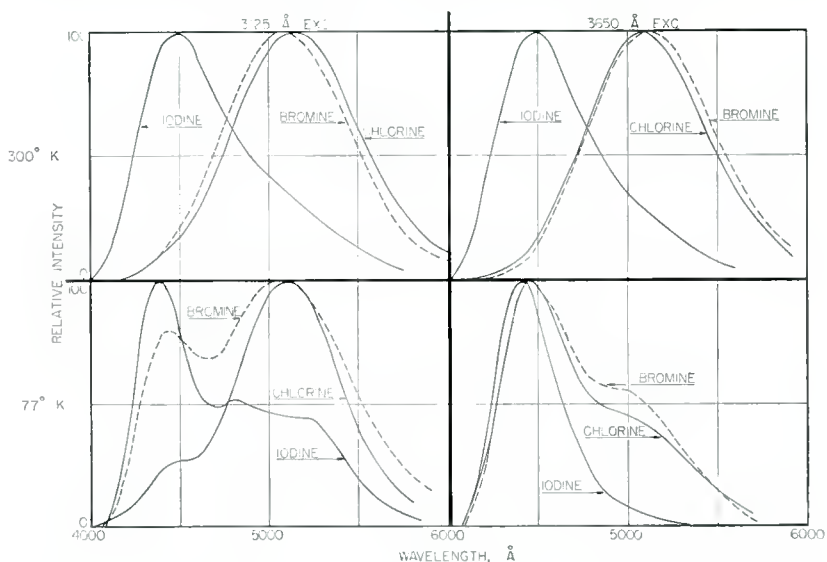


Fig. 3—Spectral distributions of the photoluminescence from ZnS:Cu phosphors prepared with chloride, bromide, or iodide as a function of exciting wavelength and temperature.

<sup>16</sup> A. L. Smith, "Influence of Fluxes on the Cathodoluminescence of Zinc Sulfide Phosphors," *Jour. Electrochem. Soc.*, Vol. 96, p. 75, August, 1949.

<sup>17</sup> F. A. Kroger and J. E. Hellingman, "The Blue Luminescence of Zinc Sulfide," *Jour. Electrochem. Soc.*, Vol. 93, p. 156, May, 1948; "Chemical Proof of the Presence of Chlorine in Blue Fluorescent Zinc Sulfide," *Jour. Electrochem. Soc.*, Vol. 95, p. 68, February, 1949.

<sup>18</sup> F. A. Kroger, H. J. Vink and J. van den Boomgaard, "Controlled Conductivity in Cadmium Sulfide Single Crystals," *Zeit. Physik Chem. (Leipzig)*, Vol. 203, p. 1, 1954.

<sup>19</sup> R. H. Bube and S. M. Thomsen, "Photoconductivity and Crystal Imperfections in Cadmium Sulfide Crystals, Part I—Effect of Impurities," *Jour. Chem. Phys.*, Vol. 23, p. 15, January, 1955.

<sup>20</sup> S. Larach and J. Turkevich, "Magnetic Properties of Zinc Sulfide and Cadmium Sulfide Phosphors," *Phys. Rev.*, Vol. 98, p. 1015, May, 1955.

<sup>21</sup> R. E. Shrader, S. Larach, and I. J. Hegyi, "Effect of Halide Coactivators on Absorption and Emission Phenomena in Zinc Sulfide Phosphors with Copper Activator," *Bull. Amer. Phys. Soc.*, Vol. I, Series II, p. 213, April 26, 1956.

Table I—Incorporated Copper, Excess Copper and Relative EL Peak Emission Intensities for ZnS:Cu Phosphor Powders

(1) Halide Type Added	(2) Cu Added (% by Wt.)	(3) Tot. Cu Found After Crystallization (% by Wt. $\pm 0.002$ )	(4) Excess Phase Cu	(5) Incorp. Cu (% by Wt. $\pm 0.002$ )	(6) Rel. El.
None	0.10	0.105	0.083	0.022	3
Cl	0.10	0.098	0.010	0.088	12
Br	0.10	0.100	0.047	0.053	80
I	0.10	0.095	0.070	0.025	100
Cl	0.03	0.029	0.000	0.029	0.2
Br	0.03	0.024	0.001	0.023	18
I	0.03	0.029	0.015	0.014	100
I	0.20	0.198	0.163	0.035	

ure 3, shows large variations in the green-to-blue ratio of the emission as a function of excitation wavelength, excitation density, and operating temperature. Table I shows that the proportion of copper in solid solution<sup>22</sup> is dependent on the halide used during preparation of the phosphors.

It has also been found that, in the presence of copper, the nature of the halide has a marked effect on the crystalline habit of the fired zinc sulfide host material. The results of X-ray analyses are summarized in Table II.

Table II

Material*	Cu	Halide	Hex (%)	Cub (%)
1	Absent	None	95	5
2	Present	Cl	99.5	0.5
3	Present	Br	50	50
4	Present	I	0.5	99.5
5	Absent	I	95	5

\* All fired at 1100° C for 20 minutes.

<sup>22</sup> Surface copper sulfide was first removed with KCN solution.

The transition temperature for the cubic-to-hexagonal conversion is usually given as 1020° C. It is not to be construed that this conversion temperature has been changed, but more likely that the conversion *rate* has been markedly affected. Long-term processing has not yet been investigated.

Figure 4 shows the spectral distributions of the *electroluminescence* emission of ZnS:Cu phosphors prepared with various halides, and Figure 5 shows similar curves for 6ZnS:O:4ZnSe:Cu phosphors. Figure 6 gives the photoluminescent excitation spectra for the sulfoselenide materials.<sup>12</sup> The effect of various halides on the spectral distribution of electroluminescence of ZnSe:Cu is shown in Figure 7. It becomes apparent that the nature of the halide coactivator affects the luminescence processes, and we may assume that association exists to some degree between activator and coactivator (acceptor and donor).

Electroluminescent materials can thus be produced in a variety of emission colors through choice of band gap by the appropriate solid solution in the general system (Zn:Cd) (S:Se:Te):Cu, with the appropriate halide coactivator.\*

#### *Electroluminescence from Boron Nitride*

Efficient electroluminescence has been obtained from boron nitride (BN).<sup>23</sup> The emission from BN is extremely complex and is, as yet, not fully explained. Excitation and emission spectra are shown in Figures 8 and 9.

#### CELL CONSTRUCTION AND CHARACTERISTICS

The electroluminescence of polycrystallites differs considerably in practice, if not in principle, from the electroluminescence of single crystals. The nature and degree of uncertainty is developed in the following discussion of the measurements and characteristics of electroluminescent cells.

Polycrystallites, when used as emitters for electroluminescence, are spread in a thin uniform layer between "parallel" electrodes. (The electrodes need not be flat, as portions of nested cones, coaxial cylinders, or concentric spheres will all serve as confining surfaces for a uniform layer of material. The material is usually applied in a binder with good dielectric properties, i.e., with low losses and high dielectric

---

\* In some cases, it is possible to use a tri-valent cation as a charge-compensating ion, or combinations of tri-valent cation and halide to achieve special results.

<sup>23</sup> S. Larach and R. E. Shrader, "Electroluminescence from Boron Nitride," *Phys. Rev.*, Vol. 102, p. 582, April, 1956; "Multiband Luminescence in Boron Nitride," *Phys. Rev.*, Vol. 104, p. 68, October, 1956.

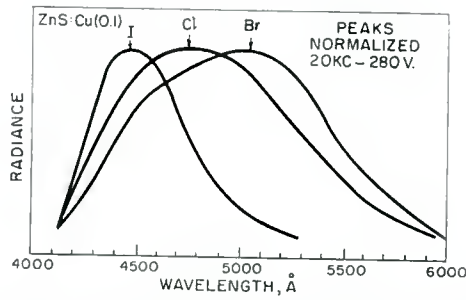


Fig. 4—Spectral distribution curves of the electroluminescence from ZnS:Cu phosphors prepared with chloride, bromide, or iodide.

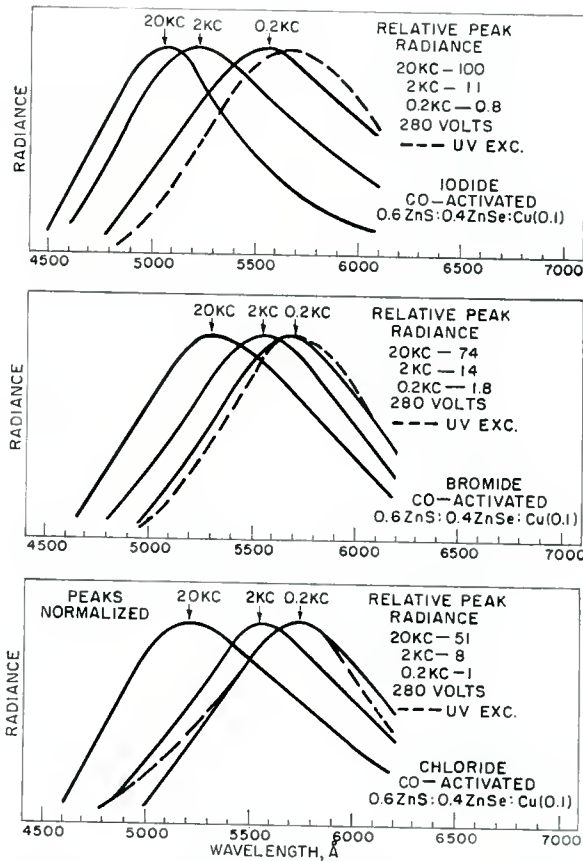


Fig. 5—Spectral distribution curves of the electroluminescence of 0.6ZnS:0.4ZnSe:Cu(0.1) coactivated with chloride, bromide, and iodide for the excitation frequencies of 20, 2, and 0.2 kilocycles; also of the photoluminescence under excitation by 3650 Å ultraviolet radiation.

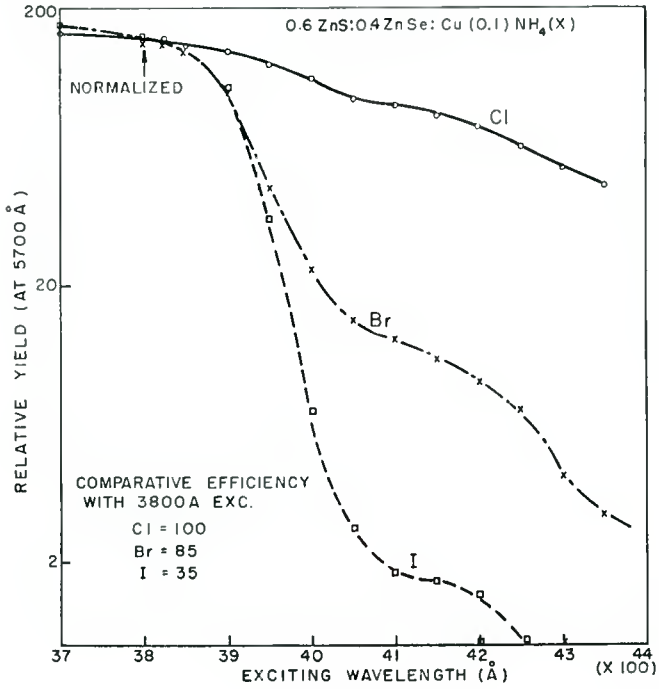


Fig. 6—Relative photoluminescent yield of the materials of Figure 5 under excitation for radiation of various wavelengths.

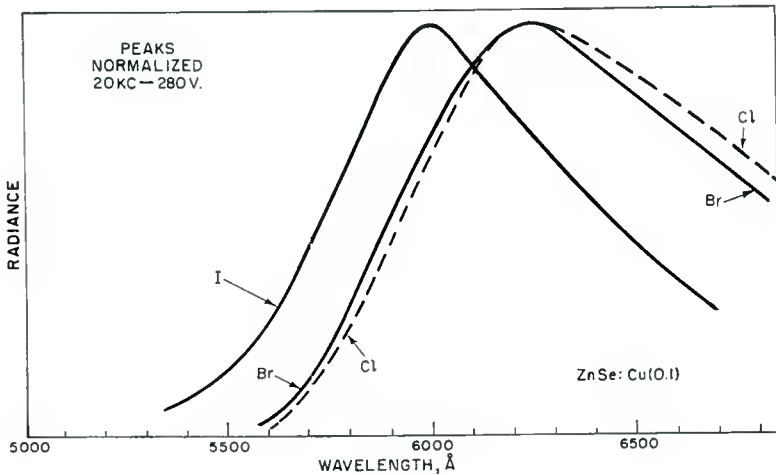


Fig. 7—Spectral distribution curves of the electroluminescence from ZnSe:Cu phosphors prepared with chloride, bromide, or iodide.

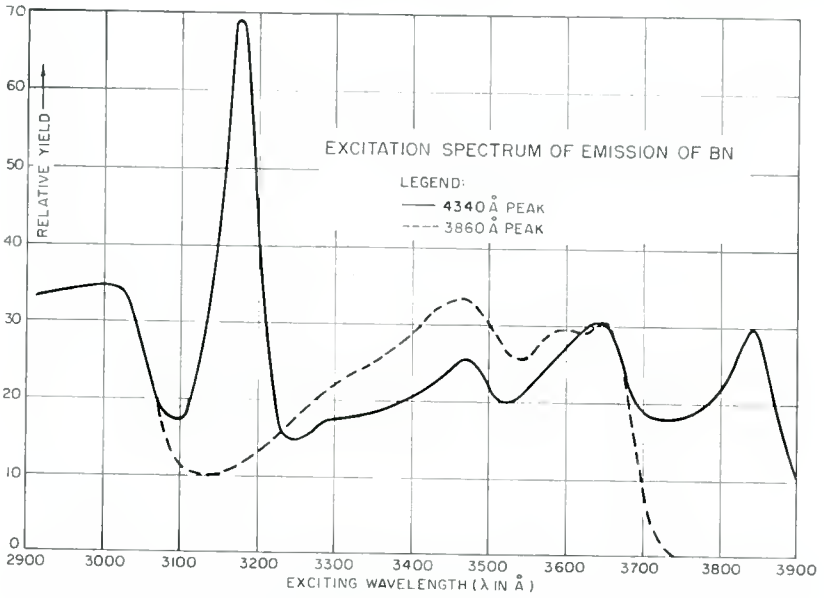


Fig. 8—Excitation spectra of two bands of the emission of boron nitride (bands 5 and 7 of Figure 9).

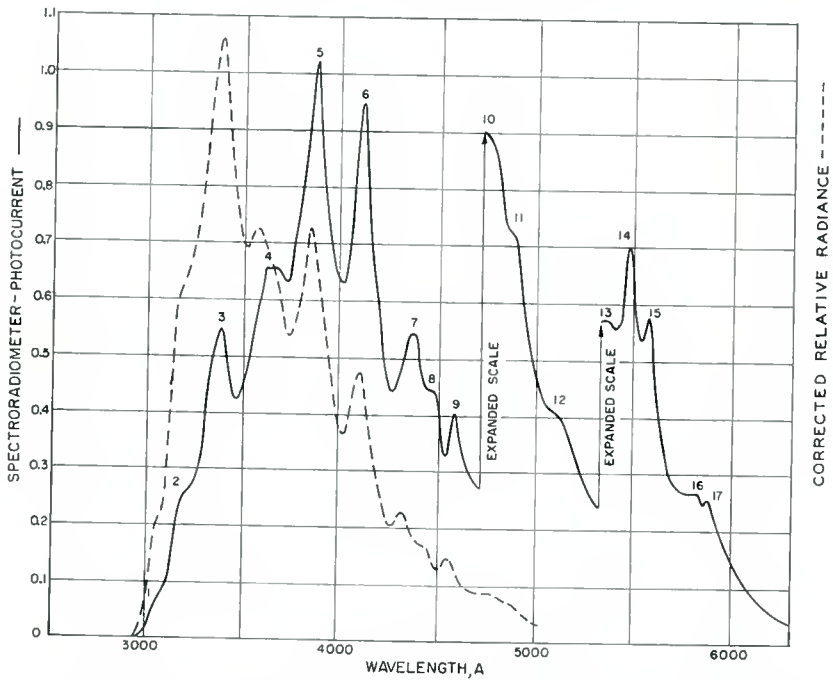


Fig. 9—Spectral distribution of the electroluminescence from boron nitride.

strength, although experimental cells have been made using air or vacuum as surrounding dielectric. The choice of binders runs from liquids, such as mineral oil, through plastics (e.g., epoxies), to ceramic frits fired on metal. Of necessity, at least one electrode must be partially transparent or translucent as well as conducting. This can be accomplished either by using glass, surface-treated so as to become conducting, or by evaporating or sputtering a sufficiently thin film of metal (usually gold) on one surface of the binder-plus-powder layers. The other electrode frequently is nontransparent, but in that case, it should be reflecting, either diffusely or specularly.

#### CELL PERFORMANCE

The performance of electroluminescent layers or cells is described empirically first. This is followed by a somewhat more brief discussion of the nature of the process.

##### *Light Output versus Frequency*

The particular characteristic most frequently discussed is the relationship of the time-averaged light output to the operating parameters—frequency and voltage.

Figure 10 shows how the light output of one experimental cell was found to vary with frequency (at constant field) over a limited range. As the frequency is increased still more, the output levels off and then falls below its maximum value. The frequency dependence may or may not be a function of the voltage used. This is determined primarily by the nature of the particular phosphor used. The output is usually given as “time-averaged” because the light output within a cycle has a complex deviation from its mean value. This variable output is called the “brightness wave form” and is discussed separately.

##### *Light Output versus Voltage*

The voltage dependence of light output has elicited a considerable amount of curve-fitting either to suggest or to check on various theoretical derivations. The currently popular curve is

$$B = A \exp \{-bV^{-1/2}\}, \quad (6)$$

known as the Alfrey–Taylor plot (Figure 11).<sup>24</sup> Since it is exceptional to be able to measure the brightness of a cell over even one decade of voltage, there is some feeling that a matched curve falls rather short of confirming the premises. Over short voltage ranges the expression

<sup>24</sup> J. B. Taylor and G. F. Alfrey, *Brit. Jour. Appl. Phys.*, Supplement #4, P. S.-44, 1956.

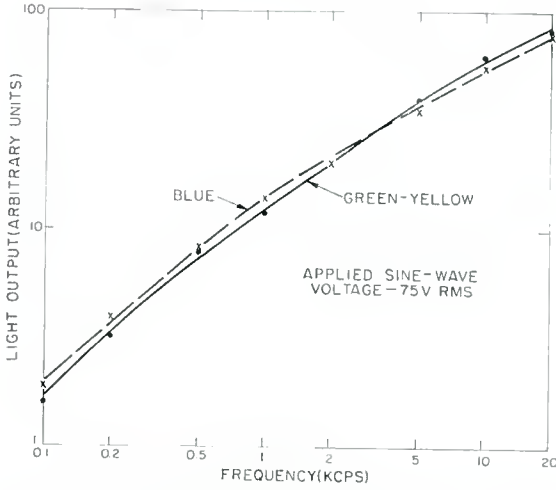


Fig. 10—Variation of light output (time-averaged) with frequency of applied sine-wave field.

$$B = A V^n$$

gives a reasonably good fit. The exponent,  $n$ , may vary from two to eight, according to the voltage range, or material.

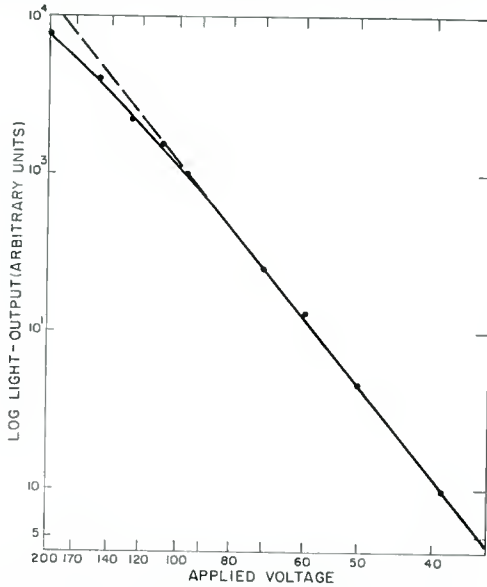


Fig. 11—Variation of light output (time-averaged) with r-m-s voltage of applied sine-wave field.

*Light Output versus Time*

Of considerable interest, of course, is the way in which the light output decreases with time of operation. The literature on the subject fails to develop any definite law of deterioration, since it is found that the operating conditions (voltage and frequency) and preconditioning markedly affect the long-term performance. Other conditions such as particle size, choice of dielectric, and protection from humidity also play significant roles. Commercial cells operated at low fields and low frequency (and therefore at low brightness) are now claimed to have a life (to half-brightness) in the range 1000 to 10,000 hours. The basic cause of cell decay is unknown, although it has been reasonably conjectured that some form of solid-state electrolysis occurs which leads to failure of the working elements where the light generation takes place.<sup>25</sup> For higher frequency operation, the life varies very nearly inversely as the frequency. If one plots the light curves (normalized at  $t = 0$ ) against cycles of operation, the plots for different frequencies very nearly coincide.<sup>26</sup>

Of more interest from the viewpoint of the basic processes involved, is the time behavior on the short time scale. When any electroluminescent cell is placed in operation, the light output rises to a steady value after several cycles. As a rough rule, it requires at least fifteen cycles before the transient processes damp out and the averaged light per cycle becomes relatively constant, although with cells with liquid dielectric there may be a slower increase for some seconds.

Within a single cycle, considerable variation of the light intensity occurs and is usually called the "brightness wave form". A Fourier analysis of the light output would show the fundamental plus many harmonics in addition to the time-averaged output. The components of greatest amplitude are usually the first two or three even harmonics. For the individual light-producing elements, not the cell as a whole, there is increasing evidence that the light output consists of only the fundamental (for roughly half of each cycle) plus odd harmonics. A working cell, containing thousands of working elements, scatters and mixes the light output so that the odd harmonics are not easily observed. The harmonic content is a function of the frequency and voltage used and this function varies with the materials. Boron nitride, for instance, when excited with sine-wave voltages, gives a light output which closely approximates a sine-squared variation with time, while

---

<sup>25</sup> S. Roberts, "Aging Characteristics of Electroluminescent Phosphors," *Jour. Appl. Phys.*, Vol. 28, p. 262, February, 1957.

<sup>26</sup> W. A. J. Thornton, "Electroluminescence Deterioration," *Jour. Appl. Phys.*, Vol. 28, p. 313, March, 1957.

most sulfide-type materials are extremely complex as to their brightness wave form (Figure 12). Any form of alternating field can be used for exciting an electroluminescent cell. The actual wave form used is determined by the experimenter<sup>27</sup> and may be tailored in order to test some hypothesis or demonstrate some special property. Each exciting wave form has its brightness wave form, and the relation is a tenuous one if it can be determined at all.

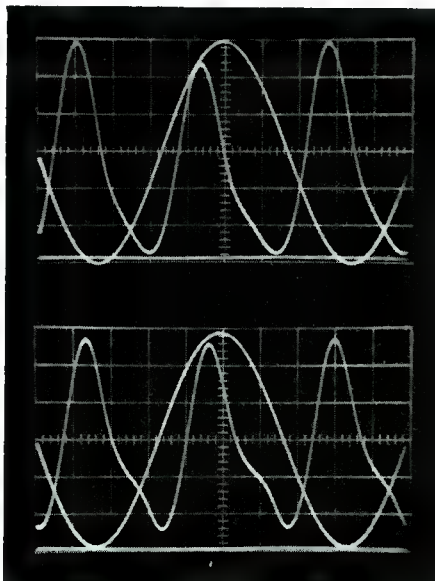


Fig. 12—Oscillogram of light output versus time and applied volts versus time in correct phase relationship. The sinusoidal curves represent voltages. The irregular curves represent light output, the bright horizontal traces representing zero light output. The upper curves are for 200 c.p.s. at 90 volts. The lower curves are for 2000 c.p.s. at 80 volts.

### *Spectral Distribution*

As may have been inferred from earlier discussions, the spectral distribution of light emission of electroluminescent phosphors under field excitation is, generally speaking, the same as would be expected for photo (ultraviolet) excitation of similar host crystal and activator composition. Many electroluminescent powders, however, have an unusual emission property which has no counterpart in the other excitation processes. This property has been called "frequency color shift." For example, one of the most efficient and easily made phosphors,

<sup>27</sup> S. Nudelman and F. Matossi, "Electroluminescence with Nonsinusoidal Fields," *Jour. Electrochem. Soc.*, Vol. 101, p. 546, November, 1954.

ZnS:Cu:Cl, at 100 cycles and in a field of 100 r-m-s volts per mil, has a broad green emission band peaking near 5200 Å. As the frequency is increased, the emission band broadens as the short-wavelength foot of the band moves toward shorter wavelengths. The shift is more or less complete at 20 kilocycles and the peak wavelength may be as far into the blue as 4900 Å. The spectrum shift is primarily a frequency characteristic and is essentially independent of the field used.

Another unusual feature of the color shift is that it really is a shift and not the emergence of one emission band at the expense of another. Under cathode-ray excitation there is evidence of a distinct blue-band peaking near 4500 Å. Under 3650 Å excitation the green band at 5200 Å alone is evident at 25° C. As the material is cooled, the separate blue band begins to appear as the green band loses intensity. These observations can be taken as strong evidence that there are at least two distinct emission processes whose relative efficiency is determined by the temperature and the excitation means. The blue-green electroluminescent emission of this phosphor (as excited by 20-kilocycle fields) is not resolvable into two emission bands whose peak wavelengths and bandwidths are similar to those excited by photons and electrons. A minimum of four to five emission bands would have to be used for adequate resolution of the blue-green emission. Color shift of another sort can be induced in cathode- or photo-excitation by use of extremely high excitation levels. This color shift differs from that of electroluminescence in that the "see-saw" action of two bands is quite evident as opposed to the "sliding shift" of the frequency effect.

Large changes in brightness level (at constant frequency) produce a barely detectable change in spectral character. Frequency-controlled color shift in ZnS:Cu can be essentially eliminated through use of aluminum as a co-activator rather than chlorine. In general, where color shift exists, it is large enough to be noticeable but hardly enough to be of any obvious practical use.

#### *Operating Efficiency*

The conversion efficiency (electrical energy to light) is of considerable interest from the practical as well as the scientific side of the electroluminescent process. From the practical side, the points to consider are (a) apparent surface brightness (since electroluminescent cells are area sources), (b) watts input per unit area, (c) power factor.

The surface is usually assumed to be Lambertian (apparent brightness independent of angle of view) for which case the lumen output per unit area is numerically equal to the brightness in foot-lamberts. For most of the unsaturated colors associated with electroluminescent

phosphors, brightness is easily measured through the use of comparison photometers or calibrated photometrically corrected photocells.

Because of the nonlinear character of the composite dielectric present between the electrodes of an electroluminescent cell, the input wattage is not as easily measured as might be thought. At low frequency and low voltage, an electroluminescent cell responds electrically as would any slightly lossy capacitor. However, at any frequency, as

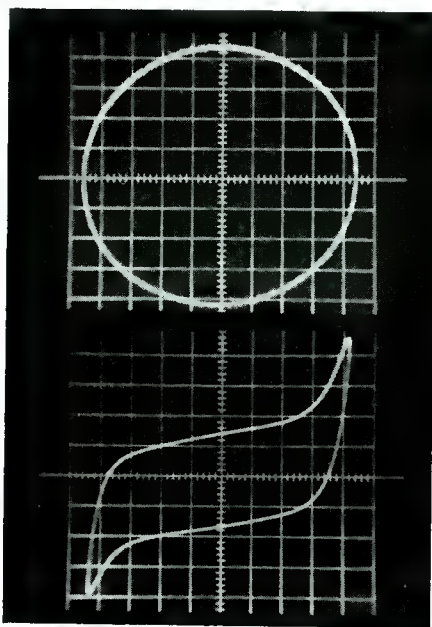


Fig. 13—Oscillogram of cell current versus cell voltage; the ordinate is voltage and the abscissa is current. The upper trace is for high voltage and the lower trace for low voltage, both at 60 cycles.

the voltage is increased beyond that necessary for the appearance of light emission, harmonic distortion in the current wave form occurs and increases with the voltage (Figure 13). For this reason, the standard bridge technique which determines the apparent capacitance<sup>28</sup>

<sup>28</sup> A number of papers have dealt with the concept of "instantaneous capacitance" which varies throughout the cycle of the applied field in non-linear systems. M. Ratner, "Capacitative Measurements on Zinc Sulfide Electroluminescent Cells," *Bull. Amer. Phys. Soc.*, Vol. 4, Series II, p. 370, August 27, 1959; H. K. Henisch, *Rectifying Semi-conductor Contact*, Oxford Clarendon Press, England, 1957; A. Hoffmann, "An Oscillograph Method for the Investigation of Barrier-Layer Properties of Metal Rectifiers," *Zeit. f. Angew. Phys.*, Vol. 2, p. 253, No. 9, 1950; K. Lehovc, "A New Method of Capacity Measurement on Dry Disk Rectifiers," *Jour. Appl. Phys.*, Vol. 20, p. 123, January, 1949.

and loss angle is extremely unreliable. Commercial dynamometer wattmeters are available for the range of frequency and watts involved with experimental cells. An electronic computing wattmeter has been found reliable for a large number of measurement situations, although it has on occasion been confronted with a circuit for which it apparently finds negative watts-input. The only other methods of determining wattage input are calorimetry and computation of  $\frac{I}{T} \int_0^T IV dt$ . Of the

two, the latter is the easier since modern two-beam or switch-beam oscilloscopes make it possible to plot both voltage and current simultaneously against time. At low distortion, this method is less accurate than the electronic wattmeter because the dissipated power in each half cycle is expressed as the difference between two very nearly equal numbers. Using the formula  $W = 2\pi f V^2 C \sin \phi$ , the efficiency of experimental cells has been measured as high as 14 lumens per watt.<sup>29</sup> The value of capacitance,  $C$ , used in the calculation, was obtained by a substitution method and the loss angle  $\phi$  by means of a phase angle meter.

The third aspect of electroluminescent cell application mentioned above refers to the fact that the power factor (regardless of light producing efficiency is only 0.2 or less. Since commercial cells can approximate 1000  $\mu\mu\text{f}$ /square inch, any installation requiring large amounts of light (and, therefore, area) will load the line and supply source with a large capacitive load. With the present trend of automatic home machinery (air conditioners, refrigerators, washers) loading the line with inductive power factor, electroluminescent lighting is in the right direction for power-factor correction.

Since both brightness and efficiency are sensitive to frequency and field, the operating conditions must be a compromise. Figure 14 shows typical performance contours of two experimental cells. This method of display of a cell's characteristics has proven very useful since it was found that the contour shapes (i.e., straight, convex, concave, or position of maximum efficiency) could in many cases, be related to many of the synthesis parameters and post-firing treatment of the various phosphors.

#### *Dielectric and Particle Size Effects*

Early in the study of electroluminescence, calculations and speculations were made as to the role of the imbedding dielectric.<sup>30</sup> It is now

<sup>29</sup> W. Lehman, "Particle Size and Efficiency of Electroluminescent Zinc Sulfide Phosphors," *Jour. Electrochem. Soc.*, Vol. 105, p. 585, October, 1958.

<sup>30</sup> S. Roberts, "Dielectric Changes of Electroluminescent Phosphor During Illumination," *Jour. Opt. Soc. Amer.*, Vol. 43, p. 590, July, 1953.

more or less generally agreed that the dielectric character of electroluminescent powders is too complex (in the broader sense of the term) to permit calculation and prediction of any specific performance in a specific dielectric surround. Empirically it has been found that, for equal applied voltage, the brightness increases monotonically with the dielectric constant of the imbedding medium. With zinc sulfide phosphors, the rate of increase is markedly reduced for dielectric constants greater than eight, the approximate value of zinc sulfide itself. Most dielectrics in this higher range have a large loss angle and are unusable for most applications.

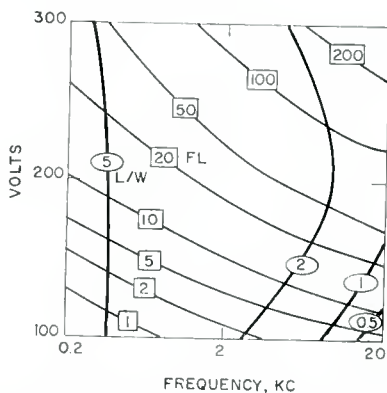


Fig. 14—Contour plots of brightness and efficiency of EL-cells at various voltages and frequencies.

Some work has been done on the effect of particle size on electroluminescence.<sup>29,31</sup> A prepared batch of electroluminescent powder was separated into fractions for which the particles were more nearly equal in size. Cells were then made using these fractions, keeping the mass per unit cell area constant. Measurable differences existed at low voltages, but at high voltage brightness was independent of particle size. The results were used by one author<sup>31</sup> to assess the relative roles of surface and volume in the electroluminescent mechanism.

There may be some valuable results available from this type of investigation, but the issue is clouded when it is realized that in most test cells, the electrode spacing may be in the range of 25 to 50 microns. Since the larger particles may run up to 20 to 25 microns, a very few particles in contact can easily bridge the cell gap. If a liquid dielectric is used, even in a dilute suspension of small particles, a bridge of

<sup>31</sup> P. Goldberg, "Particle Size Effects and the Distribution of Barriers in Electroluminescent Zinc Sulfide Phosphors," *Jour. Electrochem. Soc.*, Vol. 106, p. 34, January, 1959.

particles can be established through electrostatic forces. It seems clear that a prerequisite to a significant experiment along this line is to find some way to control the contact (or lack of it) between particles or from particles to electrodes.

#### FUNDAMENTAL PROCESSES OF ELECTROLUMINESCENCE

Thus far, the outward aspects of the electroluminescence phenomenon as displayed by particles have been described. In this section, the present state of the grasp or understanding of some aspects of the phenomenon is surveyed.

##### *Single Crystal versus Polycrystallites*

A question frequently discussed relates to the possibility that single-crystal electroluminescence is different from that of powders. Certainly there is a difference imposed by the *geometry* of the contacts. Whether this accounts for *all* the observed differences and whether it can be stated that intrinsically the two processes are essentially identical has not as yet been proven or disproven. Because of the nondefinitive nature of most of the experiments, there is still much uncertainty.

On the basis of the contact geometry, the single-crystal case *seems* to be relatively straight-forward. The position of the conducting electrodes is known and observable. The current flow and even the potential distribution (from electrode to electrode) is measurable. The crystal in the dark state is apparently homogeneous. Yet the response of the crystal to electrical stimulation is extremely complex.

With powder cells the electrodes primarily serve to place boundary conditions on the potential distribution. (Cells can be made with mica (or Mylar\*) between the electroluminescent suspension and the electrode surface.) With this cell construction, the series current in the separator is a displacement current and not a movement of free charge. Inside the suspension the current is partly displacement and partly charge movement. In a dilute electroluminescent suspension, the charge-movement current is limited to the small volume occupied by the particles. In the particles, a portion of the current may still be a displacement current, since the electroluminescent particles are essentially nonconductors rather than conductors. Because of the special preparative procedures necessary for the synthesis of the optimum performance of electroluminescent phosphors, it was concluded<sup>9</sup> that a second phase of material is necessarily present in close

---

\* Registered trade mark.

contact to the (more or less) normal luminescence phase. Under this condition, the conventional model of dielectric particles in a dielectric medium can not be realistically used to analyze the problem of field distribution and current flow in an electroluminescent layer. Since appreciable light can be obtained with fields as small as 5000 volts peak per centimeter (averaged over the layer) and since this is far too low to cause excitation by impact ionization, it is generally agreed that there must be some inhomogeneity, either chemical or electronic, distributed in such a manner as to enhance local field strengths to two or three orders stronger than the average. In addition the potential drop in this region of high field must be not less than 3 to 3.6 volts (for ZnS phosphors).

The special conditions necessary for high fields place some restrictions on the charge flow. Unless electrodes, real (a conductive layer) or virtual (surface states with surface conductivity), are coupled with the high-field region, the amount of free charge available to make use of the potential drop which exists is severely limited. In addition, oscillographic measurement of current flow shows that the light output is closely associated with a nonlinear current flow which appears when the applied voltage is sufficient to induce luminescence. This is strong evidence of the presence and necessity of barriers in powder electroluminescence. The role of barriers and local "electrodes" has received limited, but, in at least one case, careful attention in the literature.<sup>32</sup>

The chemical nature of the second phase and its physical distribution are still subjects of debate. For any specific phosphor, some very probable guesses can be made as to the chemical nature of the second phase. As mentioned earlier, in ZnS:Cu it certainly must be either  $\text{Cu}_2\text{S}$  or a Zn:Cu:S complex. In the reported cases of electroluminescent ZnS made by firing in oxidizing atmospheres, the presence of ZnO is quite possible. For BN, however, the nature of the second phase is still unknown.

The placement of the second phase has three distinct possibilities, each with its proponents. The first is that this important second phase is segregated into acicular cavities dispersed throughout each otherwise normal crystallite component. A second is that it is segregated in thin layers separating the crystallite components. The third is that the segregation occurs at the outer surfaces of the crystallites. It is probable that the proponents of each viewpoint will concede that some

---

<sup>32</sup> G. Diemer and P. Zalm, "The Role of Exhaustion Barriers in Electroluminescent Powders," *Physica*, Vol. 25, p. 232, 1959; also P. Zalm, "The Electroluminescence of ZnS Type Phosphors," *Philips Research Report*, Vol. 11, p. 353, October, 1956, and Vol. 11, p. 417, December, 1956.

segregation of each other type does exist to a limited extent. The difference of opinion concerns which mode of segregation is necessary to the electroluminescent process.

The selection of the second-phase configuration as the most probable operative one is influenced by another necessary step in the electroluminescent process. It has been shown that high fields, charge storage, and charge flow are necessary to electroluminescence. How these are connected to the excitation process is still to be determined. Impact ionization or minority injection has been discussed as possible excitation steps.<sup>33</sup> In single crystals, these possibilities can be analyzed and related to the observable parameters in a comparatively macroscopic system, since probes can be attached or microscopic observation or brightness measurement made on small fractional areas of the crystals. Our most efficient phosphors average 5 to 10 microns in size (or with BN, 0.1 micron). This scale of operations renders it difficult to extrapolate accurately and confidently the measurements and hypotheses used for single crystals. As has been mentioned, the current is largely a displacement current which masks the in-phase current. In addition, since the electroluminescent layer is a complex electrical network with nonlinear resistive and capacitive elements,\* there will be internal harmonic distortion of both the wattless and dissipative current. (By external measurement, the in-phase component of the first harmonic alone accounts for the losses when the applied voltage is an undistorted sine wave.)

Until a more exact concept of the nature of this network is obtained, it will be difficult to localize the regions of high field and high current flow. Zalm et al<sup>10</sup> have offered a concept of the equivalent network of an electroluminescent working element but have not conclusively related this element to any particular configuration in a complete cell.

Attempts have been made to show effects of d-c bias on the output of a-c induced electroluminescence. If the cells are dilute or so constructed that no direct current flows because of the bias field, there is no effect. By use of mixed frequencies, however, it is possible to demonstrate a bias effect. The oscillogram of Figure 15 shows the brightness wave form of a single cycle of a sine-wave field which is riding on a much slower triangular wave. It is seen that as the posi-

---

<sup>33</sup> M. A. Lampert, "A Simplified Theory of Two-Carrier, Space-Charge-Limited Current Flow in Solids," *RCA Review*, Vol. XX, p. 682, December, 1959.

\* These arise from the space-charge-limited currents and charge-exhaustion regions present in the crystal particles.

tion of the sine-wave cycle is varied with respect to the reversal of the triangular wave, marked changes occur in the brightness wave form. This is undoubtedly due to the transient nature of the bias induced by the  $dV/dT$  across capacitive elements in the cell.

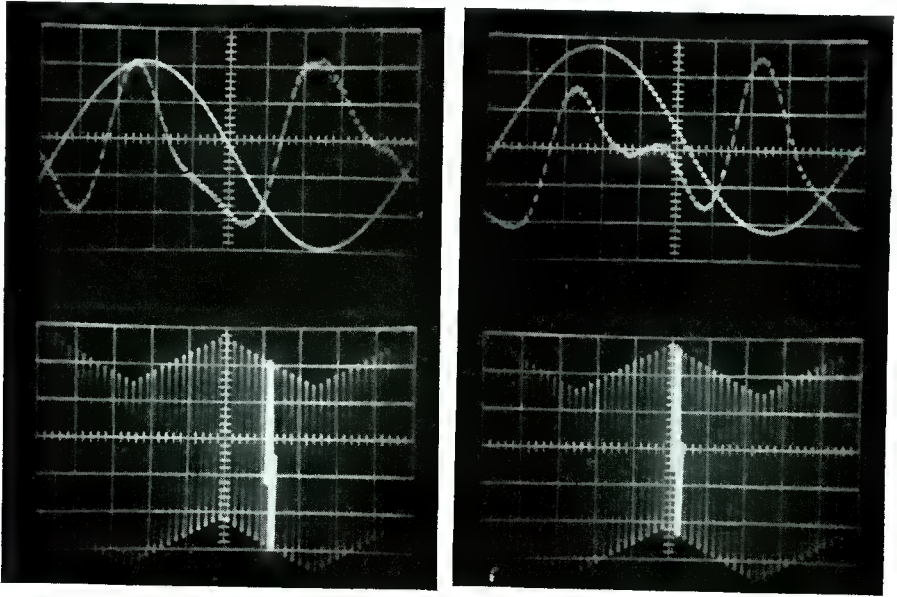


Fig. 15—Oscillogram showing the effect of superimposed voltage wave forms on the light output. (The brightened cycle in the slow trace is the single cycle displayed in the fast trace.)

When symmetrical or unsymmetrical square waves, trapezoidal waves, etc. are used, the brightness waves show a complex response to the various parameters: voltage, frequency, shape, etc. Another complicating factor arises from the frequent occurrence of color changes during a cycle. This is easily demonstrated by using filters (over the measuring photocell) which differentiate between the long- and short-wavelength portions of the emission band. Another method has been tried<sup>34</sup> using a rapid scanning monochromator slightly out of synchronism with the exciting frequency. Though potentially more complete, this method requires considerable mathematical analysis to reconstruct the spectra as a function of phase.

<sup>34</sup> E. E. Loebner, "Time-Dependent Spectra of Electroluminescent Zinc Sulfide," *Phys. Rev.*, Vol. 92, p. 846, November, 1953.

## PHYSICAL CHEMISTRY OF ELECTROLUMINESCENCE

The synthesis of phosphors is much more involved than selecting starting ingredients and firing conditions. Between the placing of a charge in the furnace and the subsequent measurement of its properties, many physical and chemical processes occur. These occur and interplay within a comparatively short period of time. Efficient phosphors are seldom obtained as the result of a process which has achieved a steady-state (equilibrium) condition, i.e., additional time at the firing temperature has no influence on the properties of the phosphor. Instead, the processes must be interrupted at a time determined empirically as optimizing one or more specific properties. At this selected time, chemical and physical characteristics of the charge and the ambient atmosphere are still changing, and yet it is these characteristics which will determine the room temperature properties. Chiefly indirect methods must be used to obtain a knowledge of these more-or-less critical characteristics, and of the changes which occur. Several experiments which illustrate how this has been done are given below.

*The Energy-Absorbing Layer*

As was pointed out earlier, the major difference between an electroluminescent and a non-electroluminescent\* material is the ability of the former to absorb and utilize energy from an electric field to produce luminescence. The existence of a Schottky-Mott type of barrier has been postulated,<sup>35</sup> but the chemical identity of the essential energy-absorbing layer has not been definitely established.

Recently, some evidence for chemical barriers as opposed to Schottky barriers in electroluminescent ZnS phosphors was reported.<sup>11</sup> Figure 16 represents the following sequence of steps:

Non-luminescent ZnS:Cu was prepared by crystallization in H<sub>2</sub>S (at 1100° C) in the absence of halide. This material had 0.117 per cent by weight of total copper and 0.019 per cent incorporated copper. Phosphors were then prepared from this starting material by two different procedures:

- (1) The diffusion, at elevated temperatures, of iodide coactivator into the material followed by digestion with alkali cyanide.
- (2) Digestion with alkali cyanide *before* the iodide diffusion.

---

\* The material should, of course, be photo- or cathodoluminescent.

<sup>35</sup> G. Diemer and P. Zalm, "Voltage Distribution Inside Electroluminescent ZnS Crystals," *Physica*, Vol. 22, p. 561, 1956.

for these results, our interpretation of this experiment is that volume iodide was obtained in materials which were prepared by either process, thereby enabling the formation of centers which gave rise to photo- and cathodo-luminescence. During the iodide diffusion, iodide apparently reacts with copper sulfide to give copper iodide, which has an appreciable vapor pressure at the temperature of diffusion. In the case of process (1), sufficient copper in excess of barrier copper is available for reaction with any iodide remaining during the period of firing, while in the case of process (2), barrier copper, if existing, is removed, the resulting phosphor being non-electroluminescent.

The capacitances of standardized cells of the above materials are shown in Figure 17(b), and the power absorbed is shown in Figure 17(c). When Figure 17(a) is compared with Figure 17(c) it is seen that electroluminescence is not a linear function of the power absorbed, and that by the surface treatment discussed above, both the energy-(power-) absorbing layer and electroluminescence are lost.

#### *Two-Step Preparation*

One example of a non-definitive but rather suggestive experiment consisted of preparing a ZnS:Cu(0.02):I phosphor at 1100° C. This material is very efficient under cathode-ray or ultraviolet excitation but showed no electroluminescence. Portions of this material were then refired at 700° C in sulphur after mixing with small amounts of unfired ZnS:Cu(.3):NH<sub>4</sub>I(10). This material normally is an efficient electroluminescent material. The relative electroluminescent brightness of the refired material as a function of the amount of added material is shown in Figure 19. Since the original copper is at the maximum which would be retained by firing the second material, the copper content of the original bulk is unlikely to change either way. The effective electroluminescent efficiency is completely out of proportion to that to be expected in a bulk-ratio basis. The conclusion strongly indicated is that the second firing has coated a large number of the particles of the first firing with a phase which is capable of being electroluminescent, and that the bulk of the original phosphor has served the purpose of allowing a proper surface to be built up on particles with luminescent capabilities.

#### *Sulfur Effect*

Another experiment<sup>37</sup> which serves to show the complexity of the physical chemistry involved in the synthesis of electroluminescent

---

<sup>37</sup> S. Larach and R. E. Shrader, "Electroluminescent Chalcogenide Phosphors," *International Conference on Solid-State Physics*, Brussels, Belgium, p. 41, June, 1958.

phosphors is illustrated by Figure 20. This shows the results of processing three materials under two different temperatures and two different atmospheres (with or without sulfur vapor present). The first material was a normal starting mix of an efficient blue-emitting electroluminescent material. The reflective color (in white light) of the materials produced by the four firings, and the responsiveness to

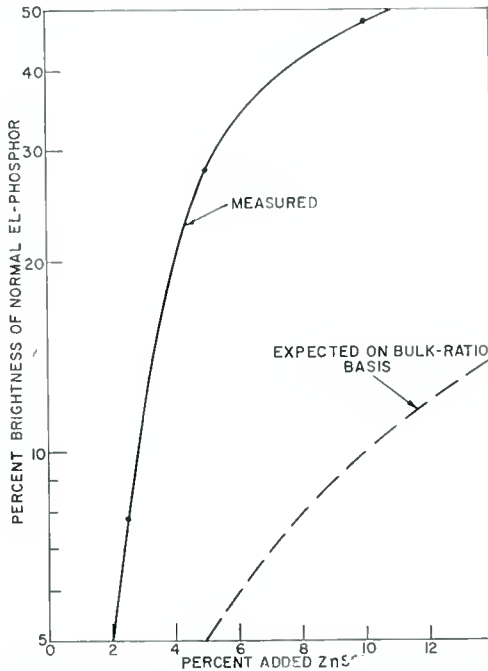


Fig. 19—Plot showing EL brightness of CR phosphor achieved on re-firing as a function of per cent of EL phosphor [ZnS:Cu (0.3)] added before re-firing.

field excitation are indicated by the notation around the outer circle of the figure. The simultaneous necessity, for electroluminescence, of 700° C temperature plus sulfur vapor is clearly indicated. The grey body color is invariably associated with the appearance of electroluminescence capabilities, at least for ZnS materials. (It does not follow that the presence of a grey color is any guarantee of electroluminescence). The material fired at 700° C without sulfur had an average particle size of 9 microns and the particles had no clear-cut planes and edges. The material fired with sulfur present had an average particle size of 14 microns and exhibited well-defined planes and edges. X-ray diffraction studies of the non-sulfur materials showed some hexagonal phase; the cubic diffraction lines were much broader than those of the sulfur material.

To determine if these results are related to the association of copper and iodine in the ZnS lattice, four processings with copper omitted were tested for photoluminescence (3650 Å excitation). The results (notations on second circle) again show the simultaneous necessity of a temperature of 700° C plus sulfur. Whether this result is a property of iodine, iodine plus lattice, or of the lattice alone is

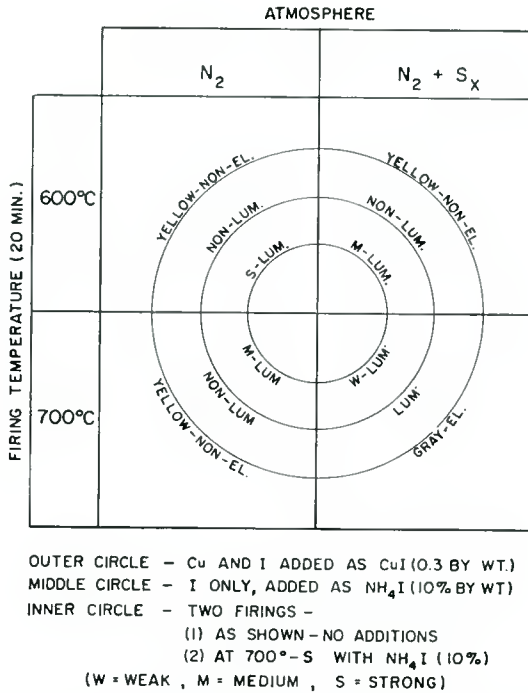


Fig. 20—Chart showing luminescent effects achieved by different firing temperatures and atmospheres.

difficult to answer in a direct manner. The following indirect approach was used: with no additive, ZnS was fired under each of the four conditions; each of the resultant materials was thoroughly admixed with the NH<sub>4</sub>I and refired under the conditions which previously had provided an efficient photoluminescent phosphor. The results of this processing are given by the inner circle in Figure 20, where the qualitative responses to photoexcitation are indicated. It seems clear that in the ZnS lattice, without copper or iodine as additive, an inhibitive effect (against subsequent activation) has been most strongly induced by the same condition which was most effective in producing luminescence capability.

As a result of this series of preparations, the following picture has developed: when the preparation temperature is above 600° C the presence of excess sulfur increases the diffusion mobility in the ZnS lattice of at least one ion, if not both. (This effect becomes less observable, the higher the preparation temperature.) The sintering of the nearly amorphous starting materials into larger aggregations proceeds with or without sulfur. During this sintering the impurities present are dispersed and incorporated into the particles although, because of disorder, the incorporation may not be complete in the usual sense of solid-solution. As the sintering proceeds, the crystallinity also improves, but more rapidly with sulfur than without. If the solid-solution limit of the copper ion is lower than the apparent incorporation limit, the excess copper is precipitated at the interfaces and outer surfaces of the crystallite domains. That this effect is rapid is illustrated by a variation in preparation whereby in a 20-minute firing at 700° C, presence of sulfur was limited to the last five minutes of the firing. The material was essentially identical to that obtained by the presence of sulfur for the entire 20 minutes.

The sintering with less disorder, which occurs in the presence of sulfur, also makes possible the luminescent center involving the halide or, if no impurities are present, reduces the mobility for the subsequent inward diffusion of impurity ions, especially iodide. The effect of this sintering is barely detectable if chloride is used.

#### CONCLUSION

The design, energy absorption, luminescence, and electrical characteristics of electroluminescent polycrystallites have been discussed. It is shown that the emission of light from a material under the action of an electric field is the result of a complex composite of phenomena. Most work on the electroluminescence from polycrystallites have been done with Group II-Group VI materials. However, even for these phosphors, a quantitative theory is still lacking.

The complete knowledge of the mechanism of electroluminescent phenomena is unlikely to be gained only by physical measurements and observations on a single species, or by synthesis variations alone. Only well-planned cooperative experiments are likely to give early insight.

#### ACKNOWLEDGMENT

The authors wish to acknowledge the considerable assistance received from Dr. S. M. Thomsen, for use of some of his data, aid in synthesis of many of the materials described, as well as helpful thoughts and discussions.

# THE ACHIEVEMENT OF MAXIMUM PHOTOCONDUCTIVITY PERFORMANCE IN CADMIUM SULFIDE CRYSTALS\*

BY

RICHARD H. BUBE AND LUCIAN A. BARTON

RCA Laboratories,  
Princeton, N. J.

*Summary*—Improved photoconductivity performance (i.e., gain  $\times$  speed) in cadmium sulfide crystals requires a decrease in trapping center concentration, probably by several orders of magnitude, over that currently available in commercial materials. The incorporation of compensating impurities (at present, the most common procedure in producing sensitive photoconductors) acts to increase the imperfection concentration. An investigation was made, therefore, of other methods of producing sensitive crystals. These methods include: (1) producing slight deviations from stoichiometry during growth, (2) incorporating a trace of donor impurity, (3) annealing conducting crystals in sulfur vapor, and (4) resubliming pure crystals under a variety of conditions. Photosensitive crystals prepared by all of these methods are discussed, and it is found that a number of crystals prepared by the first and second of these methods show marked improvement in performance over standard photoconductors. Between trap depths of 0.2 and 0.7 ev, such crystals have a total trap density in the range of  $10^{13}$   $\text{cm}^{-3}$ . For operating conditions at room temperature, the trap density near the Fermi level is at least an order of magnitude less than this density. Improvements in low-light performance by factors of  $10^3$ , and maximum-gain ( $M$ ) factors as high as 500 have been observed. Almost all crystals prepared by the third and fourth methods mentioned above show low speed of response at room temperature because of the presence of traps with depth of about 0.6 ev and density of  $10^{14}$  to  $10^{15}$   $\text{cm}^{-3}$ .

## INTRODUCTION

THE ABSORPTION of light by a photoconductor frees charge carriers which contribute to the electrical conductivity of the material until they are captured, either temporarily at a trapping center or permanently at a recombination center. Many of the important steps in this process are associated with the effects of crystal imperfections, either chemical impurities or crystal defects.<sup>1</sup>

\* Manuscript received September 16, 1959.

<sup>1</sup> For further detailed discussion of photoconductivity, see R. H. Bube, *Photoconductivity of Solids*, J. Wiley & Sons, New York, in press.

## EFFECTS OF CRYSTAL IMPERFECTIONS

All of the important properties of photoconductors—sensitivity, spectral response, speed of response, and dark conductivity—are determined, at least in part, by the nature and density of crystal imperfections present.

*Lifetime of Charge Carriers (Sensitivity)*

Although recombination between free electrons and free holes has been observed under certain conditions of high free-carrier density, free carriers are usually captured by imperfection centers. Such centers are of two types:<sup>2,3</sup> (a) trapping centers, if the probability that the captured carrier will be thermally freed to the nearest band is larger than the probability that a free carrier of opposite type will recombine with the captured carrier; or (b) recombination centers, if the probability for thermal freeing is smaller than for recombination. The recombination centers are considered in this section.

In crystals of CdS which show appreciable photosensitivity, there is evidence<sup>4,5</sup> that particular imperfections are present which have an effective negative charge with respect to the rest of the crystal, e.g., a  $\text{Cu}^+$  center, or a cation vacancy. Such centers have a large cross section for photoexcited holes, and a subsequent small cross section for photoexcited electrons. Indeed, measurements show that the cross section for hole capture is some  $10^6$  times greater than that for electron capture, probable values being about  $10^{-13}$   $\text{cm}^2$  and  $10^{-19}$   $\text{cm}^2$ , respectively. We may categorize these centers in general as compensated acceptors. The net result of the presence of such centers is to provide a long effective lifetime for the photoexcited electrons, so that for each photon absorbed many electron transits across the crystal may occur. In view of their effects, we shall call such centers "sensitizing centers." Other types of imperfections which are effective in bringing about recombination of photoexcited carriers are always present in the crystal. If sensitizing centers are absent, these other imperfections dominate and an insensitive material results. According to the above definition, high photosensitivity results under operating

---

<sup>2</sup> A. Rose, "Performance of Photoconductors," *Photoconductivity Conference*, John Wiley & Sons, New York, N.Y., 1956, p. 3.

<sup>3</sup> A. Rose, "Recombination Process In Insulators and Semiconductors," *Phys. Rev.*, Vol. 97, p. 322, January, 1955; A. Rose, "Performance of Photoconductors," *Proc. I.R.E.*, Vol. 43, p. 1850, December, 1955.

<sup>4</sup> R. H. Bube, "Photoconductivity of the Sulfide, Selenide, and Telluride of Zinc or Cadmium," *Proc. I.R.E.*, Vol. 43, p. 1836, December, 1955.

<sup>5</sup> R. H. Bube, "Analysis of Photoconductivity Applied to Cadmium-Sulfide-Type Photoconductors," *Journal of Physics & Chemistry of Solids*, Vol. 1, p. 234, January, 1957.

conditions for which the sensitizing centers are acting as recombination centers. Under operating conditions for which the sensitizing centers act only as hole traps, the photosensitivity is low and identical with that in a material without sensitizing centers.

### *Speed of Response*

In a photoconductor with only recombination levels, the time required for the conductivity to change with changes in light intensity is equal to the electron lifetime. In actual practice, particularly for low-intensity excitation, the measured response time may be several orders of magnitude greater than the electron lifetime. This low speed results from the existence in the crystal of trapping centers which trap electrons during excitation and then release them slowly when the excitation has been terminated. The observed decay time can be correlated with the lifetime by the relation<sup>6</sup>

$$\tau_0 = \tau \frac{n_t}{n}, \quad (1)$$

where  $\tau_0$  is the observed decay time,  $\tau$  is the electron lifetime,  $n$  is the density of free electrons, and  $n_t$  is the density of trapped electrons within about  $kT$  of the steady-state Fermi level during excitation. This equation, of course, holds only for  $\tau_0 \geq \tau$ . The presence of trapping centers also increases the rise time upon the beginning of excitation by draining off free carriers until a new equilibrium between trapping centers and conduction band has been established.

### *Spectral Response*

Crystal imperfections give long-wavelength spectral response. The major portion of the absorption resulting in photoconductivity usually involves absorption by the host crystal itself, i.e., intrinsic absorption with band-to-band transitions. If imperfections are present, however, with energy levels permitting excitation of an electron from the center to the conduction band, additional photoconductivity response is observed at wavelengths longer than that of the band edge. The long-wavelength cutoff of this additional response corresponds to the energy required to free an electron from the center.

### *Dark Conductivity*

Donor impurities, such as elements from Groups III and VII, tend to increase the electron conductivity of CdS, whereas acceptor impuri-

---

<sup>6</sup> A. Rose, "An Outline of Some Photoconductive Processes," *RCA Review*, Vol. XII, p. 362, September, 1951.

ties, such as elements from Groups I and V, tend to decrease the electron conductivity.<sup>7</sup> Anion vacancies can perform the same functions as donor impurities, and cation vacancies can perform the same functions as acceptor impurities. Because acceptors in CdS have energy levels about 1 ev above the top of the valence band, it is difficult to obtain high-conductivity p-type material.

#### PREPARATION OF SENSITIVE PHOTOCONDUCTING CdS

A general procedure<sup>7</sup> for preparing sensitive crystals of CdS has been to grow highly conducting crystals by incorporating a halide or a trivalent cation during the crystal growth, and then to incorporate sufficient acceptor to reduce the dark conductivity while retaining high photosensitivity. Such a procedure of incorporating too high a density of donors with back-compensation later has proven amenable as a reproducible method for preparing sensitive crystals. However, it involves a number of operational steps, each of which can act to introduce extraneous imperfections into the crystal.

In principle, and also to a limited extent in practice, it has been shown that sensitive crystals can be prepared by the incorporation of a small concentration of only the donor impurity. This increase in sensitivity can be ascribed to two possible roles of the donor: (a) compensation of acceptors already present in the crystal, either in the form of impurities or defects; or (b) creation of compensated acceptor defects directly, one cation vacancy being formed for each two donors incorporated. Actually, no chemical impurity is required to produce a sensitive crystal, anion vacancies being able to fulfill the role ascribed above to donor impurities. The control required to achieve reproducibility in the initial preparation from the vapor phase increases markedly as one proceeds from the method involving the use of two chemical impurities, to donors alone, to defects alone.

#### PHOTOCONDUCTIVITY GAIN

Thus far we have spoken of sensitivity as the measure of how "good" a photoconductor is. To speak of sensitivity quantitatively we define a specific photosensitivity,  $S$ , in units of mho cm<sup>2</sup> per watt, i.e., the product of the conductance and the square of the electrode spacing, divided by the absorbed light power.<sup>†</sup> This specific sensitivity is

<sup>7</sup> R. H. Bube and S. M. Thomsen, "Photoconductivity and Crystal Imperfections in Cadmium Sulfide Crystals. Part I—Effect of Impurities," *Jour. Chem. Phys.*, Vol. 23, p. 15, January, 1955.

<sup>†</sup> As a practical unit,  $S$  is usually determined for excitation by incandescent illumination. Since the major contribution to the sensitivity usually comes from a band near the absorption edge,  $S$  (all  $\lambda$ )  $\approx S$  (edge  $\lambda$ ).

independent of geometry, applied field, and applied light intensity if the photoconductivity varies linearly with applied field and light intensity. It turns out that this is a convenient unit to use for sensitivity, since the most sensitive CdS crystals have a value of  $S$  near unity.

Another measure of how "good" a photoconductor is, and one which is sometimes more useful than the specific sensitivity, is the photoconductivity gain. The gain,  $G$ , is defined as the number of electrons which pass between the electrodes for each photon absorbed. If the lifetime of an electron is  $\tau$  and the time required for one transit between the electrodes is  $t'$ , then<sup>6</sup>

$$G = \frac{\tau}{t'}, \quad (2)$$

or

$$G = \frac{\tau\mu V}{l^2}, \quad (3)$$

where  $\mu$  is the electron mobility,  $V$  is the applied voltage, and  $l$  is the electrode spacing. A comparison of the definitions of sensitivity and gain show that

$$G \propto \frac{V}{l^2} S, \quad (4)$$

or

$$S \propto \tau\mu. \quad (5)$$

The sensitivity is a characteristic of the material itself, whereas the gain depends on the geometry and the applied field of an operating cell.

#### MAXIMUM GAIN

Equation (3) might lead one to expect that gain may be increased indefinitely simply by increasing the applied voltage. Consideration of the physical situation, however, shows that at least three processes may interrupt the applicability of Equation (3) with increasing voltage: (a) the injection of space-charge-limited current, (b) electron multiplication by such processes as impact ionization, and (c) dielectric breakdown. Evidence indicates that processes (b) and (c) usually occur near the same values of applied voltage. Of course, if breakdown occurs before the injection of appreciable space-charge-limited current,

this in itself limits the gain obtainable. The apparently more likely case, where space-charge-limited currents become important before breakdown, has been investigated by Rose and Lampert,<sup>8,9</sup> who show that the maximum gain obtainable is given by

$$G_{\max} = \frac{\tau_0}{\tau_{RC}} M, \quad (6)$$

where  $\tau_0$  is the observed response time,  $\tau_{RC}$  is the RC time constant (the dielectric relaxation time) at the operating conditions, and  $M$  is a multiplying factor involving the actual trap distributions present, usually unity but with the possibility of being much larger. This factor  $M$  can be expressed as

$$M = \frac{N_A}{N_t}, \quad (7)$$

where  $N_A$  is the number of positive charges on the anode, corresponding to the number of traps filled by the field-injected space-charge-limited current, and  $N_t$  is the number of traps filled by the photoexcitation process (including the free electrons so created).

Traps play a dual role in that (1) they give rise to long response times by filling and emptying during photoexcitation, and (2) they also allow the achievement of higher  $G_{\max}$  by increasing the maximum field which can be applied before space-charge-limited currents become important. If the same traps are filled by both field-injected charge and photoexcitation, then  $M = 1$ , and the maximum gain is unity for many applications for which  $\tau_0 \approx \tau_{RC}$ . If, however, centers can be created which would be filled by field-injected charge but would not be filled under photoexcitation,  $M$  can take on significantly larger values.<sup>10,11</sup> In a homogeneous system, recombination centers (probably negatively charged centers) lying just above the Fermi level meet these requirements. In a nonhomogeneous system, surface traps may

<sup>8</sup> A. Rose and M. A. Lampert, "Gain-Bandwidth Product for Photoconductors," *RCA Review*, Vol. XX, p. 57, March, 1959.

<sup>9</sup> A. Rose and M. A. Lampert, "Photoconductor Performance, Space-Charge Currents, and the Steady-State Fermi Level," *Phys. Rev.*, Vol. 113, p. 1227, March, 1959.

<sup>10</sup> R. W. Smith, "Properties of Deep Traps Derived from Space-Charge-Current Flow and Photoconductive Decay," *RCA Review*, Vol. XX, p. 69, March, 1959.

<sup>11</sup> H. B. DeVore, "Gains, Response Time, and Trap Distributions in Powder Photoconductors," *RCA Review*, Vol. XX, p. 79, March, 1959.

capture the injected charge, while photocurrent flows primarily through volume regions with a much smaller trap density.

Maximum practical performance of a photoconductor cell requires maximum  $G_{\max}/\tau_0$ , or maximum gain-bandwidth product. Consider a typical case of a sandwich-type cell of area  $A$ , and thickness  $l$ . Then the capacitance of the cell,  $C$ , is

$$C = \frac{\epsilon A}{4\pi l} \times 10^{-12} \text{ farads}, \quad (8)$$

where  $\epsilon$  is the dielectric constant of the photoconductor, usually near 10; for CdS,  $\epsilon = 11.6$ . The relaxation time can then be expressed in terms of the conductivity,  $\sigma = ne\mu$ , of the material;

$$\tau_{RC} = \frac{\epsilon}{4\pi\sigma} \times 10^{-12} \text{ second}. \quad (9)$$

The gain-bandwidth product becomes

$$\frac{G_{\max}}{\tau_0} = \frac{4 \times 10^{12} \pi}{\epsilon} \sigma M, \quad (10)$$

or

$$\frac{G_{\max}}{\tau_0} = Kn \frac{N_A}{N_t} \quad (11)$$

where  $K$  is a constant depending only on  $\epsilon$  and  $\mu$ .

The gain-bandwidth product can therefore be maximized in three ways: (1) increasing the operating conductivity, (2) increasing the density of states which capture field-injected charge but not photoexcited charge, and (3) decreasing the density of states which capture photoexcited charge, i.e., the conventional electron-trapping centers. The first of these is often ruled out since many applications of photoconductors have a maximum allowable conductivity. Both of the other alternatives involve appreciable difficulty in synthesis. A number of experiments described in this paper are aimed chiefly at the third of these possible procedures, which is probably a first step in any program to increase the gain-bandwidth product. There is some reason to believe that levels required for the  $N_A$  may be present at about the right position of the forbidden gap in CdS, and that they are doubly negative recombination centers.<sup>10</sup> On the other hand, the effect of different surface and volume traps under certain geometrical arrange-

ments may be expected to lead to values of  $M$  in excess of unity. In any event, results are reported in this paper on 12 crystals with  $M \geq 10$ , resulting from experimental procedures intended only to decrease the density of trapping centers.

We can obtain an expression for the applied voltage corresponding to maximum gain by the following steps.<sup>12</sup> Space-charge-limited currents will become important when

$$\begin{aligned} V_{\max} C &= \text{total charge in crystal} \\ &= Q_{\text{free}} \frac{\tau_0}{\tau} M. \end{aligned} \quad (12)$$

Upon substitution from Equation (8) for  $C$ , and for  $Q_{\text{free}} = neAl$ ,

$$V_{\max} = \frac{8 \times 10^6 lL}{\epsilon} \tau_0 M, \quad (13)$$

where  $L$  is the light intensity in foot-candles. The trap density  $n_t$  corresponding to a given set of conditions can be expressed

$$n_t = n \frac{\tau_0}{\tau} = \frac{4 \times 10^{12}}{l} L \tau_0 \text{ cm}^{-3}. \quad (14)$$

If we assume the reasonable values  $\tau_0 = 10^{-1}$  second,  $\epsilon = 10$ , and  $l = 10^{-2}$  cm, Equations (13) and (14) become

$$V_{\max} = 8 \times 10^2 LM \text{ volts}, \quad (13a)$$

$$n_t = 4 \times 10^{13} L \text{ cm}^{-3}. \quad (14a)$$

At low light levels, the requirement for low  $n_t$  becomes very difficult to fulfill, and if it were not for the fact that this trap density is required only near the dark Fermi level rather than over the whole forbidden gap, the task of achieving low  $n_t$  would be virtually impossible.

In the special case where the photoconductor is operated with an alternating applied field of frequency  $f$ , Equation (10) for the gain-bandwidth product can be simplified since  $\sigma = 5 \times 10^{-13} \epsilon f$ :

$$\frac{G_{\max}}{\tau_0} = 2\pi f M. \quad (15)$$

<sup>12</sup> A. Rose, "Maximum Performance of Photoconductors," *Helvetica Physica Acta*, Vol. XXX, p. 242, No. 4, 1957.

## EXPERIMENT

Results are described for five different types of CdS crystals: (1) pure CdS, (2) CdS crystals containing a trace of iodine, (3) CdS crystals containing higher concentrations of iodine, (4) CdS:I crystals annealed under sulfur pressure, and (5) pure CdS crystals resublimed either in flowing nitrogen, or under pressure of sulfur or cadmium. In addition, a few results with pure CdSe are included.

CdS crystals were grown by a modified Frerichs' technique, using pre-purified nitrogen carrier gas (Matheson Co.) over cadmium and sulfur. The cadmium was held at about 650° C, the sulfur at about 325° C, the reaction zone temperature was 900° C, and the flow rate of the nitrogen over both cadmium and sulfur was about 300 cm<sup>3</sup>/min.

Thus, there are three principal ingredients: cadmium, sulfur and N<sub>2</sub>. Initially, cadmium from Johnson and Mathey was used, which showed spectrographically 3 parts per million of copper, and traces of magnesium, aluminum and silicon. Later, cadmium from Consolidated Smelting and Refining Co. of Canada was used; this cadmium showed no detectable copper and only traces of magnesium and silicon. Sulfur was obtained from Johnson and Mathey, showing about 3 parts per million of sodium and a trace of silicon; it was resublimed to remove hydrocarbons. The pre-purified N<sub>2</sub> was passed through a De-oxo Puridrier,<sup>‡</sup> through a triple liquid nitrogen trap, and then over molten cadmium pellets at 400° C in a 3-foot serpentine tube with 7-mm inside diameter, to remove oxygen and water vapor. The cadmium used to grow crystals was a very sensitive detector for oxygen in the gas stream; easily detectable CdO residues were formed with only small traces of oxygen present. Under operating conditions, no CdO was detectable. To prepare pure CdSe crystals, special halogen-free selenium from American Smelting and Refining Co. was used. Spectrographic analysis revealed the same concentration of impurities in the final CdS crystals as in the initial raw materials; i.e., when Consolidated cadmium was used, the crystals showed no spectrographically detectable copper.

Measurements were made in an atmosphere of dry helium, between temperatures of liquid nitrogen and about 100° C with ohmic indium contacts<sup>13</sup> melted onto the crystals. Monochromatic radiation was from a Bausch and Lomb grating monochromator, used with a resolution of 100Å; white light radiation was from an incandescent lamp. Variations in light intensity were achieved with neutral wire-mesh filters

<sup>‡</sup> Product of Baker and Co.

<sup>13</sup> R. W. Smith, "Properties of Ohmic Contacts to Cadmium Sulfide Single Crystals," *Phys. Rev.*, Vol. 97, p. 1525, March, 1955.

which allowed an accurate control of light intensity over seven orders of magnitude. Luminescence emission spectra were measured with a grating spectroradiometer designed and constructed by R. E. Shrader of these Laboratories.

## RESULTS

### Pure CdS

Pure crystals of CdS usually had a dark resistivity of at least  $10^{12}$  ohm cm and a specific photosensitivity of between  $10^{-5}$  and  $10^{-6}$  mho  $\text{cm}^2/\text{watt}$ . Although this photosensitivity is very low, it is by no means the lowest that can be found in CdS. Crystals<sup>14</sup> of CdS with about 100 parts per million incorporated Ni have a specific sensitivity

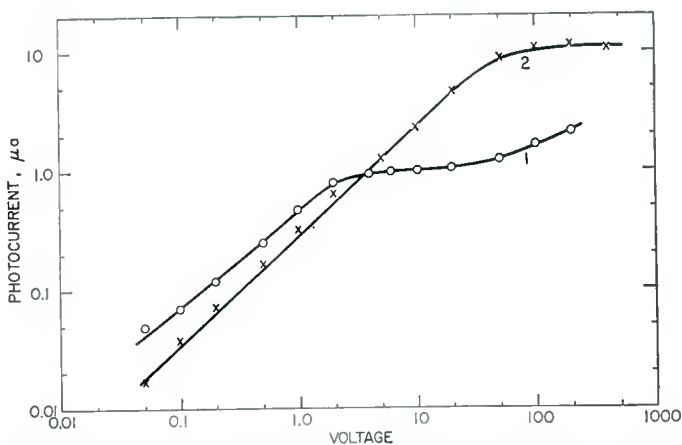


Fig. 1.—Saturation of photocurrent with applied voltage for pure CdS crystals. Curve 1 is for a crystal with 1 mm electrode spacing; curve 2 for a crystal with 7.5 mm electrode spacing.

of about  $10^{-9}$  mho  $\text{cm}^2/\text{watt}$ . (In the pure CdS, the electron lifetime is about 1 microsecond, while in the CdS:Ni it has been reduced to  $10^{-4}$  microsecond. In spite of its effective action as a recombination center, nickel extends the spectral response of CdS, adding a new band at 5400 Å.)

One of the striking characteristics of most of the pure crystals prepared was the presence of saturation of photocurrent with applied voltage. Figure 1 shows two typical examples of pure CdS with ohmic behavior at low voltages, but saturation at high voltages. Curve 1 is for a crystal with an electrode spacing of about 1 mm, whereas curve 2 is for a crystal with an electrode spacing of 7.5 mm. No dependence

<sup>14</sup> Prepared by H. A. Weakliem.

of speed of response on applied voltage was observed in the saturation range. The mechanism for the saturation is not yet understood in detail, but there is the possibility of field extraction of photoexcited holes in these pure crystals.

Pure CdS crystals were also obtained in whisker form, 10 to 20 microns in diameter. The excitation spectrum and the infrared quenching spectrum for such a crystal are shown in Figure 2. The spectral response of these crystals, like most insensitive pure crystals, had a

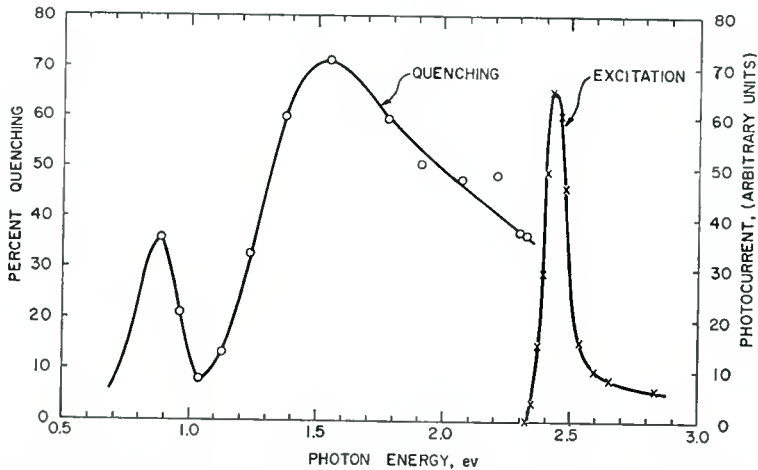


Fig. 2—Excitation and infrared quenching spectrum for a whisker of pure CdS.

sharp cutoff for wavelengths longer than that of the edge, decreasing by three orders of magnitude within 250 Å of the absorption edge. Infrared quenching was measurable to within 0.1 eV of the absorption edge, unlike previously reported data on infrared quenching in CdS which seldom extended to higher energies than about 1.8 eV.<sup>15</sup> The previous data suggested two possible explanations: (1) the infrared quenching spectrum actually was bell-shaped and no quenching occurred above 1.8 eV, thus suggesting a discrete-level to discrete-level transition, or (2) quenching actually continued above 1.8 eV (corresponding to transitions from within the valence band to a level lying about 1.0 eV above the top of the valence band as given by the low-energy cutoff), but excitation in the high-energy range became so strong that it overwhelmed the quenching effect. The second explana-

<sup>15</sup> R. H. Bube, "Infrared Quenching and a Unified Description of Photoconductivity Phenomena in Cadmium Sulfide and Selenide," *Phys. Rev.*, Vol. 99, p. 1105, August, 1955.

tion had been favored previously, and the present data confirm this choice.

A number of batches of pure CdS were grown, and a few sensitive crystals were occasionally found among them. Similar experiences had been reported previously.<sup>16</sup> The sensitive crystals probably result

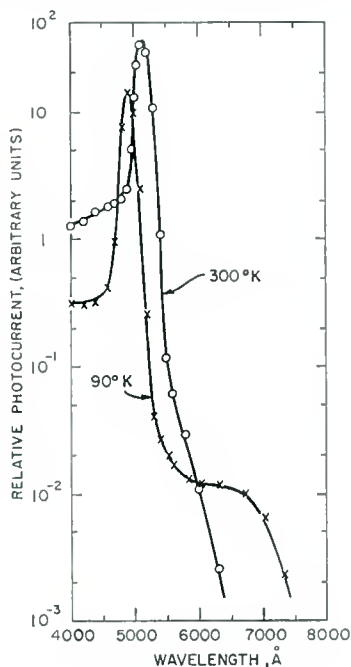


Fig. 3—Spectral response of photoconductivity for a photosensitive pure CdS crystal.

from local conditions in the growth zone favoring that departure from stoichiometry sufficient to provide photosensitivity. To produce such crystals reproducibly and with appreciable yield requires a much more detailed control of conditions in the growth zone than has been attempted to date. The properties of the sensitive crystals found in this way were of interest, however, in that most of them showed improved performance over standard crystals. Table I lists data on 5 such crystals obtained in 3 different batches. One of these crystals showed a performance improvement factor of several hundred; another showed an  $M$  value of 24. Figure 3 shows the spectral response of crystal 507A; the cutoff past the edge is very sharp, but there is evidence,

<sup>16</sup> R. H. Bube, "Comparison of Surface-Excited and Volume-Excited Photoconduction in Cadmium Sulfide Crystals," *Phys. Rev.*, Vol. 101, p. 1668, March, 1956.

Table I—Comparison of Performance Data on Improved Crystals with Data on Standard Crystals

Standard	Specific Sensitivity (S) mho cm <sup>2</sup> /watt	Light Intensity $L'$ Required for $\tau \leq 0.1$ sec, in ft-c Rise                      Decay	
CdS:Cl:Cu	$8 \times 10^{-2}$	0.4	0.1
CdSe:I:Cu	$2 \times 10^{-1}$	0.09	0.006

Crystal	Spec. Sens.	Improvement Factor* (at Equal Sensitivity) Rise                      Decay		M
CdS 409A	$7 \times 10^{-3}$	1	20	24
CdS 409B	$6 \times 10^{-1}$	360	500	5
CdS 430	$4 \times 10^{-1}$	25	25	1
CdS 507A	$8 \times 10^{-2}$	3	2	0.5
CdS 507B	$2 \times 10^{-2}$	3	8	3
CdS:I 1001A	$2 \times 10^{-2}$	10	6	
CdS:I 1001B	$7 \times 10^{-2}$	40	80	9
CdS:I 1009	$5 \times 10^{-3}$	25	20	
CdS:I 1010	$3 \times 10^{-1}$	160	200	3
CdS:I 1001C	$8 \times 10^{-2}$	10	25	3
CdS:I 1209A	$7 \times 10^{-2}$		65	540
CdS:I 1209B	$10^{-2}$		3	266
CdS:I 1216A	$4 \times 10^{-3}$		3	10
CdS:I 1216B	$2 \times 10^{-3}$			39
CdS:I 1216C	$2 \times 10^{-1}$		12	15
CdS:I 1216D	$2 \times 10^{-1}$		20	27
CdS:I 1222	$5 \times 10^{-3}$		3	3
CdS:I 224	$9 \times 10^{-2}$	2	4	16
CdS:I 326A	$4 \times 10^{-2}$	1000	250	24
CdS:I 326B	$5 \times 10^{-2}$	5	7	2
CdS:I 328A	$3 \times 10^{-3}$		1	14
CdS:I 328B	$2 \times 10^{-3}$		2	4
CdS:I 527	$10^{-1}$	4	6	2
CdS:I 605	1.6	200	200	92
CdS:I 611	$2 \times 10^{-2}$	2	62	16
CdSe (at 90°K)	1	30	30	2

$$* \text{Improvement Factor} = \frac{L'_{\text{standard}}}{L'_{\text{crystal}}} \times \frac{S_{\text{crystal}}}{S_{\text{standard}}}$$

particularly at low temperature, of imperfection response extending out to at least 7500 Å. A long-wavelength cutoff of response at 8000 Å corresponds to excitation to the conduction band from a level lying about 1 ev above the top of the valence band. Some caution must be exercised in associating the cutoff with the imperfection ionization energy because of the overlapping of excitation and quenching by the same wavelengths in this range.

Two aspects of the spectral response are worth keeping in mind in comparing the various crystals described in this paper: (1) the ratio between the flat imperfection response at low temperatures and the maximum response, here of the order of  $10^{-3}$  or  $10^{-4}$  in pure crystals; and (2) the relative difference between the shape of the response at long wavelengths between room temperature and liquid nitrogen temperature. The larger the ratio mentioned under (1) above, the greater the difference in long-wavelength shape of the response with temperature. Infrared quenching may also be involved in this difference in shape, evidence concerning which is presented later.

The thermally stimulated current curve for crystal 507A is given in Figure 4a. A total trap density of  $6 \times 10^{14}$  cm $^{-3}$  is estimated from the area under the curve and an independent measurement of photoconductivity gain at the same current levels. A summary of the different trap levels found throughout this investigation is given in Table II. There are 5 levels which occur most often, and 2 other levels which occur occasionally. The trap depths are estimated by a calculation of the location of the Fermi level from the temperature and conductivity of the thermally stimulated current maximum;

$$E_{fn} = kT \ln \left[ \frac{N_c e \mu}{\sigma} \right] \quad (16)$$

where  $N_c$  is the density of states in the conduction band,  $\mu$  is the electron mobility, taken as 100 cm $^2$ /volt/second, and  $\sigma$  is the conductivity.

For comparison, Table II also contains the thermally stimulated current peaks, calculated trap depths, and tentative identification given by Woods<sup>17</sup> from his work with CdS crystals. Two of the predominant levels found in this work are not mentioned by Woods, and two of Woods' levels are those found only occasionally in the present

<sup>17</sup> J. Woods, "Photochemical Effects and the Effect of Oxygen on Photoconducting Cadmium Sulphide Crystals," *Journal of Electronics and Control*, Vol. V, p. 417, November, 1958.

investigation; otherwise, agreement is reasonably good. Also included in Table II are trap depths reported as characteristic of CdS in a previous publication.<sup>15</sup> The agreement, especially for the five shallower traps, is quite good. The purpose of this summary is to show that there are five to seven different trap levels reasonably characteristic of defects in CdS crystals.

Inspection of Figure 4 shows that the 80° C peak does not occur in any of these faster crystals (the CdS:I crystals are discussed in the next section). Although there is thermally stimulated current at room temperature, it is small in all the crystals of Figure 4, and the

Table II—Summary of Major Trap Depths in CdS Crystals

Present Investigation T, °C	E, ev	Bube (1955) E, ev	T, °C	Woods (1958) E, ev	Defect
-170	0.20	0.21			
-135	0.25	0.30	-150	0.24	V <sub>s</sub> <sup>-2</sup>
(-90)	(0.41)	0.38	-100	0.32	V <sub>Ca</sub>
(-50)	(0.44)	0.42	- 50	0.38	
0	0.51	0.52	0	0.50	V <sub>s</sub> <sup>-</sup>
35	0.58	0.70			
80	0.63	0.77	50	0.59	V <sub>Ca</sub> · V <sub>s</sub>

improvement in room-temperature speed goes up as the current at room temperature decreases. It appears that the 80° C peak is much more influential in determining the room temperature speed than the 35° C peak; a simple calculation shows why. The time that an electron is trapped at temperature  $T$  is given by

$$\tau_t = \frac{\exp [E_t/kT]}{\nu} = \frac{\exp [E_t/kT]}{N_c S v} \quad (17)$$

where  $E_t$  is the trap depth,  $\nu$  is the attempt-to-escape frequency,  $S$  is the capture cross section of the trap for electrons, and  $v$  is the thermal electron velocity. Solving for the trap depth gives

$$E_t = kT \ln (N_c S v \tau_t). \quad (18)$$

At room temperature, for  $S = 10^{-15}$  cm<sup>2</sup>,

$$E_t = \frac{1}{40} \ln (10^{11} \tau_t). \quad (18a)$$

For  $E_t = 0.57$  ev,  $\tau_t = 0.1$  second; for  $E_t = 0.63$  ev,  $\tau_t = 1$  second. Thus, the  $35^\circ$  C traps decay in about the 0.1 second which has been taken as a standard for comparison, but the deeper  $80^\circ$  C traps require about a second to decay.

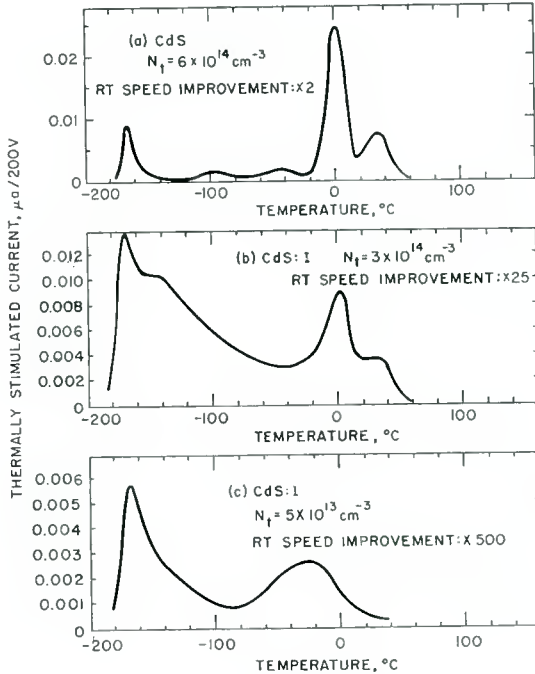


Fig. 4—Thermally stimulated current curves for (a) pure CdS crystal 507A, and for CdS with a trace of iodine, crystals (b) 1001A, and (c) 326A. Room temperature speed improvement increases markedly as the magnitude of the thermally stimulated current above room temperature decreases.

#### *CdS Crystals with a Trace of Iodine*

In view of the difficulties involved in reproducing fast sensitive crystals by deviations from stoichiometry in the preparation, an attempt was made to introduce only a trace of iodine impurity in the preparation. The nitrogen carrier gas was passed over iodine at a reduced temperature to give a vapor pressure in the range of  $10^{-4}$  to  $10^{-2}$  mm Hg. Table I shows improved performance obtained with 20 crystals from 12 different batches. Again, reproducibility remained

a problem, although not quite as severe as with the pure crystals. Occasional remarkable crystals like 326A which was 500 times faster on decay and 2000 times faster on rise than standard CdS crystals, while possessing half the sensitivity, indicate the potentialities involved; compared to standard CdSe crystals, this crystal showed an improvement factor of 45 on rise and 3 on decay.

The thermally stimulated current curves for crystals 1001A and 326A are shown in Figures 4b and 4c, respectively. The total trap densities for these two crystals were, respectively,  $3 \times 10^{14} \text{ cm}^{-3}$  and  $5 \times 10^{13} \text{ cm}^{-3}$ . The trap density relevant to room temperature operation in crystal 326A is certainly down in the  $10^{11} \text{ cm}^{-3}$  range.

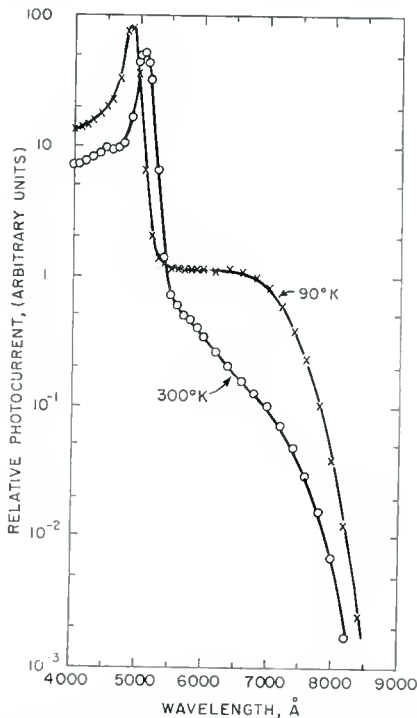


Fig. 5—Spectral response of photoconductivity for a photosensitive CdS crystal with a trace of iodine, crystal 1001A.

The spectral response of a typical crystal of this group, crystal 1001A, is given in Figure 5. In these crystals the long-wavelength cutoff still occurs at about 8000 Å, the imperfection response at low temperature is much more prominent than at room temperature, and the ratio of response at the imperfection plateau to that at the maximum is about  $10^{-2}$  instead of  $10^{-3}$  to  $10^{-4}$  found for pure crystals.

Outstanding among the  $M$  values quoted in Table I are those for crystals 1209A and 1209B. These crystals were whiskers about 25 microns in diameter. Two possible explanations for the high  $M$  values may be offered. First, because of the geometry, it was possible to approach closely the condition of Equation (12) at a sufficiently low field so that the possibility of breakdown was minimized. On this basis it would be expected that many of the other  $M$  values listed in Table I on plate-like crystals could also be increased by measuring at higher applied field as long as breakdown was avoided. Second, because of the geometry, a higher density of surface traps not involved

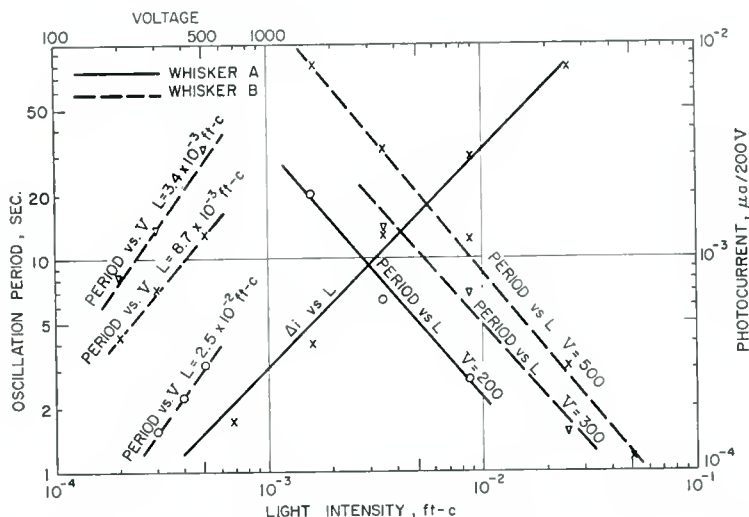


Fig. 6—Characteristics of oscillating photocurrents for whisker crystals 1209A and 1209B.

in the passage of photocurrent served to increase the  $M$  factor, as discussed in a previous section.

These whisker crystals also showed the phenomenon of oscillatory photocurrent in the presence of steady light and d-c field, previously reported both for CdS under special conditions<sup>18,19</sup> and for ZnSe.<sup>20</sup> The general behavior of the oscillatory photocurrents was very similar to that described for ZnSe. A few of the parameters are summarized

<sup>18</sup> S. H. Liebson, "Infrared Quenching of Cadmium Sulfide," *Jour. Electrochem. Soc.*, Vol. 102, p. 529, September, 1955.

<sup>19</sup> E. E. Loebner, private communication.

<sup>20</sup> R. H. Bube and E. L. Lind, "Photoconductivity in Zinc Selenide Crystals and a Correlation of Donor and Acceptor Levels in II-VI Photoconductors," *Phys. Rev.*, Vol. 110, p. 1040, June, 1958.

in Figure 6. A clue to the cause of oscillatory photocurrents in the ZnSe crystals seemed to be that oscillations occurred in a range where the photocurrent had saturated with applied field; no such saturation phenomenon was observed with these whiskers. The photocurrent varies approximately linearly with light intensity and voltage, and the period of the oscillations varies linearly with applied field and inversely as light intensity. The photocurrent values given in Figure 6 are an average of the fairly small amplitude oscillations ( $\pm 10$  per cent). The phenomenon is still too rare and unstable for a suitable explanation to be suggested. As in ZnSe, the oscillation seems to result from an abrupt cutting off of the normal current, followed by a slower build-up back to that current. If one considers the possibility of the accumulation of a space-charge up to a magnitude sufficient to cause a sudden decrease in current, after which the space-charge relaxes, it is possible to see why (1) low light intensities, giving low currents, produce longer oscillation periods because of the longer time needed to build up the space charge, and (2) higher applied fields, requiring the accumulation of more space charge to overcome them, also produce longer oscillation periods.

#### *CdS Crystals with Higher Concentrations of Iodine*

CdS crystals were also grown with higher concentrations of iodine corresponding to iodine vapor pressures between 1 and 15 mm Hg. Table III summarizes the major properties of such crystals. It appears that for very high iodine concentrations, the main effect of the iodine is to form cation vacancies; the imperfection absorption continues to increase but the free-carrier concentration reaches a maximum value.

Crystals without iodine present during the preparation showed no room temperature luminescence excited by 3650 Å ultraviolet. However, those crystals which were prepared with 1 to 5 mm Hg of iodine pressure did show a green emission at room temperature under ultraviolet excitation.\* The spectral distribution of this emission is shown in Figure 7a; it consists of two bands, one peaked within 30 Å of the room temperature absorption edge, and the other peaked about 170 Å toward longer wavelengths than the edge. The two peaks are separated by about 0.1 ev.

At liquid nitrogen temperature, all CdS crystals investigated showed green emission, but there was a significant difference in the spectrum depending on whether iodine had been incorporated. The spectra of three crystals are given in Figure 7b. The bright green

---

\* A similar emission has also been observed in CdS crystals grown with a trace of indium present.

emission involved here is that which has been frequently reported in the past;<sup>21</sup> it consists of a number of fairly narrow emission bands, the maximum of the shortest-wavelength band lying 250 Å beyond the absorption edge. This emission is temperature quenched at temperatures only slightly above that of liquid nitrogen; sometimes there

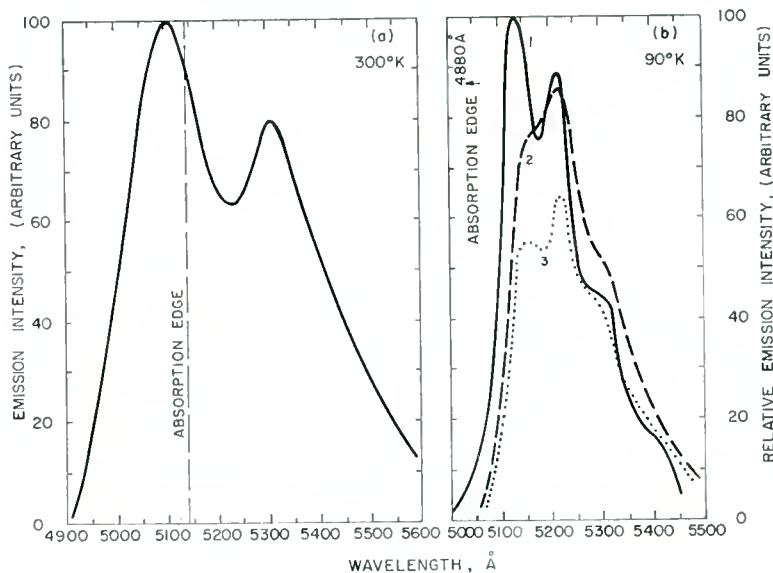


Fig. 7—(a) Room temperature emission from a CdS:I crystal excited by 3650 Å ultraviolet. (b) Liquid nitrogen emission from (1) a pure CdS crystal (2) a CdS:I crystal luminescing green at room temperature, and (3) a CdS:I crystal luminescing red at room temperature. Excited by 3650 Å ultraviolet.

is an intermediate orange or red emission before complete temperature quenching, even in pure crystals. Curve 1 in Figure 7b is for a pure crystal and has the shape of the normally reported spectrum. Curve 2 is for a crystal of CdS:I which luminesces green under ultraviolet at room temperature, and curve 3 is for a CdS:I crystal which luminesces red under ultraviolet at room temperature. The relative amplitudes of the several bands are strongly affected by the presence of the iodine.

High-conductivity CdS:I crystals are by no means insensitive. In terms of absolute conductivity change per unit light intensity, they are highly sensitive, with a typical value of  $S$  of about 50 mho  $\text{cm}^2/\text{watt}$ . The photocurrent varies very slowly with light intensity

<sup>21</sup> C. C. Klick, "Luminescence and Photoconductivity in Cadmium Sulfide at the Absorption Edge," *Phys. Rev.*, Vol. 89, p. 274, January, 1953.

in such crystals; variation of photocurrent with the 0.18 power of light intensity was observed over four orders of light intensity, down to a photocurrent equal to the dark current.

Table III—Properties of CdS:I Crystals

Vapor Pressure of Iodine During Preparation, mm Hg	$\mu$ , cm <sup>2</sup> /v sec	$\sigma$ , mho/cm	$n$ , cm <sup>-3</sup>
1	150	0.7	$3 \times 10^{16}$
5	160	30	$10^{18}$
15	250	24	$3 \times 10^{17}$

Vapor Pressure of Iodine During Preparation, mm Hg	Body Color	Room Temperature Ultraviolet-excited Luminescence
1	Yellow	Pale Green
5	Light Orange	Green or Pale Red
15	Darker Orange	Bright Red

#### *CdS:I Crystals Annealed under Sulfur Pressure*

Since high-conductivity crystals of CdS:I have a high photosensitivity, one reasonable way of making sensitive crystals with a low conductivity, without causing any major disturbance in the crystal, is to anneal under sulfur pressure. Such a process should continue to form cadmium vacancies, useful for sensitivity, and should eliminate sulfur vacancies, possibly harmful as trapping centers.

A typical annealing series, shown in Figure 8, demonstrates the times required to obtain equilibrium. The photocurrent for 900 foot-candle incandescent excitation and the dark current are plotted as a function of annealing time, for annealing at 800° C under a sulfur pressure of 2 atmospheres. The photocurrent appears to reach a stable value in about 24 hours, whereas the dark current requires a somewhat longer time.

The spectral response of a crystal annealed for 72 hours at 800° C under 2 atmospheres of sulfur pressure is given in Figure 9. The long-wavelength cutoff is still at 8000 Å, its abruptness at low-temperature being associated with infrared quenching. The ratio between the imperfection response plateau and the maximum is up to  $10^{-1}$ , and the difference between the room temperature and low temperature curves is much less than for the pure CdS or the CdS with a trace of iodine.

Sulfur-annealing of CdS crystals has a history of unusual effects, to which the present investigation also contributes. It has been reported<sup>22</sup> that crystals of CdS:I annealed at 900° C under 2 atmospheres of sulfur pressure for 4 hours showed reversible variations of sensitivity. The crystals exhibited two photosensitivity "states": (1) in state A, room-temperature sensitivity was high, and temperature

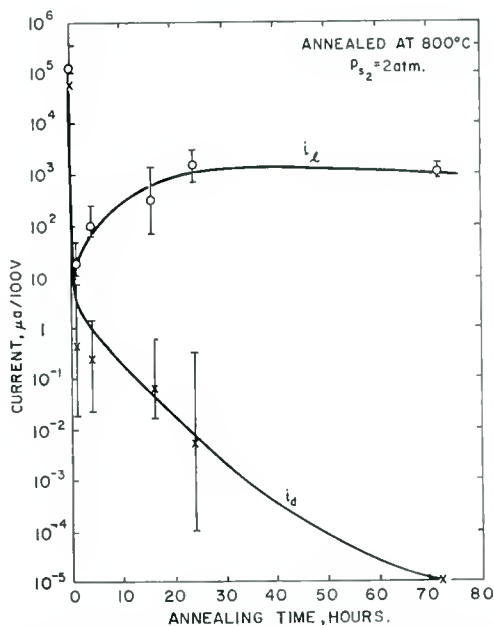


Fig. 8—Photocurrent (900 foot-candles incandescent illumination) and dark current as a function of annealing time, for high-conductivity CdS:I crystals annealed at 800° C under 2 atmospheres of sulfur pressure.

quenching was associated with thermal freeing of holes from the normal sensitizing centers lying 1 ev above the top of the valence band; (2) in state B, room-temperature sensitivity was several orders of magnitude lower, and temperature quenching was associated with thermal freeing of holes from levels about 0.2 ev above the top of the valence band. Transformation between the two states was completely reversible, a crystal in state B being transformed to state A by heating to about 250° C, and a crystal in state A being spontaneously transformed to state B by photoexcitation at room temperature. It was

<sup>22</sup> R. H. Bube, "Reversible Variations of Sensitivity in Certain Cadmium Sulfide and Selenide Photoconductors," *Jour. Chem. Phys.*, Vol. 30, p. 266, January, 1959.

postulated that a high density of defects was present, and that state A corresponded to the dispersed state of these defects, while state B corresponded to an agglomerated state. Subsequent investigation<sup>23</sup> of the dependence of hole ionization energy (from sensitizing centers) on imperfection concentration in CdS:Ga:Cu photoconducting powders

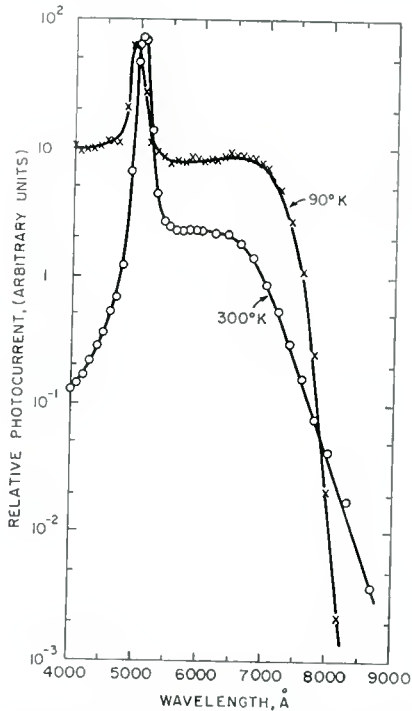


Fig. 9—Spectral response of a CdS:I crystal annealed 72 hours at 800° C under 2 atmospheres sulfur pressure.

showed that the hole ionization decreased from 1 ev to 0.3 ev upon going from low copper concentrations to copper concentrations of  $2 \times 10^{20} \text{ cm}^{-3}$  (always maintaining a constant Cu/Ga ratio). Thus, independent evidence is provided to support the contention that interacting sensitizing centers result in a decrease in the effective hole ionization energy. The present results provide a number of examples of the same type of phenomenon.

If the photocurrent of the crystal of Figure 9 is measured as a function of light intensity, it is found that the sensitivity is very

<sup>23</sup> R. H. Bube and A. B. Dreeben, "Dependence of the Hole Ionization Energy of Imperfections in Cadmium Sulfide on the Impurity Concentration," *Phys. Rev.*, September, 1959.

small at low intensities, the photocurrent varying as the 2.6 power of the intensity. Even at liquid nitrogen temperature, the photocurrent at low light intensities varies as the 1.9 power of the intensity. The photocurrent-versus-temperature curves of Figure 10 reveal this complex behavior. At high light intensities, the shape of the photocurrent-versus-temperature curve is the same as that of a crystal in state A described above, but at low light intensities, the curve shape is that

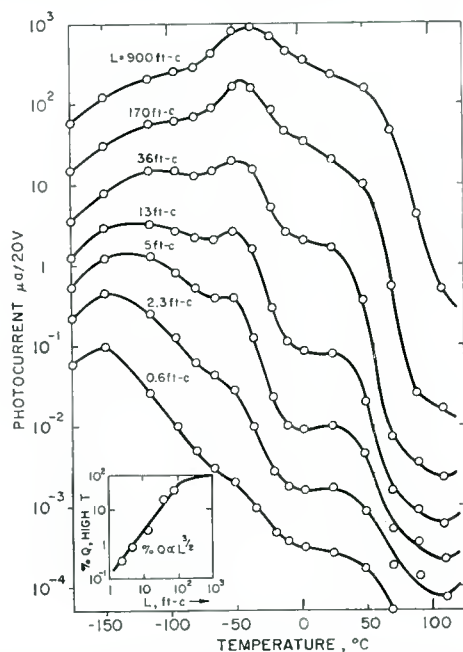


Fig. 10—Photocurrent versus temperature for the crystal of Figure 9, as a function of incandescent light intensity. The inset shows the proportion of thermal quenching associated with the high-temperature quenching process.

of state B. Stated in another way, the proportion of the sensitivity dependent on holes trapped in levels 0.2 ev above the top of the valence band increases as the light intensity decreases. The inset in the lower left hand corner of Figure 10 shows the per cent of the total quenching which is associated with freeing of holes from the levels 1 ev above the valence band. Thus, in the same crystal there is evidence of both non-interacting sensitizing centers and interacting sensitizing centers. It is proposed that the 0.2 ev levels are associated primarily with the surface, and the 1.0 ev levels primarily with the volume. The following additional evidence on another crystal helps confirm this point of view.

Figure 11 shows the spectral response curve of a crystal of CdS:I annealed at  $800^{\circ}\text{C}$  for 21 hours under 1 atmosphere of sulfur pressure. The cutoff is again at  $8000\text{ \AA}$ , but the ratio between the imperfection response plateau and the maximum is greater than  $10^{-1}$ , and there are only minor differences between the room-temperature and low-temperature curves. The temperature dependence of photocurrent for this crystal was measured (1) with light through a Corning 5113 filter peaking at  $4100\text{ \AA}$ , providing surface excitation, and (2) with light

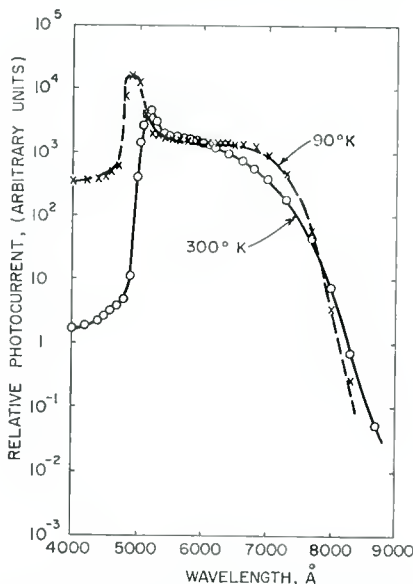


Fig. 11—Spectral response of a CdS:I crystal annealed 21 hours at  $800^{\circ}\text{C}$  under 1 atmosphere sulfur pressure.

through a Corning 2418 filter, passing all wavelengths beyond  $5900\text{ \AA}$ , providing volume excitation. The results are shown in Figure 12. The surface photoconductivity quenches at a low temperature, corresponding to a hole ionization energy of about 0.2 eV, whereas the volume photoconductivity does not quench until high enough temperatures are reached to free holes from levels 1 eV above the top of the valence band. As in previously reported cases of similar effects,<sup>22</sup> some distribution of levels above 0.2 eV also appear to be involved in low-temperature quenching, since the quenching is much more gradual than for the normal hole ionization from 1 eV levels. To explain the results of Figure 10, we must assume that surface excitation dominates at low light intensities, but that volume excitation becomes important at higher light intensities. Another example of the difference between

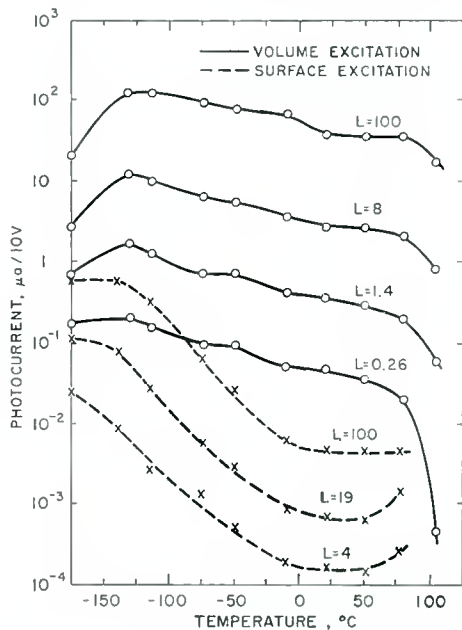


Fig. 12—Photocurrent as a function of temperature, for volume excitation and surface excitation, for different relative light intensities, for the crystal of Figure 11.

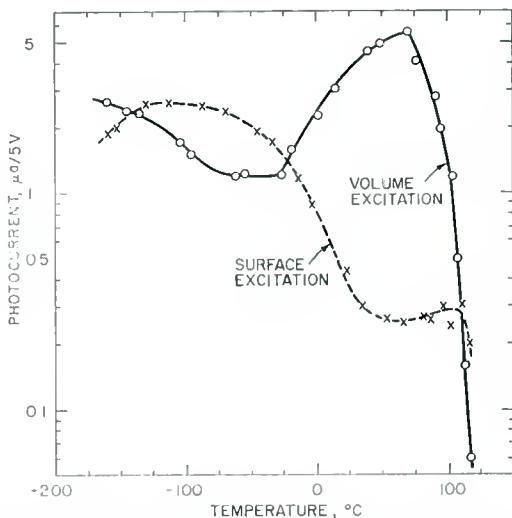


Fig. 13—Photocurrent as a function of temperature, for volume excitation and surface excitation, for a crystal of CdS:I annealed 72 hours at 800 $^{\circ}$  C under 1 atmosphere sulfur pressure.

surface and volume excitation is given in Figure 13 for a crystal of CdS:I annealed at 800° C for 72 hours under 1 atmosphere of sulfur pressure. Here the surface excitation undergoes two clearly observed quenching steps, one corresponding to a hole ionization energy of about 0.6 ev and the other corresponding to the normal ionization energy of about 1 ev.

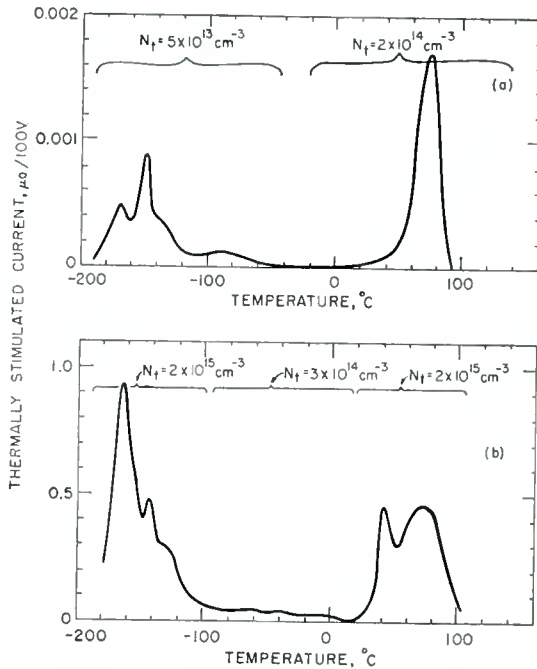


Fig. 14—Thermally stimulated current curves for (a) the crystal of Figure 13, and (b) a crystal of CdS:I annealed 21 hours at 800° C under 2 atmospheres of sulfur pressure.

Not all of the annealed CdS:I crystals were as insensitive at low light intensities as the crystal of Figure 9. Those that were more sensitive, however, showed very slow response at low light intensities. The thermally stimulated current curves given in Figure 14 for two typical crystals show the reason for this slow response. The 80° C deep-trap peak is very prominent in both crystals. The 0° C peak, so important in the curves of Figure 4, is almost completely absent, supporting the association of this peak with sulfur vacancies. The occurrence of the 80° C peak under conditions in which cadmium vacancies are likely to be formed also supports the contention that cadmium vacancies are involved in the 80° C peak. The occurrence

of the same triplet band at low temperatures in both crystals suggests that the  $-170^{\circ}\text{C}$  and  $-135^{\circ}\text{C}$  peaks usually found in this investigation, and the  $-150^{\circ}\text{C}$  peak reported by Woods, are all present and correspond to three distinctly different levels.

*Pure CdS Sublimed in Flowing Nitrogen*

Another method of making photosensitive pure CdS crystals is to take insulating insensitive crystals and to sublime them with subsequent recrystallization, taking advantage of the deviations from

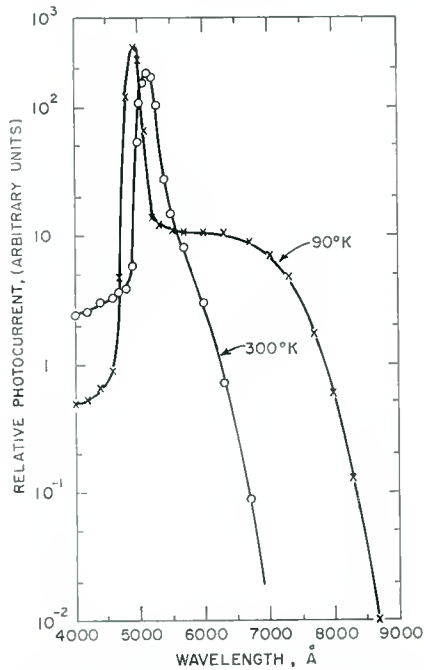


Fig. 15—Spectral response of recrystallized CdS grown from sublimed pure CdS at  $900^{\circ}\text{C}$  in flowing nitrogen.

stoichiometry occurring during this process to produce the desired sensitivity. Crystals of pure CdS were sublimed at about  $1100^{\circ}\text{C}$  and then recrystallized at about  $900^{\circ}\text{C}$ . The reproducibility and yield of this procedure were very good, almost every crystal obtained showing high sensitivity.

The spectral response of such a crystal is shown in Figure 15. Its characteristics are intermediate between those of the pure crystals of Figure 3 and the crystals with a trace of iodine of Figure 5. The difference between the room-temperature and the low-temperature curve is particularly marked, but can be at least partially explained in

terms of a difference in the infrared quenching spectra, as suggested previously. Figure 16 shows the quenching spectra for room temperature and liquid nitrogen temperature. The spectrum is appreciably sharpened at low temperatures, the onset of detectable quenching shifting from 1.8 to 1.6 ev on the high temperature side in rough agreement with the curves of Figure 15. The low-energy cutoff of the main band shifts from 1.09 ev to 1.29 ev between room temperature

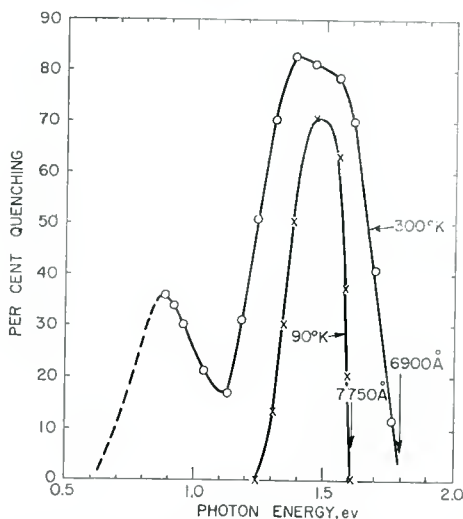


Fig. 16—Infrared quenching spectrum at 90 and 300° K for a crystal like that of Figure 15.

and liquid nitrogen temperature. Since the shift of the band gap over this temperature range is only 0.12 ev, the results imply either a simple temperature broadening phenomenon, or that the level of the sensitizing centers shifts appreciably with respect to the top of the valence band.

Every sensitive CdS crystal grown by recrystallization from sublimed pure CdS in flowing nitrogen showed a low speed of response at room temperature at low light intensities. The reason for this is illustrated in the thermally stimulated current curves of two typical crystals, given in Figure 17. The over-all trap density is high, in the range of  $10^{15}$  to  $10^{16}$   $\text{cm}^{-3}$ , and the 80° C peak is prominent in both curves. Unlike the curves obtained for crystals of CdS:I annealed under sulfur pressure (Figure 14), the curves of Figure 17 show appreciable peaks also at 0° C, tentatively associated with sulfur vacancies.

*Pure CdS Sublimed under Sulfur or Cadmium Pressure*

Pure CdS crystals were also sublimed in a sealed tube to recrystallize in a cooler portion of the tube. Two experiments were carried out: (1) pure CdS at 1025° C was sublimed and recrystallized at 990° C under 1 atmosphere of sulfur pressure for 137 hours; and (2) pure CdS at 1150° C was sublimed and recrystallized at 1100° C under 1 atmosphere of cadmium pressure for 36 hours. The results of both

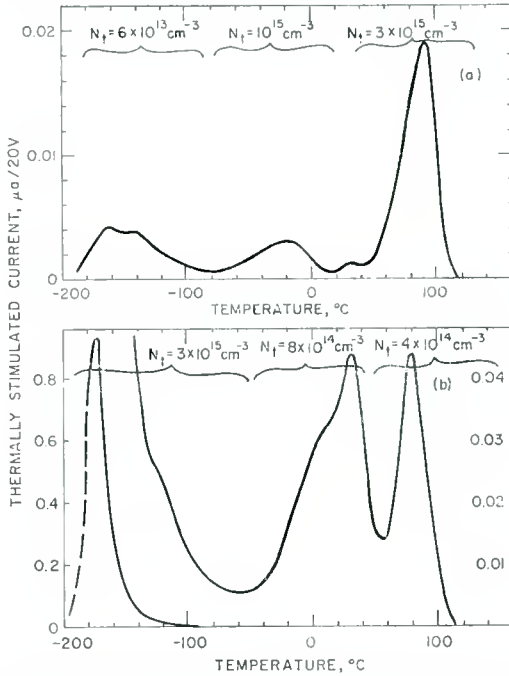


Fig. 17—Thermally stimulated current curves for CdS crystals recrystallized from sublimed pure CdS. Curve (a) is for the same crystal as Figure 15.

experiments were the same: crystals were obtained with initial high sensitivity which showed exactly the same reversible variations of sensitivity which have been previously described.<sup>22</sup> Figure 18 shows typical curves of decay of photosensitivity with time under excitation in the transformation from state A to state B. With the crystal in the dark between measurements of sensitivity, decay is negligible, but under 900 foot-candle illumination, photosensitivity decays three orders of magnitude in about 5 minutes. Curve 1 of Figure 18 is for a crystal sublimed under sulfur pressure, and curve 2 is for a crystal sublimed under cadmium pressure. Further indication of the similarity to previous results is given by the photocurrent-versus-temperature

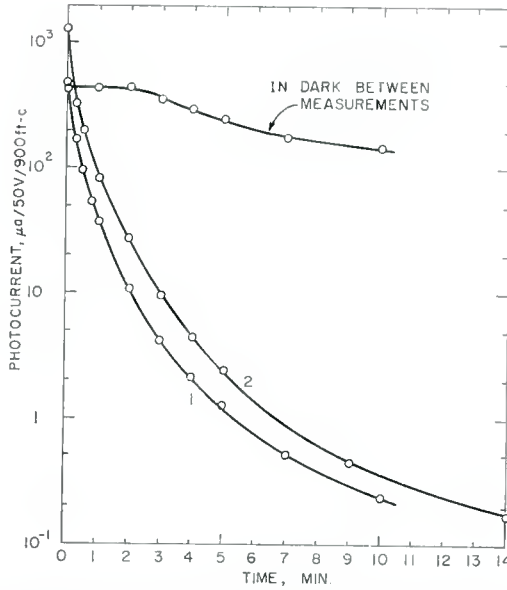


Fig. 18—Photocurrent as a function of time for crystals of CdS grown by sublimation of pure CdS, either under sulfur pressure (Curve 1) or cadmium pressure (Curve 2), under constant illumination by 900 foot-candles incandescent radiation, and in the dark except for measurements.

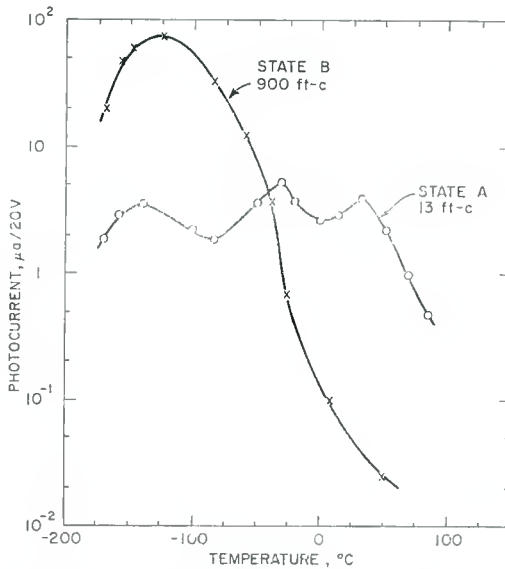


Fig. 19—Photocurrent as a function of temperature for the crystal of Curve 1 in Figure 18, both in state A and in state B.

curves of Figure 19 for the crystal sublimed under sulfur pressure. In state A, appreciable temperature quenching does not occur until above room temperature, whereas in state B, temperature quenching starts at  $-100^{\circ}\text{C}$ .

### *CdSe Crystals*

A few experiments were also performed to obtain photosensitive pure CdSe crystals directly from vapor phase growth. The spectral response of such a crystal is given in Figure 20. The low-temperature

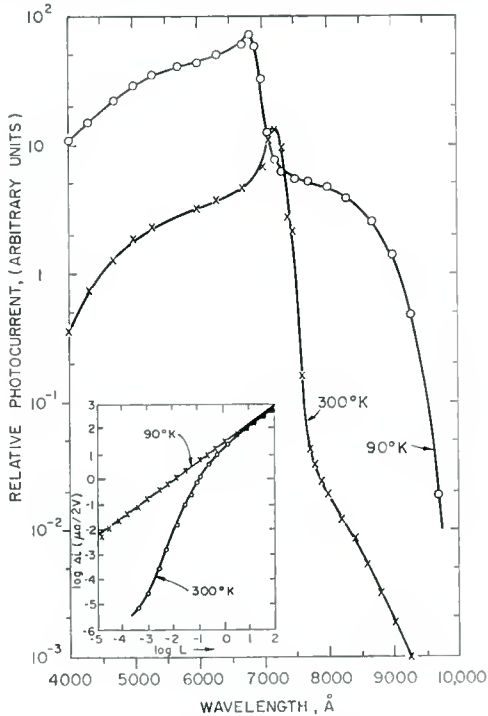


Fig. 20—Spectral response of a photosensitive pure CdSe crystal. Inset shows the variation of photocurrent with light intensity at room temperature and at liquid nitrogen temperature.

cutoff occurs at about  $10,000\text{ \AA}$ , corresponding to excitation to the conduction band from a level lying about  $0.6\text{ eV}$  above the top of the valence band. The inset shows the variation of photocurrent with light intensity at liquid nitrogen temperature and room temperature. At room temperature the sensitivity is very low for low light intensities, whereas at liquid nitrogen temperature the sensitivity is many orders of magnitude higher for these same intensities. The speed of response was measured at liquid nitrogen temperature, and the data is given

in Table I, the improvement factor being calculated relative to the room temperature data of the standard crystal. The speed of response of a standard CdSe crystal is almost always much less at liquid nitrogen temperature; therefore, the actual improvement factor should probably be still larger for operation at that temperature. The results indicate that increases in performance of CdSe can also be obtained by purification techniques.

## DISCUSSION AND SUMMARY

### *Preparation of Sensitive Crystals*

Photosensitive CdS crystals have been prepared in a number of ways without the use of impurity acceptors. (1) Advantage has been taken of random deviations from stoichiometry in the growth of pure crystals of CdS from the vapor phase. (2) Traces of iodine have been introduced into the vapor phase growth reaction, sufficient to increase sensitivity without appreciably increasing dark conductivity. (3) High-conductivity crystals of CdS:I have been annealed under sulfur pressure, to reduce dark conductivity but leave high photosensitivity. (4) Pure CdS crystals have been sublimed in flowing nitrogen and recrystallized, deviations from stoichiometry in this process giving rise to the photosensitivity.

### *Increases in Speed of Response*

Table I lists 25 crystals from 15 different preparations of pure CdS or CdS with a trace of iodine incorporated, which show increased low-light speed of response over standard CdS crystals. This increase in speed has been accomplished by purification of the ingredients used in the preparation, and by use of a preparation method which interferes as little as possible with the regular vapor phase growth of the crystals. Four of these crystals show increases in low-light speed (at constant sensitivity) by factors of several hundred, and nine others show increases by factors greater than ten. In most of the crystals, greater improvements were effected in the decay time than the rise time. In a few cases the opposite occurred.

### *M Values in Excess of Unity*

Table I lists 12 crystals with maximum-gain  $M$  factor (see Equation (6)) equal to 10 or greater. One whisker crystal gave  $M$  of 540. It is likely that many of the  $M$  values given in Table I could be increased still further by increasing the applied field above that used. Since no imperfections were deliberately incorporated to provide the large  $M$  values, it may be concluded either that suitable centers are inherently present in the crystals, or that (particularly in the case of the whiskers)

crystal geometry was such that surface traps were able to affect the injected current while not affecting the volume photocurrent.

### Trapping Centers

A comparison of the present results with others previously published shows that there are at least five, and probably seven, definitely different trapping centers, with trap depth between 0.2 and 0.7 ev. It is the deepest of these traps, with thermally stimulated current peak near 80° C, which exerts the largest influence on the low-light speed of response at room temperature. In the crystals with improved speed,

Table IV—Suggested Transitions Involving Cation Vacancies

	<i>Excitation</i>	<i>Recombination</i>
(1)	$[V_c^+]^- + h \rightarrow [V_c^{+2}]^0 + e \rightarrow [V_c^+]^-$	
(2)	$[V_c^-]^{-2} + h \rightarrow [V_c^+]^- + e \rightarrow [V_c^-]^{-2}$	
	<i>Trapping</i>	<i>Freeing</i>
(3)	$[V_c^+]^- + e \rightarrow [V_c^-]^{-2} \rightarrow e + [V_c^+]^-$	

Superscripts inside brackets represent localized charges at the center. Superscripts outside brackets represent effective charge of center with respect to rest of crystal.

Underline represents nonequilibrium configuration.

this peak was effectively absent, corresponding to a trap density no greater than about  $10^{11} \text{ cm}^{-3}$ . Total trap densities of the order of  $10^{13} \text{ cm}^{-3}$  were obtained in these faster crystals. The 80° C peak was prominent, however, in crystals made sensitive by annealing or recrystallization after sublimation, with trap densities of the order of  $10^{15} \text{ cm}^{-3}$ . Variations of the thermally stimulated current peaks with preparation conditions suggest that cation vacancies may be involved in the 80° C peak, whereas anion vacancies may be involved in the 0° peak. Table IV summarizes suggested electronic transitions involving cation vacancies. Transitions (1) and (2) are those previously proposed for the role of these centers as sensitizing centers for photoconductivity.<sup>1</sup> Transition (3) shows how cation vacancies might act like trapping centers; the location of the  $[V_c^-]^{-2}$  level, as suggested by space-charge-limited currents,<sup>10</sup> is reasonably close to that calculated for the 80° C peak. If this identification were correct, it would explain both why sensitive crystals are so frequently slow and why the imperfection response (assumed proportional to the  $[V_c^+]^-$  concentration)

is so much higher in the slower crystals of the present investigation than in the faster crystals.

#### *Shallow Sensitizing Centers*

Additional evidence has been presented for the existence of sensitizing centers with a hole ionization energy of only about 0.2 ev, instead of the 1 ev characteristic of normal sensitizing centers. These low-energy centers seem to be the result of interaction between sensitizing centers under conditions where the density of such centers is high. In some crystals, such an interaction appears to be controllable and reversible; in other crystals the interaction between centers appears to occur mainly at the surface where the density is highest.

# INFRARED PHOTOCONDUCTIVE DETECTORS USING IMPURITY-ACTIVATED GERMANIUM- SILICON ALLOYS\*†

By

G. A. MORTON, M. L. SCHULTZ AND W. E. HARTY

RCA Laboratories,  
Princeton, N. J.

*Summary*—A new class of sensitive infrared photoconductors is described wherein the long-wavelength limit can be adjusted to meet the requirements of their application in detectors. This makes it possible to minimize the cooling needed to obtain a given detectivity and to reduce background radiation noise.

The general theory of impurity-activated photoconductors and the noise which determines their sensitivity in a detector are discussed. The class of extrinsic photoconductors consisting of germanium-silicon alloys is the principal subject of this paper. The long-wavelength limit is determined by the activator impurity, the alloy composition, and the activator compensation. The performance of gold- and zinc-activated alloys is described in detail. The peak detectivity,  $D_m^*$ , of the two materials for a given long-wavelength limit and temperature is approximately the same, but the shapes of their spectral response curves are very different. A zinc-activated alloy with a 14-micron long-wavelength limit will have a detectivity of the order of  $D_m^* = 2 \times 10$  cm/watt when cooled to temperatures attainable with a liquid oxygen-nitrogen mixture at reduced pressure. Such a photoconductor is well suited for application in the long-wavelength atmospheric window. Optical and electronic problems of adapting these photoconductors to detector cells for this and other applications are considered.

## INTRODUCTION

A LARGE PART of our knowledge of the external world reaches us through the intermediary of electromagnetic radiation. The role of visible light in this respect needs no comment. Much valuable information is also contained in the infrared spectrum from the edge of visibility at 0.8 micron to many hundreds of microns where it merges with the radio spectrum. Of particular interest is the region around 10 microns, for in this region lies the maximum of emission intensity of black bodies at room temperature (300°K), and also because the region corresponds to the center of a

\* This work has been performed under ONR contract.

† Manuscript received September 18, 1959.

relatively transparent window in an otherwise nearly opaque atmosphere. Therefore, objects which differ only slightly in temperature from their ambient can be detected at great distances by infrared sensors operating in this portion of the spectrum. This class of detector is therefore of considerable importance to science, technology, and the military.

Only within the last few years has it been possible to synthesize photoconductive detectors which are sensitive in this portion of the spectrum. Earlier detectors operating in this region were what we shall term "temperature-sensitive" detectors, which are detectors whose output depends upon a temperature change of the sensitive area due to the absorption of incident infrared radiation. The most sensitive detector of this type is the bolometer, which consists of an electrical conductor of low thermal capacity whose resistance depends upon its temperature and whose surface is blackened to absorb a large fraction of the infrared radiation falling on it. Other examples of temperature-sensitive infrared detectors are thermocouples, the Evaporograph,<sup>‡</sup> and thermally sensitive phosphors.

Photoconductive detectors, on the other hand, are members of the class of devices known as photon-responsive detectors. A photoconductor is a semiconductor whose conductivity is altered by the absorption of photons of the appropriate wavelength. For a given applied voltage across a photoconductive cell, therefore, there will be a change of current which is proportional to the rate of arrival of photons of sufficient energy to excite current carriers. As a practical means for detecting infrared radiation, photoconductors have many advantages over bolometer detectors. For a given speed of response, photoconductive detectors can be much more sensitive than bolometers. Their speed of response can be greater, and they can be synthesized to have response in any portion of the spectrum desired.

#### INFRARED DETECTOR APPLICATIONS

Before discussing infrared photoconductors in any detail, it is desirable to review some of their applications, since the applications determine the characteristics sought in the photoconductive material. Two principal areas of application of infrared detectors are the fields of chemical technology and military devices.

Most organic molecules have characteristic infrared absorption lines by which they can be identified. Infrared spectrometers are therefore used extensively in the oil, medical and food industries.

---

<sup>‡</sup> Registered trade mark.

The spectral response must extend over the range of the absorption bands being used for chemical identification, and the response should be relatively independent of wavelength over this band. For practical reasons associated with the amplifier and electronics used in connection with these detectors, their electrical frequency response should be relatively high (e.g., from 100 to 1000 cycles per second), although in the past when bolometers and thermocouples were used, the frequency response was perforce considerably lower.

In military applications, the requirements for infrared detectors are much more stringent. Here they are used to detect at a distance targets which have temperatures only slightly different from their ambient. These targets may be aircraft, missiles, trucks, tanks, or ships. Except for rather special cases, the aforementioned targets have temperatures in the neighborhood of 300° K and emit as black bodies. The peak of the radiation intensity is, therefore, about 10 microns. The earth's atmosphere is relatively opaque to infrared radiation from wavelengths of about 5.5 microns out to very long wavelengths except for a narrow transmission band extending from 8.5 microns to around 13.5 microns. An infrared detector that is to be effective for these targets should therefore have a spectral response extending to 14 microns, and, as will become apparent as the discussion proceeds, should be insensitive to longer wavelengths.

Another application now rapidly gaining importance is the detection of satellites and vehicles in space. For nonterrestrial applications such as the detection of one satellite by another, the problem of atmospheric absorption is not involved. The factors determining the long-wavelength cutoff which gives optimum results under these circumstances are more complicated and depend upon things other than the detector itself (for example, upon the electrical characteristics of the amplifier associated with the cell).

#### LIMITS OF DETECTOR PERFORMANCE

The lower limit of infrared radiation intensity which can be detected by a photoconductive detector is set by the random fluctuations in current through the cell. When the photoconductive current due to the detected radiation becomes comparable with or smaller than the random fluctuations in output current, it becomes impossible to distinguish the signal from the noise. In considering these random fluctuations or limiting noise of an infrared detector system, it is convenient to classify them according to their sources into background-radiation noise, photoconductor noise, and noise from the amplifier and associated circuitry.

Background-radiation noise arises because infrared radiation exhibits a quantum characteristic in its interaction with a photoconductor. Therefore the photocurrent is excited by a flux of photons arriving randomly in time. There will be a root-mean-square deviation in the number of photons arriving in any preassigned interval. This deviation is equal to the square root of the number. The change in flux representing the signal must be greater than this deviation.

The dark current of a photoconductor is due to the random thermal excitation of current carriers within the material, and, therefore it has a statistical fluctuation. As discussed in a later section, this fluctuation decreases exponentially with the reciprocal of the product of the temperature and the long-wavelength limit of the photoconductor.

The circuit noise is due to the Johnson noise in the coupling circuit and the noise of the amplifiers. It is similar to the noise which sets the limit to the performance of a radio receiver and many other types of electronic equipment.

The concept of noise limitation is used to specify the sensitivity of a photoconductive detector. The term specifying the sensitivity is "noise equivalent power" (NEP). This is the flux in watts of infrared radiation required to give a signal which is just equal to the root-mean-square noise from the detector. In specifying the NEP of a detector cell, the frequency bandwidth and the frequency at which the radiation supplied to the cell is chopped must be given. Also, the nature of the infrared radiation must be stated. The two common test conditions are with either the total black-body radiation reaching the cell from a source at a stated temperature (e.g., 500° K) or monochromatic radiation of a given wavelength.

Certain inadequacies of the noise equivalent power as a specification of sensitivity have led to the adoption of "detectivity" as an alternative. The detectivity  $D^*$  of a photoconductive cell is defined in terms of its NEP as follows:

$$D^* = (\text{NEP})^{-1} A^{1/2} \Delta f^{1/2} \quad (1)$$

where  $A$  is the working area of the cell and  $\Delta f$  the frequency bandwidth for the given NEP.

#### BACKGROUND NOISE

In designing an infrared detector system for use as a means of sensing remote objects under terrestrial environment, one of the objectives for obtaining optimum performance is that it shall be

limited by background radiation noise. The detector and target are immersed in a nearly opaque atmosphere which is at a temperature in the neighborhood of  $300^{\circ}$  K. The signal being received by the detector is, as mentioned previously, transmitted through a narrow atmospheric window extending from 8.5 to 13.5 microns. However, the detector also sees background radiation from the atmosphere emitted over the entire infrared spectrum and having an intensity distribution corresponding to a black body at  $300^{\circ}$  K. If this background radiation were strictly constant, it would result in a d-c current through the detector which would bias the signal current but would not limit the sensitivity of the cell. However, the background is constituted of photons which arrive at the detector essentially randomly in time and, therefore, as has been stated, have a root-mean-square statistical fluctuation equal to the square root of their number. It is this statistical fluctuation which determines the amount of radiation which must be received from the target to insure detection.

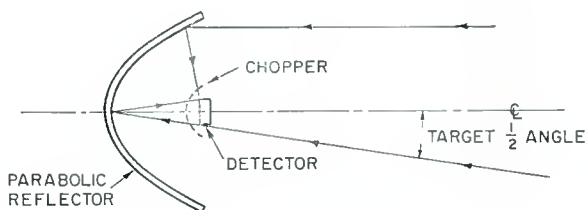


Fig. 1—Detector optical system.

The limit imposed by the statistical fluctuations of the background on the sensitivity of a detector can be evaluated quantitatively as follows:

Consider the system shown in Figure 1. The cell is assumed to have an area of  $1 \text{ cm}^2$  and to be in a reflective optical system which has an angular aperture of  $180^{\circ}$ . Consequently, the cell sees radiation coming from an infinite plane which is a black body at  $300^{\circ}$  K. Under these circumstances, the amount of radiation that the cell receives is equal to the amount of radiation emitted by a black body of  $1 \text{ cm}^2$  area at this temperature. Since the cell responds to all photons with wavelengths shorter than its long-wavelength limit,  $\lambda_m$ , the number of photons,  $Q$ , can be calculated from Planck's radiation equation expressed in terms of photons as follows:

$$Q_{0-\lambda_m} = \int_0^{\lambda_m} \frac{2\pi c}{\lambda^4} \exp\left\{-\frac{hc}{\lambda kT}\right\} d\lambda \text{ photons/cm}^2/\text{second.} \quad (2)$$

The number of photons ( $Q_{0-\lambda_m}$ ) reaching the surface of the cell in the wavelength range from zero to the long-wavelength limit,  $\lambda_m$ , is given in Table I for long-wavelength limits of from 2 to 30 microns.

Table I

$\lambda_m$ microns	$Q_{0-\lambda_m} = a \times 10^b$		$\sqrt{Q_{0-\lambda_m}} = c \times 10^d$	
	<i>a</i>	<i>b</i>	<i>c</i>	<i>d</i>
2	6.1	10	2.5	5
4	1.8	15	4.2	7
6	4.9	16	2.2	8
8	2.2	17	4.7	8
10	5.0	17	7.0	8
12	8.2	17	9.0	8
14	1.2	18	1.1	9
16	1.5	18	1.2	9
18	1.8	18	1.3	9
20	2.0	18	1.4	9
25	2.6	18	1.6	9
30	2.9	18	1.7	9

The root-mean-square noise produced by this radiation is given in the second column of the same table. The noise equivalent photon flux (paralleling the NEP defined above) is therefore just equal to this number. From the noise equivalent photon flux, the NEP for a black body source of approximately 300° K can be calculated from the relation

$$\text{NEP} = \frac{H_{300^\circ\text{K}}}{Q_{0-\lambda_m}} \times (\text{noise equivalent photon flux}) = \frac{H_{300^\circ\text{K}}}{\sqrt{Q_{0-\lambda_m}}} \quad (3)$$

where  $H_{300^\circ\text{K}}$  equals watts radiated by a black body of 1 cm<sup>2</sup> area at 300° K. The value thus calculated is the noise equivalent power of a perfect detector whose performance is limited by the radiation background.

The curve for this limiting noise equivalent power, which is the power radiated from a minimum detectable target, is shown as a function of the long-wavelength limit in curve (1) of Figure 2. The

preceding estimate of the power received at the detector from a target to give a signal equal to the noise assumes no atmospheric absorption. Actually, the power from the target will be received only over a narrow spectral region around 10 microns. This transmission band begins

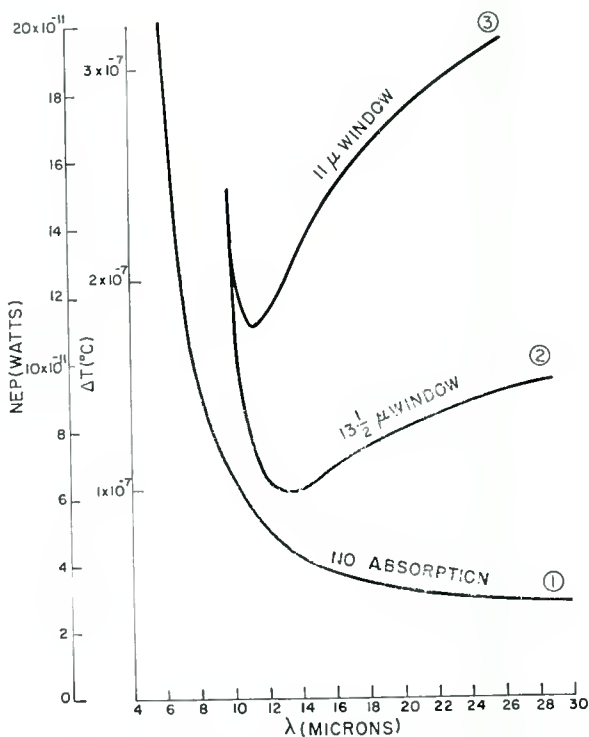


Fig. 2—Background radiation limit as a function of detector long-wavelength limit.

at 8.5 microns with a rather sharp edge and extends to 11 microns where the absorption begins to rise slowly, until at 13.5 microns the atmosphere again becomes nearly opaque. For short ranges (a few thousand feet), the atmospheric window can be considered as extending from 8.5 to 13.5 microns; at greater distances (beyond 7 or 8 miles), however, the window extends from about 8.5 to 11 microns.

Although the signal is transmitted only over this narrow band, the background includes the entire spectral range to which the detector is sensitive, since the atmosphere radiates in those portions of the spectrum where its absorption is high. Consequently, the performance of any detector falls off rapidly if the long-wavelength response of the detector extends appreciably beyond the atmospheric window.

This is shown in curves 2 and 3 of Figure 2. Curve 2 shows the amount of radiation that would be received at the detector in the absence of atmospheric absorption when the radiated signal is such that with atmospheric absorption the detector would have a signal-to-noise ratio of unity. Curve 3 is a similar calculation where the target is many miles from the detector and the window extends from 8.5 to 11 microns. It must be pointed out that in this case, complete transmission through the window is assumed. Actually, some absorption exists; for example, if the target is 10 miles from the detector, the window has a transmission of about 30 per cent. Under these conditions, the value of the ordinate (NEP) must be increased by a factor of 3.

An alternative way of indicating the performance of the detector system is to give the temperature difference between the target and its background (assuming the image of the target fills the detector) such that the increased radiation will give a signal just equal to the noise. This temperature ( $\Delta T$ ) is also given on the ordinate of Figure 2. These curves clearly show that under terrestrial conditions, a short-range detector should have a long-wavelength limit around 13.5 to 14 microns and a long-range detector, a limit of 11 to 12 microns.

The rapid deterioration of performance as the long-wavelength limit increases beyond the optimum indicates the importance of accurate control of the long-wavelength limit of a photoconductive detector. Since the background imposes a limit to the performance of the system, there is little advantage in increasing the sensitivity of a detector beyond that set by the background; in other words, for photoconductors which are to be used as infrared detectors, there is no advantage in reducing the noise generated beyond the point at which the background noise becomes dominant. This makes it possible to estimate the peak detectivity,  $D^*_m$ , which corresponds to the radiation-noise limit under a given set of conditions by the following relationship:

$$D^*_m = [\text{NEP}_m (1 \text{ cm}^2)]^{-1} = \left( \sqrt{Q_{0-\lambda_m}} \times \frac{hc}{\lambda_p} \right)^{-1}. \quad (4)$$

This expression is derived by assuming that the number of photons from the target during the integration period equals the square root of the background photons to which the target is sensitive and that each of these photons has an energy corresponding to that carried by a photon of the wavelength  $\lambda_p$  for the peak of the spectral response of the photoconductor. For the application in question, this peak should be at approximately 10 microns, and, therefore, the detectivity

obtained from the above relation is about  $4.5 \times 10^{10}$  cm/watt.

The preceding has assumed an ideal atmosphere where the photon fluctuation is due only to the random arrival of photons. In an actual atmosphere, turbulent air currents, temperature nonuniformity, and similar factors would probably double this noise. Therefore, a more realistic value of the limiting detectivity required of a practical optimum short-range detector is about  $2 \times 10^{10}$  cm/watt. This figure serves as a useful guide in the development of practical infrared photoconductive materials.

In treating the astronomical application, other factors must be brought into consideration. Here, both the detector and the target are no longer immersed in a relatively opaque emissive atmosphere. Instead, the detector looks at a background which is close to absolute zero temperature. Furthermore, there is no absorption between the target, which is assumed to be at a temperature between 250 and 300° K, and the detector. Therefore, radiation background imposes no limit to the sensitivity of the detector system.

As has been pointed out earlier, the generation-recombination noise in a photoconductive detector decreases exponentially with the reciprocal of the product of cell temperature and long-wavelength limit. If unlimited cooling is available for the detector, the obvious procedure is to use a photoconductor with a very long wavelength response and to use a cell temperature which brings the generation-recombination noise below the Johnson noise and the input noise of the amplifier associated with the detector.

When only limited cooling is available, the procedure giving optimum results is to cool the cell to the limiting temperature and adjust the long-wavelength limit until the generation-recombination noise equals the combined Johnson noise of the cell and load resistor, and the input noise of the amplifier.<sup>1</sup> The reasons for this are given in the section entitled Electrical Considerations. In both these examples, the circuit noise sets the limit of performance of the system. This is a very important point, and a section of this paper is devoted to a discussion of the amplifier problem in general.

#### INFRARED PHOTOCONDUCTORS

Two types of photoconductors are recognized — intrinsic photoconductors and extrinsic or impurity-activated photoconductors. Excitation of photocurrent in an intrinsic photoconductor occurs when

---

<sup>1</sup>W. E. Spicer, "Relationship between Signal-to-Noise Ratio and Threshold Response of Infrared Photoconductors Limited by Generation-Recombination Noise," *Jour. Appl. Phys.*, Vol. 30, p. 1331, September, 1959.

a photon having an energy equal to or greater than the forbidden-band-gap energy is absorbed by the material and produces an electron-hole pair. These freed carriers can move through the crystal under the influence of an applied field and give rise to the photoconductive current. The excitation of an impurity-activated photoconductor occurs by the absorption of a photon by the impurity causing an electron or hole to be excited into the conduction band or valence band, respectively. For this, the photon must have an energy equal to or greater than the ionization energy of the impurity. The excited current carrier is then free to move through the lattice and give rise to a photoconductive current.

It should be pointed out that in this type of photoconductivity the minority carrier (the ionized impurity) is immobile and only the majority carrier can move. Ohmic contacts to the photoconductor must allow current carriers to enter or leave the material at the contacts. When an excited current carrier moves away from its parent atom, there is a redistribution of potential throughout the photoconductor which permits another carrier of the same sign to move in to take its place. A current flow corresponding to the freed charge continues until recombination with the minority carrier occurs.

With both types of photoconductors, the thermal motion of the lattice can also excite carriers. These, of course, give rise to a dark current in exactly the same way that photon-excited carriers produce the photocurrent. If this dark current were perfectly uniform, it would not limit the performance of the material used as a detector. However, it is subject to a statistical fluctuation or noise and this generation-recombination noise is, as has been pointed out, one of the limiting factors to detector performance. Although it appears that the ultimate sensitivity which could be achieved with an "ideal" intrinsic photoconductor is probably about the same as for an impurity-activated photoconductor, there are many factors which are very difficult to evaluate at this time.<sup>2</sup> In terms of today's technology, however, impurity-activated photoconductors for the detection of long-wavelength radiation are far superior to known intrinsic photoconductors. Therefore, the discussion which follows is restricted almost exclusively to impurity-activated photoconductors.

Quantitatively, the photoconductive current,  $\Delta i$ , is given (to a close approximation) by the expression

$$\Delta i = \frac{e \tau \mu E}{L} \frac{dN}{dt} \quad (5)$$

<sup>2</sup> W. E. Spicer, private communication.

Here  $dN/dt$  is the rate of excitation of carriers,  $\tau$  the carrier lifetime,  $\mu$  the mobility,  $L$  the length of the crystal, and  $E$  the applied electric field. The rate of excitation of carriers depends upon the number of activator centers from which excitation can take place, upon the radiation cross section,  $\alpha_p$ , of each center, and upon the infrared radiant flux,  $F$ . In a photoconductor of the type in which acceptors are the activator centers, if the activator concentration is  $N_A$ , the total number of active centers is  $N_A V$  where  $V$  is the volume of the crystal. Frequently, an impurity-activated photoconductor will contain, in addition to the activator centers, centers of the opposite sign; in other words, there will be a certain concentration of compensating donor levels,  $N_D$ . When this condition obtains, the number of active centers available for excitation will be  $N_A - N_D$ . For this type of photoconductor, the expression for the photocurrent,  $\Delta i_s$ , is

$$\Delta i_s = \frac{e\tau\mu E}{L} (N_A - N_D) V \alpha_p F. \quad (6)$$

The dark current,  $i_d$ , is given by

$$i_d = \frac{e\mu E}{L} nV, \quad (7)$$

where  $n$  is the concentration of carriers due to thermal excitation, and is given by

$$n = N_C \exp\left(-\frac{E_f}{kT}\right). \quad (8)$$

$N_C$  is the effective number of states in the valence band and  $E_f$  is the Fermi energy. For a partially compensated impurity level, the Fermi energy will be essentially equal to the impurity ionization energy,  $E_i$ . Under these conditions, the expression for  $n$  is

$$n = N_C \left(\frac{N_A - N_D}{N_D}\right) \exp\left(-\frac{E_i}{kT}\right). \quad (9)$$

Generation-recombination noise is related to the dark current since both the thermal excitation and the recombination of carriers are purely random processes. It may be shown that the root-mean-square

noise current,  $\Delta i_N$ , due to the thermally excited dark current is given by<sup>3</sup>

$$\Delta i_N = \frac{e\mu E}{L} \left( \frac{2N_C(N_A - N_D) V \tau \Delta f}{N_D} \right)^{1/2} \exp\left(-\frac{E_i}{2kT}\right), \quad (10)$$

where  $\Delta f$  is the frequency bandwidth over which measurements are taken. It should be pointed out that the bandwidth is approximately reciprocally related to the integration time. This time is the period over which a physical phenomenon is allowed to integrate when an observation is made. If an exponential cutoff is assumed for the frequency band, it can be readily shown by means of a Fourier transform that  $\Delta f = 1/(2t)$  where  $t$  is the integration time.

The signal-to-noise ratio is given by

$$\frac{S}{N} = \frac{\Delta i_s}{\Delta i_N} = \alpha_p F \left[ \frac{\tau V N_D (N_A - N_D)}{2N_C \Delta f} \right]^{1/2} \exp\left(\frac{E_i}{2kT}\right), \quad (11)$$

and the noise equivalent power by

$$\text{NEP} = F(S/N)^{-1} = \alpha_p^{-1} \left[ \frac{2N_C \Delta f}{\tau V N_D (N_A - N_D)} \right]^{1/2} \exp\left(-\frac{E_i}{2kT}\right). \quad (12)$$

The expression for the detectivity  $D^*$  will be given for the case of a generation-recombination noise-limited, impurity-activated photoconductor mounted in an ideal integrating chamber.<sup>†</sup> It is

$$D^* = \left( \frac{\tau N_D \alpha_p}{2N_C} \right)^{1/2} \exp\left(\frac{E_i}{2kT}\right). \quad (13)$$

If the photoconductive threshold,  $\lambda_m$ , is expressed in terms of the impurity ionization energy

$$E_i = \frac{hc}{\lambda_m}, \quad (14)$$

the expression for  $D^*$  becomes:

<sup>3</sup> K. M. van Vliet, "Noise in Semiconductors and Photoconductors," *Proc. I.R.E.*, Vol. 46, p. 1004, June, 1958. The expression for both the signal and the noise current should include a term  $(1/1 + \omega^2\tau^2)^{1/2}$  where  $\omega = 2\pi f$  and  $f$  is the chopping frequency. For values of  $f$  likely to be encountered in practice and for photoconductors of the type being discussed,  $\omega\tau \ll 1$ . In any event, the signal-to-noise ratio will be independent of  $f$  regardless of whether or not the above inequality is satisfied.

<sup>†</sup> A discussion of the properties of the integrating chamber is given later. By an ideal chamber is meant one with perfectly reflecting walls.

$$D^* = \left( \frac{\tau N_D \alpha_p}{2N_0} \right)^{1/2} \exp \left( \frac{hc}{2k} \frac{1}{\lambda_m T} \right). \quad (15)$$

Since the coefficient preceding the exponential term is nearly temperature independent, it is possible to write an approximate general expression for the detectivity of an impurity-activated photoconductor as follows:

$$D^* = KM^* \exp \frac{hc}{2k} \frac{1}{\lambda_m T} \quad (16)$$

and

$$\log D^* = \log K + \log M^* + .434 \frac{hc}{2k} \frac{1}{\lambda_m T}. \quad (17)$$

In this expression,  $K$  contains physical constants which are essentially independent of the photoconductor;  $M^*$ , the merit factor, contains the radiation absorption cross section, carrier lifetime, and other factors which may vary from photoconductor to photoconductor. The final factor, which is exponential in form, interrelates photoconductor temperature and long-wavelength limit. This expression is very convenient as a first-order approximation for the performance of photoconductors at different operating temperatures and with different long-wavelength limits and photoconductive characteristics. The merit factor,  $M^*$ , is also useful in comparing the fundamental performance of different kinds of photoconductors.

#### GERMANIUM, SILICON AND THEIR ALLOYS

Both germanium and silicon exhibit strong photoconductivity in the near-infrared region, but their band gaps are far too large to be excited by long-wavelength infrared radiation. The two elements can be alloyed in all proportions and grown into good single crystals. X-ray analyses of the alloy single crystals thus produced show that their lattice is the same as that of the elementary semiconductors and that there is a monotonic decrease in the lattice constant going from germanium to silicon. The X-ray lines of the diffraction patterns are sharp, there is no indication of segregation or nonuniform mixing, and there is no indication of the formation of a super lattice in any portion of the composition range thus far examined.

Measurements of the band gap show that there is a continuous increase in width from the 0.7 ev of germanium to the 1.2 ev of silicon. The increase is not uniform with composition but increases rather

rapidly as small amounts of silicon are added to germanium up to 12 to 15 per cent. From then on, the band-gap energy increases more slowly as silicon is added. This behavior of the alloy system has been explained by F. Herman with his analysis of the energy-band structure in *k*-space of this system of semiconductors.<sup>4</sup>

Both silicon and germanium are excellent hosts for activator impurities to form impurity-activated photoconductors. The ionization energies of a large number of impurity atoms in both germanium and silicon have been measured. Table II lists some of these observed levels.<sup>5</sup> The impurities listed are potential activators for photocon-

Table II

	Impurity Levels in Germanium			Donors
	Acceptors			
Au	0.05 <sup>c</sup>	0.20 <sup>c</sup>	0.16 <sup>v</sup>	0.05 <sup>v</sup>
Ag	0.09 <sup>c</sup>	0.28 <sup>c</sup>	0.13 <sup>v</sup>	
Cu	0.26 <sup>c</sup>	0.33 <sup>v</sup>	0.04 <sup>v</sup>	
Fe	0.27 <sup>c</sup>	0.35 <sup>v</sup>		
Co	0.30 <sup>c</sup>	0.25 <sup>v</sup>		0.09 <sup>v</sup>
Ni	0.30 <sup>c</sup>	0.23 <sup>v</sup>		
Mn	0.37 <sup>c</sup>	0.16 <sup>v</sup>		
Cd		0.16 <sup>v</sup>	0.05 <sup>v</sup>	
Zn		0.095 <sup>v</sup>	0.035 <sup>v</sup>	
S				0.18 <sup>c</sup>
Se			0.28 <sup>c</sup>	
Te			0.30 <sup>c</sup>	0.14 <sup>c</sup>
				0.11 <sup>c</sup>

<sup>c</sup> Measured from conduction band.  
<sup>v</sup> Measured from valence band.

ductors. Where an impurity shows a multiplicity of levels and it is desired to use one of the levels above the lowest, the levels with lower ionization energies can be compensated with impurities of the opposite type. The gold level at .15 eV above the valence band was the first used in practical long-wavelength infrared photoconductors. This level was found early in 1953 in this investigation of long-wavelength photoconductors.<sup>6</sup> By its use, a photoconductor having a long-wavelength

<sup>4</sup> F. Herman, "Speculations on the Energy Band Structure of Ge-Si Alloys," *Phys. Rev.*, Vol. 95, p. 847, August, 1954.

<sup>5</sup> W. W. Tyler, "Deep Level Impurities in Germanium," *International Conference on Semiconductors*, Pergamon Press, Inc., New York, N. Y., 1958, p. 59.

<sup>6</sup> Thirteenth Interim Report, Contract N6onr-23603, January 15, 1953 to April 15, 1953.

limit\* in the neighborhood of 10 microns, and excellent response characteristics at liquid nitrogen temperature can be achieved.

An examination of Table II shows that none of the impurity levels found thus far are entirely suited for a photoconductor with a long-wavelength limit in the neighborhood of 14 or 14.5 microns. The second level of gold just described has a cutoff at too short a wavelength to be really satisfactory in the atmospheric transmission window. On the other hand, the second level of zinc in germanium has a long-wavelength limit of more than 17 microns, and, as a consequence, the cell must be cooled to a very low temperature to obtain adequate detectivity. Furthermore, in terrestrial applications, the cell will respond to radiation beyond the long-wavelength edge of the atmospheric window.

Impurities can be introduced into the alloy giving acceptor or donor levels in the forbidden band, and their ionization energies adjusted simply by adjusting the alloy composition.<sup>7</sup> The ionization energy of an acceptor lying close to the valence band in pure germanium increases as silicon is added to the germanium. Similarly, the ionization energy of an acceptor in silicon decreases as germanium is added to the silicon. Figure 3 shows the variation of the ionization energy of a number of impurities in this alloy system. It should be mentioned at this point that the ionization energy of an impurity in the alloy is, as discussed later, also somewhat dependent upon the compensation of the level involved.

Of the activator elements examined to date for photoconductors operating in the 10-micron atmospheric window, the two most promising from the point of view of high absolute sensitivity are the lowest level of gold and the second level of zinc. Since both of these activators have several levels in the forbidden band, the appropriate level must be selected by suitable compensation with a second foreign atom impurity of the opposite type.

The lowest level of gold in germanium has a long-wavelength cutoff of about 25 microns. The ionization energy is so small that, because of the high thermal excitation, the photoconductor would be virtually useless at liquid nitrogen temperature or any temperature that could be obtained by maintaining liquid nitrogen at a reduced pressure. However, in an alloy containing approximately 11 atomic per cent of silicon, the long-wavelength limit is about 14 microns. The ionization energy has increased to a point where a detectivity of the order of

\* Long-wavelength limit is defined in this discussion as the wavelength,  $\lambda_m$ , at which the photoconductive response is 10 per cent of its peak value.

<sup>7</sup> M. L. Schultz, "Ionization Energies of Some Impurities in Germanium-Silicon Alloys," *Bull. Am. Phys. Soc.*, Ser. II, Vol. 2, No. 3, p. 135, March 21, 1957.

$10^{10}$  cm/watt is realizable at temperatures attainable with a liquid oxygen-nitrogen mixture at reduced pressures. Similarly, with the second level of zinc, as the silicon content of the alloy is increased, the long-wavelength limit decreases from 17 microns in pure germanium. Figure 4 shows a series of spectral response curves of zinc-activated alloys of compositions ranging from 0 to 7.5 per cent silicon. The continuous decrease of the long-wavelength limit is readily apparent.

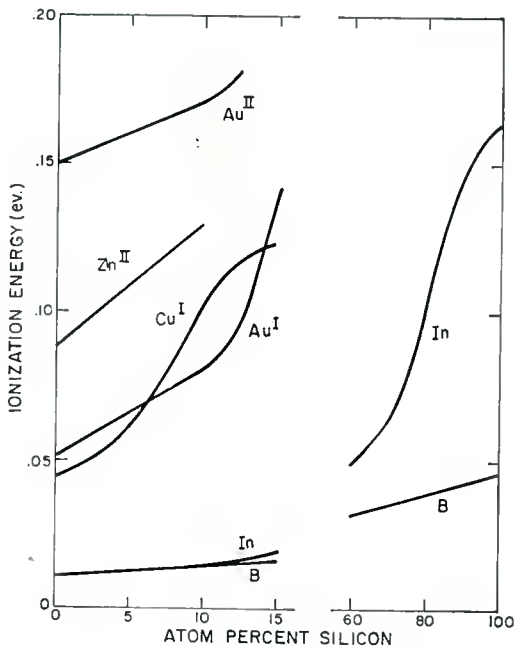


Fig. 3—Impurity ionization energies as a function of alloy composition.

Both the 89.1 per cent Ge, 10.9 per cent Si:Zn<sup>II</sup> photoconductors have approximately the same long-wavelength limit and, at a given temperature, essentially the same maximum detectivity. The shape of the spectral response curve of the two impurity-activated alloys is quite different, however, as shown in Figure 5. It will be noted that the gold-activated alloy has a maximum around 7 microns and a gradual decrease in response out to its long-wavelength limit at 14.5 microns. The zinc-activated photoconductor, on the other hand, has its maximum at 10 microns and falls sharply to its long-wavelength limit of 14.5 microns. The shape of the curve for the zinc-activated alloy is much better suited for

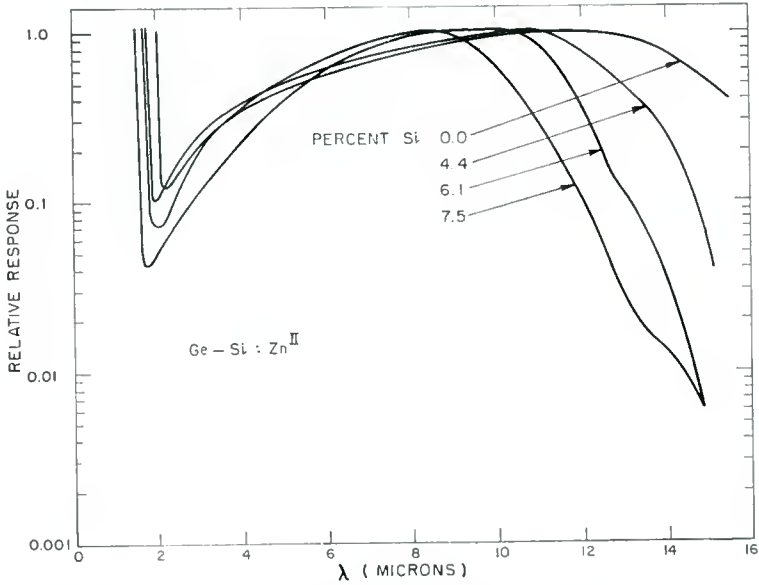


Fig. 4—Spectral-response characteristics for zinc-activated alloys as a function of alloy composition.

applications involving the transmission of the signal radiation through the atmospheric window than that of the gold-activated alloy. However, other applications may require the broader response band of the gold-activated material.

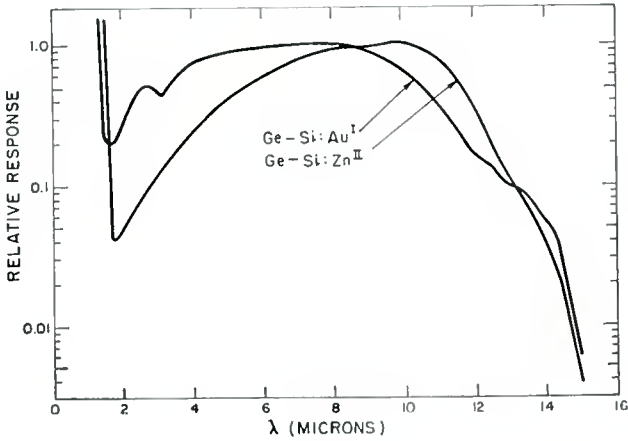


Fig. 5—Comparison of spectral-response characteristics of zinc- and gold-activated alloys.

It is interesting to examine this class of photoconductor in comparison with other photoconductors in terms of the general expression for detectivity given above. This comparison can most easily be made by plotting  $\log D^*$  as a function of  $1/(\lambda_m T)$  as has been done in Figure 6. An estimate for  $\log K$  has been made which, although very

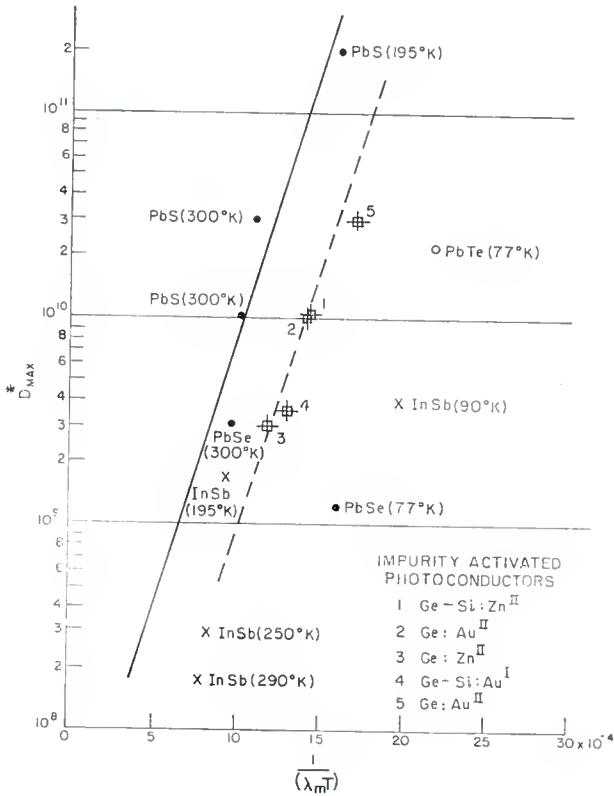


Fig. 6—Relationship between peak detectivity and temperature-long-wavelength limit product.

unreliable because of the uncertainty in a number of the constants involved, serves to locate the (solid) line corresponding to  $M^* = 1$ .<sup>†</sup> The performance of a number of different types of photoconductors is indicated. Many of these are barrier type such as the lead sulfide and lead telluride photoconductors, others are junction type such as the lead high-temperature indium antimonide, and a few are intrinsic such as

<sup>†</sup> Note: For comparison purposes, this may be considered a purely arbitrary line.

the low-temperature indium antimonide.

The high-temperature, short-wavelength, lead sulfide photoconductors seem to lie very close to the line for  $M^* = \text{unity}$ . (This is probably entirely fortuitous in that the expression is derived for impurity-activated photoconductors.) However, even if the solid line in Figure 6 is considered purely arbitrary, the position of various photoconductors relative to it is in one sense a measure of their merit, for it indicates the detectivity for a given long-wavelength limit that can be achieved with a specified amount of cooling. It should be noted that the relatively long-wavelength lead telluride, lead selenide and indium antimonide detectors which operate at liquid nitrogen temperature all have values for  $M^*$  of  $10^{-3}$  or less.

The position of a number of impurity-activated germanium and germanium-silicon alloy cells is also plotted in this figure. These cells cover a variety of types including the second level of gold in pure germanium, the first level of gold in an alloy, and the second level of zinc in an alloy. It is interesting to note that these all lie approximately on a line (dashed) corresponding to  $M^* = 0.1$  which is parallel to the solid curve for  $M^* = 1$ . At the time of writing, the dashed curve on which the impurity-activated alloys lie appears to be representative of what can be expected from these types of photoconductors. They are markedly superior to low-temperature lead telluride and indium antimonide. On the basis of what is presently known about the impurity-activated alloys, it is probably safe to extrapolate over several orders of magnitude from the given experimental points.

#### PREPARATION OF IMPURITY-ACTIVATED ALLOY PHOTOCONDUCTORS

The growing of germanium-silicon alloy crystals is somewhat more complicated than that of either germanium or silicon alone, since both the lattice constant and the melting point of the alloy crystals are functions of alloy composition. Inasmuch as both the gold-activated and zinc-activated photoconductors lie in the germanium-rich portion of the alloy composition range, this discussion of methods of preparation will be limited to crystals containing less than 20 per cent silicon.

The crystals are grown in a zone-melting furnace. The construction is illustrated in Figure 7. The furnace is heated by three Globar\* elements oriented perpendicular to the direction of crystal growth. These heater elements are enclosed in fire brick for heat insulation. The furnace is mounted on a platform which is moved by a lead screw. A normal growing rate is two inches per 24 hours for most of the

---

\* Registered trade mark.

alloys under consideration. The furnace temperature must be precisely controlled (to approximately  $\pm 1^\circ \text{C}$  at  $1000^\circ \text{C}$ ) so that fluctuations in the growth rate at the growing liquid-solid interface are eliminated. The charge is contained in a silica boat coated to prevent wetting of the boat surface by the liquid alloy. A slow stream of dry oxygen-free helium is passed through the silica furnace tube in which the boat is placed during the growth of the crystal.

A single crystal of germanium is used as seed and the crystal grows from the seed through an intermediate transition region in which the silicon content increases to a region where the silicon content is maintained constant at the desired final value. The charge

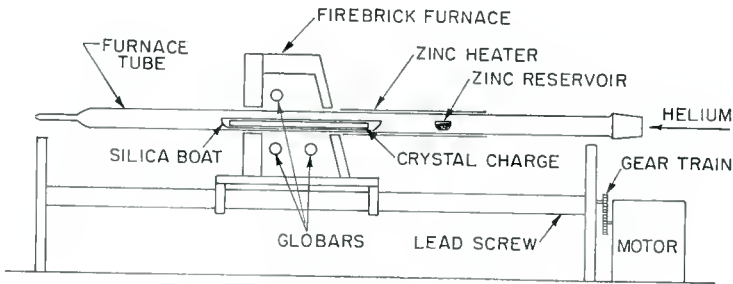


Fig. 7—Crystal growing apparatus.

consists of an ingot of purified germanium of uniform cross section and a piece of pure silicon cut to a size and shape which gives the final alloy composition desired. To maintain a constant molten zone length in the transition region from the seed to the final alloy, the furnace temperature must be increased because the melting-point temperature of the alloy increases as the silicon content increases. This is done by a motor-driven programmer.

Where gold is the activator, it may be introduced into the alloy in one of two ways, either during growth of the alloy crystal by placing the appropriate amount of pure gold into the first zone length of the charge or, more conveniently, by diffusion into previously grown undoped alloy. Diffusion can be carried out as follows. The alloy ingot is cut into the shape required for the final detector element. After cutting, the surfaces are cleaned by etching with CP-4. Next, a thin layer of gold is electroplated over the entire surface of the sample. The sample is placed in a graphite boat which, in turn, is inserted into a silica furnace tube containing an argon atmosphere, and diffusion is carried out at a temperature of approximately  $900^\circ \text{C}$ . The diffusion time required to give a homogeneous distribution of activator centers

depends, of course, upon the sample dimensions. If the smallest dimension is of the order of 3 or 4 mm, a diffusion time of about 250 hours is required. After diffusion, the samples are annealed at 500° C for 48 hours to precipitate any copper which may have accidentally diffused into the alloy. After this, the surfaces are cleaned by lapping and etching, and electrical contacts are applied.

The doping procedure for the zinc-activated alloy detector material is somewhat more complicated for several reasons. Since the rate of diffusion of zinc in the solid material is too small for practical diffusion doping, the doping must be done from the melt as the crystal is being grown. Since the zinc level of interest is the deeper lying of the two levels, the shallower level must be completely compensated by the addition of the proper concentration of a donor impurity. Finally, because of the volatility of zinc, a doping technique which maintains the proper zinc concentration in the melt must be employed.

The furnace arrangement for zinc-doping is shown in Figure 7. The zinc source is a reservoir located ahead of the crystal growing boat so that the flow of inert gas carries the zinc vapor over the molten material. An auxiliary heater maintains the temperature in the vicinity of the zinc reservoir at that which gives the desired steady-state concentration of zinc in the molten zone. This is maintained, of course, by an interchange of zinc between the melt and the vapor phase. By growing calibration crystals doped with zinc only, the relationship between the zinc heater temperature and zinc concentration in the finished crystal can be determined.

Antimony is most frequently used as the n-type impurity to compensate the shallow level of zinc. The appropriate amount is placed in the first zone length of the alloy crystal charge. Although antimony is much less volatile than zinc, some is lost from the charge during the growth of the crystal. This loss requires that the zinc reservoir temperature be programmed in order to maintain constant conditions of compensation throughout the crystal.

After a zinc-doped crystal has been grown, a preliminary survey at room temperature and liquid nitrogen temperature by means of a four-point resistivity probe is made of the ingot to determine its suitability as a photoconductor. This probe survey is quite essential because of the difficulty of maintaining the correct compensation throughout the ingot. The ratio of resistance at room temperature and liquid nitrogen temperature is a relatively good guide to the number of uncompensated centers in the alloy.

Both gold- and zinc-activated materials, after the samples have been lapped to shape, etched and the contacts applied, are subjected

to a series of measurements in a demountable test cryostat before they are considered ready for mounting in a permanent cell. These measurements include (a) dark resistance, (b) noise at 100 cps, (c) signal from a 500° K black body chopped at 100 cps, and (d) the relative spectral response. All of these measurements are made over a range of temperatures from 77° K to 50° K or lower. In general, both signal and noise measurements at each temperature are made with several values of applied voltage. If these tests are satisfactory, the material is then ready for mounting in a cell.

#### PERFORMANCE OF IMPURITY-ACTIVATED GERMANIUM-SILICON ALLOY PHOTOCONDUCTORS

##### *Zinc-Activated Alloy*

Figure 8 shows in detail the spectral response curve of a zinc-activated alloy which is considered very suitable for meeting the requirements of target detection through the earth's atmosphere. The

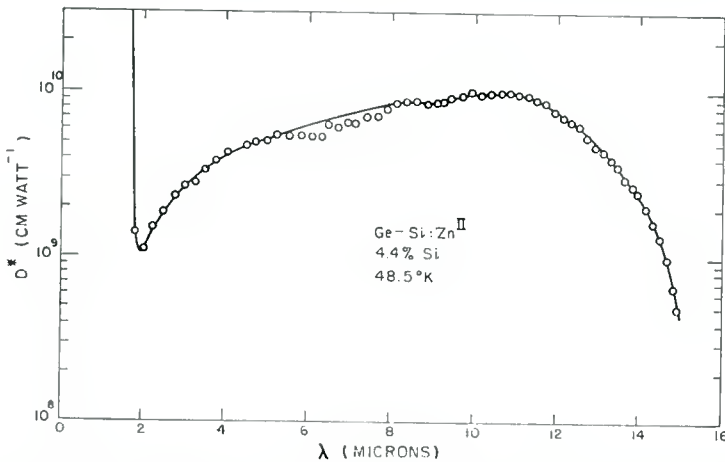


Fig. 8—Absolute spectral response characteristic for a zinc-activated alloy.

ordinate of the spectral response curve is the differential detectivity (i.e., detectivity per unit wavelength) at each wavelength given on the abscissa. It will be seen that the response rises sharply from the long-wavelength limit of 14 microns to a maximum at 10.5 or 11 microns and then falls slowly with decreasing wavelength.

The performance of this photoconductor as a function of temperature is given in Figure 9. Curves are shown for the signal  $\Delta\sigma_s$ , the root-mean-square noise  $\Delta\sigma_n$ , and the detectivity  $D^*$  for a 500° K source chopped at 100 cps with a 1-cycle bandwidth for the noise. It can be

seen that the signal is very nearly independent of temperature. The noise falls rapidly until a temperature of 55° K is reached and then falls more slowly. The slope of the low-temperature portion of this curve is that expected from the ionization energy of the activator centers (also from the long-wavelength limit of photoconductivity). The more rapid drop in the high-temperature portion of the curve probably has no fundamental significance and may be due to the behavior of the contacts or to surface contamination of the material.

The detectivity at 48.5° K of the particular sample shown in these curves for a 500° K source is  $5.3 \times 10^9$  cm watt<sup>-1</sup>. The peak detectivity for materials having a spectral response of the shape of that observed for the zinc-activated alloy is about double the detectivity measured for a 500° K source.

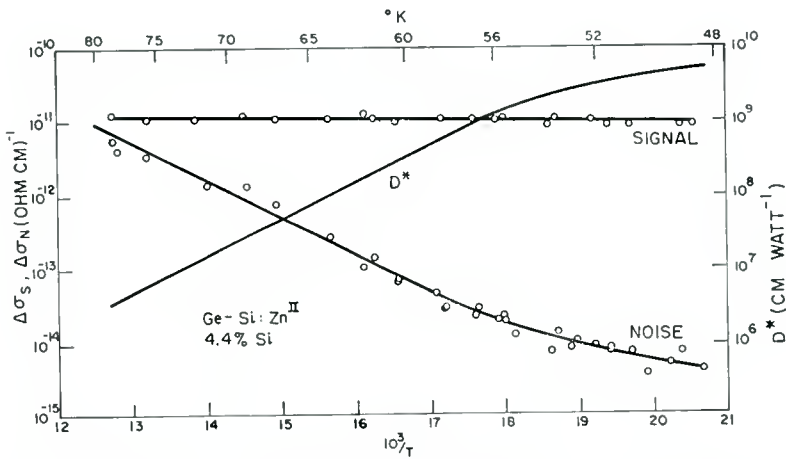


Fig. 9—Temperature dependence of signal, noise, and detectivity for a zinc-activated alloy.

The variation of long-wavelength limit with alloy composition was discussed in an earlier section. However, the alloy composition does not uniquely determine the long-wavelength limit for zinc-activated materials. The extent to which the active level (the Zn<sup>II</sup> level) is compensated by antimony strongly affects the long-wavelength limit. This can readily be seen in Figure 10 which shows a series of spectral response curves of a group of activated alloys of approximately the same silicon ratio but with different degrees of compensation.

On the basis of data available at the present, an empirical expression has been worked out for the long-wavelength limit in terms of alloy composition and compensation as follows:

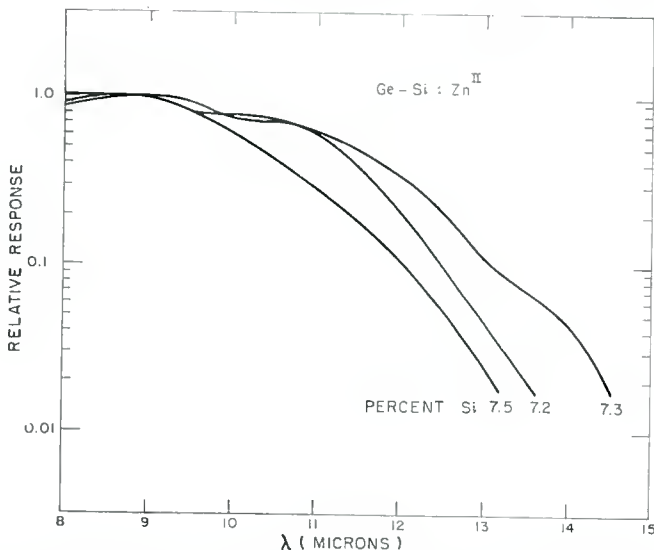


Fig. 10—Effect of degree of compensation upon the long-wavelength limit of zinc-activated alloys.

$$\lambda_m = 17.1 - 58R - 8RC, \quad (18)$$

where 
$$R = \frac{\text{Si}_{\text{atoms}}}{\text{Ge}_{\text{atoms}} + \text{Si}_{\text{atoms}}} \text{ and } C = \left( \frac{N_D}{N_A - N_D} \right)^{1/2}. \quad (19)$$

Figure 11 is a plot of the presently available samples on a curve

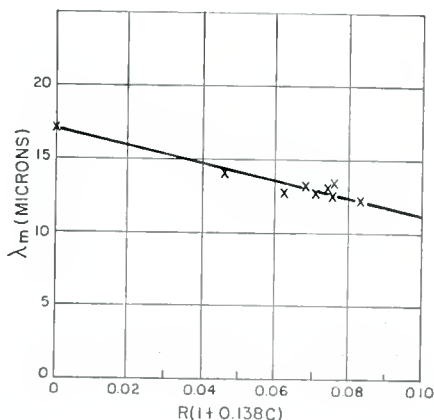


Fig. 11—Correlation between long-wavelength-limit alloy composition and degree of compensation.

with long-wavelength limit as ordinate and the composition-compensation parameter as abscissa. The fit to the empirical curve is within the accuracy to which compensation is known.

*Gold-Activated Alloy*

The gold-activated alloy system appears to be somewhat more complex than the zinc-activated system, and many aspects of it remain to be investigated. The spectral characteristic differences seen in Figure 5 make it evident that it is somewhat less suitable than zinc for a detector operating in the 8.5 to 13.5 micron atmospheric window. However, its apparent greater photoconductive gain discussed below gives it certain advantages in astronomical applications.

The other general features of the two systems, for appropriately

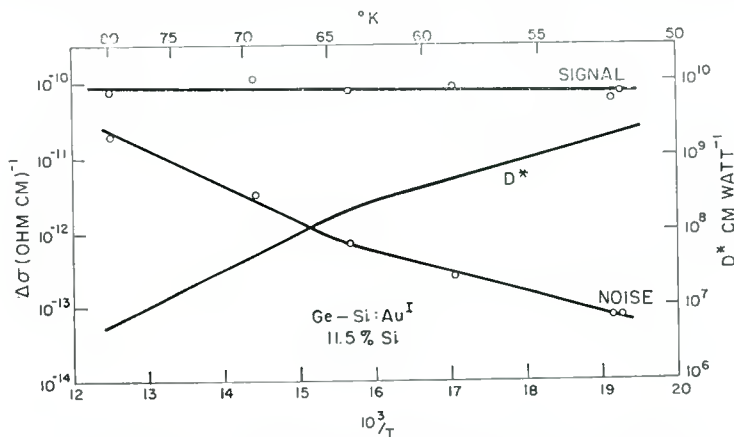


Fig. 12—Temperature dependence of signal, noise, and detectivity for a gold-activated alloy.

chosen alloy compositions, are similar. Curves giving the variation with temperature of the signal conductivity, the r-m-s noise conductivity, and the 500° K black-body detectivity for a typical gold-activated alloy sample are given in Figure 12. The signal conductivity is nearly temperature independent. The noise conductivity decreases rapidly with decreasing temperature. Below about 64° K, the  $\Delta\sigma_n$  curve exhibits the exponential dependence upon  $1/T$  predicted by Equation (10) and has a slope which corresponds approximately to  $E_i/2$  as required by this equation. The 500° K black-body detectivity,  $D^*$ , derived from these signal and noise data increases with  $1/T$  at a rate determined primarily by the temperature dependence of the noise. The value at 50° K is  $3.1 \times 10^9$  cm watt<sup>-1</sup>. This is to be compared with a value of  $4.0 \times 10^9$  cm watt<sup>-1</sup> for the zinc-doped sample of Figure 9 at the same temperature.

It may be noted that the values of  $\Delta\sigma_s$  (for the same incident radiant flux) and  $\Delta\sigma_p$  are both roughly one order of magnitude larger for the gold-doped alloy sample than for the zinc. The dark conductivities also exhibit approximately this same ratio. This difference appears to be typical of the two types of material. At the present time, however, it is not possible to say which of the parameters (mobility, lifetime, etc.) characteristic of the materials are responsible for this difference.

Some observations have been made which indicate that the properties of the gold-doped alloys depend upon the degree of compensation in a manner similar to that discussed above for the zinc-doped alloys. The investigation of these effects has not yet been carried to a state which would warrant any detailed discussion at this time.

In an earlier section, it was pointed out that both gold- and zinc-activated alloy photoconductors appear to lie on a straight line when log detectivity is plotted against the reciprocal of the product of long-wavelength limit and cell temperature. A nomograph which gives detectivity in terms of photoconductor temperature and long-wavelength limit is shown in Figure 13. This nomograph, which applies to the activated photoconductors discussed here, is very useful for determining the operating conditions of a cell which must meet certain wavelength and detectivity requirements. It should be mentioned that there is some variation from cell to cell for any one type so that the nomograph cannot replace detailed measurements of a particular cell for critical systems application.

#### OPTICAL CONSIDERATIONS

The concentration of activator atoms of a given impurity which can be introduced into the alloy is definitely limited. This limit is set by two factors, (1) the limited solubility in the semiconductor of the impurity in question and (2) the tendency to approach impurity banding if the concentration is too high (i.e., the tendency of impurities to form "conduction" bands lying below the true conduction band of the material or a "valence" band above the true valence band.)

Experimentally it was found that when gold is used as the activator, a concentration of about  $3 \times 10^{15}$  atoms/cm<sup>3</sup> is the maximum concentration practical due to the limited solubility of gold in the alloy. With zinc, the activator concentration should not be higher than about  $10^{16}$  atoms/cm<sup>3</sup>. This limit is not set by the solubility of zinc but rather by the fact that at higher concentrations the material shows excess conductivity at low temperatures due to impurity banding.

After compensation, the concentration of activator centers avail-

able for photoconductive excitation is in the range of  $2 \times 10^{15}$  to  $6 \times 10^{15}$  centers/cm<sup>3</sup>. Each activator center presents a radiation absorption cross section of the order of  $10^{-16}$  cm<sup>2</sup>. Therefore, these photoconductors are relatively transparent to radiation between the long-wavelength limit and the intrinsic absorption edge. Transmission measurements at liquid nitrogen temperature of an alloy of 7.5 per

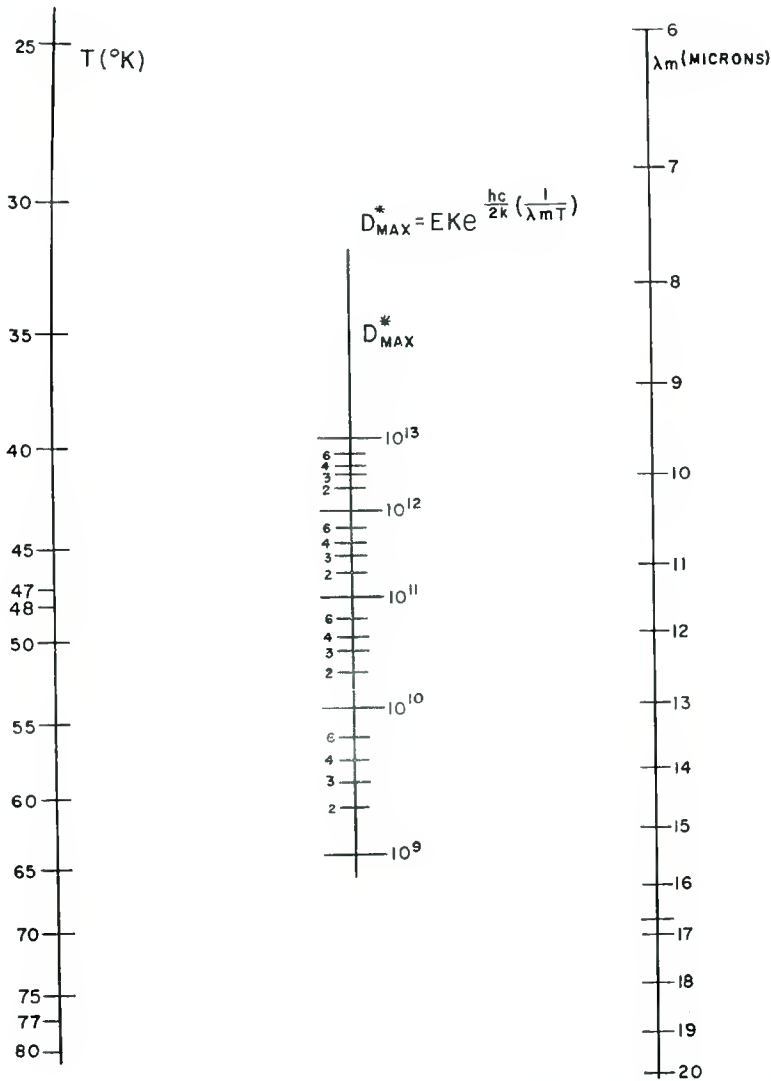


Fig. 13—Nomograph relating detectivity, operating temperature, and long-wavelength limit.

cent silicon in germanium activated with zinc to have about  $5 \times 10^{15}$  uncompensated activator centers have been made. There is a sharp rise in transmission at the intrinsic absorption edge. From this wavelength to about 10 microns, the transmission remains relatively constant and then rises again until 12 microns is reached. This rise is the long-wavelength edge of the activator band. The absorption coefficient calculated from these transmission measurements, shown in Figure 14, is about  $1 \text{ cm}^{-1}$  in the useful range of the photoconductor. Similar measurements at room temperature show no rise in transmission at the long-wavelength limit of the impurity response. This is to be expected inasmuch as all the impurity-activator centers are ionized and the absorption observed is that due to the free carriers.

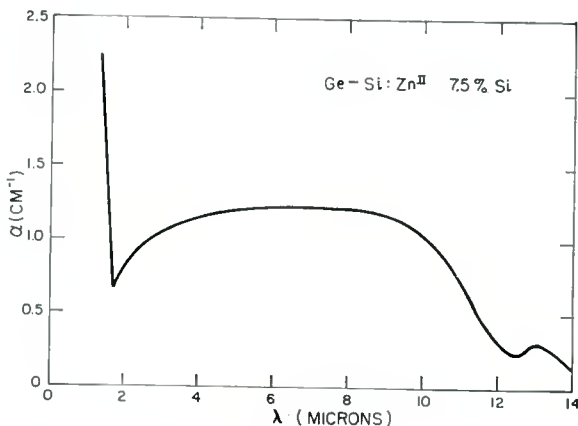


Fig. 14—Optical absorption coefficient of a zinc-activated alloy.

The relatively high transparency of this class of photoconductor means that the material cannot be used in the form of a thin film as is done with the opaque intrinsic photoconductors such as lead telluride and indium antimonide. Instead, special cell forms have been worked out which permit efficient usage of the radiation in spite of the transparency of the material. In the case of very small cells, the material is placed in an integrating chamber so that radiation which enters through the aperture of the chamber passes through the crystal many times before it is finally absorbed or lost. For larger cells, it is possible to take advantage of the high index of refraction of the material and shape the cell so that there is a large number of total internal reflections.

The integrating chamber is a small chamber with highly reflecting

sides within which the crystal is mounted. An aperture in this chamber serves as the working area of the detector cell. The chamber and crystal are maintained at a low temperature. The optimum size of crystal and chamber can be worked out from the following signal-to-noise ratio considerations.

Radiation which enters the cell is (a) usefully absorbed by the crystal, (b) absorbed by the walls or electrical contacts of the crystal, or (c) escapes through the aperture. The radiation producing a photoconductive signal is therefore given by the following expression:

$$F = \left( \frac{4\alpha_p(N_A - N_D)V}{A + A'\beta + 4\alpha_p(N_A - N_D)V} \right) P, \quad (20)$$

where

$A$  is the aperture area

$A'$  is the wall area

$(1 - \beta)$  is the wall reflectivity

$P$  is the radiation flux entering the chamber.

The generation-recombination noise of the crystal has the form given by Equation (10). Therefore, the signal-to-noise ratio in terms of size of the crystal and area of the aperture can be expressed as follows:

$$\frac{S}{N} = 2\alpha_p \left[ \frac{2(N_A - N_D)\tau N_D}{N_C \Delta f} \right]^{1/2} \frac{V^{1/2}}{A + A'\beta + 4\alpha_p(N_A - N_D)V} \exp\left(\frac{hc}{2k\lambda_m T}\right). \quad (21)$$

For a given aperture, this expression can be maximized in terms of volume of photoconductor yielding the following expression for the optimum value:

$$V_{\text{opt}} = \frac{A + A'\beta}{4\alpha_p(N_A - N_D)}. \quad (22)$$

This expression gives the design parameters for the optimum detector cell for use where small sensitive areas are required. Figure 15 is an outline of a typical detector showing the arrangement of photoconductor, its electrical contacts, and the integrating chamber.

For larger cells, the ratio of crystal volume to aperture area makes an integrating chamber inadvisable. Instead, advantage can be taken of the high index of refraction of the material to obtain long radiation path lengths by using a number of total internal reflections. A ray entering the face of the cell will be refracted toward the normal by the large index of refraction. The maximum deviation from a normal to the surface for a ray entering at approximately grazing incidence is  $14^\circ$ , the critical angle for total internal reflection. If the bottom of the crystal is cut in the form of a "roof" prism (the two planes defining the prism making angles to the normal from the front face of  $62^\circ$ ), radiation from the front face will be totally reflected first by the bottom prism and then by the sides of the crystal and will stay within the crystal over a path approximately three times the length of the crystal. The expression for the signal-to-noise ratio under these circumstances in terms of the geometrical factors of the crystal is given as follows:

$$\frac{S}{N} = \frac{K_1(1 - e^{-3\alpha x})}{K_2 A^{1/2} x^{1/2}}, \quad (23)$$

where  $\alpha$  is the absorption coefficient,  $x$  the depth of the crystal and  $A$  the area of the face. Differentiating this equation with respect to  $x$  and equating to zero to obtain the maximum, the following result is obtained:

$$\frac{S}{N} = K(1 - e^{-3\alpha x})x^{-1/2}$$

$$\frac{d}{dx} \left( \frac{S}{N} \right) = K \left[ -\frac{1}{2} x^{-3/2} (1 - e^{-3\alpha x}) + 3\alpha e^{-3\alpha x} x^{-1/2} \right] = 0 \quad (24)$$

$$e^{-3\alpha x} = (1 + 6\alpha x)^{-1}$$

$$x = 0.47 \text{ cm.}$$

An efficient cell, therefore, is one with a face having dimensions of  $0.5 \times 0.5$  cm and a depth of 0.5 cm shaped as shown in Figure 16(a).

As has been pointed out, the bottom of the photoconductor must be slanted in order to receive total internal reflection. The exact angle to preserve total internal reflection depends upon two factors; (1) the maximum angle of incidence of radiation upon the surface of the cell, and (2) the index of refraction of any bonding material used to mount the crystal. For example, if a plastic resin is used to mount the crystal both for structural reasons and to provide good thermal contact

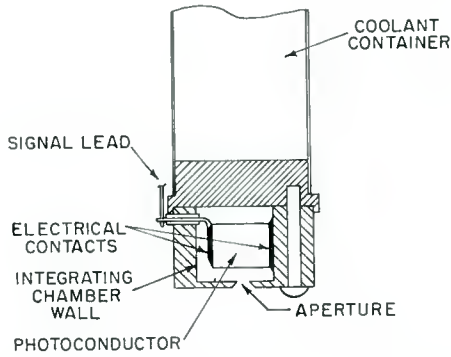
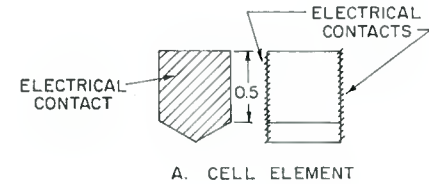


Fig. 15—Typical integrating chamber assembly.

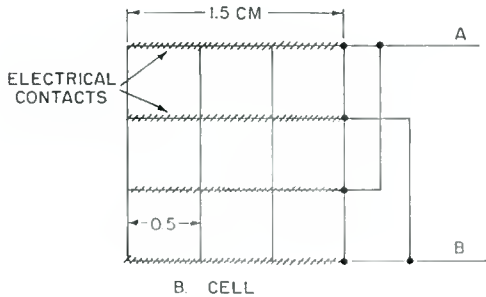
with a cooling chamber, this index of refraction will be approximately 1.5. Under these circumstances, the angle of total internal reflection at surfaces thus bonded will be:

$$\sin \theta = \frac{1.5}{4.0},$$

$$\theta = 22^\circ.$$



A. CELL ELEMENT



B. CELL

Fig. 16—(a) Cell element shaped to enhance internal reflections, and (b) Multiple element cell configuration.

Consequently, instead of the bottom faces making an angle of  $62^\circ$  to the normal from the front face, they must make an angle of  $54^\circ$ . Again, if the maximum angle of rays entering the crystal surface is less than  $90^\circ$  due to limitations of the angular aperture of the system, the angle of the bottom faces lies between the two values calculated above.

Where the detector requires a very large sensitive area, arrays of cells of the type illustrated in Figure 16(a) will give the required area. In addition to optical efficiency and good signal-to-noise ratio, certain electrical advantages are obtained using a multi-element arrangement. Figure 16(b) illustrates a nine-element multiple cell having a working area of  $1.5 \times 1.5$  cm.

#### ELECTRICAL CONSIDERATIONS

As is clear from the foregoing, the response of a photoconductive cell to infrared radiation near threshold levels is a small change in conductivity superimposed on the dark conductivity of the material. In the range of flux levels of interest, the electrical circuitry must be able to distinguish fractional changes in conductivity of the order of  $10^{-7}$ . Furthermore, the performance of the detector improves exponentially with the reciprocal temperature of the material as long as the cell generation-recombination noise exceeds the amplifier noise. Therefore, it is critically important for a high-sensitivity detector to use the most sensitive, low-noise, high-impedance amplifier possible, with a frequency pass band which can be accurately controlled. The amplifier problem has not yet been wholly solved, but amplifiers are available which will allow detector systems to operate under conditions where the noise equivalent power is  $10^{-11}$  to  $10^{-12}$  watt.

The amplifier most frequently used with this type of detector is shown schematically in Figure 17. It consists of a low-noise cathode-follower first stage followed by several stages of voltage amplification working into either a synchronous detector or a sharply tuned filter as, for example, two stages of twin "T" coupled amplifiers. At the low temperature where these photoconductive materials operate to best advantage, their impedance is quite high. Typical cells will have resistances ranging from 5 to 20 megohms. Therefore the load resistors and amplifier vacuum tube for the first stage must be selected with considerable care. Since there is considerable voltage across the load resistors during operation (100 to 200 volts), it is frequently desirable to use wire-wound or metalized resistors to avoid the possibility of current noise. A number of tube types are acceptable as in the first stage of the amplifier. For example, type 12AX7 is found

to have relatively low flicker noise and to operate satisfactorily in conjunction with a high-impedance input circuit.

At low temperatures the capacitance of the material is an important consideration in amplifier design. As a working figure, the dielectric constant may be considered the same as that of germanium, namely, 16. A typical cell having a photoconductor 5 mm on an edge will have a capacitance of about .7 micromicrofarad. At a chopping frequency of 100 cycles, the capacitive reactance of such a cell will be about  $10^9$  ohms, and, at 1000 cycles, it will be about  $10^8$  ohms. These values are high enough so that the cell may be considered as essentially resistive in its electrical behavior at these frequencies.

In designing the coupling between the cell and the amplifier, it should be borne in mind that the objective is to minimize amplifier

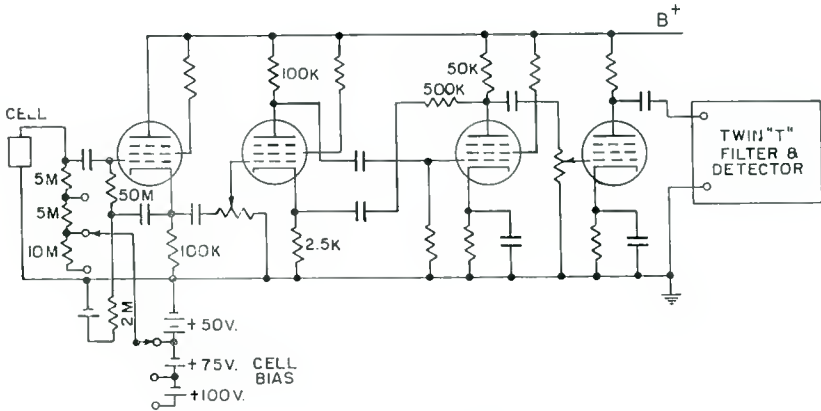


Fig. 17—Cell amplifier.

noise rather than to obtain maximum coupling efficiency. Therefore, it is frequently expedient to use a load resistor which is much lower than the cell resistance. In general, the most practical design is one where the load resistance is just high enough so that generation-recombination noise (or radiation-background noise) limits the performance of the system. Further increase of load resistance above this value does not improve the signal-to-noise ratio of the system and only serves to enhance microphonic and other difficulties.

The following specific problem of the amplifier required for an assumed cell illustrates some of the considerations involved in the design of the associated circuits.

The schematic diagram of the cell and amplifier is shown in Figure 18. The cell element has an area 0.25 cm<sup>2</sup> and a depth of 0.5 cm. The

dielectric constant is 16 and the resistivity at operating temperature is  $10^8$  ohm cms. The resistance of the cell is therefore

$$R_C = 200 \text{ megohms,}$$

$$C = 1 \text{ } \mu\text{f.}$$

The capacitance represents a reactive impedance of about 2000 megohms and can be neglected in comparison with the resistive component.

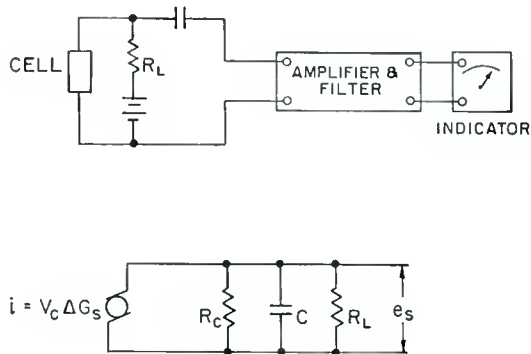


Fig. 18—Equivalent cell circuit.

The signal voltage  $e_s$  supplied to the first stage of the amplifier can be calculated from the following relation:

$$e_s = V_C Z(\Delta G), \quad (25)$$

where

$$|Z| = \frac{R_L R_C}{\sqrt{(R_L + R_C)^2 + 4\pi^2 C^2 R_C^2 R_L^2}}.$$

If it is assumed that  $R_L \ll R_C$ , which is permissible in this example, Equation (25) simplifies to

$$e_s = V_C R_L \Delta G_s. \quad (26)$$

$V_C$  is the maximum voltage that can be applied to the cell without noise breakdown and is approximately 100 volts. If a radiation flux of  $2 \times 10^{-11}$  watt is assumed,  $\Delta G_s$  has a value of about  $4 \times 10^{-16}$  ohm $^{-1}$ . With  $R_L = 20$  megohms,

$$e_s = 8 \times 10^{-7} \text{ volt.}$$

A well-designed amplifier with a type 12AX7 input stage will have a noise voltage of  $\sim 2 \times 10^{-8}$  volt. Clearly, therefore, the system will be limited by generation-recombination noise when employing a cell operating at  $\sim 50^\circ$  K.

In general, a well designed conventional amplifier using commercially available low-noise tubes is adequate for detectors working in the 8.5 to 13.5 micron window in terrestrial environment. Such a system, with a detector cooled to temperatures which can be achieved by liquid air under reduced pressures, will not be limited by noise generated by the amplifier or coupling circuits, but rather by either background radiation noise (if a large-angular-aperture optical system is employed) or by excitation-recombination noise (when the optical system employed severely limits the incident radiation).

When a detector system is operated at the very low temperatures which will yield best results for use in satellites and space craft outside the earth's atmospheric blanket, less conventional amplifiers must be employed to obtain full utilization of the capabilities of this class of photoconductive detector. Several types of amplifiers offer promise in this capacity. One which may be particularly suitable with low-noise photoconductors is a parametric amplifier using a mechanically driven variable condenser. Where such a system is used with a detector having a signal frequency  $f_1$  and pumped at a much higher frequency  $f_2$ , the expression for the gain of the system will be

$$G = \beta \frac{\Delta C}{C_A} \frac{f_2}{f_1}, \quad (27)$$

where  $\Delta C/C_A$  is the fractional change of the variable capacitor and  $\beta$  is the transfer function. For example a gain of 10 to 100 is practical with an amplifier in which the output is taken off the idler circuit at a frequency  $f_2 - f_1$ , where the chopping frequency  $f_1$  is 100 cycles and the pumping frequency  $f_2$  is 10,000 cycles, and a capacitor designed to have  $\Delta C/C_A \approx 1$  is employed. If, now, the idling circuit and capacitor are cooled to the same low temperature at which the cell is operated, a signal will be amplified by an extremely low-noise amplifier up to a level where it can be introduced into a conventional tube amplifier. This type of parametric amplifier will give an improvement in signal-to-noise ratio of one to two orders of magnitude for cases where the input coupling circuit and first tube of the conventional amplifier is the source of the limiting noise. The similarity between this type of amplifier and a vibrating-reed electrometer is quite apparent.

The possibility of using impurity-activated alloys for the detection of shorter-wavelength infrared radiation, for example, around 5 microns, has also been investigated. Detectors of this type, even when cooled to liquid nitrogen temperature, have very low generation-recombination noise because of the relatively high ionization energy of the activator impurities. Here, again, an amplifier with a noise lower than that which can be achieved with commercially available vacuum tubes may be required. The type of parametric amplifier discussed in the preceding paragraph may represent the solution in this application also.

### CONCLUSION

In the preceding sections, some of the principal characteristics required of photoconductive infrared detectors for both terrestrial and astronomical applications have been discussed and a class of photoconductors meeting many of these requirements has been described. This class of photoconductors, which is constituted of the impurity-activated germanium-silicon alloys, is extremely flexible. It permits an adjustment of the long-wavelength limit to fit the application and the selection of a spectral response shape giving the most favorable results.

Zinc-activated alloy with a composition giving a 14-micron long-wavelength limit has, when cooled to temperatures that can be reached by liquid air at a reduced pressure, a photoconductive detectivity which is high enough so that it is essentially background limited when used in a large-aperture optical system. Such a detector is extremely useful for the detection of low-temperature objects through the atmospheric window around 10 microns.

Other activators in these alloys yield photoconductors with high photoconductive gain, as, for example, the lowest level of gold when operated at very low temperatures and used with a low noise amplifier. These photoconductors offer unique possibilities as detectors of satellites and space vehicles under nonterrestrial conditions.

In terms of detectivity for a given operating temperature and long-wavelength limit, this class of infrared photoconductors has a merit factor  $M^*$  more than two orders of magnitude higher than those calculated from the published performance characteristics of such low-temperature materials as PbTe and InSb. However, the merit factor for PbS at room temperature is nearly ten times greater than that of the activated germanium-silicon alloy photoconductors. Therefore research should continue on this class of photoconductors with the objective of improving its performance still further.

# SINTERED CADMIUM SULFIDE PHOTO- CONDUCTIVE CELLS\*

BY

C. P. HADLEY AND E. FISCHER

RCA Electron Tube Division,  
Lancaster, Pa.

*Summary*—This paper discusses the properties of sintered cadmium sulfide photoconductive cells. The information which is presented has been gathered during a long program leading to the large-scale commercial production of such cells. Fabrication techniques are discussed, as are properties of the host materials, activation impurities, electrodes, and packaging. Theory is presented regarding energy-level structure, sensitivity, time effects, geometry, ohmic contacts, and gamma. Finally, characteristics are discussed with respect to the practical application of the cells.

## INTRODUCTION

ALTHOUGH THE phenomenon of photoconductivity has been known for more than 75 years, large-scale commercial use of cadmium sulfide photoconductive cells is rather recent. Only within the last few years, since the development of techniques for fabricating large-area polycrystalline surfaces, has general use of such devices for control applications been possible. This paper summarizes information which has been gathered by RCA during the development and production of these cells.

## PREPARATION OF CELLS

Two types of cadmium sulfide photoconductive cells are shown in Figure 1. The important elements of such cells are the supporting substrate, the photoconductive layer, the metallic electrodes, and a protective enclosure.

The substrate must be strong, chemically inert, and able to withstand the sintering temperature required for processing the photoconductive material. Alumina and Pyrex<sup>†</sup> are among the useful materials for substrate construction.

The photoconductive layer is made in a manner similar to that described by Thomsen and Bube.<sup>1</sup> A water suspension containing

<sup>†</sup> Registered trade mark.

\* Manuscript received October 1, 1959.

<sup>1</sup> S. M. Thomsen and R. H. Bube, "High-Sensitivity Photoconductor Layers," *Rev. Sci. Instr.*, Vol. 26, p. 664, July, 1955.

cadmium sulfide, a copper salt, and excess chloride is applied to the substrate. The coated substrate is then fired in air at a temperature in the range of 500 to 700° C for a period which may vary between ten minutes and two hours.

The electrodes are applied by evaporation. Various metals may be used as electrode materials, the essential criteria being chemical stability and relatively low work function. The latter requirement is necessary to provide ohmic contacts, which are desirable if polarity effects are to be avoided. Because the properties of tin provide a good compromise between these two conflicting criteria, the use of this material produces cells having superior characteristics.

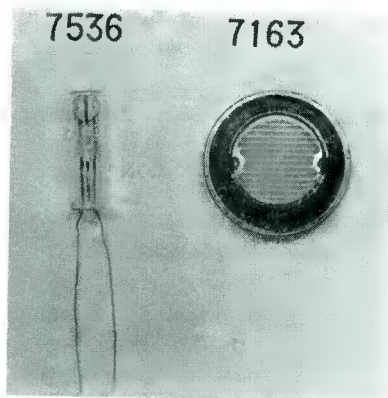


Fig. 1—Photograph of CdS cells.

It is essential that the finished cell be protected from moisture. Even a very small amount of water vapor will cause an erratic increase in the photocurrent and dark current. Slightly larger amounts of water encourage a chemical reaction between the electrode material and the cadmium sulfide which will in a short time cause catastrophic failure of the cell. It would, of course, be desirable from the point of view of cost to use a plastic material as the encapsulating medium. Exhaustive tests have shown, however, that even the best plastics which have been tried thus far are not sufficiently effective as a moisture barrier, and a cell enclosed in such a material may fail in moderate humidity in a matter of weeks. A long-life quality product requires the use of glass and glass-metal constructions such as those shown in Figure 1.

After the cell is completed, an aging schedule involving the application of heat, light, and voltage is usually required. This aging process insures a stable, sensitive, long-life product.

## PROCESSING CONTROLS

The properties of a photoconductor can be altered by the application of certain processing controls during design and production. These controls are discussed below with respect to their effect on the fundamental operation of the photoconductor.

A photoelectric event in cadmium sulfide proceeds approximately as follows.<sup>2-4</sup> An incident photon creates a hole-electron pair by exciting an electron from the valence band to the conduction band. Although the hole is captured immediately by a recombination center in the forbidden band, the electron remains in the conduction band for some time and is available to carry current. Finally, the electron and hole recombine to end the process.

The conductivity during excitation by photons,  $\sigma$ , is given by

$$\sigma = n_e e \mu$$

where  $n_e$  is the density of electrons in the conduction band,  $e$  is the electron charge, and  $\mu$  is the mobility of the electrons. The density of conduction electrons,  $n_e$ , is related to the incident photon flux as follows:

$$n_e = f \tau$$

where  $f$  is the rate of electron excitation per unit volume and  $\tau$  is the mean life of the excited electron. Creation of a sensitive photoconductor, therefore, depends on an increase in the mean life, which, in turn, is related to the density and character of centers within the forbidden band. A considerable number of such levels have been detected,<sup>4</sup> some of which are listed below.

**Chloride Level:** This donor level near the conduction band is caused by replacement of a sulfide ion in the lattice by a chloride ion and a loosely attached electron.

**Copper Level:** This level is caused by substitution of copper for cadmium in the lattice. The result is an acceptor level located about 1.7 electron volts below the conduction band.

---

<sup>2</sup> A. Rose, "An Outline of Some Photoconductive Processes," *RCA Review*, Vol. XII, p. 362, September, 1951.

<sup>3</sup> A. Rose, "Performance of Photoconductors," *Proc. I.R.E.*, Vol. 43, p. 1850, December, 1955.

<sup>4</sup> R. H. Bube, "Photoconductivity of the Sulfide, Selenide, and Telluride of Zinc or Cadmium," *Proc. I.R.E.*, Vol. 43, p. 1836, December, 1955.

**Sulfide Vacancy:** The absence of sulfide produces donor levels located between the chloride and copper levels.

**Cadmium Vacancy:** Cadmium vacancies produce acceptor levels located between the chloride and copper levels.

**Other Levels:** A number of other levels have been observed, but not identified.

The general statement may be made that any process which raises the Fermi level in the cadmium sulfide tends to increase sensitivity and dark current, to reduce the speed of response, and to reduce gamma in the useful illumination range. Gamma is defined as the fractional change in photoconductivity per incremental fractional change in incident illumination.

Various process controls may cause a change in the Fermi level, as follows:

1. An increase of chloride in the lattice tends to raise the Fermi level. In the method of surface preparation described previously, the amount of chloride added to the suspension is usually far in excess of the amount desired in the lattice, and the controlling factor is the solubility of the chloride in the cadmium sulfide.
2. An increase of copper in the lattice lowers the Fermi level.
3. Vacuum treatment tends to raise the Fermi level.
4. Air baking raises the Fermi level.
5. Treatment with strong light lowers the Fermi level.

#### GEOMETRICAL CONSIDERATIONS

A typical photoconductive element consists of a sensitive layer having a thickness  $S$  and an electrode pattern such as that shown in Figure 1. Such an electrode structure can be said to have a gap length  $l$  and a gap width  $w$ . If the cadmium sulfide layer is thin enough so that the conductive electrons are uniformly distributed, the conductance,  $g$ , is given by the following relation:

$$g = \sigma \frac{lS}{w} \quad (1)$$

where  $\sigma$  is the bulk conductivity. Both the photosensitivity and dark current are raised by an increase in the thickness of the cadmium

sulfide layer, although the rate of increase becomes small if the layer is much thicker than about 0.002 centimeter. If the product  $\sigma S$  is replaced by  $\sigma_s$ , the specific sensitivity, the conductance then is given by

$$g = \nu \sigma_s \quad (2)$$

where  $\nu$  is the number of conductive squares ( $\nu = l/w$ ). For the 7163 cell, shown in Figure 1, the geometrical factor,  $\nu$ , is 270 squares and the thickness  $S$  is 0.0006 centimeter. The current at an illumination

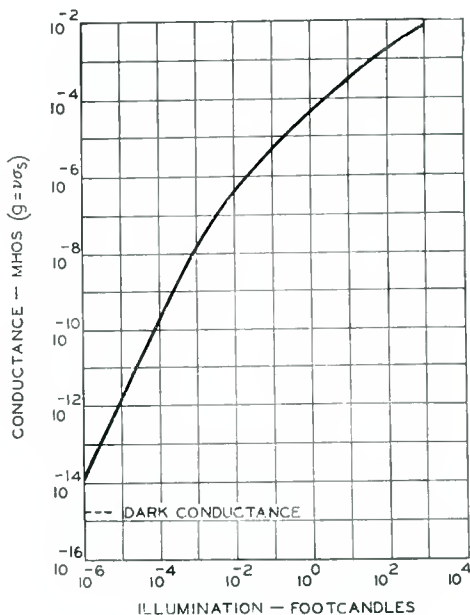


Fig. 2—Conductance versus illumination.

of one foot-candle of tungsten light (2870° K color temperature) and a voltage of 50 volts is two milliamperes. The specific sensitivity,  $\sigma_s$ , is not a constant but depends on the illumination, as shown in Figure 2.

For more complicated electrode patterns, the geometrical factor,  $\nu$ , is given by

$$\nu = \frac{A}{a w} \quad (3)$$

where  $A$  is the gross area of the surface and  $a$  is the distance of repetition of the electrode pattern.

## GAMMA AND SENSITIVITY

Over limited ranges of illumination, the specific sensitivity may be represented by

$$\sigma_s = \sigma_{s0} L^\gamma \quad (4)$$

where  $L$  is the illumination and  $\sigma_{s0}$  and  $\gamma$  are constants. For the complete device, the conductance  $g$  is given by

$$g = \nu \sigma_s = g_0 L^\gamma \quad (5)$$

where  $g_0 = \nu \sigma_{s0}$ .

Equation (5) is applicable over one or two orders of magnitude of illumination. For greater ranges,  $\gamma$  may not be considered a constant, as shown by the curve in Figure 2. Over the useful range of input radiation,  $\gamma$  tends to decrease as the illumination increases. Bube and Rose<sup>2-4</sup> have explained this behavior of  $\gamma$  on the basis of the energy-level picture described previously and have pointed out that the effect is due to a rise in the quasi Fermi level with increasing illumination and to the distribution of energy states within the band gap (the quasi Fermi level is defined by the equation  $n_c = N_c \exp(e\zeta'/kT)$ , where  $N_c$  is the effective density of states in the conduction band and  $\zeta'$  is measured from the bottom of the conduction band). Because the Fermi level can be affected by chemical composition as well as by light, it may be inferred that any processing control which raises the Fermi level tends to decrease  $\gamma$ . Extensive measurements have shown that a decrease in copper, for example, decreases  $\gamma$ . The curve shown in Figure 2 may be considered as the characteristic curve of a particular cadmium sulfide photoconductive device. This characteristic may be controlled as follows:

1. Any process which raises the Fermi level (addition of chloride, reduction of copper, or the like) tends to shift the characteristic curve to the left.
2. Any change in geometrical design which increases the number of conductive squares will raise the characteristic curve.
3. An increase in the thickness of the photoconductive layer tends to raise the characteristic curve, but only to a limited degree because the material is relatively opaque.

## TIME EFFECTS

For a given condition of input radiation, the conductivity may be expressed as follows:

$$\sigma = N_c e \mu \exp \left[ \frac{e \zeta'}{kT} \right]$$

If the input radiation is suddenly removed, the rate of change of conductivity may be found by differentiation of this equation as follows:

$$\frac{d\sigma}{dt} = \sigma \frac{e}{kT} \frac{d\zeta'}{dt}.$$

The quantity  $d\zeta'/dt$  may be determined as a function of the density of states in the energy range  $d\zeta'$  and the recombination rate  $n_c/\tau$ :

$$\frac{d\zeta'}{dt} = - \frac{n_c}{\tau N(\zeta')}.$$

The rate of change of conductivity can then be expressed as follows:

$$\frac{d\sigma}{dt} = - \frac{\sigma e f}{kTN(\zeta')} \quad (6)$$

where  $N(\zeta')$  is the density of states per unit energy range at the level  $\zeta'$ .

Figures 3 and 4 show the time effects for various conditions of illumination and previous history. Although the rise or decay of photocurrent is not entirely an exponential function of time, an exponential function may be assumed for approximate analyses. The time constant is then dependent on the illumination in the following manner:

$$\tau_L = \frac{\alpha}{L\beta} \quad (7)$$

where  $\tau_L$  is the time constant associated with the illumination  $L$ , and  $\alpha$  and  $\beta$  are constants.

#### OHMIC CONTACTS

In the discussion thus far, it has been assumed that the effect of the contacts cannot be detected in the performance of the cell. This assumption is the operational definition of an ohmic contact. Physically, the ohmic contact is obtained by use of a metal whose work

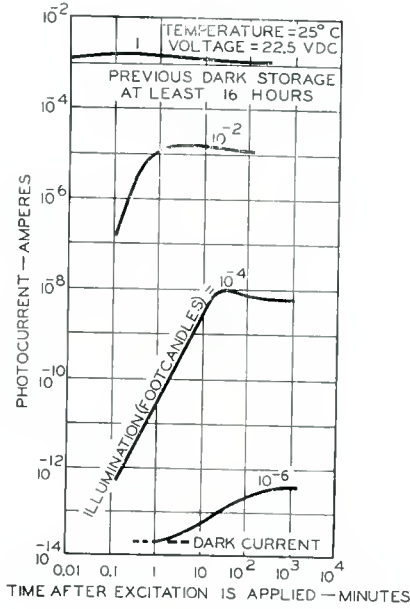


Fig. 3—Rise characteristics.

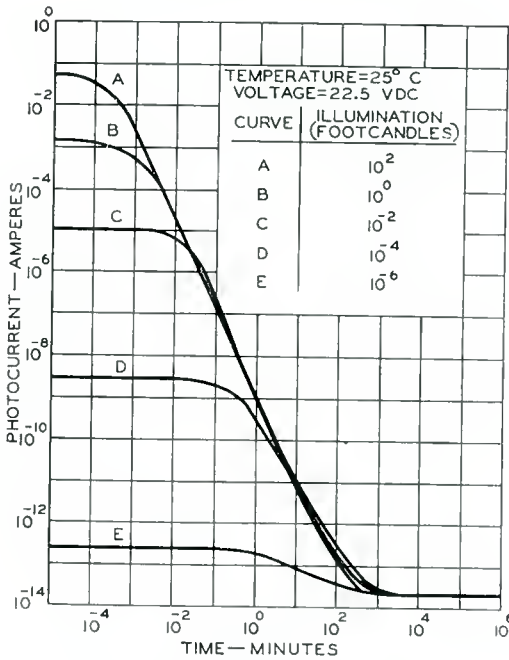


Fig. 4—Decay characteristics.

function is at least as low as that of the semiconductor. The three electrode materials which have had general use in the industry are gold, tin, and indium. Some of their pertinent properties are listed below:

<u>Material</u>	<u>Work Function (electron volts)</u>	<u>Contact on CdS</u>
Gold	4.9	nonohmic
Tin	4.3	ohmic
Indium	4.0	ohmic

One of the disadvantages of a nonohmic contact is the nonlinear relationship between current and voltage. Figure 5 shows a potential-energy diagram of the conditions near a nonohmic contact between a metal and a semiconductor. The contact is assumed to be at the negative end of the circuit. Only a single energy level is drawn, and surface states are assumed to be unimportant. The current, voltage, and thickness of the depletion layer are related in a manner which has been calculated by Schottky. This calculation is summarized by Mott and Gurney.<sup>5</sup> The solution predicts nonlinear behavior of the current-voltage characteristic, but suggests that linearity would be obtained for applied voltages much in excess of  $kT/e$ . Experimental results show, however, that if gold electrodes are used on cadmium sulfide, for example, the current varies almost as the square of the applied voltage over rather wide ranges. Presumably, the height of the barrier is modified by the field, possibly in a manner similar to that observed as the Schottky effect in thermionic cathodes.

A second disadvantage of nonohmic contacts is the introduction of a time delay in current-voltage phenomena. If the voltage across the cell shown in Figure 5 is suddenly increased, an increase in the width of the depletion layer is indicated. This increase in width is delayed, however, because it must be accompanied by an emptying of some of the occupied states. The emptying of these states is not instantaneous, but requires a time similar to that described in Equation (6). Thus, the time constant of the current-voltage change is controlled by the illumination in the same manner as shown in Figures 3 and 4.

One result of the effect just described is that the photoelectric response of the cell is less under a-c than d-c conditions. Under an illumination of one foot-candle, for example, when 60-cycle-per-second alternating voltage is applied to a cadmium sulfide cell having gold electrodes, the photocurrent will be only about one half of that obtained when a constant voltage is used. When tin or indium electrodes are used, this effect is much smaller.

<sup>5</sup> N. F. Mott and R. W. Gurney, *Electronic Processes in Ionic Solids*, The Clarendon Press, Second Edition, Oxford, 1948, p. 174.

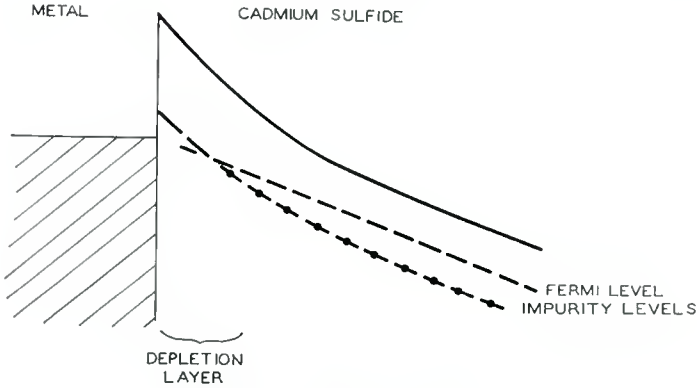


Fig. 5—Nonohmic contact.

#### ADDITIONAL CHARACTERISTICS

The spectral sensitivity curve of the 7163 is given in Figure 6. The peak of the response occurs at a wavelength of 5800 angstroms, which is slightly longer than that which would be expected if the band gap of cadmium sulfide were considered. The response tends to shift toward the red region as more copper is added.

As the temperature of the photoconductor rises, the sensitivity decreases, as shown in Figure 7. The effect is marked at lower input levels, and becomes negligible for illuminations above ten foot-candles.

Figure 8 shows that current is proportional to voltage when tin electrodes are used on the sintered cadmium sulfide. The linearity

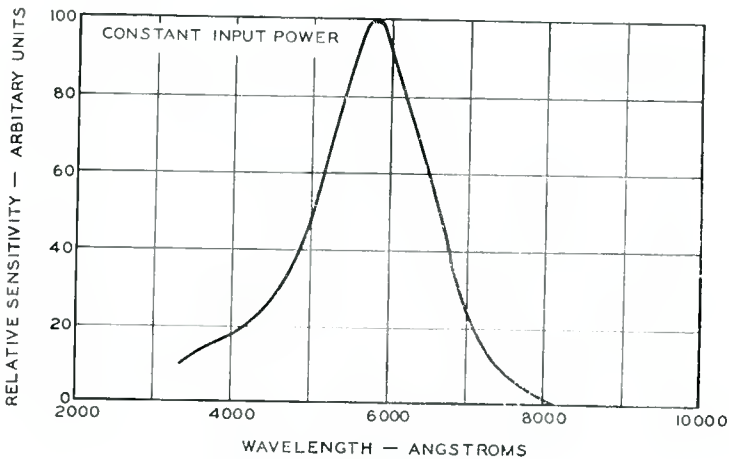


Fig. 6—Spectral response.

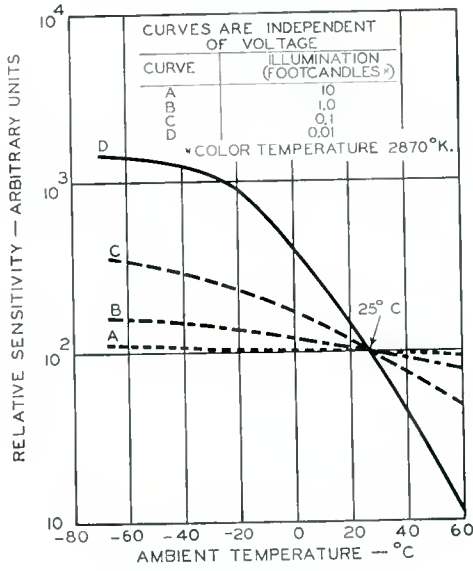


Fig. 7—Photoconductivity versus temperature.

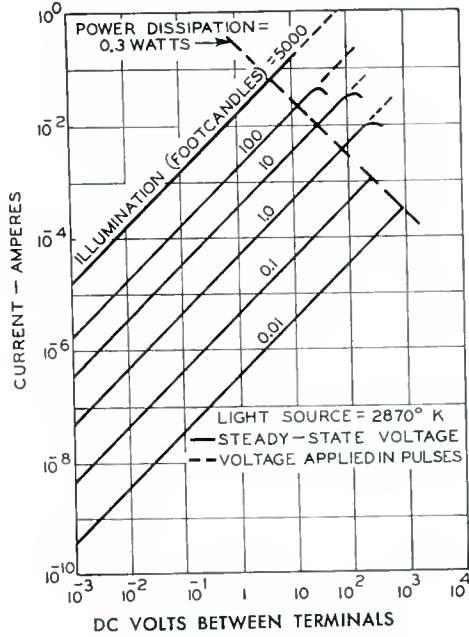


Fig. 8—Current versus voltage.

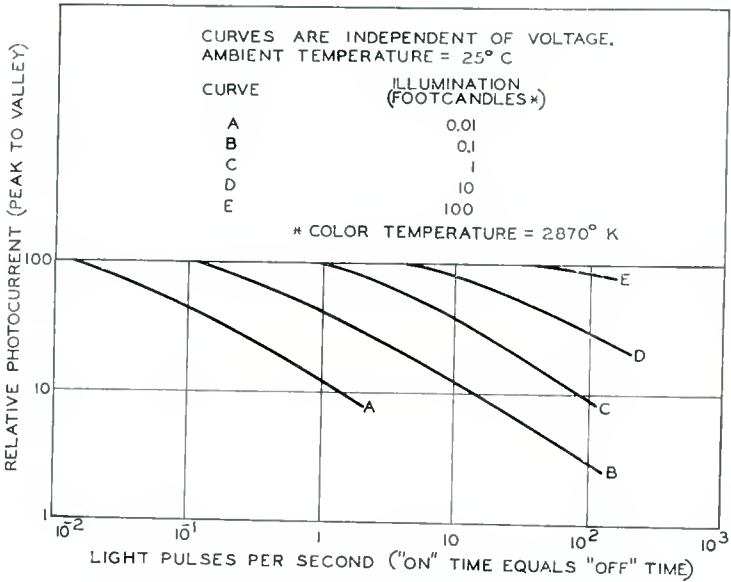


Fig. 9—Response to intermittent illumination.

extends over six orders of magnitude of applied voltage starting as low as 0.001 volt. At the higher dissipation ranges, the decrease in sensitivity with increasing temperature causes a decrease in photocurrent. If pulsed voltages are applied, however, linearity extends to at least 1000 volts.

In applications in which it is necessary to detect rapid light pulses of a repetitive nature, such as in particle counting, it is useful to know the peak-to-valley response as a function of the frequency of square-wave light input. Figure 9 shows such data. As would be expected, the frequency response is better for higher illumination.

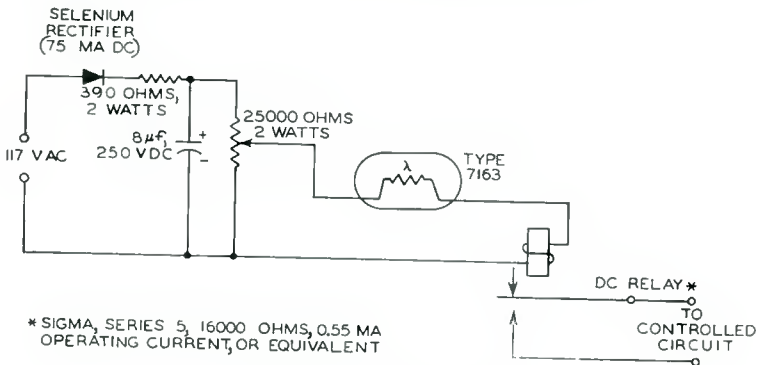


Fig. 10—Typical circuit.

A typical circuit for the 7163 cadmium sulfide cell is shown in Figure 10. In this circuit, the relay is normally energized when light is incident on the cell. When the light is interrupted, or the light level drops to a predetermined value, the relay opens. The potentiometer is employed to adjust the value of the photocurrent at which the relay activates. Light levels as low as one foot-candle may be used. The circuit of Figure 10 is intended for both "on-off" applications and applications in which the light level changes gradually.

#### ACKNOWLEDGMENT

The results reported on the previous pages obviously depend on work by many people. The authors acknowledge especially the contributions of G. S. Briggs, R. W. Christensen, and H. W. Kuzminski.

# THE ROLE OF SPACE-CHARGE CURRENTS IN LIGHT AMPLIFIERS\*

BY

A. ROSE AND R. H. BUBE

RCA Laboratories,  
Princeton, N.J.

*Summary*—The light-gain, the operating input light level and the exposure for single pictures are derived for light amplifiers of the sandwich type using adjacent layers of photoconductor and electroluminescent material. A key parameter in these relations is the voltage  $V_m$  at which space-charge current flow is initiated in the photoconductor. Also involved is a factor  $M$  which measures the ratio of recombination centers to traps, both evaluated near the Fermi level. Present photoconductors should permit: (a) light-gains of over 100-fold to be achieved at television frame rates, (b) operation at television frame rates with input light intensities as low as  $10^{-1}$  foot-candle, and (c) exposures for single pictures approaching photographic speeds. Improved performance depends strongly on attaining higher values of  $M$  in photoconductors.

## INTRODUCTION

THE LIGHT AMPLIFIER,<sup>1</sup> as developed by F. H. Nicoll and B. Kazan, consists essentially of a thin layer of electroluminescent (EL) powder adjacent to a thin layer of photoconductor (PC). The two layers form a sandwich between two outer electrodes across which an a-c voltage of several hundred volts is applied. Successful operation has been demonstrated with a-c frequencies ranging from less than 100 to about 10,000 cycles per second. In the dark, more than half the a-c voltage is across the PC. Under illumination, the PC becomes more conducting and the voltage shifts to the EL and generates light. Light gains of 100 to 1000 have been achieved. Response times from fractions of a second to tens of seconds are encountered and input-light intensities range from about  $10^{-2}$  to 1 foot-candle.

It is natural to inquire about the possibilities of extending the performance of the light amplifier toward higher gains, faster response times, shorter exposures, and lower input-light intensities. It is natural also to inquire about the internal properties or parameters of the photoconductor needed to achieve these extensions. A quick review shows that a dozen parameters need to be explored in order to define the performance of a light amplifier.

---

\* Manuscript received October 6, 1959.

<sup>1</sup> B. Kazan and F. H. Nicoll, "An Electroluminescent Light-Amplifying Picture Panel," *Proc. I.R.E.*, Vol. 43, p. 1888, December, 1955.

The purpose of this analysis is to derive a number of relatively simple relations both for the key performance parameters and for the hidden material parameters in terms of observables convenient for the designer of a light amplifier. This turns out to be possible only because space-charge current flow in insulators plays a dominant role in setting the limits of performance.<sup>2</sup> It is convenient, therefore, to express all of the parameters in terms of that voltage  $V_m$  at which space-charge current flow sets in.

#### ANALYSIS

Consider, as in the light amplifier, an a-c voltage applied across two adjacent layers of insulator. One layer is the PC and the second is the EL material. A significant shift of voltage from the PC to the EL will take place when the resistance of the PC is reduced to a value equal to its capacitive reactance. We take this as the operating point of the light amplifier.\* Under these conditions the increase in a-c power across the EL is approximately equal to the increase in power dissipated in the PC. We can then write

$$G_L = G_P \mathcal{E}, \quad (1)$$

where  $G_L$  is the light gain, or ratio of light power out to light power in,  $G_P$  is the power gain in the PC, and  $\mathcal{E}$  is the efficiency of the EL in watts of output light per volt-ampere across the EL. For the PC<sup>3,4</sup>

$$\begin{aligned} G_P &= \text{voltage gain} \times \text{current gain}, \\ &= G_V \times G_I, \end{aligned} \quad (2)$$

<sup>2a</sup> R. W. Smith and A. Rose, "Space-Charge-Limited Currents in Single Crystals of CdS," *Phys. Rev.*, Vol. 97, p. 1531, March, 1955.

<sup>b</sup> A. Rose, "Space-Charge-Limited Currents in Solids," *Phys. Rev.*, Vol. 97, p. 1538, March, 1955.

<sup>c</sup> M. A. Lampert, "A Simplified Theory of Space-Charge-Limited Currents," *Phys. Rev.*, Vol. 103, p. 1648, September, 1956.

<sup>d</sup> A. Rose and M. A. Lampert, "Photoconductor Performance, Space-Charge Currents and the Steady-State Fermi Level," *Phys. Rev.*, Vol. 113, p. 1227, March, 1959; also "Gain-Bandwidth Product for Photoconductors," *RCA Review*, Vol. XX, p. 57, March, 1959.

<sup>e</sup> R. W. Redington, "Maximum Performance of High-Resistivity Photoconductors," *Jour. Appl. Phys.*, Vol. 29, p. 189, February, 1958.

\* This condition is close to the point of *maximum* gain. The gain of the light amplifier will begin to exceed unity already at smaller light intensities and correspondingly smaller changes in resistance of the PC (see ref. 9).

<sup>3</sup> A. Rose, "Performance of Photoconductors," *Proc. I.R.E.*, Vol. 43, p. 1850, December, 1955.

<sup>4</sup> A. Rose, "La Photoconductivite," *L'Onde Electrique*, Vol. 34, p. 645, October, 1954.

$$G_V = \frac{eV}{h\nu}, \quad (3)$$

$$G_I = \frac{\tau_f}{T} = \frac{V\mu\tau_f}{d^2}, \quad (4)$$

where  $V$  is the voltage applied across the PC and  $h\nu/e$  is the volt equivalent of the photons.  $\tau_f$  is the lifetime of a free carrier in the photolayer,  $T$  is the transit time of a free carrier through the photoconductor, and  $\mu$  its mobility.  $d$  is the thickness of photolayer. Combining Equations (2), (3) and (4) with Equation (1), using 2.5 volts for  $h\nu/e$ ,

$$G_L = \frac{2V^2\mu\tau_f}{5d^2} \mathcal{E}. \quad (5)$$

The free-carrier density  $n_f$  is excited by the incident light intensity  $L$  (foot-candles) and for visible light may be written as

$$n_f = \frac{L}{d} \tau_f \times 10^{13} \text{ cm}^{-3}. \quad (6)$$

A lumen of visible light is taken to be  $10^{16}$  photons/second. Equation (6) is rewritten in the form

$$L = \frac{n_f d}{\tau_f} \times 10^{-13} \text{ foot-candles}. \quad (7)$$

Multiplying both sides by  $\tau_0$ , the photoconductive response time, gives

$$\text{Exposure} \equiv L\tau_0 = \frac{n_f d \tau_0}{\tau_f} \times 10^{-13} \text{ foot-candle seconds}. \quad (8)$$

Equations (5), (7), and (8) are purely formal relations for the performance properties of a light amplifier. They give, respectively, the light-gain, the operating input light intensity, and the exposure required for single pictures. At this point, the physics of space-charge current flow is introduced by computing that voltage  $V_m$  at which space-charge current flow is initiated. The expression for  $V_m$  will be inserted into Equations (5), (7), and (8) to transform them into relations containing only readily accessible design parameters.

The reason that space-charge currents play a significant part in the performance of light amplifiers is that they set an upper limit to the voltage that can be applied across the photoconductor.\* Suppose, for example, that the dark conductivity of the PC is just under its capacitive admittance so that a doubling of the conductivity will shift the voltage from the PC layer to the EL layer and cause the emission of light.\*\* This doubling of the conductivity should, in normal operation, be brought about by the input light intensity. It should not be brought about by the applied voltage, that is, by the addition of space-charge current. If space-charge current were to flow, the light emitted by the amplifier *with no light input* would be more than half of the maximum possible light output. The maximum permissible voltage is accordingly somewhat under that voltage at which the density of free carriers is doubled by the application of a voltage alone.

From previous work on space-charge current flow,<sup>2</sup> the voltage required to double the free carrier density is

$$\begin{aligned} V_m &= \frac{Q}{2C} \\ &= \frac{1}{2} n_f \frac{\tau_0}{\tau_f} ed \left( \frac{1}{C} \right) M \\ &= \frac{2\pi}{K} n_f ed^2 \frac{\tau_0}{\tau_f} M \times 10^{12} \text{ volts.} \end{aligned} \quad (9)$$

In the above relations,  $Q$  is the total charge that must be injected by the applied voltage in order to double the free-carrier density. Since the charge is distributed in the space between the cathode and anode faces rather than residing at the faces as in a normal capacitor, the effective capacitance is about twice the geometric capacitance, or  $2C$ . The total charge that must be injected is composed of both free and trapped charge. When the free-carrier density is doubled, so must the density of *all* electrons in trapping states down to the Fermi level also be doubled. Now the ratio of trapped to free charge, as measured by

---

\* The present analysis assumes that the contact to the photoconductor is ohmic. This is the common condition for high-gain photoconductors. On the other hand, if one could arrange to apply sufficiently high fields to the photoconductor through a blocking contact to achieve impact ionization, it is likely that even better performance would be attained. The present analysis does not cover impact ionization.

\*\* If the dark conductivity is less than this value, a bias light can be used to adjust it to the operating point.

the ratio of photoconductive response time to life time, is<sup>5</sup> just  $\tau_0/\tau_f$ . This ratio counts only those trapped charges that are effectively in thermal contact with the conduction band under illumination. Under many conditions these are all the trapped charges down to the Fermi level. Under some preferred conditions,<sup>24</sup> however, the total number of trapped charges is  $M$  times larger than those measured by the photoconductive response time. Hence the total charge density to be injected by the applied voltage is, as shown in Equation (9),

$$en_f \frac{\tau_0}{\tau_f} M.$$

Equation (9) may be simplified by incorporating into it the conditions that hold at the operating point of the light amplifier.

$$\text{Resistance of PC per cm}^2 \equiv R = \frac{1}{2\pi fC},$$

$$R = \frac{d}{n_f e \mu}.$$

Therefore,

$$n_f e \mu = \frac{d}{R},$$

$$= 2\pi f d C,$$

$$= \frac{Kf}{2} \times 10^{-12} \text{ cm}^{-3}. \quad (10)$$

Here  $K$  is the dielectric constant,  $e$  the electronic charge in coulombs, and  $f$  the frequency of a-c voltage applied across the light amplifier. Equation (10) is inserted in Equation (9) to give

$$V_m = \pi \frac{d^2 f \tau_0}{\mu \tau_f} M \text{ volts.} \quad (11)$$

We solve Equation (11) for  $\tau_f$  and insert the result in Equations (5), (7), and (8) to get

$$G_L = \frac{2\pi}{5} V_m f \tau_0 M \mathcal{E}, \quad (12)$$

<sup>5</sup> A. Rose, "An Outline of Some Photoconductive Processes," *RCA Review*, Vol. XII, p. 362, September, 1951.

$$L = \frac{KV_m}{2\pi d\tau_0 M} \times 10^{-6} \text{ foot-candles,} \quad (13)$$

$$L\tau_0 = \frac{KV_m}{2\pi dM} \times 10^{-6} \text{ foot-candle seconds,}$$

$$\doteq \frac{KV_m}{2\pi dM} \times 10^{-5} \text{ meter-candle seconds.} \quad (14)$$

Further useful relations are obtained by solving Equation (11) for the lifetime of a free carrier,

$$\tau_f = \frac{\pi d^2 f \tau_0}{\mu V_m} M \text{ seconds,} \quad (15)$$

and by solving Equations (10) and (11) for the density of electron-occupied traps,

$$n_t \doteq n_f \frac{\tau_0}{\tau_f} = \frac{KV_m}{2\pi d^2 M} 10^7 \text{ cm}^{-3}. \quad (16)$$

For the usual trap distribution, this is the density of traps near the Fermi level in the dark, that is, about 0.6 volt below the conduction band.<sup>5</sup>

## DISCUSSION

### *Light Gain*

We repeat Equation (12),

$$G_L = \frac{2\pi}{5} V_m f \tau_0 M \mathcal{E},$$

$$= \frac{1}{5} f \tau_0 M \quad \text{for } V_m = 200 \text{ volts}$$

$$\epsilon = 10^{-3},$$

and conclude that light gains of 100 or more are possible at television frame rates provided the frequency of the a-c voltage is 10,000 cycles per second.

*Low-Light Operation*

We repeat Equation (13),

$$L = \frac{KV_m}{2\pi d\tau_0 M} \times 10^{-6} \text{ foot-candles.}$$

By inserting a representative set of values for the parameters,

$$\begin{aligned} K &= 10, \\ V_m &= 200 \text{ volts,} \\ d &= 10^{-2} \text{ cms,} \\ \tau_0 &= 10^{-1} \text{ second,} \end{aligned}$$

we get

$$L = \frac{4 \times 10^{-1}}{M} \text{ foot-candles.}$$

Operation of the light amplifier at lower light intensities can come chiefly from  $M$  values greater than unity. Response times longer than  $10^{-1}$  second can, of course, be used to attain lower light levels if such slower frame rates are tolerable. Also, a significant advantage would be gained if  $V_m$  were reduced from 200 to 2 volts, but this requires the development of a new highly efficient EL process, such as low-voltage injection. The increased efficiency is needed in Equation (12) to offset the lower  $V_m$  and retain the same light gain.

*Exposure*

It is frequently suggested that a photographic film might be backed up with a light amplifier to extend the range of film towards lower lights or to shorter exposure times at a given light intensity. For this arrangement to be successful, the exposure required for the light amplifier should be less than that required for films. But from Equation (14) the exposure for a light amplifier is

$$\begin{aligned} L\tau_0 &= \frac{KV_m}{2\pi dM} \times 10^{-5} \text{ meter-candle seconds} \\ &= \frac{4 \times 10^{-1}}{M} \text{ meter-candle seconds} \end{aligned}$$

for  $K = 10$ ,  $V_m = 200$ , and  $d = 10^{-2}$  cm. Since the exposures required

for sensitive film are in the range of  $10^{-2}$  to  $10^{-3}$  meter-candle seconds, the light amplifier can not offer any advantage unless  $M$  values larger than 10 to 100 are achieved.

It should be noted that the expression for the exposure (Equation (14)) does *not* contain any parameters involving the sensitivity of the photoconductor. Actually, if we use Equation (8) for the exposure, we find that the number of photons needed is just the number required to raise the Fermi level by  $kT$ , that is, the number required to double the pre-existing number of free plus trapped electrons.

#### Trap Densities

It is evident from the discussion of light gains, low-light operation, and exposures that large  $M$  values would directly aid the performance of the light amplifier in all these respects. But large  $M$  values mean that the freedom from traps must be insured to a high order. In Equation (16),

$$n_t = \frac{KV_m}{2\pi d^2 M} \times 10^7 \text{ cm}^{-3},$$

we use the values  $K = 10$ ,  $V_m = 200$ ,  $d = 10^{-2}$ , and  $M = 100$  to compute an electron-occupied trap density near the Fermi level of

$$n_t = 4 \times 10^{11} \text{ cm}^{-3}.$$

While total trap densities in insulator materials are normally found to be  $10^{14} \text{ cm}^{-3}$  and greater, trap densities of  $10^{12} \text{ cm}^{-3}$  per  $kT$  at a depth of 0.5 to 1.0 volt from the band edge have been reported.<sup>6</sup>

#### Experimental

Finally, it is of interest to test the analytic results against the data on a single-element light amplifier reported by F. H. Nicoll<sup>7</sup> and the data by H. B. DeVore<sup>8</sup> on the  $M$  values of the type of CdSe cell used by Nicoll (see Table I). There are a number of uncertainties

<sup>6a</sup> R. W. Smith, "Some Aspects of the Photoconductivity of Cadmium Sulfide," *RCA Review*, Vol. XII, p. 350, September, 1951; also "Properties of Deep Traps Derived From Space-Charge-Current Flow and Photoconductive Decay," *RCA Review*, Vol. XX, p. 69, March, 1959.

<sup>6</sup> R. H. Bube and L. A. Barton, "The Achievement of Maximum Photoconductivity Performance in Cadmium Sulfide Crystals," *RCA Review*, Vol. XX, p. 564, December, 1959.

<sup>7</sup> F. H. Nicoll, "Properties of a Single Element Light Amplifier Using Sintered Cadmium Selenide Photoconductive Material," *RCA Review*, Vol. XX, p. 658, December, 1959.

<sup>8</sup> H. B. DeVore, "Gains, Response Times and Trap Distributions in Powder Photoconductors," *RCA Review*, Vol. XX, p. 79, March, 1959.

Table I—Comparison of Analytical Results with Data of F. H. Nicoll and Data of H. B. DeVore

$f$ (cycles/sec)	Data from Nicoll <sup>7</sup>			Data from DeVore <sup>8</sup>	Analytical Results	
	$\tau_0^*$ (seconds)	$G_L^\dagger$ $\left( \frac{\text{yellow light in}}{\text{yellow light out}} \right)$	L $\ddagger$ foot candles		$G_L$ computed from Eq. (12)	L $\#\#$ computed from Eq. (13)
420	1	1200	$2 \times 10^{-3}$	8	1600	$2 \times 10^{-3}$
2000	0.3	680	$10^{-2}$	3	850	$2 \times 10^{-2}$
4200	0.18	380	$2 \times 10^{-2}$	3	1050	$4 \times 10^{-2}$
10,000	0.05	110	0.1	0.5	120	0.8

\* Nicoll gives the rise and decay for times to within 80 per cent of the final values. We have taken these times and divided by two to approximate the time to rise or decay to 50 per cent of the final value. These response times are taken at the peak of the gain versus input light curves.

† Nicoll states that the light gain of these cells would be expected to be somewhat greater than the yellow-yellow gain since the photo cell does not peak in the yellow.

‡ DeVore estimates that  $1.4 \times 10^{16}$  photons per second per incandescent lumen is used by the CdSe cell. This is close enough to the figure  $10^{16}$  per second used in the analysis that no correction was made. The light intensities are taken at the peak of the gain versus input light curves.

# Equation (13) was modified to fit the geometry of the CdSe cell and takes on the form  $L = K' V_m / (d\tau_0 M) \times 10^{-6}$  foot-candles where  $d$ , the electrode separation, is 0.05 cm. and  $K'$  is an averaged value between air and the ceramic substrate of the cell. We have taken its value to be 2.

Table II—Comparison of Experimental and Analytical Results for a CdS Powder Light Amplifier

	Experimental (Hadley and Christensen) <sup>9</sup>	Computed from Eqs. (13) and (14)
Input light intensity at maximum gain	$4 \times 10^{-3}$ foot-candle	$3 \times 10^{-3}$ foot-candle
Input exposure at maximum gain	2 meter-candle seconds	0.6 meter-candle second

<sup>9</sup> C. P. Hadley and R. W. Christensen, "Solid-State Image Intensifier Under Dynamic Operation," *RCA Review*, Vol. XX, p. 670, December, 1959.

in data and interpretation such that the comparison of experiment and analysis should have only order of magnitude significance. That the experimental and computed values of  $G_L$  and  $L$  agree generally within a factor of 3 is probably fortuitous. The comparison is useful chiefly in giving some confidence in the analysis. For the computed values of  $G_L$ ,  $V_m$  was taken from Nicoll's work to be 400 volts and  $\mathcal{E}$  was estimated to be  $10^{-3}$ . The EL efficiency is probably the most uncertain factor.

Table II shows data of C. P. Hadley and R. W. Christensen<sup>9</sup> on the input light intensity for maximum gain and the single-picture exposure, also for maximum gain, for a CdS powder light amplifier. The corresponding values computed from Equations (13) and (14) are shown also in Table II. The value of  $M$  was taken to be 0.4 from DeVore's measurements on CdS powder. The value of  $M$  is, of course, subject to some variation from one powder sample to another since it depends on the intimate trap structure of the material.

#### ACKNOWLEDGMENT

We are indebted to F. H. Nicoll, H. B. DeVore and E. G. Ramberg for critical readings of the manuscript.

# PROPERTIES OF A SINGLE-ELEMENT LIGHT AMPLIFIER USING SINTERED CADMIUM SELENIDE PHOTOCONDUCTIVE MATERIAL\*

BY

F. H. NICOLL

RCA Laboratories,  
Princeton, N. J.

*Summary*—The use of photoconductive sintered cadmium selenide as the control element in a light amplifier offers the possibility of improved gain and speed of response. Such a single-element light amplifier has been made and tested. The results show that moderate gains with high output luminance are possible with speeds in a range suitable for moving pictures. Very high gains are possible if slow response can be tolerated.

Measurements were made over a range of operating frequencies and for various input levels. Data on rise time, decay time, and gain for tungsten-light input are given in curve form. From these curves the operating range and input-output light levels for useful picture reproduction can be determined.

## INTRODUCTION

SINCE THE first light-amplifier or solid-state image-intensifier panels were made,<sup>1</sup> the techniques for making the panels have been improved considerably. However, the performance of the various designs continues to be limited by the performance of the photoconductor. For example, in the application of the device to X-ray fluoroscopy,<sup>2</sup> the gain or amplification is in a useful range, but the device is limited to viewing of stationary objects because of the slow response of the photoconductor.

Many applications of image intensifiers require high gain and a speed of response sufficient for moving images. There are other applications, however, where gain could be sacrificed to obtain faster response if this were possible. Intensifiers have been made mainly with cadmium sulfide powder as the light- or X-ray-sensitive material. One of the most promising new photoconductive materials is sintered cadmium selenide. This material was first made experimentally by S. M.

---

\* Manuscript received October 6, 1959.

<sup>1</sup> B. Kazan and F. H. Nicoll, "An Electroluminescent Light-Amplifying Picture Panel," *Proc. I.R.E.*, Vol. 43, p. 1888, December, 1955.

<sup>2</sup> B. Kazan, "A Solid-State Amplifying Fluoroscope Screen," *RCA Review*, Vol. XIX, p. 19, March, 1958.

Thomsen,<sup>3</sup> and similar material is now available in a glass enclosed mounting as the C7218 photoconductive cell. This material is attractive because of its high sensitivity and relatively fast response. In addition, it is sensitive over the visible region of the spectrum and can be excited by most cathodoluminescent phosphors, fluorescent lamps, and tungsten light sources. The measurements described here were made on a photoconductive cell and an electroluminescent cell, without optical feedback, connected in series to form a single-element light amplifier.

The theory of light-amplifier operation has been described in a number of publications<sup>1,4,5</sup> and is not discussed here. Instead, a purely experimental approach is taken with a view to discovering what can be expected of the sintered cadmium selenide when it is used in a light amplifier. Of course, the performance of a large panel cannot exceed, and may even be inferior to the performance of a single-element amplifier.

#### PROPERTIES OF THE SINTERED CADMIUM SELENIDE PHOTOCONDUCTIVE CELL

The preliminary data sheet on the C7218 photoconductive cell\* gives sensitivity, decay and rise times, and spectral response. These are all given for low d-c fields which are not useful in light-amplifier operation. For this reason, tests were made to determine the behavior of a sintered cadmium selenide photoconductive cell at high fields (800 volts per mm). Results for d-c and a-c voltages are compared and these results are later compared with the cell's behavior with a-c in a light-amplifier arrangement. In the case of the light amplifier, the photoconductive operation is quite different since the field across the photoconductor changes as the current rises and decays.

Figure 1 is a plot of photocurrent as a function of applied d-c voltage for various levels of incident illumination. These results are not highly accurate, but do give a general indication of the interdependence of various parameters. At high currents and high voltage some heating occurs. This heating was reduced by keeping the time for readings to a minimum. The curves of Figure 1 are reduced to the

---

<sup>3</sup> S. M. Thomsen and R. H. Bube, "High Sensitivity Photoconductor Layer," *Rev. Sci. Instr.*, Vol. 26, p. 664, July, 1955.

<sup>4</sup> R. K. Orthuber and L. R. Ullery, "A Solid-State Image Intensifier," *Jour. Opt. Soc. Amer.*, Vol. 44, p. 297, April, 1954.

<sup>5</sup> G. Diemer, H. A. Klasens and J. G. van Santen, "Solid-State Image Intensifiers," *Philips Research Report*, Vol. 10, p. 401, December, 1955.

\* Tentative Data Sheet, RCA Developmental Type No. C7218, Radio Corporation of America, Electron Tube Division, Lancaster, Pennsylvania.

equivalent of the "standard" gap such as was used in the tests on powders, i.e., a gap 0.5 mm by 5 mm.

If the curves for low voltages are compared with the C7218 data sheet, it can be seen that the particular cell used in these tests is actually less sensitive.

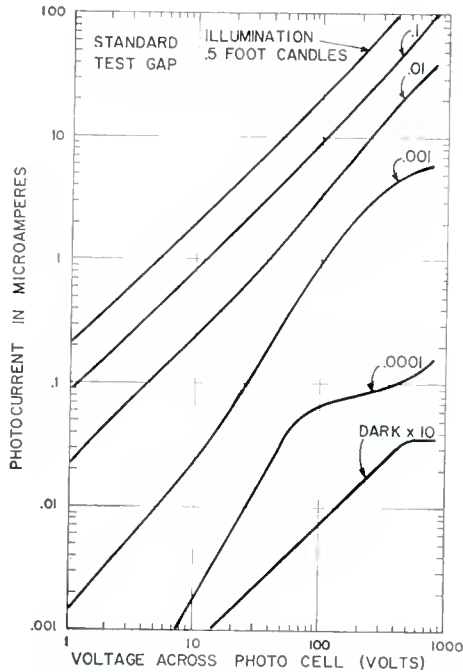


Fig. 1—Photocurrent versus voltage for sintered CdSe cell.

Figure 2 is a replot of Figure 1 and shows curves of photocurrent versus light for various d-c fields. These curves are extended much beyond the range of the C7218 data sheet in the direction of higher light levels and higher fields. No particular peculiarities show up in the operation of the cells under these conditions. Photocurrent is approximately proportional to voltage and rises somewhat less than linearly with input illumination. This is in contrast to the behavior of photoconductive powders in which current varies as the third or fourth power of the voltage, and the variation of current with light is superlinear. These differences are reflected in improved performance of the sintered-cell light amplifier.

Figures 3 and 4 show decay and rise curves measured on an oscilloscope for various incident light levels for 500 volts d-c and for 300

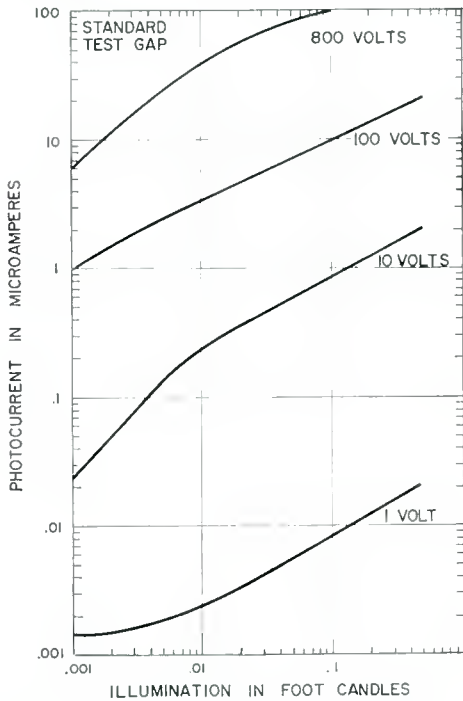


Fig. 2—Photocurrent versus illumination for sintered CdSe cell.

volts (rms) at 420 cps, respectively. This was done to establish the fact that the behavior with a-c and d-c is essentially the same. Values of decay and rise to 20 and 80 per cent of the initial values were used

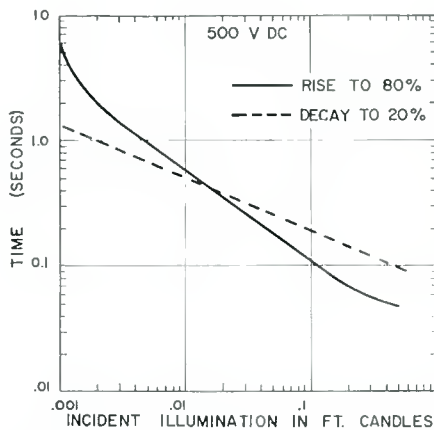


Fig. 3—Rise time and decay time for sintered CdSe cell, d-c applied voltage.

in the curves, since these values should be significant in indicating the performance of the photoconductor in a picture device. The actual rise and decay times when the photoconductive cell is used in series with an electroluminescent element will be quite different, partly because the output versus voltage characteristic of the electroluminescent layer is nonlinear and partly because the voltage across the photoconductor varies with light input. Nevertheless, the curves show that the photoconductor alone is capable of rise and decay times of 50 to 100 milliseconds if operated at sufficiently high light levels.

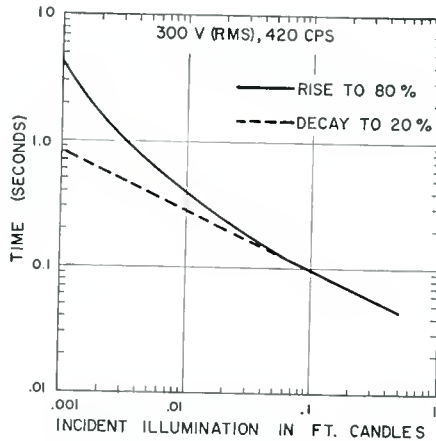


Fig. 4—Rise time and decay time for sintered CdSe cell, a-c applied voltage.

#### PROPERTIES OF A SINTERED CADMIUM SELENIDE CELL IN SERIES WITH AN ELECTROLUMINESCENT ELEMENT

To make the tests on the single-element light amplifier simulate the operation of a light-amplifier panel, the ratio of electroluminescent area to photoconductor area was made the same as would exist on a grooved photoconductor amplifier of the usual type.<sup>1</sup> An electroluminescent area of approximately .04 square inch was used. The capacitance of this layer is about 50 micromicrofarads. Care was taken to ensure that light from the electroluminescent layer did not feed back to the photoconductive cell.

Some experiments were first made to determine the most suitable operating voltage for the light-amplifier element. Six hundred volts rms was found to be a suitable value, since it is not so low that gain is greatly reduced nor so high that light is emitted from the electroluminescent layer when the photoconductor is in the dark. Therefore,

the measurements were made at this voltage and the frequency was varied.

Generally, input light was obtained from a 25-watt tungsten light bulb with no filter, conveniently variable over several orders of magnitude without color change. To evaluate energy gain, some tests were also made with yellow electroluminescent light input identical with the light output. The output was measured with a calibrated electron multiplier, and gain curves were plotted from the resulting input-output curves. Rise and decay times were measured for a range of input light levels and for various frequencies. Input light of the desired intensity was turned on or off by means of a shutter, and the rise or decay of the output light was measured with an electron multiplier and oscilloscope.

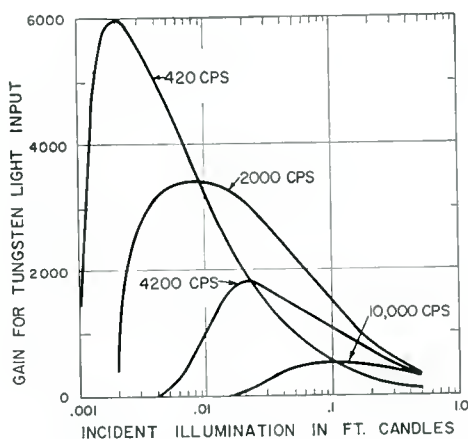


Fig. 5—Gain as a function of incident illumination for simple light-amplifier element.

Figure 5 shows luminous-gain curves as a function of tungsten light input for applied frequencies of 420, 2000, 4200, and 10,000 cps. It was found that the gain figure with yellow excitation was  $\frac{1}{5}$  that obtained with tungsten light. Real-energy gains with yellow excitation are, however, somewhat greater than this figure since the yellow light input does not match the response peak of the photoconductor.

In general, maximum gain is considerably reduced as the frequency is increased. This is also characteristic of the behavior of powder photoconductor light amplifiers and is partly due to the decrease in impedance of the electroluminescent layer at the higher frequencies. While the gain is reduced, the actual light output is increased and the device simply operates at higher input light levels where response is

faster. Higher input levels are desirable from the point of view of reducing rise time and decay time, provided gain does not drop below a useful figure.

The maximum gain, shown on the curves of Figure 5, is 6000, which corresponds to an *energy gain* greater than 1200. This is of special interest since powder-type light amplifiers having *energy gain* greater than 1200 are extremely slow in response, whereas the CdSe sintered type is considerably faster although still short of the speed required for observing motion at very low input levels. The increase in maximum gain as frequency is reduced was checked experimentally, and it appears that 420 cps is about the frequency of maximum gain. At 60 cps, for example, the gain is about 3000, or  $\frac{1}{2}$  of that at 420 cps.

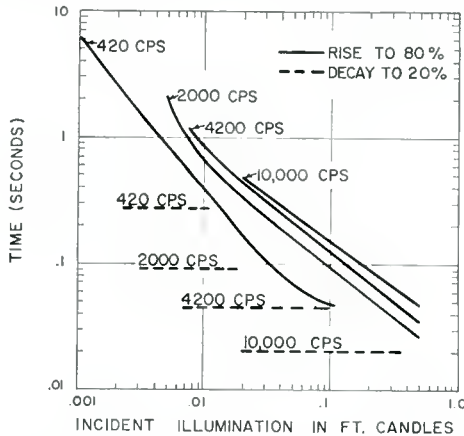


Fig. 6—Rise and decay as a function of incident illumination for simple light-amplifier element.

Figure 6 shows curves of rise and decay time as a function of incident illumination for various frequencies of operation. Decay time changes very little with light level and is shown as dotted horizontal lines. This may be due to the fact that as output light decreases, the voltage across the photoconductor increases, thus changing the shape of the decay curve from that of the photoconductor alone. For high light levels, the voltage excursion on the photoconductor is greater than for low-level excitation, thus counteracting the normally faster decay at high inputs.

Decay time decreases considerably as the frequency of operation is increased. At 10 kilocycles it is in the neighborhood of 20 milliseconds, and the operating range of the panel is at higher light levels.

Rise times are indicated by the solid lines in Figure 6. For a given light level, rise time is longer for higher frequencies, but at any

particular frequency, rise time decreases with increasing illumination.

The rise-time range or decay-time range which is of interest in a picture panel is, of course, determined by the input-light range which can be used in producing a satisfactory picture. The usable input range is determined by the transfer characteristic or gamma of the panel which can be deduced from the light-input-light-output curves and is considered later. It can be seen, for example, that with a rise time of 50 milliseconds at an input light of 0.1 foot-candle, gain is quite small and the output has reached saturation.

Figure 7 shows curves of input light versus output light for a range of operating frequencies applied to the single-element light amplifier. These curves show that at low levels the gamma is greater than unity.

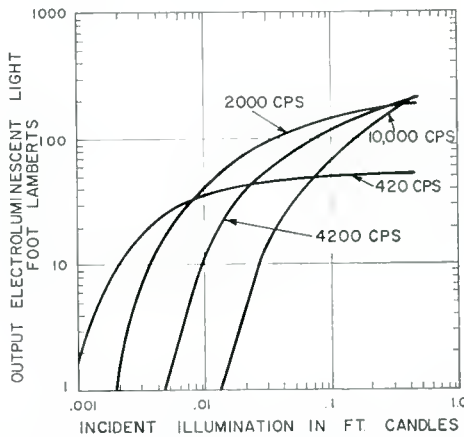


Fig. 7—Light output as a function of incident illumination for simple light-amplifier element.

It reaches unity as the level is increased and finally becomes less than unity at the highest levels. The highest input-light level for satisfactory picture reproduction at a given frequency occurs at some selected point where the gamma is less than unity, and this point is higher for higher frequencies. The useful light output for high-frequency operation is therefore greater than for low-frequency operation, but the increased output is obtained at the expense of gain.

These results were obtained using a 25-mil gap and approximately equivalent areas of photoconductor and electroluminescent layers. This was done to simulate normal panel construction.

For some applications requiring fewer elements and in which special construction could be used, the impedance of the electroluminescent layer may be artificially decreased by the addition of a parallel capac-

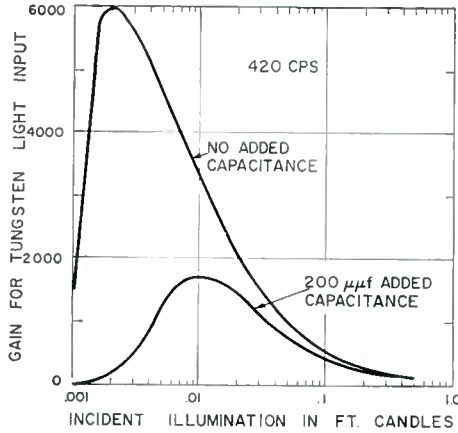


Fig. 8—Gain as a function of incident illumination for light-amplifier element with added capacitance.

itor. The operation of the light-amplifier element with added capacitance then resembles to some extent the operation of the original element at higher frequency. Figures 8, 9, and 10 compare the operation of a light amplifier element with added capacitance to that of the same element operated normally. Figure 8 shows that the gain is reduced by the addition of the capacitance so that the gain curve taken at 420 cps with added capacitance is similar to that for the original element operated at 4200 cps.

Figure 9 shows curves of rise and decay times for light-amplifier elements with and without added capacitance. Adding capacitance to

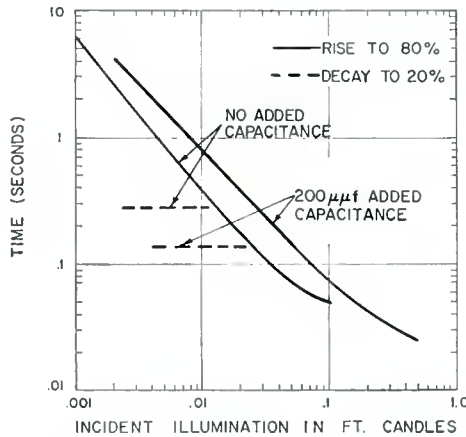


Fig. 9—Rise and decay as a function of incident illumination for light-amplifier element with added capacitance.

the electroluminescent element increases the rise time and decreases decay time. In this respect, the operation is again similar to that of the original element at higher frequency.

Figure 10 shows curves for light input versus light output with no added capacitance and with 200 micromicrofarad added as in the other curves. In this case, operation with added capacitance is not so similar to operation at 4200 cps without added capacitance. The sensitivity with added capacitance is reduced, and, in addition, the curve flattens off at the same output level as the 420-cps curve for no added capacitance. Thus, in the over-all device, while the use of added capacitance

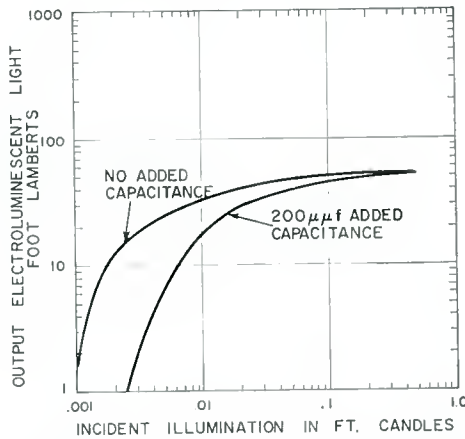


Fig. 10—Light output as a function of incident illumination for light-amplifier element with added capacitance.

across the electroluminescent layer decreases decay time, it also reduces gain and provides no increase in output over operation at the same frequency without the added capacitance. The use of added capacitance complicates the structure of a light-amplifier panel and actually gives less output than that obtained by operating in the conventional manner at higher frequency. Except for special applications then, the use of added capacitance would seem to be undesirable.

Practical panel operation is best illustrated, then, by the curves of Figures 5, 6, and 7, covering as they do the simplest combination of photoconductor and electroluminescent layer. To evaluate what might be expected from a sintered CdSe light amplifier, an estimate of operating range (maximum and minimum useful input-light levels) must be made for each frequency. Maximum useful light output is determined as the point at which low gamma would be expected to impair the reproduction of halftones. These points were determined for the different frequencies from a linear input-output characteristic,

since these curves were easier to interpret than log-log plots. These maximum output levels correspond to maximum useful input levels.

Since the final device is for picture reproduction, a maximum contrast of 50 to 1 is used to calculate the minimum input required. Inputs below this value are considered as black and are disregarded.

## RESULTS

Table I gives the useful operating range of input and output light levels along with the range of rise and decay time and the maximum gain. These results are tabulated for four different frequencies. The

*Table I—Useful Operating Range for Sintered CdSe Light-Amplifier Element with 50-1 Contrast in Output Image*

Operating Frequency (cps)	10,000	4200	2000	420
Input Light Level (foot-candles)	.4 to .02	.2 to .007	.1 to .003	.01 to .0008
Output at Maximum Input (foot-lamberts)	160	150	140	35
Rise time to 80% (seconds)	.06 to .5	.07 to 1.0	.07 to 2.0	.4 to 6.0
Decay Time to 20% (seconds)	.02	.05	.09	.28
Maximum Tungsten Light Gain	555	1900	3400	6000

Table shows clearly that to obtain decay times of 50 milliseconds or less the amplifier must be operated above 420 cps. This is advantageous in terms of maximum light output, but less gain is obtained at these frequencies. Faster response can, therefore, be obtained at the expense of gain.

From the table it is clear that decay times small enough for moving pictures can only be obtained by operating near 10,000 cps where the tungsten-light gain is 555 or the energy gain about 100. Under these conditions rise time at the low inputs is .5 second, and, therefore, light output on a moving picture will depend on the length of time a given portion of photoconductor is exposed. Thus, the gamma of the various portions of the picture will vary somewhat with the input level. The decay time is not so much a function of the input level and should therefore have little deleterious effect on picture reproduction.

The results of the experiments on a single-element light amplifier using sintered cadmium selenide as the photoconductor should be indicative of the results attainable with a panel amplifier using the same constituent parts. Since the measurements described in this paper were made, more sensitive photoconductive cells have become available. Improvements in the performance of light amplifiers could also result from the development of more efficient electroluminescent materials.

#### ACKNOWLEDGMENTS

The author wishes to thank E. W. Herold and D. W. Epstein for their continued interest in this work. Many of the measurements were made by H. Ogawa and the electroluminescent cells used in the experiments were made by L. Korsakoff.

# SOLID-STATE IMAGE INTENSIFIER UNDER DYNAMIC OPERATION\*

BY

C. P. HADLEY AND R. W. CHRISTENSEN

RCA Electron Tube Division,  
Lancaster, Pa.

*Summary*—This paper describes the performance of photoconductor-electroluminescent-phosphor image intensifiers under dynamic conditions of operation. Both experimental data and theory are presented. The theory is based on some simplifying assumptions which allow easy analysis and permit an insight into the importance of the various parameters. The experimental data, however, confirm the applicability of the analysis. Some suggestions concerning the possible improvement of intensifier performance are made.

## INTRODUCTION

THIS PAPER presents experimental and theoretical analyses of time-delay phenomena exhibited by solid-state image intensifiers of the photoconductor-electroluminescent-phosphor type.<sup>†</sup> These phenomena are usually caused by the photoconductor, frequently cadmium sulfide or cadmium selenide, which responds slowly to changes in the level of input radiation. The following three cases of intensifier operation are considered:

(1) *Static characteristic*: The output is observed after the input radiation has been incident for a long time. This condition is of interest when gain is desired but time is not a factor.

(2) *Instantaneous dynamic characteristic*: The output is considered immediately after a short input exposure. This condition is of interest for visual observation with an X-ray input.

(3) *Integrated dynamic characteristic*: The output energy is considered as a function of the input energy associated with a short exposure. This situation results when an X-ray input is used and the output is recorded on photographic film.

Two models of the image intensifier are considered. Figure 1 shows a grooved structure which can be used for either visible-light

---

\* Manuscript received October 20, 1959.

† This work was supported in part by a Wright Air Development Center Contract.

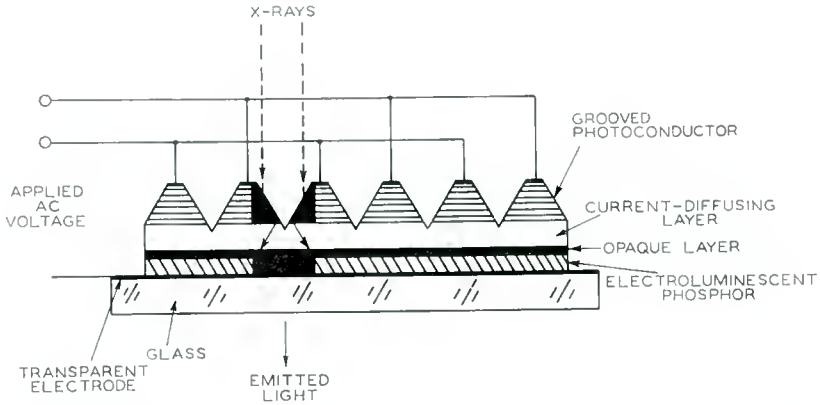


Fig. 1—Grooved image-intensifier structure for use with either visible-light or X-ray input.

or X-ray input. Figure 2 shows a non-grooved structure which is applicable only for X-ray input. Both designs have a photoconductor on the input side, an electro luminescent layer to provide the light output, and an opaque layer which separates them to prevent optical feedback.

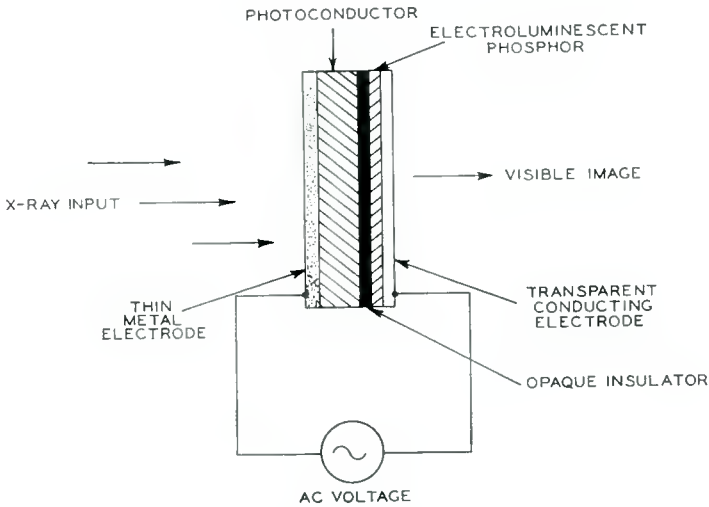


Fig. 2—Ungrooved image-intensifier structure for use with X-ray input only.

## BASIC CONSIDERATIONS

Electrically, the image intensifier acts as a capacitor (the electroluminescent layer) in series with a resistor (the photoconductor). Although the photoconductor (a powder with a plastic binder) is far from ohmic in behavior,<sup>1</sup> it is more convenient for the purpose of discussion to assume the photoconductor to be ohmic; the simplicity of presentation justifies some inaccuracy in the conclusion. Therefore, the conductance  $G_L$  of the photoconductive layer is given by

$$G_L = G_0 L^n, \quad (1)$$

where  $L$  is the illumination and  $n$  and  $G_0$  are constants. Equation (1) applies after the illumination has been incident for a long time.

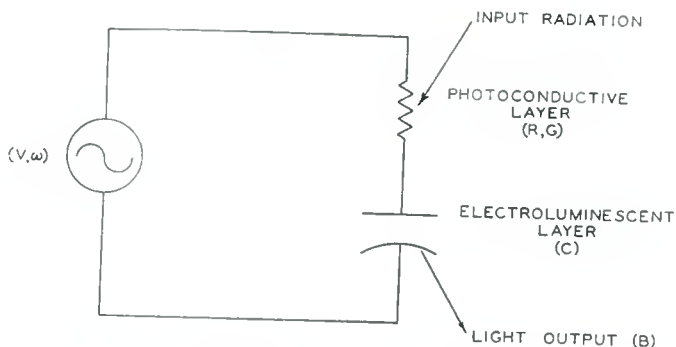


Fig. 3—Equivalent circuit for image intensifier.

The output or brightness,  $B$ , of the electroluminescent layer is represented by the expression

$$B = B_0 \omega^a V_C^m, \quad (2)$$

where  $\omega/(2\pi)$  is the frequency of the applied voltage,  $V_C$  is the voltage across the layer, and  $B_0$ ,  $a$ , and  $m$  are constants.

## STATIC CHARACTERISTIC

The equivalent circuit for the image intensifier is shown in Figure 3. From simple alternating-current theory, the output for the static characteristic,  $B_s$ , is given by

<sup>1</sup> B. Kazan and F. H. Nicoll, "An Electroluminescent Light-Amplifying Picture Panel," *Proc. I.R.E.*, Vol. 43, p. 1888, December, 1955.

$$B_s = B_m \frac{G^m}{[G^2 + (C\omega)^2]^{m/2}}, \quad (3)$$

where  $B_m$  is substituted for  $B_0 \omega^a V^m$ ,  $C$  is the capacitance of the electro-luminescent layer, and  $G$  is the conductance of the photoconductor. Figure 4 shows a plot of Equation (3) over the various illumination regions of interest. These regions are discussed separately.

*Low-input region:* For low input levels, the conductance is caused by leakage and is usually small compared to the susceptance. The output  $B_s$  is given by

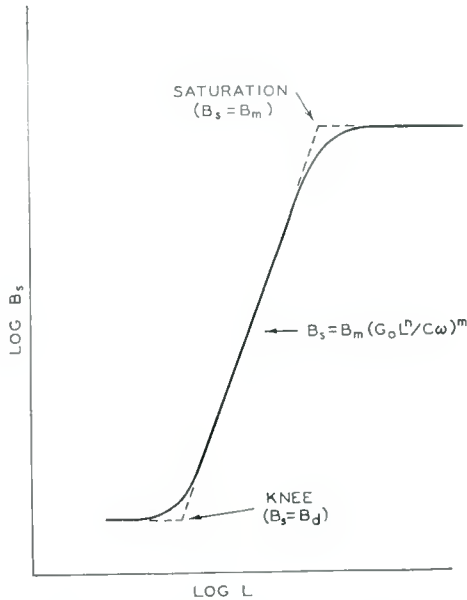


Fig. 4—Idealized curve for static characteristic.

$$B_s = B_d = B_m \left( \frac{G_d}{C\omega} \right)^m, \quad (4)$$

where  $B_d$  is the background, and  $G_d$  is the leakage conductance.

*Intermediate region:* In this region, the conductance, given by Equation (1), is small compared to the susceptance. The output is as follows:

$$B_s = B_m \left( \frac{G_0 L^n}{C\omega} \right)^m. \quad (5)$$

The static characteristic in the intermediate region is a straight line having a slope of  $mn$ .

*Saturation region:* At high input levels, the conductance is much greater than the susceptance, and the static characteristic is given by

$$B_s = B_m. \quad (6)$$

The lowest useful input radiation may be determined from the position of the knee on the curve of Figure 4. The knee is defined as the intersection of the straight-line portions of the low-input region and the intermediate region of the curve. At the knee, the conductance  $G$  of the intensifier is given by

$$G = G_0 L^n = G_d. \quad (7)$$

The lowest useful input is defined by this equation.

Similarly, the saturation point of the curve is defined as the intersection of the saturation and intermediate portions of the static characteristic, and is given by

$$G_0 L^n = C\omega. \quad (8)$$

Another quantity of interest is the gain under static conditions. This quantity is defined as  $B/L$  and may be determined from Equations (1) and (3). The maximum gain is determined by solution of the following equation:

$$\frac{d}{dL} \left( \frac{B}{L} \right) = 0.$$

Maximum gain occurs when

$$G_0 L^n = [\sqrt{mn-1}] C\omega, \quad (9)$$

and is given by

$$\text{Gain (max)} = B_m \left( \frac{G_0}{C\omega} \right)^{\frac{1}{n}} \left[ \frac{(mn-1)^{\frac{mn-1}{2n}}}{(mn)^{m/2}} \right], \quad (10)$$

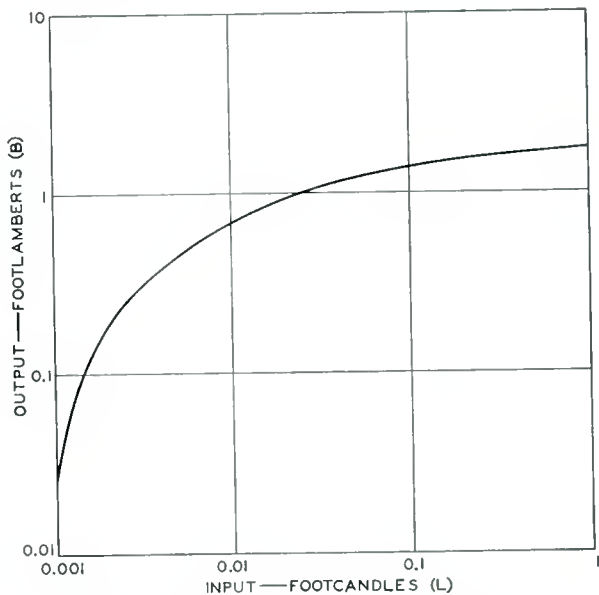


Fig. 5—Static characteristic (light input).

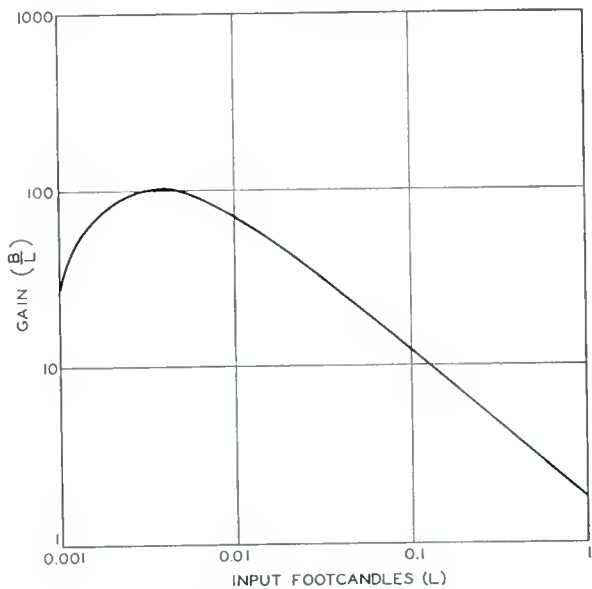


Fig. 6—Gain (light input).

Some experimental results illustrating the previous equations are given in Figures 5, 6, and 7. Figures 5 and 6 show the static characteristic and gain for the intermediate and saturation regions when a grooved intensifier (CdS) with visible-light input is used. The static curve is much rounder than predicted because of the non-ohmic character of the photoconductor. The maximum gain comes close to the saturation point, as expected. The fact that the intermediate region is very steep is expected, because  $m$  is about 3.5 for the zinc sulfo-selenide phosphor used,  $n$  is near 0.7 for the photoconductor, and the slope, given by  $mn$ , is about 2.5. Although the curve of Figure 5

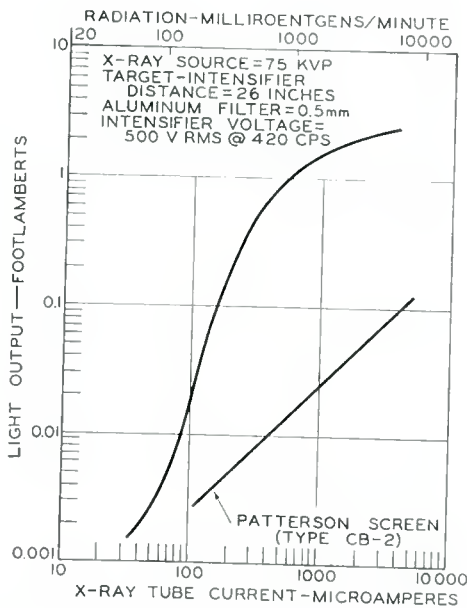


Fig. 7—Static characteristic for X-ray input.

does not extend to extremely low levels, it can be seen by extrapolation that the lowest useful input is about 0.001 foot-candle. This figure is consistent with the photocurrent-to-dark current properties of the cadmium sulfide photoconductor.

Figure 7 shows a static characteristic of an image intensifier (CdS) for X-ray input. The maximum intensification occurs with an input of about 1000 milliroentgens per minute. At this point, the output is about 100 times that which would be obtained, under the same conditions, from a Patterson CB-2 screen.

INSTANTANEOUS DYNAMIC CHARACTERISTIC

For some applications, it is desirable to apply a short pulse of radiation to the input of the intensifier and to view the output visually. An example of such applications is the use of the device for medical fluoroscopy. The property of interest in such an application is the output of the panel directly after completion of the exposure. The curve of the logarithm of this output as a function of the logarithm of the input exposure is defined as the instantaneous dynamic characteristic. A hypothetical curve is given in Figure 8.

The conductivity of the photoconductor is approximately an exponential function of time. Therefore, the conductance  $G$  of the intensifier is given by

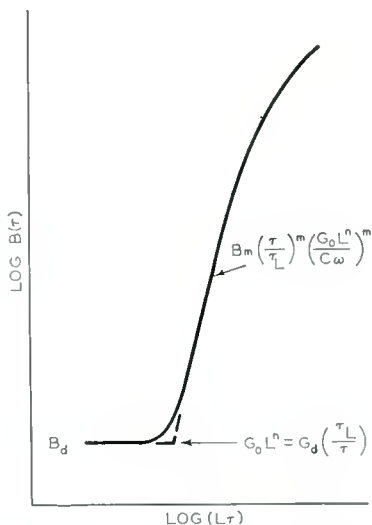


Fig. 8—Hypothetical curve for instantaneous dynamic characteristic.

$$G = G_0 L^n \left( 1 - \exp \left\{ - \frac{\tau}{\tau_L} \right\} \right)$$

where  $\tau$  is the exposure time and  $\tau_L$  is the time constant associated with the illumination  $L$ . For the usual case,  $\tau$  is much smaller than  $\tau_L$ , and the output of the panel at time  $\tau$  is

$$B(\tau) = B_m \left( \frac{\tau}{\tau_L} \right)^m \left( \frac{G_0 L^n}{C \omega} \right)^m \tag{11}$$

The minimum illumination which can be used pertains at the knee of the curve, and is given by

$$G_0 L^n = G_d \left( \frac{\tau_L}{\tau} \right). \quad (12)$$

### INTEGRATED DYNAMIC CHARACTERISTIC

For applications in which the output image of the intensifier is to be recorded (for example, on photographic film), the characteristic of interest is  $\int_0^{\tau_i} B dt$  as a function of  $L\tau$ . The time during which

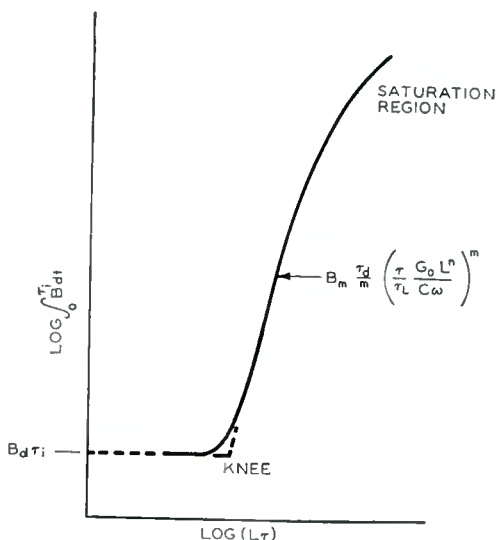


Fig. 9—Idealized curve of integrated dynamic characteristic.

the output is observed is the integration time  $\tau_i$ . Figure 9 shows an idealized logarithmic curve of this characteristic. The three regions of this curve which are of interest are discussed separately below.

*Low-input region:* At low light levels, the output of the image intensifier is constant at the background value  $B_d$ , and the dynamic output is given by

$$\int_0^{\tau_i} B dt = B_d \tau_i. \quad (13)$$

*Intermediate region:* In the intermediate region, the conductance of the photoconductive layer rises during exposure (as discussed previously for the instantaneous dynamic characteristic), and the brightness reaches the level given by Equation (11). At the end of the exposure, the conductance has not risen very far toward its ultimate value, and decays with a time constant,  $\tau_d$ , which is characteristic of a very low input level. The decay of the output is given by

$$B(t) = B(\tau) \exp \left\{ \frac{-mt}{\tau_d} \right\}. \quad (14)$$

For all practical purposes, therefore, the integrated output is approximately equal to the integral of Equation (14) from zero to infinity;

$$\int_0^{\tau_i} B dt = B_m \left( \frac{\tau_d}{m} \right) \left( \frac{\tau}{\tau_L} \frac{G_0 L^n}{C_w} \right)^m. \quad (15)$$

*Saturated region:* At still higher input-illumination levels, a saturation region is reached. The exact nature of the characteristic in the saturation region depends on whether the photoconductor saturates or whether the intensifier saturates because of impedance relationships.

The lowest useful exposure which can be used is determined from the position of the knee of the curve shown in Figure 9. This point is determined by the intersection of the two straight-line portions of the characteristic. Thus, at the knee, the lowest useful exposure is given by

$$\frac{m \tau_i}{\tau_d} = \left( \frac{\tau G_L}{\tau_L G_d} \right)^m. \quad (16)$$

If it is assumed that the integration time is of the order of the low-light response time, then the minimum exposure time is expressed as follows:

$$\tau_{\min} = \tau_L m^{\frac{1}{m}} \left( \frac{G_d}{G_L} \right). \quad (17)$$

The dynamic gain is defined as  $\int_0^{\tau_i} B dt / (L \tau)$  and is given by

$$\text{Gain (dyn)} = B_m \left( \frac{\tau_d}{m} \right) \left( \frac{G_0}{\tau_L C \omega} \right)^m L^{m-1} \tau^{m-1} \tag{18}$$

Figure 10 shows an integrated dynamic characteristic for a grooved structure (CdS) when a visible-light input (2870° K) is used.

DISCUSSION

It is interesting to compare the performance of the image intensifier with theoretical predictions based on data for a typical sintered cadmium sulfide photoconductive cell, the 7163. Because the intensifier

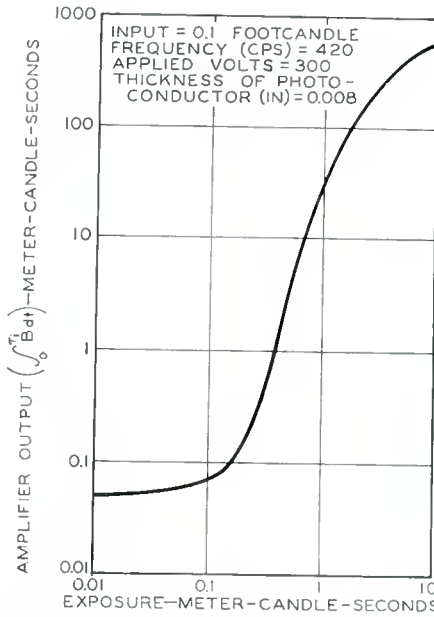


Fig. 10—Integrated dynamic characteristic for a grooved image-intensifier structure with a visible-light input of 2870° K.

uses a powdered photoconductor, completely accurate predictions using these data should not be expected. The results of the comparison are as follows:

<i>Static Characteristic</i>	<i>Theory</i>	<i>Experiment</i>
<i>L</i> (min) (foot-candles) .....	.005	.001
gamma .....	2.5	3.9
 <i>Integrated Dynamic Characteristics</i>		
<i>Lτ</i> (min) (meter-candle-seconds) .....	.05	.2
gamma .....		4.3

The results of this analysis indicate that certain improvements in intensifier performance are possible. The quantity  $\gamma$ , both for static and dynamic operation, is so large that it produces a high-contrast output. As shown in Equations (5) and (15), the important factors in this quantity are  $m$  and  $n$ . The photoconductor affects  $\gamma$  through  $n$ , and only moderate reduction in this factor is to be expected. The quantity  $m$ , however, which is a property of the electroluminescent phosphor, depends on the field which is applied to the material. A considerable reduction in  $m$  can be achieved if the thickness of the layer is reduced while the applied voltage is maintained. Equation (3) shows, however, that the photoconductive layer must also be reduced in thickness if the operating range, with regard to input radiation, is to remain the same.

With respect to the integrated dynamic characteristic, it might be desirable to extend the minimum exposure toward lower levels. By use of Equation (17) and data for a developmental sintered cadmium selenide photoconductive cell (RCA-Dev. No. C-7218), it can be shown that intensifiers using cadmium selenide as the photoconductor should be faster, photographically speaking, by about three orders of magnitude than those using cadmium sulfide. Indeed, the intensifier using cadmium selenide should be about as fast as the best photographic film.

# A SIMPLIFIED THEORY OF TWO-CARRIER, SPACE-CHARGE-LIMITED CURRENT FLOW IN SOLIDS\*

BY

M. A. LAMPERT

RCA Laboratories,  
Princeton, N.J.

*Summary*—Two-carrier, space-charge-limited current flow is analyzed by an extension of the simple, but effective, method introduced by Rose to treat the one-carrier problem. The analysis is carried out for those situations where most of the injected carriers and their concomitant space charge are free, and where the currents are field-driven. The analysis does not require specific assumptions about the dependence of carrier drift velocities on field intensity. Results are obtained for both monomolecular and bimolecular recombination. Where exact theoretical results are available (recent work of Parmenter and Ruppel), the present, simplified theory checks remarkably well.

## INTRODUCTION

ONE-CARRIER SCLC (space-charge-limited currents) in solids are known to exhibit a richness of behavior<sup>1-6</sup> which foretells wide application to electronics.<sup>7-10</sup> Of particular interest to

\* Manuscript received October 19, 1959.

<sup>1</sup> N. F. Mott and R. W. Gurney, *Electronic Processes in Ionic Crystals*, Oxford Clarendon Press, England, 1940, p. 172.

<sup>2</sup> W. Shockley and R. C. Prim, "Space-Charge Limited Emission in Semiconductors," *Phys. Rev.*, Vol. 90, p. 753, June, 1953.

<sup>3</sup> G. C. Dacey, "Space-Charge Limited Hole Current in Germanium," *Phys. Rev.*, Vol. 90, p. 759, June, 1953.

<sup>4</sup> R. W. Smith and A. Rose, "Space-Charge-Limited Currents in Single Crystals of Cadmium Sulfide," *Phys. Rev.*, Vol. 97, p. 1531, March, 1955.

<sup>5</sup> A. Rose, "Space-Charge-Limited Currents in Solids," *Phys. Rev.*, Vol. 97, p. 1538, March, 1955.

<sup>6</sup> M. A. Lampert, "Simplified Theory of Space-Charge-Limited Currents in an Insulator With Traps," *Phys. Rev.*, Vol. 103, p. 1648, September, 1956.

<sup>7</sup> W. Shockley, "Transistor Electronics: Imperfections, Unipolar and Analog Transistors," *Proc. I.R.E.*, Vol. 40, p. 1289, November, 1952.

<sup>8</sup> G. T. Wright, "Space-Charge Limited Currents in Insulating Materials," *Nature*, Vol. 182, p. 1296, November, 1958.

<sup>9</sup> E. O. Johnson and A. Rose, "Simple General Analysis of Amplifier Devices with Emitter, Control and Collector Functions," *Proc. I.R.E.*, Vol. 47, p. 407, March, 1959.

<sup>10</sup> W. Ruppel and R. W. Smith, "CdS Analog Diode and Triode," *RCA Review*, Vol. XX, p. 702, December, 1959.

photoelectronics is the recent discovery<sup>11-13</sup> that the performance of a one-carrier<sup>14</sup> photoconductor with ohmic contacts is limited ultimately by the onset of (one-carrier) SCLC. The performance of a light amplifier with a photoconductor element is limited in like fashion.<sup>15</sup> Finally, the use of one-carrier SCLC furnishes an extraordinarily sensitive technique<sup>16</sup> for the study of defects in pure crystals.

It seems reasonable to expect that a comparable yield of new, interesting, and perhaps useful results will ensue from the study, both experimental and theoretical, of *two-carrier* SCLC in solids. The double-injection experiments of Tyler<sup>17</sup> on germanium and Smith<sup>18</sup> on CdS are possibly examples of this phenomenon (the uncertainty arises from the unknown role of the hole-injecting contact in these experiments). On the theoretical side, the recent work of Parmenter and Ruppel<sup>19</sup> represents the first analytical inroad into the two-carrier SCLC problem.

The recondite nature of the exact solution for the simplest (trap-free) problem,<sup>19</sup> plus the unavailability of exact solutions for the more general problems of this class, make it clear that what is needed is a simplified approach, i.e., a theoretical framework based on a set of simple, basic, physical concepts that can be easily manipulated to obtain approximate solutions. The simple physical concepts introduced by A. Rose<sup>5,6</sup> to deal with the problem of one-carrier SCLC in solids is an example of the type of approach which is sought. In the present paper, the concepts of Rose are extended to provide a simplified

---

<sup>11</sup> A. Rose, "Maximum Performance of Photoconductors," *Helvetica Physica Acta*, Vol. 30, p. 242, No. 4, 1957.

<sup>12</sup> R. W. Redington, "Maximum Performance of High-Resistivity Photoconductors," *Jour. Appl. Phys.*, Vol. 29, p. 189, February, 1958.

<sup>13</sup> A. Rose and M. A. Lampert, "Photoconductor Performance, Space-Charge Currents, and the Steady-State Fermi Level," *Phys. Rev.*, Vol. 113, p. 1227, March, 1959.

<sup>14</sup> One-carrier in the sense that the second, or minority, carrier gets trapped very quickly into recombination centers, and hence makes negligible contribution to the photocurrent.

<sup>15</sup> R. H. Bube and A. Rose, "The Role of Space-Charge Currents in Light Amplifiers," *RCA Review*, Vol. XX, p. 648, December, 1959.

<sup>16</sup> M. A. Lampert, A. Rose, and R. W. Smith, "Space-Charge Limited Currents as a Technique for the Study of Imperfections in Pure Crystals," *Jour. Phys. Chem. Solids*, Vol. 8, p. 465, January, 1959.

<sup>17</sup> W. W. Tyler, "Injection Breakdown in Iron-Doped Germanium Diodes," *Phys. Rev.*, Vol. 96, p. 226, October, 1954.

<sup>18</sup> R. W. Smith, "Low-Field Electroluminescence in Insulating Crystals of Cadmium Sulfide," *Phys. Rev.*, Vol. 105, p. 900, February, 1957.

<sup>19</sup> R. H. Parmenter and W. Ruppel, "Two-Carrier Space-Charge Limited Current in a Trap Free Insulator," *Jour. Appl. Phys.*, Vol. 30, p. 1548, October, 1959.

approach to the two-carrier SCLC problem. The underlying principles of the solution were first recognized by Rose<sup>20</sup> several years ago, and were applied to a special problem. Recently the author independently rediscovered the necessary concepts and has applied them in greater generality. In the following solution, the analytical result of Parmenter and Ruppel<sup>19</sup> is (approximately) reproduced and generalized, both bimolecular and monomolecular (constant lifetime) recombination of the two-carriers being considered. The extension of this simplified approach to cover the important cases where a sizable fraction of the injected carriers and space charge are held in deep traps or recombination centers remains to be done.

Except where otherwise stated, MKS units are employed throughout this paper. Further, only steady-state currents are analyzed.

#### THE BASIC ARGUMENT

The principles underlying the (approximate) solution to the two-carrier SCLC problem are a simple extension of those used in the study of the one-carrier SCLC problem.<sup>5</sup>

*One-carrier SCLC* (All injected carriers free)

For the sake of definiteness, it is assumed the current carriers are electrons (subscript  $n$ ).

Two elementary relations yield the solution to this problem:

$$Q = e\mathcal{N} = CV, \quad (1)$$

$$I = \frac{e\mathcal{N}}{t_n}, \quad (2)$$

where  $Q$  is the total charge in the solid,  $\mathcal{N}$  the total number of free electrons (the free electrons present in the solid at thermal equilibrium are neglected),  $e$  is the magnitude of the charge on the electron,  $C$  the capacitance of the solid,  $V$  the applied voltage,  $I$  the current, and  $t_n$  the transit time of electrons from cathode to anode. Noting that  $t_n = L/v_n$ , where  $L$  is the cathode-anode spacing and  $v_n$  the free-electron drift velocity, Equations (1) and (2) can be combined to give the desired current-voltage relationship:

$$I = v_n C \frac{V}{L}. \quad (3)$$

<sup>20</sup> A. Rose, unpublished notes, 1955.

The drift-velocity  $v_n$  can be a complicated function of the applied field  $V/L$  ( $v_n = v_n(V/L)$ ) and can even saturate (become constant) over a range of applied fields.<sup>21</sup> At sufficiently low fields ( $v_n = \mu_n V/L$ ),

$$I = \mu_n C \frac{V^2}{L^2}. \quad (4)$$

For a one-dimensional geometry ( $L$  small compared to the smaller transverse dimension of the electrodes), it is convenient to refer to the current-density,  $J$ . In this case,  $C$  is the capacitance per unit area;  $C = \epsilon/L$ , with  $\epsilon$  the static dielectric constant of the solid. Then,

$$J = \epsilon \mu_n \frac{V^2}{L^3}. \quad (5)$$

The exact analytical solution<sup>1</sup> differs from Equation (5) only in that it is larger by the factor 9/8.

#### *Two-Carrier SCLC* (All injected carriers free)

The extension of Equation (2) for this case is straightforward. Since current is now carried by injected holes as well as by injected electrons,

$$I = e \left( \frac{\mathcal{N}}{t_n} + \frac{\mathcal{P}}{t_p} \right) \approx e \mathcal{N} \left( \frac{1}{t_n} + \frac{1}{t_p} \right), \quad (6)$$

where  $\mathcal{P}$  is the total number of free holes and  $t_p$  their transit time. Here, it is assumed that the two-carrier current,  $I$ , is much larger than the one-carrier SCL current at voltage  $V$ ; this requires that  $\mathcal{N} \approx \mathcal{P}$ .

The modification of Equation (1) is not quite so trivial. Clearly, all of the injected holes and electrons do not contribute to space charge since they largely neutralize each other. The electrically unbalanced portion of the carriers, i.e., the space charge, is obtained from the spatial variation of  $\mathcal{N}$  and  $\mathcal{P}$ , and is given by

$$Q \approx e \mathcal{N} \frac{t_n + t_p}{\tau} = CV, \quad (7)$$

<sup>21</sup> J. B. Gunn, "High Electric Field Effects in Semiconductors," *Progress in Semiconductors*, John Wiley & Sons, Inc., New York, New York, Vol. 2, 1957, p. 213.

where  $\tau$  is the common lifetime for the injected electrons and holes. Here  $e\mathcal{N}t_n/\tau$  and  $e\mathcal{P}t_p/\tau \approx e\mathcal{N}t_p/\tau$  represent the unbalanced portions of the injected electrons and holes, respectively. These are additive because the injected electron and hole densities vary spatially in an opposite sense; the electrons decrease in density from cathode to anode and the holes from anode to cathode. The argument is presented more fully in the next section.

Combining Equations (6) and (7),

$$I = v_n v_p \tau C \frac{V}{L^2}. \quad (8)$$

At sufficiently low fields, where the carrier mobilities are field-independent,

$$I = \mu_n \mu_p \tau C \frac{V^3}{L^4}. \quad (9)$$

For a one-dimensional geometry, replacing  $I$  by the current-density  $J$  and taking  $C = \epsilon/L$  as in Equation (5),

$$J = \epsilon v_n v_p \tau \frac{V}{L^3} \rightarrow \epsilon \mu_n \mu_p \tau \frac{V^3}{L^5} \text{ at low fields.} \quad (10)$$

#### DETAILED DISCUSSION

Two-carrier SCL currents require a cathode and anode which are capable of injecting electrons and holes, respectively. Two suitable structures for the observation of these currents are shown, by means of schematic energy-band diagrams, in Figure 1. Figure 1a shows an n-i-p semiconductor structure. The n-i junction is the electron-injecting contact and the i-p junction the hole-injecting contact. The two-carrier SCL currents flow in the intrinsic region. If the n and p regions are both degenerate, this structure will be useful down to the lowest temperatures. Figure 1b shows an insulator or semiconductor with the usual type of electron-injecting contact and with the thyristor-type of hole-injecting contact.<sup>22</sup>

In this report, for the sake of simplicity, the discussion of two-carrier currents is restricted to those situations in which

<sup>22</sup> This type of contact has been invoked by D. O. North in explanation of thyristor action: C. W. Mueller and J. Hilibrand, "The 'Thyristor'—A New High Speed Switching Transistor," *Trans. I.R.E. PGED*, p. 2, January, 1958.

- (a) the injected carriers and their unbalanced portions (space charge) are free, i.e., not in traps or recombination centers,
- (b) the applied voltage,  $V$ , is of such a magnitude that the resultant current-density,  $J$ , greatly exceeds both the Ohm's law current<sup>23</sup> and the one-carrier SCL current that would correspond to the voltage  $V$ ,
- (c) carriers are injected only at the contacts; no carrier multiplication (breakdown) takes place in the body of the sample,
- (d) the current is field-driven; diffusion currents are neglected. (With regard to n-i-p semiconductor structures, this last assumption restricts the discussion to those situations in

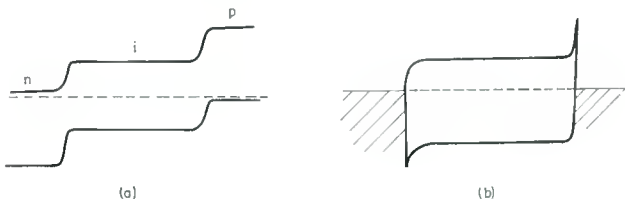


Fig. 1—Schematic energy-band diagrams of two structures which are suitable for the observation of two-carrier, space-charge-limited currents; (a) n-i-p semiconductor; (b) insulator, or semiconductor, with ordinary ohmic type of electron-injecting contact and with thyristor-type of hole-injecting contact.

which the length,  $L$ , of the intrinsic section is substantially larger than the diffusion length,  $L_D$ , corresponding to the carrier densities present in this section under injection conditions. Those situations where  $L < L_D$  have already been discussed in the literature).

Under the above conditions, the plots of  $n$  (free-electron density) and  $p$  (free-hole density) versus position in the sample must have the general shape shown in Figure 2 (solid lines). The most important feature of these plots is their relatively slight variation with position over the main body of the sample. The two curves cross at position  $\bar{x}$ ;  $n(\bar{x}) = \bar{n} = p(\bar{x}) = \bar{p}$ . It is shown later that  $\bar{x} \approx L/2$ . The short-dashed lines are plots of  $n$  and  $p$  in thermal equilibrium.

Let  $Q_-$  denote the total negative charge per unit area between the

<sup>23</sup> Here we mean the current resulting from the flow of the *thermal-equilibrium* density of free carriers in response to the applied voltage. Depending on the field-dependence of the mobility, this current may or may not be linear with voltage in any given range.

cathode,  $x=0$ , and the neutrality point,  $\bar{x}$ . Similarly, let  $Q_+$  denote the positive charge between  $\bar{x}$  and  $L$ . Then  $(1/e)|Q_-|$  is simply the area between the  $n$  and  $p$  curves from 0 to  $\bar{x}$ , and  $(1/e)Q_+$  the area from  $\bar{x}$  to  $L$ . The above-listed conditions require:

$$\frac{1}{e} |Q_-| \ll \bar{n} \frac{L}{2} \quad \text{and} \quad \frac{1}{e} Q_+ \ll \bar{n} \frac{L}{2}. \quad (11)$$

For, if  $(1/e)|Q_-| \gtrsim \bar{n} L/2$ , the observed current,  $J$ , would be essentially

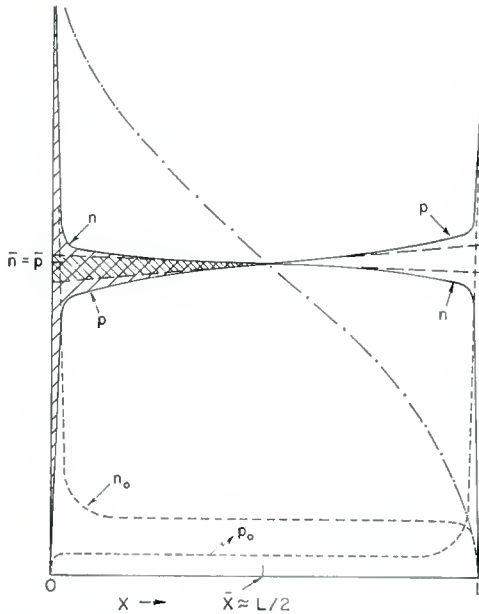


Fig. 2—Schematic representation of free-electron and hole density distributions (solid curves) in a solid carrying a significant (i.e., appropriately large) two-carrier current. Short-dashed curves indicate schematic free-carrier distributions in thermal equilibrium (no current).

the *one-carrier* SCL current, in violation of condition (b). Thus, a variation of  $n$  with  $x$  such as that shown by the dot-dashed curve in Figure 2 is impossible under the stated conditions. With such a variation, the space charge associated with  $n$  would be comparable with  $e\bar{n}L$ , and the magnitude of the resultant current would be of the order obtainable from *one-carrier* SCLC, in violation of assumption (b).

Physically, the situation may be described by saying that there is a plasma of electrons and holes in the main body of the sample—the departures from charge neutrality over this region are *relatively* small.

Since the relative variations of  $n$  and  $p$  over the main body of the sample are small, it is a reasonable approximation to write

$$\left. \begin{aligned} n(x) &\approx \bar{n} \exp \frac{\bar{x} - x}{\bar{v}_n \bar{\tau}} \approx \bar{n} \left\{ 1 + \bar{\theta}_n \frac{(\bar{x} - x)}{L} \right\} \text{ with } \bar{\theta}_n = \frac{L}{\bar{v}_n \bar{\tau}}, \\ p(x) &\approx \bar{p} \exp \frac{x - \bar{x}}{\bar{v}_p \bar{\tau}} \approx \bar{p} \left\{ 1 - \bar{\theta}_p \frac{(\bar{x} - x)}{L} \right\} \text{ with } \bar{\theta}_p = \frac{L}{\bar{v}_p \bar{\tau}}. \end{aligned} \right\} \quad (12)$$

A bar over a quantity denotes the value of that quantity at  $x = \bar{x}$ .  $v_n$  and  $v_p$  are the electron and hole drift velocities, respectively,  $\tau$  is the common lifetime for electrons and holes at  $x = \bar{x}$  (since  $\bar{n} = \bar{p}$ , equality of the electron and hole recombination rates—required for the steady-state—dictates that electrons and holes have a common lifetime at  $x = \bar{x}$ ), and  $\bar{\theta}_n$  and  $\bar{\theta}_p$  are the (approximate) transit-time-to-lifetime ratios for the electrons and holes, respectively, over the body of the plasma. Clearly, the inequalities in Equation (11) require that  $\bar{\theta}_n \ll 1$  and  $\bar{\theta}_p \ll 1$ . The linear variations of  $n$  and  $p$  with  $x$  in Equation (12) are represented by the two long-dashed straight lines in Figure 2. From the opposite signs of the slopes of the two lines, it is obvious that where the electrons are in excess ( $n > \bar{n}$ ) the holes are deficient ( $p < \bar{p}$ ): the converse is also true. Thus the resultant space charge due to each is additive, as assumed in Equation (7).

Thus, over the body of the plasma, the excess charge is given by

$$e(n - p) \approx e\bar{n} (\bar{\theta}_n + \bar{\theta}_p) \frac{\bar{x} - x}{L}. \quad (13)$$

At this point, the crucial assumption of the theory is made: *The total space-charge  $Q_-$  between 0 and  $\bar{x}$  consists mainly of space charge in the body of the plasma.* This also applies for the charge  $Q_+$  between  $\bar{x}$  and  $L$ .

Then the limiting density  $\bar{n}$ , to which the plasma builds up, is determined precisely by this condition.

Integrating Equation (13) and taking  $\bar{x} = L/2$

$$|Q_-| = e \int_0^{\bar{x}} (n - p) dx \approx e\bar{n} (\bar{\theta}_n + \bar{\theta}_p) \frac{L}{8}. \quad (14)$$

As stated earlier,  $(1/e)|Q_-|$  is rigorously the area between the true  $n$  and  $p$  curves in Figure 2 from  $x = 0$  to  $x = \bar{x}$ . This area is shaded.

The approximate value for  $(1/e) |Q_-|$  in Equation (14), obtained by approximating  $n$  and  $p$  by Equation (12), is the triangular area in Figure 2 which is cross-hatched. The assumption that the total space charge consists mainly of space charge in the body of the plasma is equivalent to saying that  $(1/e) |Q_-|$  is reasonably well approximated by the triangular area in Figure 2. Our assumption that the cathode and anode are both perfect injecting contacts, i.e., that the cathode is an infinite reservoir of electrons and the anode an infinite reservoir of holes, requires that the over-all sample be neutral (see the Appendix):  $|Q_-| = Q_+$ . Since  $(1/e) Q_+$  is approximated by the triangular area to the right of the point  $(\bar{x}, \bar{n})$ , equality of the two triangular areas clearly requires that  $\bar{x} \approx L/2$ , as used in Equation (14).

It remains to relate  $Q_-$  to the applied voltage. Following Rose,<sup>5</sup> the elementary parallel-plate capacitor relationship is used:

$$|Q_-| = CV \approx \frac{\epsilon V}{L}. \quad (15)$$

For  $C$  we have taken the geometric capacitance corresponding to cathode-anode separation  $L$ ;  $C = \epsilon/L$ .

Combining Equations (14) and (15)

$$V \approx \frac{L|Q_-|}{\epsilon} \approx \frac{e\bar{n}(\bar{v}_n + \bar{v}_p) L^2}{8\epsilon} = \frac{e\bar{n}L^3}{8\epsilon\bar{\tau}} \left( \frac{1}{\bar{v}_n} + \frac{1}{\bar{v}_p} \right). \quad (16)$$

Finally, we relate  $\bar{n}$  to  $J$ ,

$$J = e(nv_n + pv_p) = e\bar{n}(\bar{v}_n + \bar{v}_p). \quad (17)$$

Combining Equations (16) and (17),

$$V \approx \frac{JL^3}{8\epsilon\bar{\tau}\bar{v}_n\bar{v}_p}. \quad (18)$$

Equation (18) is the basic formula from which all results are derived. Except for a numerical factor, it is seen to be identical with Equation (10).

A somewhat more consistent treatment of the problem, following Equation (13), changes the numerical factor in Equation (18) by 50 per cent. The Poisson equation,  $\epsilon d\mathcal{E}/dx = e(n-p)$ , integrates, through the use of Equation (13) and  $\bar{x} = L/2$  and  $\mathcal{E}(0) = 0$ , to

give  $\epsilon\mathcal{E} = e\bar{n} (\bar{\theta}_n + \bar{\theta}_p) [x - (x^2/L)]/2$ . Another integration, from 0 to  $\bar{x} = L/2$ , gives the applied voltage,

$$V = 2 \int_0^{L/2} \mathcal{E} dx = e\bar{n} (\bar{\theta}_n + \bar{\theta}_p) \frac{L^2}{12\epsilon}. \quad (16')$$

The different numerical factors in (16) and (16') arise from our taking  $C$  = the geometrical capacitance =  $\epsilon/L$  in (15), thus giving (16), whereas, more accurately,  $C = (3/2) \times$  the geometrical capacitance =  $3\epsilon/2L$ , giving Equation (16'). The "enhanced" capacitance is due to the distributed space charge. Use of Equation (16') leads to the voltage-current relationship:

$$V \approx \frac{J L^3}{12\epsilon \bar{\tau} \bar{v}_n \bar{v}_p}. \quad (18')$$

#### APPLICATIONS

**Bimolecular Recombination:**  $\bar{\tau} = 1/\alpha\bar{n}$  and  $\alpha = v_T s$ , where  $v_T$  is the thermal velocity and  $s$  the bimolecular recombination cross section.

Substituting for  $\bar{\tau}$  in Equation (18) and using (17):

$$V \approx \frac{\mu_0 J^2 L^3}{4\epsilon^2 \bar{v}_n \bar{v}_p (\bar{v}_n + \bar{v}_p)} \rightarrow J \approx \left\{ \frac{4\epsilon^2 \bar{v}_n \bar{v}_p (\bar{v}_n + \bar{v}_p)}{\mu_0} \right\}^{1/2} \frac{V^{1/2}}{L^{3/2}}, \quad (19)$$

with  $\mu_0 = \frac{\epsilon\alpha}{2e}$ .

Further particularization depends on detailed knowledge of the dependence of the drift velocities  $\bar{v}_n$  and  $\bar{v}_p$  on the electric field intensity  $\bar{\mathcal{E}} \approx V/L$ .

*Low-field mobility case:*  $\bar{v}_n = \mu_n \bar{\mathcal{E}}$  and  $\bar{v}_p = \mu_p \bar{\mathcal{E}}$ .

Equation (19) gives:

$$J \approx 2\epsilon \left\{ \frac{\mu_n \mu_p (\mu_n + \mu_p)}{\mu_0} \right\}^{1/2} \frac{V^2}{L^3}. \quad (20)$$

The conditions  $\bar{\theta}_n \ll 1$  and  $\bar{\theta}_p \ll 1$ , which must be satisfied if our treatment is to be valid, are easily shown to be equivalent to the conditions  $(\mu_n/\mu_0)^{1/2} \gg 1$  and  $(\mu_p/\mu_0)^{1/2} \gg 1$ . (Note that this criterion,

and hence the transit-time-to-lifetime ratio, is independent of applied voltage.) Under these same conditions, R. H. Parmenter and W. Ruppel<sup>19</sup> have solved the problem rigorously (i.e., integrated the differential equations given in the Appendix). Their result is:

$$J_{P-R} = \frac{3\sqrt{2\pi}}{4} \epsilon \left\{ \frac{\mu_n \mu_p (\mu_n + \mu_p)}{\mu_0} \right\}^{1/2} \frac{V^2}{L^3}. \quad (20')$$

It is seen that our result (20) differs from their exact result (20') only by a constant factor — it is larger by the factor  $8/(3\sqrt{2\pi}) = 1.06$ . The fact that our approximate result is so extremely close to the exact result is fortuitous. The use of Equation (18') instead of (18) would have resulted in an error of approximately 25 per cent.

The quantity  $\mu_0$  was first introduced by Parmenter and Ruppel<sup>19</sup> and is called by them the "recombination mobility."

Assuming, for the sake of definiteness, that  $\mu_n \gtrsim \mu_p$ , Equation (20) can be rewritten as:

$$J \approx 2\epsilon \mu_n \left\{ \frac{\mu_p}{\mu_0} \right\}^{1/2} \frac{V^2}{L^3}. \quad (21)$$

In practical units,  $J$  (amperes/cm<sup>2</sup>)  $\approx 2 \times 10^{-13} K \mu_n (\mu_p/\mu_0)^{1/2} (V^2/L^3)$ , where  $K$  is the relative dielectric constant,  $\mu_n$  is in cm<sup>2</sup>/volt sec,  $V$  in volts, and  $L$  in cm.

Equation (21) differs from the one-carrier, electron SCL current equation only through the enhancement factor  $2(\mu_p/\mu_0)^{1/2}$ . As Parmenter and Ruppel<sup>19</sup> have pointed out, for reasonable values of  $s$ , namely  $s \approx 10^{-19}$  cm<sup>2</sup>,  $\mu_0$  is very small —  $\mu_0 \sim 10^{-5}$  cm<sup>2</sup>/volt sec. Thus, enhancement factors of the order of  $10^3$  to  $10^4$  may be expected.

*Saturated drift-velocity case:*  $\bar{v}_n = v_{n,s}$  and  $\bar{v}_p = v_{p,s}$ , both independent of the applied field  $\bar{E}$ :

Equation (19), unmodified, gives the current-voltage ( $J$ - $V$ ) characteristic.

Assuming, for the sake of definiteness, that  $v_{n,s} > v_{p,s}$ , Equation (19) can be rewritten:

$$J \approx 2\epsilon v_{n,s} \left\{ \frac{v_{p,s}}{\mu_0} \right\}^{1/2} \frac{V^{1/2}}{L^{3/2}}. \quad (22)$$

In practical units,  $J$  (amps/cm<sup>2</sup>)  $\approx 2 \times 10^{-13} K v_{n,s} (v_{p,s}/\mu_0)^{1/2} (V^{1/2}/L^{3/2})$  with  $v_{n,s}$  and  $v_{p,s}$  in cm/sec,  $\mu_0$  in cm<sup>2</sup>/volt sec,  $V$  in volts, and  $L$  in cm. Attainable values of the coefficients in Equation (22) are

indicated, for present materials, in Table I, which presents the available data on saturated drift velocities in semiconductors.

Table I—Saturated Drift-Velocities in Semiconductors

Material	Lattice Temperature (degrees Kelvin)	$v_{n,s}$ (cm/second)	$v_{p,s}$ (cm/second)
Ge	300	$7 \times 10^6$	$5.5 \times 10^6$
	77	$9 \times 10^6$	$9 \times 10^6$
Si	300	$8.2 \times 10^6$	$4 \times 10^6$
	77	$> 3.4 \times 10^7$	
InSb	300	$> 5.4 \times 10^7$	
	77	$> 5.4 \times 10^7$	
InAs	77	$1.5 \times 10^7$	

Since the transit times of electrons and holes are saturated, whereas the lifetime decreases with voltage because of increased injection of carriers, there will be a critical voltage  $V_{cr} = Lv_{p,s}/16\mu_0$  at which the hole transit time becomes equal to the lifetime. For  $V > V_{cr}$ , the current is essentially one-carrier, space-charge-limited. Considering the magnitudes of  $v_{p,s}$  and  $\mu_0$ , this is a truly academic point. Long before  $V_{cr}$  could be reached, the sample would break down under the high field.

*One-carrier saturated drift-velocity case:*  $\bar{v}_n = v_{n,s}$  independent of the applied field,  $\bar{v}_p = \mu_p \bar{C}$ , and  $v_{n,s} > \bar{v}_p$ .

Equation (19) reduces to:

$$J \approx 2\epsilon v_{n,s} \left\{ \frac{\mu_p}{\mu_0} \right\}^{1/2} \frac{V}{L^2}. \quad (23)$$

In practical units,  $J$  (amps/cm<sup>2</sup>)  $\approx 2 \times 10^{-13} K v_{n,s} (\mu_p/\mu_0)^{1/2} (V/L^2)$ .

**Recombination Through Localized Centers:**  $\bar{\tau} = \tau = \text{constant}$ , independent of  $\bar{n}$ .

For  $\bar{n} = \bar{p}$ , as required by our assumptions, it will generally be necessary that  $\bar{n} > N_R$ , where  $N_R$  is the density of the effective recombination centers. Actually the more stringent requirement comes from our assumption that the space charge, which is the *unneutralized* portion of  $n$ , is also mainly *free* charge. For this to be true, it will generally be required that  $(1/e) |Q_-| = (1/e) Q_+ > N_R L/2$ . From Equation (14) we see that this inequality reduces to  $\bar{n} > 4N_R/(\bar{\theta}_n + \bar{\theta}_p)$  with  $\bar{\theta}_n \ll 1$  and  $\bar{\theta}_p \ll 1$ .

Throughout the plasma, the common lifetime  $\tau$  is given by

$$\frac{1}{\tau} = v_T N_R \frac{s_n s_p}{s_n + s_p}, \quad (24)$$

where  $s_n$  and  $s_p$  are the capture cross sections of the recombination center for electrons and holes, respectively.

*Low-field mobility case:*  $\bar{v}_n = \mu_n \bar{E}$ ,  $\bar{v}_p = \mu_p \bar{E}$ .

Equation (18) gives:

$$J \approx 8\epsilon \tau \mu_n \mu_p \frac{V^3}{L^5}. \quad (25)$$

In practical units,  $J$  (amps/cm<sup>2</sup>)  $\approx 10^{-12} K \tau \mu_n \mu_p V^3/L^5$ .

*Saturated drift-velocity case:*  $\bar{v}_n = v_{n,s}$  and  $\bar{v}_p = v_{p,s}$ , both independent of the applied field  $\bar{E}$ .

Equation (18), unmodified, gives:

$$J \approx 8\epsilon \tau v_{n,s} v_{p,s} \frac{V}{L^3}. \quad (26)$$

In practical units,  $J$  (amps/cm<sup>2</sup>)  $\approx 10^{-12} K \tau v_{n,s} v_{p,s} V/L^3$ .

*One-carrier saturated drift-velocity case:*  $\bar{v}_n = v_{n,s}$  independent of the applied field  $\bar{E}$ ,  $\bar{v}_p = \mu_p \bar{E}$ , and  $v_{n,s} > \bar{v}_p$ .

Equation (18) gives:

$$J \approx 8\epsilon \tau v_{n,s} \mu_p \frac{V^2}{L^4}. \quad (27)$$

In practical units,  $J$  (amps/cm<sup>2</sup>)  $\approx 10^{-12} K \tau v_{n,s} \mu_p V^2/L^4$ .

The various current-voltage formulas of this section, expressed in practical units, are collected together in Table II.

#### CONCLUDING REMARKS

The successful reproduction of the Parmenter-Ruppel exact result (20') by our simplified theory leaves no doubt that the simplified theory presented in this paper predicts the correct current-voltage characteristics for those two-carrier problems where the injected carriers, as well as their resultant space charge, are substantially free. The inclusion in the theory of shallow trapping of the injected carriers

Table II—Current-Voltage Relationships for Various Situations  
(All quantities in practical units).

Lifetime	Drift-velocity Field-Dependence	Current-Voltage Characteristic
$\tau_p = \frac{1}{\alpha n}$	$v_n = \mu_n \mathcal{E}, v_p = \mu_p \mathcal{E}$ $\mu_n \gtrsim \mu_p$	$J \approx 2 \times 10^{-13} K \mu_n \left\{ \frac{\mu_p}{\mu_0} \right\}^{1/2} \frac{V^2}{L^3}$ amps/cm <sup>2</sup>
$\tau_n = \frac{1}{\alpha p}$ $\alpha = v_T s$	$v_n = v_{n,s}, v_p = \mu_p \mathcal{E}$ $v_{n,s} > v_p$	$J \approx 2 \times 10^{-13} K v_{n,s} \left\{ \frac{\mu_p}{\mu_0} \right\}^{1/2} \frac{V}{L^2}$
$\mu_0 = \frac{\epsilon \alpha}{2e}$	$v_n = v_{n,s}, v_p = v_{p,s}$ $v_{n,s} \gtrsim v_{p,s}$	$J \approx 2 \times 10^{-13} K v_{n,s} \left\{ \frac{v_{p,s}}{\mu_0} \right\}^{1/2} \frac{V^{1/2}}{L^{3/2}}$
$\tau = \text{constant}$	$v_n = \mu_n \mathcal{E}, v_p = \mu_p \mathcal{E}$	$J \approx 10^{-12} K \tau \mu_n \mu_p \frac{V^3}{L^3}$
	$v_n = v_{n,s}, v_p = \mu_p \mathcal{E}$ $v_{n,s} > v_p$	$J \approx 10^{-12} K \tau v_{n,s} \mu_p \frac{V^2}{L^4}$
	$v_n = v_{n,s}, v_p = v_{p,s}$	$J \approx 10^{-12} K \tau v_{n,s} v_{p,s} \frac{V}{L^3}$

requires only slight modifications. It remains to apply the theory to those situations in which deep trapping of injected carriers plays an important role.

In concluding, the author would like to stress the invaluable contribution of Parmenter and Ruppel.<sup>10</sup> Their work provided the one available exact result against which to test the approximate results of this paper. It is precisely this check that gives us confidence in our approach and results.

ACKNOWLEDGMENT

The author is indebted to Dr. A. Rose for calling attention to his earlier work on these problems, and to Dr. M. Glicksman for supplying the data for Table I. He is also grateful to Dr. Rose and Dr. Parmenter for their careful reading of the manuscript.

APPENDIX

The most rigorous method for discussing two-carrier current flow proceeds directly from the differential equations appropriate to the

problem. These equations are a current-flow equation (28), Poisson's equation (29), and the conservation equations (30):

$$J = e (nv_n + pv_p) = \text{constant} \quad (28)$$

$$\frac{\epsilon}{e} \frac{d\mathcal{E}}{dx} = n - p \quad (29)$$

$$-\frac{d}{dx} (nv_n) = \frac{d}{dx} (pv_p) = \frac{n}{\tau_n} = \frac{p}{\tau_p}. \quad (30)$$

For the bimolecular-recombination case,  $\tau_n = 1/\alpha p$  and  $\tau_p = 1/\alpha n$  with  $\alpha = v_p s$ .

In the current-flow equation (28), we are clearly neglecting diffusion currents. The form of the Equations (28) through (30) is such that it is convenient to regard the current  $J$  as given and to solve for the corresponding applied voltage and potential distribution. This same procedure is followed in the analysis of one-carrier SCLC.<sup>6</sup>

The boundary conditions that complete the mathematical characterization of the problem are determined by the nature of the injecting contacts. Throughout this paper we are assuming that these are *perfect* injecting contacts, i.e., that the cathode is an infinite reservoir of electrons and the anode an infinite reservoir of holes. In the simplified theory, which neglects diffusive current flow in the region of the contacts, the appropriate boundary conditions are simply that the electric field intensity vanish at the cathode and anode:

$$\mathcal{E} = 0 \text{ at } x = 0 \text{ and at } x = L. \quad (31)$$

Integrating Equation (29) from 0 to  $L$  and using Equation (31), it is seen that the over-all sample is neutral:

$$\int_0^L (n - p) dx = 0.$$

Equations (30) can be rewritten

$$\frac{d(nv_n)}{nv_n} = -\theta_n \frac{dx}{L}; \quad \frac{d(pv_p)}{pv_p} = \theta_p \frac{dx}{L} \quad (32)$$

with  $\theta_n = L/v_n\tau_n$  and  $\theta_p = L/v_p\tau_p$ .  $\theta_n$  and  $\theta_p$  are, so to speak, the *local*

transit-time-to-lifetime ratios for electrons and holes respectively. Integration of Equations (32) gives, rigorously,

$$n v_n = \bar{n} \bar{v}_n \exp \int_x^{\bar{x}} \theta_n \frac{dx}{L} ; \quad p v_p = \bar{n} \bar{v}_p \exp - \int_x^{\bar{x}} \theta_p \frac{dx}{L} \quad (33)$$

where  $\bar{x}$  defines the plane of neutrality, and  $\bar{n} = \bar{p}$ .

In the range of currents of interest, we know that over the main portion of the sample there is a plasma of electrons and holes, and that the various quantities of interest cannot change drastically over the body of the plasma. Further, for all the situations discussed in this paper,  $\bar{\theta}_n \ll 1$  and  $\bar{\theta}_p \ll 1$ . Thus,  $\theta_n \ll 1$  and  $\theta_p \ll 1$  throughout the plasma. Under these conditions the exponentials appearing in Equation (33) can be expanded to give:

$$\begin{aligned} n v_n &= \bar{n} \bar{v}_n \left\{ 1 + \int_x^{\bar{x}} \theta_n \frac{dx}{L} \right\} \\ p v_p &= \bar{n} \bar{v}_p \left\{ 1 - \int_x^{\bar{x}} \theta_p \frac{dx}{L} \right\} \end{aligned} \quad (34)$$

Using the boundary conditions given in Equations (31), Equation (29) integrates directly to give,

$$\bar{E} = - \frac{e}{\epsilon} \int_0^{\bar{x}} (n - p) dx = \frac{|Q_-|}{\epsilon} = - \frac{e}{\epsilon} \int_{\bar{x}}^L (p - n) dx = \frac{Q_+}{\epsilon}. \quad (35)$$

Equations (12) clearly are obtained from Equations (34) by taking  $\theta_n = \bar{\theta}_n$ ,  $\theta_p = \bar{\theta}_p$ ,  $v_n = \bar{v}_n$ , and  $v_p = \bar{v}_p$ . These approximations are equivalent to replacing the differential Equations (30) by the simpler equations:

$$- \bar{v}_n \frac{dn}{dx} = \frac{n}{\bar{\tau}_n}, \quad \bar{v}_p \frac{dp}{dx} = \frac{p}{\bar{\tau}_p}. \quad (30')$$

The relations given in Equations (12) are indeed the solutions to (30'). An essential approximation made in obtaining Equations (30') from (30) is

$$\frac{d}{dx} (n v_n) = v_n \frac{dn}{dx} + n \frac{dv_n}{dx} \approx v_n \frac{dn}{dx},$$

and likewise

$$\frac{d}{dx} (pv_p) \approx v_p \frac{dp}{dx}.$$

These approximations are valid only so long as  $\left| \frac{n \frac{dv_n}{dx}}{v_n \frac{dn}{dx}} \right| < 1$  and

$$\left| \frac{p \frac{dv_p}{dx}}{v_p \frac{dp}{dx}} \right| < 1. \text{ For the case of saturated drift velocities, } \frac{dv_n}{dx} \approx 0$$

and  $\frac{dv_p}{dx} \approx 0$ , and the approximations are automatically justified.

However, for the low-field case,  $v_n = \mu_n \mathcal{E}$  and  $v_p = \mu_p \mathcal{E}$ ,

$$\left| \frac{n \frac{dv_n}{dx}}{v_n \frac{dn}{dx}} \right| = \left| \frac{n \frac{d\mathcal{E}}{dx}}{\mathcal{E} \frac{dn}{dx}} \right| \approx \left| \frac{\bar{n} (n-p)}{\bar{n} \theta_n \int_0^{L/2} (n-p) dx} \right| \approx \frac{|\bar{x} - x|}{\bar{\theta}_n} \frac{L}{8}.$$

It follows that, in this case, Equations (30') are good approximations to Equation (30) over only a very small portion of the sample

near the center:  $\left| \frac{L}{2} - x \right| \leq \frac{\bar{\theta}_n \bar{\theta}_p}{\bar{\theta}_n + \bar{\theta}_p} \frac{L}{8}$ . It is concluded that a

rigorous justification of the results of the preceding sections requires a more careful analysis. Before this finer analysis is undertaken, it is noted that the source of the difficulty lies in the neglect of the variations of  $v_n$  and  $v_p$  with position in Equations (34). Note that it is permissible to neglect the variations of  $\theta_n$  and  $\theta_p$  with position, i.e., to take  $\theta_n = \bar{\theta}_n$  and  $\theta_p = \bar{\theta}_p$  inside the integrals appearing in Equations (34) since  $\theta_n$  and  $\theta_p$  are small quantities to begin with. That this approximation cannot produce large errors will be argued further with a calculation appearing at the end of this Appendix.

We return to Equations (34) and consider them for the particular case of low-fields:  $v_n = \mu_n \mathcal{E}$  and  $v_p = \mu_p \mathcal{E}$ . Equations (34) are re-written

$$n\mathcal{E} = \bar{n}\bar{\mathcal{E}} \left( 1 + \int_x^{\bar{x}} \theta_n \frac{dx}{L} \right) \tag{36}$$

$$p\mathcal{E} = \bar{n}\bar{\mathcal{E}} \left( 1 - \int_x^{\bar{x}} \theta_p \frac{dx}{L} \right)$$

Subtracting the second equation from the first and using Equation (29):

$$(n - p) \mathcal{E} = \frac{\epsilon}{2e} \frac{d\mathcal{E}^2}{dx} = \bar{n}\bar{\mathcal{E}} \int_x^{\bar{x}} (\theta_n + \theta_p) \frac{dx}{L} . \tag{37}$$

As discussed above, we take  $\theta_n = \bar{\theta}_n$ ,  $\theta_p = \bar{\theta}_p$  in Equation (37) and integrate:

$$\frac{d\mathcal{E}^2}{dx} = \frac{2e\bar{n}\bar{\mathcal{E}}(\bar{\theta}_n + \bar{\theta}_p)(\bar{x} - x)}{\epsilon L} . \tag{38}$$

Integration of Equation (38) gives

$$\mathcal{E} = \bar{\mathcal{E}} \left\{ 1 - \frac{e\bar{n}(\bar{\theta}_n + \bar{\theta}_p)(\bar{x} - x)^2}{\epsilon\bar{\mathcal{E}}L} \right\}^{1/2} . \tag{39}$$

Since  $\mathcal{E} = 0$  at  $x = 0$  (Equations (31)):

$$\epsilon\bar{\mathcal{E}} = |Q_-| = e\bar{n}(\bar{\theta}_n + \bar{\theta}_p) \frac{L}{4} . \tag{40}$$

Equation (40) differs only by a factor of 2 from Equation (14). Using (40),  $\mathcal{E}$  can be written

$$\mathcal{E} = \bar{\mathcal{E}} \left\{ 1 - \frac{4(\bar{x} - x)^2}{L^2} \right\}^{1/2} . \tag{41}$$

Equations (29), (39), and (41) give

$$n - p = \frac{\bar{n}(\bar{\theta}_n + \bar{\theta}_p)(\bar{x} - x)}{\left\{1 - \frac{4(\bar{x} - x)^2}{L^2}\right\}^{1/2}} = \frac{\left(4\epsilon \frac{\bar{\mathcal{E}}}{e}\right)(\bar{x} - x)}{\left\{1 - \frac{4(\bar{x} - x)^2}{L^2}\right\}^{1/2}}. \quad (42)$$

Comparing Equation (42) with (13), we see that the "triangular" approximation for  $(n - p)$ , namely (13), underestimates the charge  $|Q_-| = Q_+$ .

Integrating Equation (41) to obtain the applied voltage:

$$V = 2 \int_0^{L/2} \mathcal{E} dx = \bar{\mathcal{E}}L \int_0^{\pi/2} \cos^2 \theta d\theta = \frac{\pi}{4} \bar{\mathcal{E}}L, \quad (43)$$

Equations (40) and (43) give

$$V = \frac{e\bar{n}(\bar{\theta}_n + \bar{\theta}_p)L^2}{\epsilon 16/\pi}. \quad (44)$$

Equation (44) differs by less than a factor of 2 from Equation (16).

It is instructive to examine the variations of  $\theta_n$  and  $\theta_p$  with position:

$$(\bar{x} = L/2): \frac{\bar{\theta}_n}{\theta_n} = \frac{\bar{n}}{\bar{v}_n} \frac{v_n}{p} = \frac{\bar{n}}{p} \frac{\mathcal{E}}{\bar{\mathcal{E}}} = \frac{\bar{n}\bar{\mathcal{E}}}{p\mathcal{E}} \frac{\mathcal{E}^2}{\bar{\mathcal{E}}^2} = \frac{1 - 4\frac{(\bar{x} - x)^2}{L^2}}{1 - \bar{\theta}_p \frac{(\bar{x} - x)}{L}}, \quad (45)$$

$$(\bar{x} = L/2): \frac{\bar{\theta}_p}{\theta_p} = \frac{\bar{n}}{\bar{v}_p} \frac{v_p}{n} = \frac{\bar{n}}{n} \frac{\mathcal{E}}{\bar{\mathcal{E}}} = \frac{\bar{n}\bar{\mathcal{E}}}{n\mathcal{E}} \frac{\mathcal{E}^2}{\bar{\mathcal{E}}^2} = \frac{1 - 4\frac{(\bar{x} - x)^2}{L^2}}{1 + \bar{\theta}_n \frac{(\bar{x} - x)}{L}}. \quad (46)$$

From Equation (46) it follows that  $\theta_p$  decreases monotonically from  $\infty$  at  $x = 0$  to  $\bar{\theta}_p$  at  $x = \bar{x}$ . From Equation (45) it follows that

$\theta_n$  decreases monotonically from  $\infty$  to  $\bar{\theta}_n$  at  $x = \bar{x} - \bar{\theta}_p L/4$ . Between  $x = \bar{x} - \bar{\theta}_p L/4$  and  $\bar{x}$ ,  $\theta_n < \bar{\theta}_n$  but  $\theta_n/\bar{\theta}_n \approx 1$ . Thus, except over a narrow interval of width  $(\bar{\theta}_n + \bar{\theta}_p) L/4$  about  $\bar{x} = L/2$ ,  $\theta_n$  and  $\theta_p$  are everywhere greater than  $\bar{\theta}_n$  and  $\bar{\theta}_p$ , respectively.

Therefore, the other extreme from taking  $\theta_n = \bar{\theta}_n$ ,  $\theta_p = \bar{\theta}_p$  in Equation (37) is to take  $\theta_n$  and  $\theta_p$  equal to their values at the *other* limit of integration. Equation (37) then reduces to:

$$\frac{\epsilon}{e} \mathcal{E} \frac{d\mathcal{E}}{dx} = \bar{n} \bar{\mathcal{E}} (\theta_n + \theta_p) \frac{(\bar{x} - x)}{L} = \frac{\alpha L \bar{n} \bar{\mathcal{E}}}{\mu_n \mu_p \mathcal{E}^2} (p v_p + n v_n) \frac{\bar{x} - x}{L}. \quad (47)$$

From Equations (34),

$$p v_p + n v_n \approx \bar{n} \left[ (\bar{v}_n + \bar{v}_p) + \frac{\bar{x} - x}{L} (\bar{v}_n \theta_n - \bar{v}_p \theta_p) \right]. \quad (48)$$

In substituting Equation (48) into (47) it is necessary to keep only the leading term:

$$\mathcal{E}^3 \frac{d\mathcal{E}}{d\bar{x}} \approx \frac{e \alpha L \bar{n}^2 \bar{\mathcal{E}}^2}{\epsilon} \left( \frac{1}{\mu_n} + \frac{1}{\mu_p} \right) \frac{(\bar{x} - x)}{L}. \quad (49)$$

Integrating Equation (49):

$$\bar{\mathcal{E}}^4 - \mathcal{E}^4 = \frac{2 e \alpha \bar{n}^2 \bar{\mathcal{E}}^2}{\epsilon} \left( \frac{1}{\mu_n} + \frac{1}{\mu_p} \right) (\bar{x} - x)^2. \quad (50)$$

Requiring that  $\mathcal{E} = 0$  at  $x = 0$  (taking  $x = L/2$ ):

$$|Q_-| = \epsilon \bar{\mathcal{E}} = \frac{e \bar{n} L}{2} \left\{ \frac{\alpha \bar{n} L}{\mu_n \bar{\mathcal{E}}} + \frac{\alpha \bar{n} L}{\mu_p \bar{\mathcal{E}}} \right\} = e \bar{n} (\bar{\theta}_n + \bar{\theta}_p) \frac{L}{2}. \quad (51)$$

This result differs from Equation (40) only by the factor 2. Thus we have verified our earlier contention that no large error would be incurred by neglecting the variations with position of  $\theta_n$  and  $\theta_p$  in Equation (37).

# A CdS ANALOG DIODE AND TRIODE\*

By

W. RUPPEL<sup>‡</sup> AND R. W. SMITH<sup>†</sup>

*Summary*—An ideal insulator represents the “electrical analog” of a vacuum since it is devoid of free charge carriers. Space-charge-limited excess carriers can be drawn through an insulator across an ohmic contact which provides the reservoir of excess carriers. Diode and triode operation that is precisely analogous to the corresponding vacuum devices is obtained by applying ohmic and blocking contacts to the insulator. Analog diode and triode operation is demonstrated using an insulating cadmium sulfide single crystal.

## INTRODUCTION

IN THE last twenty years, as an outgrowth of the rapidly increasing knowledge of the physics of the solid state, a number of solid-state devices have been constructed which have proven in many respects to be superior to vacuum devices. It is interesting to note, however, that none of the actual solid-state devices which have found widespread application represents the true analog of the vacuum diode or triode.

If one is to build an analog solid-state diode or triode, what is required conceptually is to fill the space between the electrodes with a solid through which a space-charge-limited current flow of injected free charge carriers can be achieved. Since a vacuum in thermal equilibrium does not contain any free charge carriers, the proper solid-state analog to a vacuum is the perfect insulator.

Space-charge-limited currents through highly perfect insulating cadmium sulfide single crystals have been observed by Smith and Rose.<sup>1</sup> On the basis of these observations the construction of solid-state analog devices has become possible. A cadmium sulfide single-crystal diode and triode are described showing the principle of solid-state analog operation.

## ANALOG DIODE

One of the simplest vacuum-tube devices is a diode. It is based on the principle that a space-charge-limited electron current can flow

---

\* Manuscript received October 22, 1959.

<sup>‡</sup> Laboratories RCA, Limited, Zurich, Switzerland.

<sup>†</sup> RCA Laboratories, Princeton, N. J.

<sup>1</sup> R. W. Smith and A. Rose, “Space-Charge-Limited Currents in Single Crystals of Cadmium Sulfide,” *Phys. Rev.*, Vol. 97, p. 1531, March, 1955.

through vacuum provided that the cathode emits electrons. The other electrode retains electrons and, hence, blocks the current flow in the opposite direction. In a solid-state analog diode the vacuum inter-electrode space is replaced by an insulator. In an ideal insulator in thermal equilibrium, as in vacuum, there are no free charge carriers. The current through an ideal insulator in the dark or through vacuum is carried entirely by carriers injected from the contacts if field emission of electrons from impurity or lattice atoms in the insulator is excluded. Therefore, in an analog diode one of the two contacts to the insulators must inject free carriers into the insulator. It is called the "ohmic" contact. The other contact must retain free carriers and is therefore known as the "blocking" contact. In the following, the nature of ohmic and blocking contacts to an insulator is discussed, and then the space-charge-limited current flow through an insulator is considered and compared with that through vacuum.

#### *Ohmic Contact*

The injection of excess majority free carriers into the insulator requires a reservoir of free carriers at the contact. The carriers enter into the insulator by diffusion; the electric field vanishes close to the contact. Conceptually, either electrons at the cathode or holes at the anode or both of them simultaneously at the two electrodes can enter the insulator by diffusion. The injection of carriers across such ohmic contacts is always limited by the space charge which is formed by the injected carriers in the insulator, both with and without applied voltage.

The hot oxide cathode in a vacuum tube may be considered to form an ohmic contact for electrons to the vacuum, as long as emission is limited by space charge and not by temperature. Similarly, current injected into an insulator can be considered as a thermal emission current from the cathode. There is, however, one important difference with respect to the vacuum case. In the vacuum case the work function of the cathode determines the emissivity. In an electrical contact to an insulator, it is the difference in work functions between the contact material and the insulator that determines the energy difference between a conduction electron in the contact material and one in the volume of the insulator. In principle, an ohmic contact is formed when the work function of the contact material is smaller than that of the insulator. However, the work functions of the two materials can be modified by surface layers and by surface reactions when the two materials are brought together. Therefore, this rule has to be applied to practical cases with some caution, since the exact nature of these surface processes will be unknown in most cases.

The difference between the work functions of the contact material and the insulator will in general be smaller than the work function of the contact material itself. This difference can even be made smaller than the work function of an oxide cathode. For this reason it is easier to achieve electron injection into an insulator than into a vacuum, and large space-charge-limited excess carrier injection currents can be drawn across an ohmic contact into an insulator at room temperature.

### *Blocking Contact*

A contact is blocking if no free carriers can enter from it into the insulator. The work function of almost any metal is large enough so that only a negligible emission current is drawn from the room-temperature electrode in a vacuum diode. Since, in contrast to the vacuum case, it is the difference in work functions that determines the maximum emission current for a contact to an insulator, a good blocking contact can only be formed by a high-work-function material. If, for example, the insulator is n type, then a p-type semiconductor is likely to form a good blocking contact, since in the p-type semiconductor the Fermi level is likely to lie deeper in energy below the vacuum level than in the n-type insulator.

### *Space-charge-limited Current Flow*

As stated above, the diffusion of electrons across an ohmic contact into vacuum or into an insulator is limited by the space charge of the injected carriers. The space-charge-limited current flow in a vacuum tube is a well-known phenomenon; space-charge-limited one-carrier current flow through insulators has been analyzed by Rose<sup>2</sup> and Lampert.<sup>3</sup> For the illustration of the operation of an analog device, the main physical differences between space-charge-limited current flow through vacuum and through an insulator are outlined briefly.

In a vacuum diode the electrons make no collisions en route from cathode to anode and therefore are accelerated continuously in their transit. In an insulator, the electrons move in general with constant velocity.\* This results in a difference in the dependence of the transit time and, hence, of the space-charge-limited current on the voltage

---

<sup>2</sup> A. Rose, "Space-Charge-Limited Currents in Solids," *Phys. Rev.*, Vol. 97, p. 1538, March, 1955.

<sup>3</sup> M. A. Lampert, "Simplified Theory of Space-Charge-Limited Currents in an Insulator with Traps," *Phys. Rev.*, Vol. 103, p. 1648, September, 1956.

\* For the case of one-carrier current flow through insulators with field-dependent mobility see M. A. Lampert, "Simplified Theory of One-Carrier Currents with Field Dependent Mobilities," *Jour. Appl. Phys.*, Vol. 29, p. 1082, July, 1958.

and the interelectrode distance for an electron in vacuum and in an insulator. While the space-charge-limited current through vacuum is proportional to  $V^{3/2}/d^2$ , where  $V$  is the applied voltage and  $d$  the interelectrode distance, the one-carrier current through a semiconductor or trap-free insulator<sup>4</sup> is proportional to  $V^2/d^3$ . The difference in voltage dependence is even more pronounced when the insulator contains traps and part of the injected space charge is bound in traps. Alternatively, the concentration and distribution in energy of traps can be deduced according to the theory of Rose<sup>2</sup> and Lampert<sup>3</sup> from the particular shape of the current-voltage characteristic of a space-charge-limited current. In this way, trap distributions have been determined in CdS<sup>5</sup> and ZnS<sup>6</sup>.

In addition to modifying the shape of the current-voltage curve, trapping of the free carriers and scattering by the thermal vibrations of the insulator lattice and by imperfections lowers the absolute magnitude of a space-charge-limited current in an insulator relative to that in vacuum. Large space-charge-limited currents can therefore be drawn only through very thin and highly perfect insulators.

#### A CdS ANALOG DIODE

A CdS single crystal was used as the insulator to substitute for the vacuum in the construction of an actual analog diode. The crystal was a platelet of 10 microns thickness. It was grown by sublimation of CdS in an H<sub>2</sub>S atmosphere. Although it was not deliberately activated, it showed some photosensitivity. The resistivity of the crystal in the dark and at low voltages exceeded 10<sup>12</sup> ohm-centimeters.

An ohmic and a blocking contact, each about 1 mm<sup>2</sup> in area, were applied to opposite sides of the crystal, giving an interelectrode spacing of 10 microns. Indium metal, which is known to form an ohmic contact to CdS,<sup>7</sup> was evaporated onto the crystal. Tellurium was chosen for the blocking contact.

---

<sup>4</sup> N. F. Mott and R. W. Gurney, *Electronic Processes in Ionic Crystals*, Oxford Clarendon Press, England, 1940; W. Shockley and R. C. Prim, "Space-Charge Limited Emission in Semiconductors," *Phys. Rev.*, Vol. 90, p. 753, June, 1953; G. C. Dacey, "Space-Charge Limited Hole Current in Germanium," *Phys. Rev.*, Vol. 90, p. 759, June, 1953.

<sup>5</sup> R. W. Smith, "Properties of Deep Traps Derived from Space-Charge-Current Flow and Photoconductive Decay," *RCA Review*, Vol. XX, p. 69, March, 1959.

<sup>6</sup> G. F. Alfrey and I. Cooke, "Electric Contact to Zinc Sulphide Crystals," *Phys. Soc. Proc.*, Vol. 70B, p. 1096, November, 1957; W. Ruppel, "Space-Charge-Limited Currents in ZnS Single Crystals," *Helv. Phys. Acta*, Vol. 31, p. 311, 1958.

<sup>7</sup> R. W. Smith, "Properties of Ohmic Contacts to Cadmium Sulfide Single Crystals," *Phys. Rev.*, Vol. 97, p. 1525, March, 1955.

The d-c current-voltage characteristic of a CdS analog diode with one indium and one tellurium contact is shown in Figure 1. The upper curve, the forward characteristic of the rectifier, is obtained with the indium contact negative and the tellurium contact positive. The lower curve shows the back current.

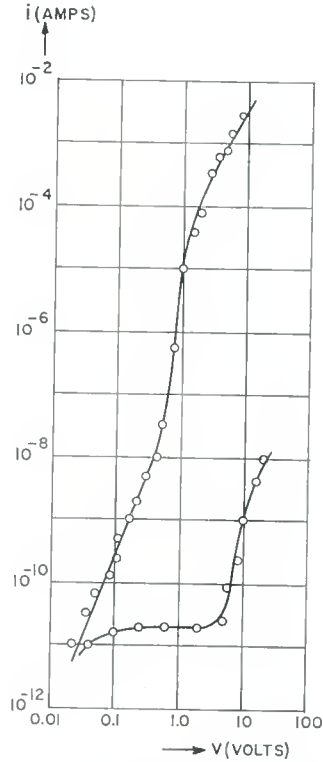


Fig. 1—D-C characteristic of CdS analog diode with indium cathode and tellurium anode (contact area  $1 \text{ mm}^2$ ).

### Forward Current

The forward current shows the behavior that is expected for a space-charge-limited current through an insulator with traps.<sup>3</sup> At low voltages the current increases approximately with the square of the applied voltage. The square law indicates trapping of the injected excess electrons predominately in a single level lying above the quasi Fermi level for electrons. From the slight deviation from the square law, it must be concluded that the quasi Fermi level moves through an energy region in the forbidden gap with a small distribution of traps. With increasing applied voltage the quasi Fermi level moves

towards the single trap level. When the quasi Fermi level crosses the trap level, the current increases steeply with voltage. The transition from square-law to an almost vertical current-voltage curve determines position and concentration of the single trap level.<sup>5</sup> At still higher voltages the current increases again with the square of the applied voltage. The square law at high voltages has also been observed in CdS<sup>8</sup> and in ZnS.<sup>6</sup> The interpretation of this branch, on the basis of the theory of Rose<sup>2</sup> and Lampert,<sup>3</sup> is that a high density of shallow traps is present. On the other hand, the observation of electroluminescence in the range points to some two-carrier injection. The forming of the anode that precedes the injection of holes is often indicated by irreversible current changes.<sup>9</sup>

### Back Current

When the tellurium is biased negatively, the diode is operated in its back direction, since the tellurium makes a blocking contact to the CdS crystal. Little is known about the precise nature of this heterogeneous junction. The number of recombination centers in the junction region is readily affected by slight variations in the preparation and subsequent treatment of the junction. The magnitude and voltage dependence of the back current of the rectifier accordingly lack reproducibility in time and from sample to sample. The magnitude of the saturated portion of the back current in Figure 1 can be accounted for by a high generation and recombination rate of carriers due to a high concentration of centers at the junction. The mechanism of the low-voltage breakdown at 5 volts ( $E = 5 \times 10^3$  volts/cm), however, is not clear.

### HIGH TEMPERATURE ANALOG DIODE

The principle of analog operation lends itself to high-temperature performance since large-band-gap materials can readily be used.

Neither indium nor tellurium provided suitable contacts at elevated temperatures. The evaporated uniform indium layer decomposes into separate droplets and the tellurium layer re-evaporates. A gallium<sup>7</sup> ohmic contact and graphite<sup>8</sup> blocking contact were therefore used at high-temperature measurements.

The magnitude of a space-charge-limited injection current increases with increasing temperature since the ratio of free to trapped injected

---

<sup>8</sup> G. T. Wright, "Space-Charge-Limited Currents in Insulating Materials," *Nature*, Vol. 182, p. 1296, November, 1958.

<sup>9</sup> R. W. Smith, "Low-Field Electroluminescence in Insulating Crystals of Cadmium Sulfide," *Phys. Rev.*, Vol. 105, p. 900, February, 1957.

carriers is larger at higher temperature.<sup>2</sup> The forward current of the rectifier is therefore expected to increase at elevated temperature. At the same time, the back current across the blocking contact will also be higher and should show a temperature dependence even stronger than that of the forward current, owing to a higher activation energy.

In Figure 2 the current-voltage characteristic of a CdS crystal with gallium and graphite electrodes, taken at 1000 cycles/sec, is shown at

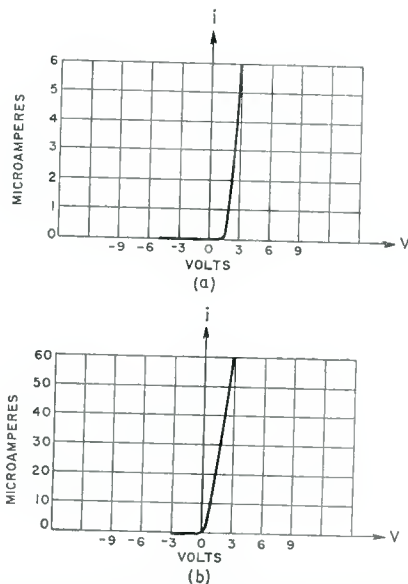


Fig. 2—A-C characteristics of CdS analog diode with gallium cathode and graphite anode (a) at 20 degrees Centigrade and (b) at 300 degrees Centigrade.

room temperature and at 300° C in vacuum. The space-charge-limited forward current at 300° C is about ten times larger than the corresponding current at room temperature, and the back current has increased by an even larger factor. The variation of the forward and back current with temperature was essentially reversible.

### ANALOG TRIODE

#### *The Principles of Solid-State Triodes*

The early solid-state triodes were of the unipolar type, i.e., the motion of charge carriers of only one sign was involved. One example is the modulation by a neighboring metal plate of the current carried

by the thermal equilibrium free-carrier concentration in a semiconductor.<sup>10</sup> The metal plate forms a capacitor with the semiconductor. By applying a voltage of the proper sign to the metal plate, part of the semiconductor is depleted of free carriers, and the current is reduced. Another example is the modulation of an electron current and the corresponding motion of F-centers through KCl at elevated temperatures by introducing a blocking control electrode into the KCl crystal.<sup>11</sup> Finally, in the unipolar transistor<sup>12</sup> a current through a semiconductor is modulated by depletion of part of the current path of free carriers. The depletion is achieved by biasing a p-n junction in the back direction.

It is to be emphasized, however, that in all of these devices no space charge is present in the absence of the control electrode. The current between source and drain electrode is not carried by injected excess space charge but rather by carriers already existing in the semiconductor in thermal equilibrium. Space charge is introduced by the current control only. The sign of the space charge is opposite to that of the conduction carriers, and the free-carrier density is reduced by the control electrode.

In vacuum the thermal equilibrium free-carrier density is zero. Current flow is achieved by the introduction of excess carriers with the concomitant formation of space charge. Current control is effected by modulating the space charge, thus modulating the limitation of the excess carrier injection.

A solid-state analog triode, termed the "analog transistor," was proposed by Shockley.<sup>12</sup> It makes use of space-charge-limited majority carrier injection from a highly doped semiconductor region into an intrinsic region. The injection current is modulated across a back-biased p-i or n-i junction. However, the construction of an analog transistor of the proposed structure containing homogeneous p-i and n-i junctions has, to the writers' knowledge, not been reported.

The CdS analog triode described here is based on the same principle of analog operation. A space-charge-limited excess carrier injection current is drawn through insulating CdS. In the semiconductor analog transistor, the space-charge-limited current would be injected across a forward-biased homogeneous n-i or p-i junction and controlled across

---

<sup>10</sup> O. Heil, British Patent 439, 457, 1935; W. Shockley and G. L. Pearson, "Modulation of Conductance of Thin-Films of Semi-Conductors by Surface Charges," *Phys. Rev.*, Vol. 74, p. 232, July, 1948.

<sup>11</sup> R. Hilsch and R. W. Pohl, "Model of Blocking Layer and Control of Electron Current by Three-Electrode Crystal," *Zeits. f. Physik.*, Vol. 111, p. 399, 1938.

<sup>12</sup> W. Shockley, "Transistor Electronics: Imperfections, Unipolar and Analog Transistors," *Proc. I.R.E.*, Vol. 40, p. 1289, November, 1952.

a back biased homogeneous p-i or n-i junction. In the CdS analog triode, the excess carriers are injected across an ohmic metal-semiconductor contact and controlled across a back-biased heterogeneous semiconductor-insulator junction. Table I summarizes the salient features of analog and unipolar devices.

It may be mentioned at this point that the common bipolar transistor is based upon a different principle of operation. Here, the motion of both carriers—electrons and holes—is essential. Bipolar transistor action depends upon the injection of minority carriers. Space-charge neutrality in regions outside the junctions is maintained due to the short relaxation time of the majority carriers in the semiconductor. While space-charge neutrality has permitted high current densities and relatively high frequency response to be achieved at low voltages, it has not yielded devices in the very-high-impedance range such as can be achieved by the analog triode.

TABLE I

	<i>Unipolar Operation</i>		<i>Analog Operation</i>	
	Free Carrier Concentration	Space Charge	Free Carrier Concentration	Space Charge
Without Control	thermal equilibrium	none	above thermal equilibrium	same sign as free carriers
With Control	below thermal equilibrium	opposite sign to free carriers (depletion layer)	above thermal equilibrium	same sign as free carriers

#### A CdS ANALOG TRIODE

An analog triode is made by adding a grid to the previously described diode in order to control the space-charge-limited forward current. Since a blocking contact is required for the control grid, it is made in the same way as the blocking electrode of the diode. The problem of applying the control grid in such a position as to optimize the modulation of the space-charge-limited current flow is obviously more difficult in a crystal than in vacuum. The electrode arrangement chosen for the demonstration of insulator triode operation is shown in Figure 3.

The grid and the anode are evaporated onto the same face of the CdS crystal with an interelectrode distance of 20 microns. The cathode is applied opposite to the grid electrode, but shifted by about half the

grid-anode distance towards the anode (see Figure 3). The area of each electrode is about 1 square millimeter. The input capacitance of the grid is about 10 micromicrofarads. This electrode geometry is not optimized, but permits the demonstration of analog current control.

The cathode is again formed of indium while the grid and anode are tellurium. The choice of the anode material is not critical for the operation of the triode. Tellurium was chosen for the convenience of simultaneous application with the control-grid electrode.

Figure 3 shows the basic circuit connections for the operation of the triode. A current of excess electrons injected from the indium is drawn between cathode and anode. This injection is limited by the

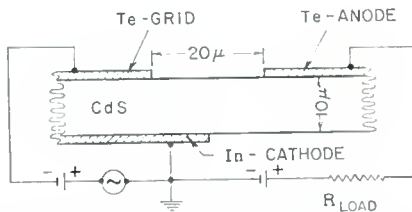


Fig. 3—Cross-sectional view of CdS analog triode showing electrode arrangement and basic circuit connections.

electron space charge accumulated in the interelectrode space. By applying a negative voltage to the grid electrode the negative-space-charge barrier is enhanced, the space-charge limitation becomes more pronounced and the anode current is reduced. It should be emphasized, that for practical design considerations, the CdS crystal should be as thin and as pure as possible. This is necessary in order to obtain high currents. Figure 4 shows the reduction in anode current with negative grid voltage for several anode voltages. The corresponding transconductance is  $(\partial i_a / \partial V_g)_{V_a} \approx 10$  micromhos.

The d-c input resistance of the triode can be taken from Figure 1 to be in the order of  $10^{11}$  ohms since the grid resistance is essentially determined by the back current of the diode. From these values, it follows that the current and the power amplification for d-c are in the order of  $10^5$ , while the voltage amplification is about unity.

The ratio of the a-c to d-c output signal versus frequency is plotted in Figure 5. The frequency response for the present samples extends from d-c through the audio frequency range. Around 1000 cycles per second, an enhanced response is observed. The same effect is observed at lower frequencies as a transient undershoot of about a millisecond duration of the anode current when a negative grid voltage is applied.

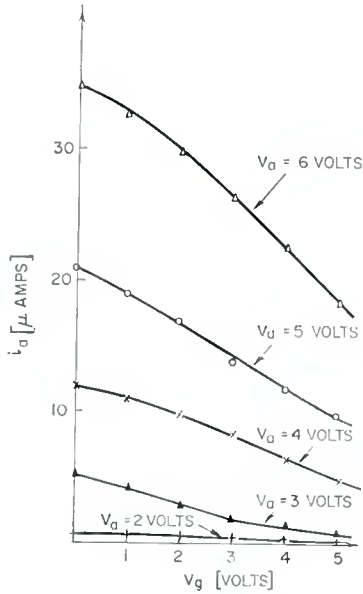


Fig. 4—Anode current as a function of grid voltage for several anode voltages.

The upper frequency limit is expected to be given by the relaxation time of the injected space charge, which is simply the dielectric relaxation time of the insulator under the operating conditions of increased conductivity brought about by excess carrier injection. This argument

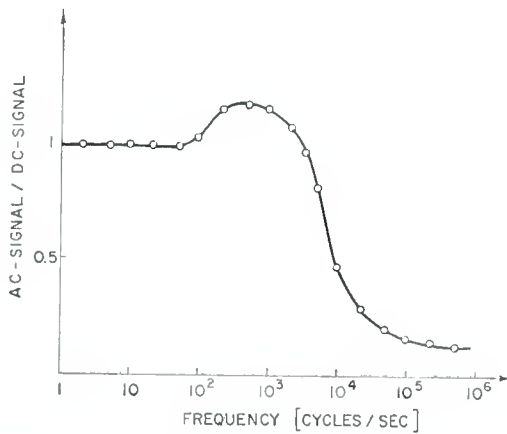


Fig. 5—Ratio of a-c to d-c output signal as a function of frequency ( $V_a = 6$  volts,  $V_g = 3$  volts,  $\Delta V_g = \pm 1$  volt).

assumes that free and trapped charge are in thermal equilibrium. It is evident that the relaxation time will be a minimum when all the injected carriers are free. This underlines the need for more nearly trap-free insulator crystals. Furthermore, a reduction of the inter-electrode dimensions is also expected to lead to higher frequency operation, since the space-charge-limited current at constant electric field, is thereby increased and with it the speed of relaxation.

### CONCLUSIONS

In the investigation of the solid-state analogs of vacuum tube devices, the first step is of course, the demonstration of the principle of operation. One may at this point evaluate the further possibilities and limitations of these devices.

Improvement in the performance will depend mainly on further experimental and theoretical developments in three fields — the technique of growing insulator single crystals, studies of the nature of ohmic and blocking contacts to an insulator, and finally the application of these contacts to the insulator with very small interelectrode dimensions.

Crystals with a still higher degree of perfection than are available now will lead to a higher forward current of the diode and a higher transconductance and power output of the triode, since the magnitude of space-charge-limited currents has an extremely sensitive dependence on the degree of perfection of the insulator up to the point where the free-carrier density exceeds the trap density. For the analog triode to compete in frequency range with the vacuum triode, the electron transit time in the solid must match that in a vacuum. To do this, closer electrode spacings must be used to counterbalance the smaller electron velocities in solids.

Contacts are of crucial importance for the operation of an analog device. The quality of the ohmic contact will determine essentially the noise properties of any analog device. An excellent blocking contact will permit higher voltage, higher impedance and higher-temperature operation. The advantages of higher-voltage operation are apparent — a larger forward to back current ratio for the diode, and greater amplification and better frequency response of the triode due to higher conductivity at the operating point.

An interesting possibility is that of making the cathode ohmic for electron flow and the anode ohmic for hole flow. This arrangement would no longer represent a true analog device but rather a useful extension of it. The current flow, now a two-carrier space-charge-limited current, is expected to exceed the one-carrier current by orders

of magnitude.<sup>13,14</sup> The space-charge limitation to the current is weakened by simultaneous injection of electrons and holes. This is in contrast to the vacuum case where the emission of positive ions by the anode adds only little to the electron current since the cancellation of space charge in the vacuum tube is not as efficient as in a solid owing to the accelerated motion of carriers in vacuum in contrast to constant velocity motion in a solid. The two-carrier space-charge-limited current through an insulator may be controlled either by one grid, as in the analog device, or, more efficiently, by two grids controlling the negative space-charge region at the cathode and the positive space-charge region at the anode separately. The experimental difficulty in the construction of such a device is that of finding ohmic contacts to the insulator for both electrons and holes. The insulator itself should be very highly perfect so as to achieve a long life time for both electrons and holes.

Finally, the great flexibility in the application of contacts by vacuum or electrolytic deposition may lead also to a great versatility in the design of new analog devices. The analog principle therefore seems to be especially well suited for the construction of integrated devices, since it combines small dimensions with the possibility of applying a pattern of ohmic and blocking contacts to an insulator.

#### ACKNOWLEDGMENT

The authors wish to acknowledge the helpful discussions with Dr. Albert Rose relating to this work. Thanks are also due to Dr. Rudolf Nitsche, Laboratories RCA, Ltd., Zurich, Switzerland, for the preparation of the CdS single crystals.

---

<sup>13</sup> R. H. Parmenter and W. Ruppel, "Two-Carrier Space-Charge Limited Current in a Trap Free Insulator," *Jour. Appl. Phys.*, Vol. 30, p. 1548, October, 1959.

<sup>14</sup> M. A. Lampert, "A Simplified Theory of Two-Carrier, Space-Charge-Limited Current Flow in Solids," *RCA Review*, Vol. XX, p. 682, December, 1959.

# SOLID-STATE OPTOELECTRONICS\*†

BY

E. E. LOEBNER

RCA Laboratories,  
Princeton, N.J.

*Summary*—A discussion of the harnessing of photoelectric and luminescent phenomena is preceded by a brief classification and explanation. This is followed by a description of optoelectronic modulators and amplifiers, i.e., devices which have mixed optical and electrical signal and power access. The technology of assembling image-transmitting, image-storing, and picture-reproducing panels from optoelectronic elements is reviewed.

The functioning of various optoelectronic logic nets and computer components is treated in detail. Finally, a synthesis of panel technology and logic circuitry into novel picture-processing panels and computer systems is proposed. The similarity between the organizational structure of such parallel processing systems and that of the neuron network of vertebrate retinas is pointed out.

## INTRODUCTION

INTERACTIONS of light and electricity within matter have been known and studied for nearly a hundred years. However, a systematic exploration of the many relations among optical and electronic phenomena has a more recent history. Solid-state optoelectronics is concerned with the technological exploitation of these relations and employs techniques which are an outgrowth of allied solid-state technologies such as those of semiconductors, phosphors, and photoconductors. In addition to reviewing the past and present work in this area, this paper attempts to outline roughly the likely directions that future developments in optoelectronics will take.

Attention is focused on several unique features of photons which make them more suitable than electrons especially for use in data-handling systems where the information appears in pictorial form and can be processed in parallel in neuron-like networks. The design of photogeometrical pattern processing panels is discussed.

## PHOTON INTERACTIONS WITH SOLIDS

The interactions of photons with matter fall into several categories. Figure 1 is an attempt to represent graphically three categories of interactions of light quanta or photons,  $h\nu$ , incident upon matter.

---

\* Based on a key-note address before the Symposium on Electroluminescent Devices at the Electrochemical Society meeting, May 6, 1959, Philadelphia, Pa.

† Manuscript received October 23, 1959.

Category A is photon or quantum conserving. This means that the photon does not suffer annihilation during its interaction with the solid. These phenomena are part of classical optics. The result of such interactions might be a deflection of the photon from its original path.

Category B is quantum converting, but does not produce ionization within the solid. Photon  $h\nu$  can be converted into another photon,  $h\nu'$ , where frequency  $\nu'$  is usually smaller than the frequency  $\nu$  of the

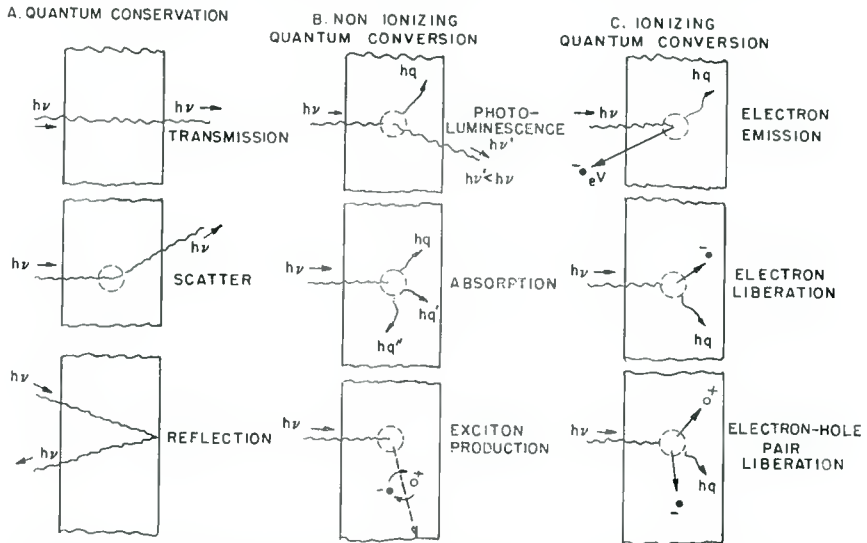


Fig. 1—Graphical representation of interactions of photons incident upon solids ( $h\nu =$  energy of photon,  $hq =$  energy of phonon): (a) quantum conserving, (b) quantum converting without ionization, and (c) quantum converting with ionization.

incident photon. Since the total energy and total momentum of the system has to remain constant in all these interactions, a vibrational quantum,  $hq$ , called a phonon, carries the surplus energy away in the form of heat. This phenomenon is known as photoluminescence. The law which requires  $\nu' \leq \nu$  is known as Stokes' law. In the rare cases where a phonon is absorbed rather than emitted during the process, we speak of anti-Stokes luminescence,<sup>1</sup> since  $\nu' > \nu$  is then permitted. In those instances where all the photon energy is dissipated into heat through the emission of several phonons, the phenomenon is referred to as light or photon absorption. Another case, which could be considered an intermediate case between ionizing and non-ionizing proc-

<sup>1</sup> H. W. Leverenz, *An Introduction to Luminescence of Solids*, Wiley & Sons, New York, New York, 1950, p. 125.

esses, is photon-to-exciton conversion. An exciton<sup>2</sup> is an electron-hole pair where both particles are partially ionized in the sense of being able to propagate through the solid but still remain together because they lack sufficient energy to separate. Although composed of electronic entities, the exciton will not respond to the application of uniform electric fields. However, it can transport the energy of the annihilated photon throughout the solid. The role of the exciton in various optoelectronic phenomena is still controversial.<sup>3</sup>

Category C is quantum converting, just as category B, but ionization in the solid does result. All the phenomena in this category are designated photoelectric phenomena. They result in the photons liberating electrons which are normally confined to the vicinity of certain atoms. If the energy or speed of the liberated electron is sufficient to overcome the pull exerted on it at the surface of the solid (quite similar to the escape velocity of a space-bound rocket), we speak of electron emission or photoelectric emission.

Often the liberated electron does not possess enough speed or energy and remains confined within the walls of the solid. It can still be utilized, however, through the application of external influences such as electric or magnetic fields, microwaves, infrared rays, and others. Its presence is manifested by such phenomena as increased conductivity and changes in the electric and magnetic susceptibilities. Substances which suffer an appreciable change in conductivity because of photon irradiation are known as photoconductors. Photoconductivity is not, however, a simple energy- or power-conversion photoelectric phenomenon; this is discussed in more detail in a later section. If the photon liberates an electron-hole pair, where both the electron and the hole persist long enough in this liberated state to move independently, and if there is within the solid or near its wall an internal electrical field acting on the pair, the field will separate them and generate an electromotive force tending to oppose this field. This phenomenon is known as the photovoltaic effect or the Becquerel photoelectric effect. It has been exploited for many years to power photographic exposure meters and recently has increased in prominence as a potential means for solar energy conversion, competing with thermoelectric and other photoelectric conversion phenomena. Recent discoveries<sup>4</sup> of the unique photo-

---

<sup>2</sup> C. Kittel, *Introduction to Solid State Physics*, Wiley & Sons, New York, New York, 1953, p. 320.

<sup>3</sup> *Proceedings of 1958 International Conference on Semiconductors*, Pergamon Press, Inc., New York, New York, Vol. 8, Various papers and following discussions, pp. 166-195.

<sup>4</sup> S. G. Ellis, F. Herman, E. E. Loebner, W. J. Merz, C. W. Struck and J. G. White, "Photovoltages Larger than the Band Gap in Zinc Sulfide Crystals," *Phys. Rev.*, Vol. 109, p. 1860, March, 1958.

electric properties of planar crystallographic defects, known to occur in certain polymorphic compounds such as ZnS, indicate that monocrystalline photovoltaic power generators can provide outputs of many hundred volts.

### LIGHT PRODUCTION IN SOLIDS

It is a well-established principle in physics that, on an atomic scale, all processes are reversible. A word of caution is necessary. The existence of micro-reversibility does not imply that the probabilities of the reversible processes are the same in both directions nor that

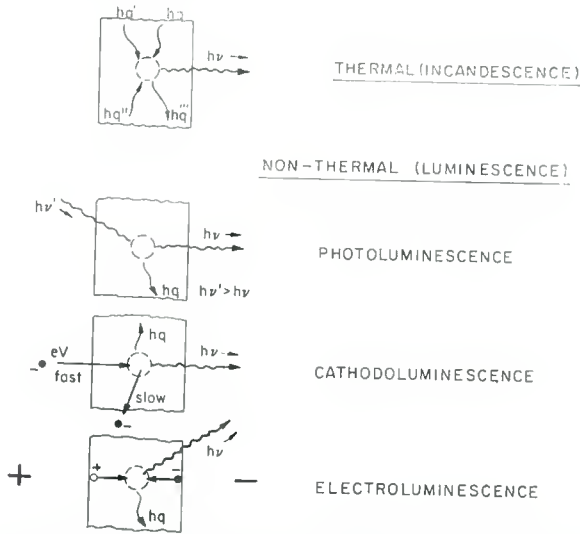


Fig. 2—Graphical representation of photon-producing processes ( $h\nu =$  energy of photon,  $hq =$  energy of phonon).

their efficiencies are the same. However, it does say that each process and phenomenon has its reverse or inverse process and phenomenon. This principle can be applied to photon interactions with matter. Four light-production processes are shown graphically in Figure 2. Two of these are the inverse of processes from category B and two from category C. They have been grouped here in the more conventional manner as thermal (incandescent) and nonthermal (luminescent) processes.

Incandescence can be considered the inverse process of photon absorption accompanied by heat dissipation. Here a number of phonons combine and pool their energies to produce a photon. The incandescent light bulb is the best example of an incandescent device. Photoluminescence becomes its own inverse process if one neglects the

frequency conversion of the photon discussed earlier. Cathodoluminescence becomes the inverse of photoelectric emission. An energetic electron is incident onto the solid, and part of the energy is converted into photon emission while the rest turns into phonons either directly or via secondary electrons.

Electroluminescence can be formally assumed to be the inverse phenomenon of the photovoltaic effect, since photons are produced upon the application of an electromotive force. That this formalism does have a physical justification, at least in some instances, did not escape one of the earliest investigators of electroluminescence, O. V. Lossyev,<sup>5</sup> who also described p-n junctions in SiC as early as 1931.<sup>6</sup> He showed in 1940 that the very same junction was responsible for photovoltaic as well as electroluminescent phenomena.<sup>7</sup> Since this was many years before the recognition of minority carrier injection,<sup>8</sup> a detailed exploration of these effects could not be made and had to await later developments.<sup>9</sup> Recent work at RCA Laboratories<sup>10</sup> has shown striking agreement between electroluminescent and photovoltaic effects generated in a GaP p-n junction and the behavior expected from theory for the case of free electron-hole radiative recombination and generation. Figure 3 is a photograph of injection electroluminescence in GaP due to bimolecular recombination of free majority and minority carriers, and Figure 4 shows the spectral distributions of the electroluminous and photovoltaic responses. Interest in GaP electroluminescence is based on the intermediate position that it occupies physically, chemically, theoretically, and technologically between a "classical phosphor" ZnS on one hand and the classical semiconductors germanium and silicon on

---

<sup>5</sup> O. V. Lossyev, "Luminous Carborundum Detector and Crystal Oscillator," *Telegrafia i Telefonija bez provodov*, (Wireless Telegraphy and Telephony), Vol. 18, p. 61, 1923, and Vol. 26, p. 403, 1924.

<sup>6</sup> O. W. Lossew (O. V. Lossyev), "Glow II of Carborundum Detectors, Electrical Conductivity of Carborundum, and Unipolar Conductivity of Crystal Detectors," *Physik Z.*, Vol. 32, p. 692, 1931.

<sup>7</sup> O. W. Lossew (O. V. Lossyev), "The Spectral Distribution of the Barrier-Layer Photo-Effect in Single Crystals of Carborundum," *Doklady, Akad. Nauk. USSR*, Vol. 29, p. 363, 1940.

<sup>8</sup> W. H. Brattain and J. Bardeen, "Nature of the Forward Current in Germanium Point Contacts," *Phys. Rev.*, Vol. 74, p. 231, July, 1948.

<sup>9</sup> K. Lehovc, C. A. Accardo and E. Jamgochian, "Injected Light Emission of Silicon Carbide Crystals," *Phys. Rev.*, Vol. 83, p. 603, August, 1951; J. N. Shive, "Properties of the M-1740 P-N Junction Photocell," *Proc. I.R.E.*, Vol. 40, p. 1410, November, 1952.

<sup>10</sup> E. E. Loebner and E. W. Poor, Jr., "Bimolecular Electroluminescent Transitions in GaP," *Phys. Rev. Letters*, Vol. 3, p. 23, July, 1959.

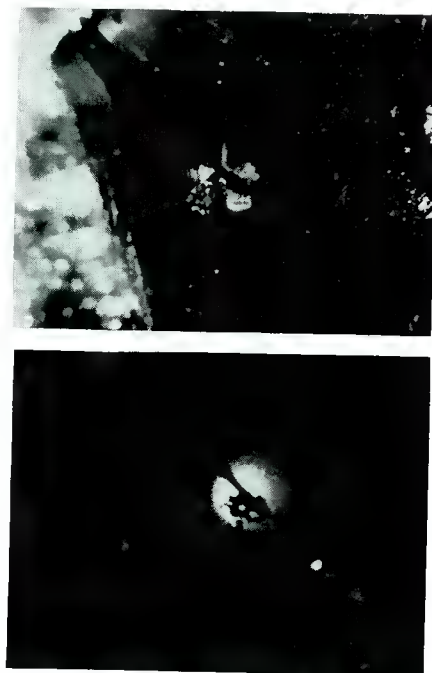


Fig. 3—Photograph of a single crystal GaP diode. (a) Illuminated view of the (111) face to which a gallium-tipped electrode makes contact; (b) electroluminescent emission of 565  $\mu$  light produced through bimolecular recombination of carriers injected across a junction during forward bias.

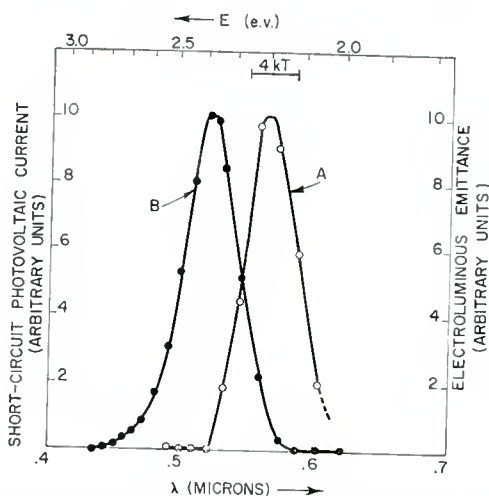


Fig. 4—Spectral distributions of optoelectronic phenomena in GaP. Curve A shows electroluminescent emittance; Curve B short-circuit photo-voltaic current.

the other hand. Electroluminescence in ZnS is discussed at length in a paper by S. Larach and R. E. Shrader.<sup>11</sup>

### MODULATORS AND AMPLIFIERS

Phenomena that give rise to light-responsive and light-producing devices of the converter class, i.e., photoelectric and luminescent power converters, were discussed in the preceding sections. Such converters have two places of access, called ports; one port serves as a supply of the input power, the other delivers the output of the device.

A modulator or amplifier requires the addition of a third port, which we shall call gate since it provides a place of control or gating.

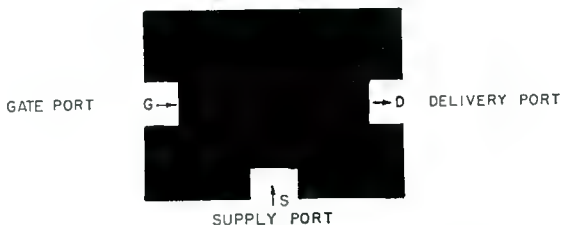


Fig. 5—Schematic representation of a generalized three-port optoelectronic modulator. G is the gate or signal input port, S the supply or power port, and D the delivery or output port.

Formally, any modulator or amplifier can be represented by the proverbial black box as shown in Figure 5. A modulator is capable of amplification if the magnitude of a parameter at the delivery port exceeds the magnitude of the same parameter at the gate port. Any of the three ports can be either optic or electric depending on the form of the energy or power which passes through them.

A classification of optoelectronic modulators by port topology is attempted in Figure 6 by means of a cube. Each port is represented by a face of the cube. Optic ports are shown by diagonal lines on a white background and electric ports by diagonal lines on a grey background. The control or gating ports through which the input signals pass are represented by the front and rear faces, the power-supply ports by the left and right side faces, and the output ports by the top and bottom faces. Each of the eight possible classes of modulator devices is graphically represented by one corner of the cube, its ports by the three faces intersecting in this corner.

<sup>11</sup> S. Larach and R. E. Shrader, "Electroluminescence of Polycrystallites," *RCA Review*, Vol. XX, p. 532, December, 1959.

Let us first consider the four top corners of the device topological cube. Since we have eliminated incandescence from our considerations, they all represent classes of luminescence modulators. The top-left front corner can be considered to represent the all-optical devices. To this group, belong devices employing the well known phenomena of optical enhancement and quenching of photoluminescence, usually by longer wavelength radiation. More recently, several workers<sup>12</sup> called attention to so-called quantum-mechanical amplifiers which are analogous to optical masers, except that they are not coherent amplifiers since spontaneous emission replaces the induced emission of the maser.

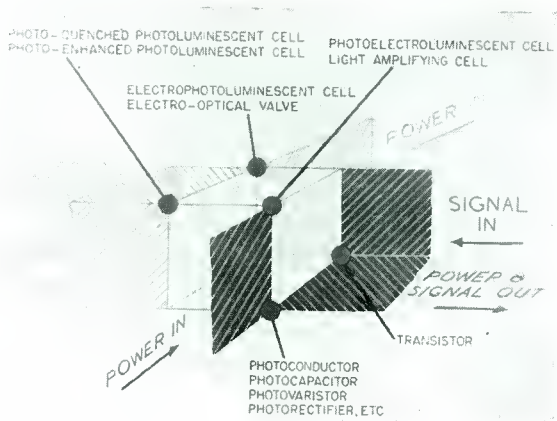


Fig. 6—Topological diagram of the eight classes of optoelectronic modulators. The devices are represented as corners of a cube whose faces designate the functions and nature of the ports. The thinly hatched faces represent optic ports and the thickly hatched faces represent electric ports.

Quite recently, Halsted and coworkers<sup>13</sup> demonstrated the presence of two-stage optical excitation in ZnS and CdS, and thus indicated the possibility of using these and similar materials for the construction of all-optical amplifiers.<sup>14</sup>

Electrical gating of photoluminescence, represented by the top-left

<sup>12</sup> J. Weber, "Maser Noise Considerations," *Phys. Rev.*, Vol. 108, p. 537, November, 1957; N. Bloembergen, "Solid State Infrared Quantum Counters," *Phys. Rev. Letters*, Vol. 2, p. 84, February, 1959.

<sup>13</sup> R. E. Halsted, E. F. Apple and J. S. Prener, "Two-Stage Optical Excitation in Sulfide Phosphors," *Phys. Rev. Letters*, Vol. 2, p. 420, May, 1959.

<sup>14</sup> E. E. Loebner, "Luminescence Modulators and Amplifiers," presented at the *Conference on Solid State Dielectric Devices*, Birmingham, England, September, 1959.

rear corner of the cube, has been referred to as electrophotoluminescence. Halsted<sup>15</sup> has shown that power amplification is possible in an electrophotoluminor cell. Although attempts have been made to explain this phenomenon,<sup>16</sup> the detailed mechanism of this effect is still obscure.<sup>14</sup> Optical gating of electroluminescence (top-right-front corner of the cube) in an integrated solid-state device was reported by Cusano<sup>17</sup> five years ago. Some care has to be exercised in determining the amplification<sup>18</sup> of the device since it also exhibits mixer properties.

When Figure 6 was prepared, the top-right rear corner of the cube stood empty, but since then one device using electrical gating of electroluminescence has been described.<sup>19</sup> Recently the author reported ex-

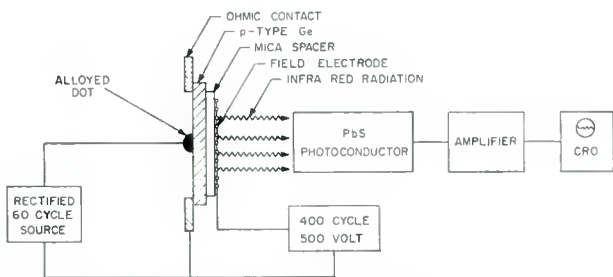
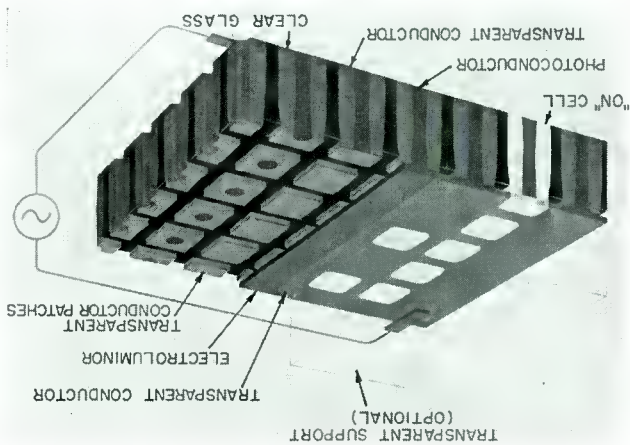


Fig. 7—Diagram of the "Field Effect Modulation of Radiative Recombinations in Germanium" experiment.

periments he carried out jointly with Dr. Braunstein<sup>20</sup> at RCA Laboratories. Figure 7 shows the experimental set-up which was used to demonstrate power gain in a field-modulated germanium diode between electrical gating and radiative output. Modulation of the output is by control of the surface recombination rate, which competes for the minority carriers with radiative recombination centers in the bulk.

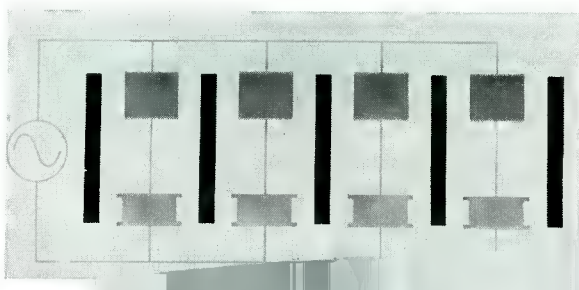
- <sup>15</sup> R. E. Halsted, *Bull. Amer. Phys. Soc.*, Ser. II, Vol. 2, p. 155, 1957.
- <sup>16</sup> R. E. Halsted, "Photoluminescent Modulation in Nonuniformly Excited ZnS Phosphors," *Phys. Rev.*, Vol. 99, p. 1897, September, 1955; P. J. Daniel, R. F. Schwarz, M. E. Lasser, and L. W. Hershinger, "Control of Luminescence by Charge Extraction," *Phys. Rev.*, Vol. 111, p. 1240, September, 1958; Y. T. Sihvonen, D. R. Boyd, and C. D. Woelke, "Some Properties of Green and Red-Green Luminescing CdS," *Phys. Rev.*, Vol. 113, p. 965, February, 1959.
- <sup>17</sup> D. A. Cusano, "Radiation-Controlled Electroluminescence and Light Amplification in Phosphor Films," *Phys. Rev.*, Vol. 98, p. 546, April, 1955.
- <sup>18</sup> E. E. Loebner, "Luminous and Radiant Power Gains of Light-Amplifying Devices," *Jour. Opt. Soc. Amer.*, Vol. 46, p. 227, March, 1956.
- <sup>19</sup> E. E. Loebner, U. S. Patent, 2,817,783.
- <sup>20</sup> R. Braunstein and E. E. Loebner, "Field Effect Modulation of Radiative Recombinations in Germanium," presented at the *AIEE-IRE Solid State Device Research Conference*, Columbus, Ohio, June, 1958.

Fig. 11—Cross-sectional diagram of the cellular image storing panel. Photo-etched holes in a plate of Corning Fotofilm glass are mutually separated by a photo-darkened grid, though surrounded by more transparent glass. The holes contain photoconductor powder in contact with square electrode patches on one side and a continuous electrode on the other. An electroluminescent layer, topped with another electrode, is deposited on the patches.



and constructions of storage light-intensifiers is given by H. O. Hook.<sup>27</sup> Two important attributes of devices of this type are small size of the individual light amplifier elements (permitting a density of several hundred per square centimeter) and small power consumption (approximately 10 milliwatts per square centimeter). Figures 11 and 12 show the construction and operation of one of the earlier designs. It consists of a Corning Fotofilm\* glass plate containing photoconductor-

Fig. 10—Schematic diagram of an optical feedback cellular image-storing panel.



<sup>27</sup> H. O. Hook, "Optical Feedback Type Storage Light Intensifiers," *RCA Review*, Vol. XX, p. 744, December, 1959. \*Registered trade mark.

The bottom face of the device topological cube of Figure 6 contains labels of two quite well known devices, the photoconductor and the transistor. The filling-in of the two other corners of the cube is left as an exercise to the reader of this paper.

It is evident that over half a dozen optoelectronic components are available for incorporation into optoelectronic networks. Most of those built in recent years,<sup>21</sup> however, depend for their control and gain characteristics on incorporated photoconductors. In the following sections, the discussion is limited to cases where the devices and systems are built up from electrically and optically coupled photoconductors and electroluminors. It should be apparent from the discussion in this section that this limitation is probably a temporary one and that the future might bring more complex systems.

OPTICAL TRANSMISSION AND STORAGE PANELS

The most common optoelectronic transmission circuit<sup>22</sup> is a series combination of a photoconductor and electroluminor as shown in Figure 8. It can be shown<sup>23</sup> that the gating photon flux  $h\nu$  controls the

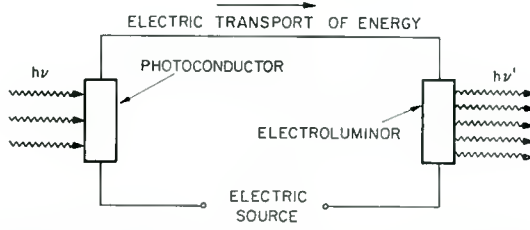


Fig. 8—Optoelectronic photon transmission or conversion circuit. Photons incident on a photoconductor generate electronic charge carriers which gain energy from the electric source and transport some of it to the electroluminor, where part of this energy is reconverted into photons.

transport and conversion of electric power of the source and that the photon flux output  $h\nu'$  can exceed the flux  $h\nu$  by two to three orders of magnitude. If the frequencies  $\nu$  and  $\nu'$  are both in the visible region of the spectrum, this circuit is referred to as a light-amplifier

<sup>21</sup> E. E. Loebner, "Recent Developments in Image Transducers," presented at the *Proceedings of the International Conference on Solid State Physics in Electronics and Telecommunications*, Brussels, Belgium, June, 1958; to be published by Academic Press in a book entitled *Physics of the Solid State*.

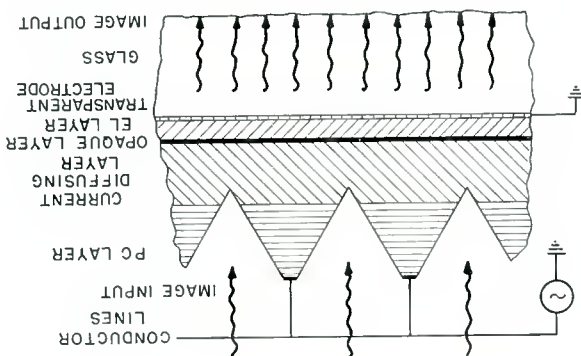
<sup>22</sup> E. E. Loebner, "Opto-Electronic Devices and Networks," *Proc. I.R.E.*, Vol. 43, p. 1897, December, 1955.

<sup>23</sup> A. Rose and R. H. Bube, "The Role of Space-Charge Currents in Light Amplifiers," *RCA Review*, Vol. XX, p. 648, December, 1959.

Another panel device is the storage light-intensifier panel shown schematically on Figure 10. This device differs from the previous ones in that it employs optical feedback for storage functions.<sup>24</sup> It is important that the optical feedback be restricted to within each amplifier element and that crossfeed of light be minimized. This leads to a cellular construction. A more detailed discussion of various designs

versa. Electroluminor-photoconductor light amplifiers are either slow or have a low output level, or they are insensitive to very low input levels. Multistage panels<sup>25</sup> might prove effective in solving this problem. Another possible function of light-transmission panels is that of light inversion,<sup>26</sup> i.e., inverting a negative image into a positive and vice versa.

Fig. 9—Cross-sectional diagram of a portion of the grooved-line photoconductor image-intensifying panel.



The function of these panel devices is to provide a very large number of optic gain ports and only one or two electric power supply

rear corner of the cube, has been referred to as electrophotoluminescence. Halsted<sup>15</sup> has shown that power amplification is possible in an electrophotoluminor cell. Although attempts have been made to explain this phenomenon,<sup>16</sup> the detailed mechanism of this effect is still obscure.<sup>14</sup> Optical gating of electroluminescence (top-right-front corner of the cube) in an integrated solid-state device was reported by Cusano<sup>17</sup> five years ago. Some care has to be exercised in determining the amplification<sup>18</sup> of the device since it also exhibits mixer properties.

When Figure 6 was prepared, the top-right rear corner of the cube stood empty, but since then one device using electrical gating of electroluminescence has been described.<sup>19</sup> Recently the author reported ex-

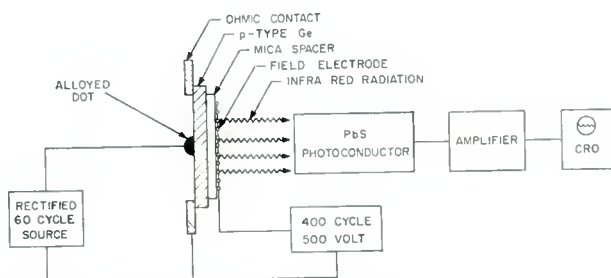


Fig. 7—Diagram of the "Field Effect Modulation of Radiative Recombinations in Germanium" experiment.

periments he carried out jointly with Dr. Braunstein<sup>20</sup> at RCA Laboratories. Figure 7 shows the experimental set-up which was used to demonstrate power gain in a field-modulated germanium diode between electrical gating and radiative output. Modulation of the output is by control of the surface recombination rate, which competes for the minority carriers with radiative recombination centers in the bulk.

<sup>15</sup> R. E. Halsted, *Bull. Amer. Phys. Soc.*, Ser. II, Vol. 2, p. 155, 1957.

<sup>16</sup> R. E. Halsted, "Photoluminescent Modulation in Nonuniformly Excited ZnS Phosphors," *Phys. Rev.*, Vol. 99, p. 1897, September, 1955; P. J. Daniel, R. F. Schwarz, M. E. Lasser, and L. W. Hershinger, "Control of Luminescence by Charge Extraction," *Phys. Rev.*, Vol. 111, p. 1240, September, 1958; Y. T. Sihvonen, D. R. Boyd, and C. D. Woelke, "Some Properties of Green and Red-Green Luminescing CdS," *Phys. Rev.*, Vol. 113, p. 965, February, 1959.

<sup>17</sup> D. A. Cusano, "Radiation-Controlled Electroluminescence and Light Amplification in Phosphor Films," *Phys. Rev.*, Vol. 98, p. 546, April, 1955.

<sup>18</sup> E. E. Loebner, "Luminous and Radiant Power Gains of Light-Amplifying Devices," *Jour. Opt. Soc. Amer.*, Vol. 46, p. 227, March, 1956.

<sup>19</sup> E. E. Loebner, U. S. Patent, 2,817,783.

<sup>20</sup> R. Braunstein and E. E. Loebner, "Field Effect Modulation of Radiative Recombinations in Germanium," presented at the *AIEE-IRE Solid State Device Research Conference*, Columbus, Ohio, June, 1958.

The bottom face of the device topological cube of Figure 6 contains labels of two quite well known devices, the photoconductor and the transistor. The filling-in of the two other corners of the cube is left as an exercise to the reader of this paper.

It is evident that over half a dozen optoelectronic components are available for incorporation into optoelectronic networks. Most of those built in recent years,<sup>21</sup> however, depend for their control and gain characteristics on incorporated photoconductors. In the following sections, the discussion is limited to cases where the devices and systems are built up from electrically and optically coupled photoconductors and electroluminors. It should be apparent from the discussion in this section that this limitation is probably a temporary one and that the future might bring more complex systems.

### OPTICAL TRANSMISSION AND STORAGE PANELS

The most common optoelectronic transmission circuit<sup>22</sup> is a series combination of a photoconductor and electroluminor as shown in Figure 8. It can be shown<sup>23</sup> that the gating photon flux  $h\nu$  controls the

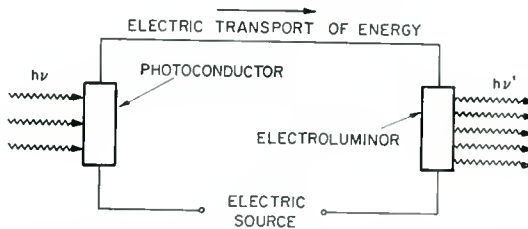


Fig. 8—Optoelectronic photon transmission or conversion circuit. Photons incident on a photoconductor generate electronic charge carriers which gain energy from the electric source and transport some of it to the electroluminor, where part of this energy is reconverted into photons.

transport and conversion of electric power of the source and that the photon flux output  $h\nu'$  can exceed the flux  $h\nu$  by two to three orders of magnitude. If the frequencies  $\nu$  and  $\nu'$  are both in the visible region of the spectrum, this circuit is referred to as a light-amplifier

<sup>21</sup> E. E. Loebner, "Recent Developments in Image Transducers," presented at the *Proceedings of the International Conference on Solid State Physics in Electronics and Telecommunications*, Brussels, Belgium, June, 1958; to be published by Academic Press in a book entitled *Physics of the Solid State*.

<sup>22</sup> E. E. Loebner, "Opto-Electronic Devices and Networks," *Proc. I.R.E.*, Vol. 43, p. 1897, December, 1955.

<sup>23</sup> A. Rose and R. H. Bube, "The Role of Space-Charge Currents in Light Amplifiers," *RCA Review*, Vol. XX, p. 648, December, 1959.

circuit or cell. A cross section of a light-amplifying picture panel designed and built by Kazan and Nicoll<sup>24</sup> is seen in Figure 9. It is known as the photoconductor groove-type light amplifier, and improvements in X-ray fluoroscopy using this construction have been reviewed recently.<sup>21</sup>

The function of these panel devices is to amplify or convert images. Such panels have a very large number of optic gating ports, an equal number of optic output ports and only one or two electric power supply

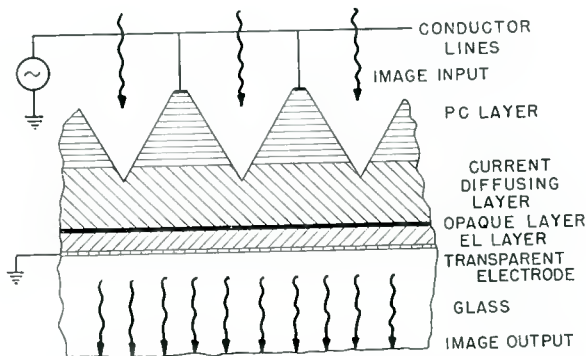


Fig. 9—Cross-sectional diagram of a portion of the grooved-line photoconductor image-intensifying panel.

ports. Thus far, panel image devices promise early application only as converters of X-ray,  $\gamma$ -ray, or infrared ray images to visible images. Electrolumino-photoconductor light amplifiers are either slow or have a low output level, or they are insensitive to very low input levels. Multistage panels<sup>25</sup> might prove effective in solving this problem. Another possible function of light-transmission panels is that of light inversion,<sup>26</sup> i.e., inverting a negative image into a positive and vice versa.

Another panel device is the storage light-intensifier panel shown schematically on Figure 10. This device differs from the previous ones in that it employs optical feedback for storage functions.<sup>22</sup> It is important that the optical feedback be restricted to within each amplifier element and that crossfeed of light be minimized. This leads to a cellular construction. A more detailed discussion of various designs

<sup>24</sup> B. Kazan and F. H. Nicoll, "An Electroluminescent Light-Amplifying Picture Tube," *Proc. I.R.E.*, Vol. 43, p. 1888, December, 1955.

<sup>25</sup> B. Kazan and F. H. Nicoll, "Solid-State Light Amplifiers," *Jour. Opt. Soc. Amer.*, Vol. 47, p. 887, October, 1957.

<sup>26</sup> D. A. Jenny and E. E. Loebner, U. S. Patent 2,883,556 (1959).

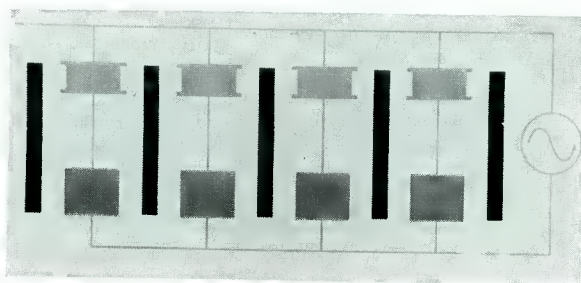


Fig. 10—Schematic diagram of an optical feedback cellular image-storing panel.

and constructions of storage light-intensifiers is given by H. O. Hook.<sup>27</sup> Two important attributes of devices of this type are small size of the individual light amplifier elements (permitting a density of several hundred per square centimeter) and small power consumption (approximately 10 milliwatts per square centimeter). Figures 11 and 12 show the construction and operation of one of the earlier designs. It consists of a Corning Fotoform\* glass plate containing photoconductor-

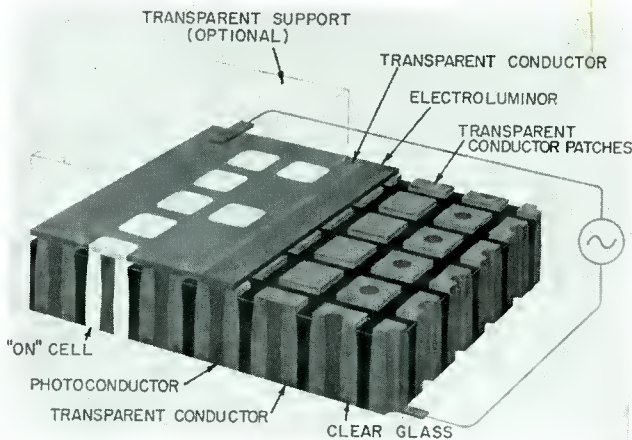


Fig. 11—Cross-sectional diagram of the cellular image storing panel. Photo-etched holes in a plate of Corning Fotoform glass are mutually separated by a photo-darkened grid, though surrounded by more transparent glass. The holes contain photoconductor powder in contact with square electrode patches on one side and a continuous electrode on the other. An electro-luminor layer, topped with another electrode, is deposited on the patches.

<sup>27</sup> H. O. Hook, "Optical Feedback Type Storage Light Intensifiers," *RCA Review*, Vol. XX, p. 744, December, 1959.

\* Registered trade mark.

filled holes surrounded by clear glass and partitioned by a mesh of darkened glass.

Storage intensifier panels of the type described here have a port topology identical to that of the transmission panels. The inputs and outputs to each picture element are optical; the power supply is elec-

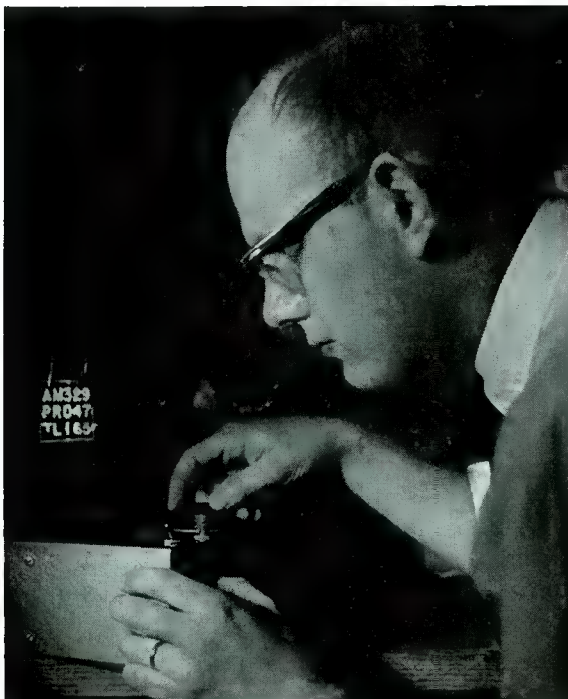


Fig. 12—Photograph of a "Fotoform" glass image-storing panel in operation. It has an area of 25 cm<sup>2</sup>, a resolution of 200 elements per cm<sup>2</sup>, a trigger sensitivity of 10<sup>-1</sup> lux-seconds, and an output of up to 100 lumens per m<sup>2</sup>.

trical. There is no provision for selective erasing of the stored information; the power supply must be interrupted and the whole panel extinguished.

#### PICTURE REPRODUCING PANELS

A much-discussed approach to planar solid-state picture reproducers consists of the use of two mutually perpendicular grids of parallel electrodes to enable a dot-sequential method of picture reproduction. The simple sandwich of an electroluminor layer between the two elec-

trode grids<sup>28</sup> is an approach which suffers from an extremely low contrast and low output level in those cases where the duty cycle of single picture elements is short. Many attempts have been made to improve this situation by introducing an additional solid-state circuit component at each picture element, but thus far, none has proven so feasible as to threaten the dominant role of cathode-ray tubes in the picture-reproducing area. Suggestions to improve the contrast by using diodes<sup>29</sup> or ferroelectric capacitors<sup>30</sup> have been made. In none of these cases have the problems of scanning, switching, and low

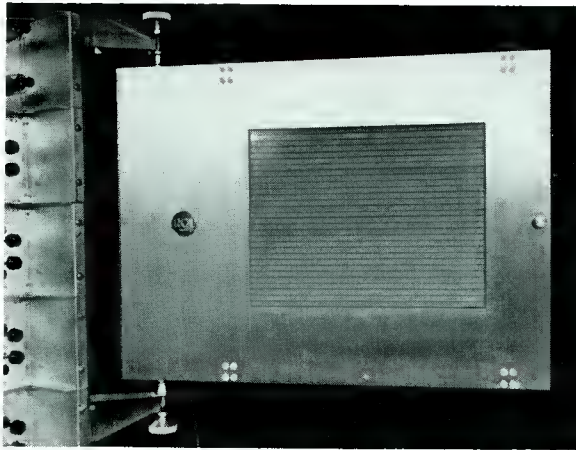


Fig. 13—Front view photograph of the transfluxor-controlled electroluminescent picture display panel. The panel contains an array of 1200 cells, each having an output area of about 1 cm<sup>2</sup>. The panel is less than 4 cm thick. Its area, which is less than 0.5 m<sup>2</sup> also accommodates the magnetic horizontal and vertical scanning systems.

output levels been considered. The first experimental solution of the problem has been provided by Rajchman and associates<sup>31</sup> at the RCA Laboratories. It consists of a transfluxor-controlled mosaic<sup>32</sup> of electroluminor elements as shown in Figure 13. The scanning is accomplished in the panel itself through the use of current-coincident non-

<sup>28</sup> W. W. Piper, U. S. Patent 2,698,915 (1955).

<sup>29</sup> D. C. Livingston, U. S. Patent 2,774,813 (1956); and S. C. Peek, Jr., U. S. Patent 2,818,531 (1957).

<sup>30</sup> E. A. Sack, "ELF—A New Electroluminescent Display," *Proc. I.R.E.*, Vol. 46, p. 1694, October, 1958; B. Kazan, U. S. Patent 2,873,380 (1959).

<sup>31</sup> J. A. Rajchman, G. R. Briggs, and A. W. Lo, "Transfluxor Controlled Electroluminescent Display Panels," *Proc. I.R.E.*, Vol. 46, p. 1808, November, 1958.

<sup>32</sup> J. A. Rajchman and A. W. Lo, "The Transfluxor—A Magnetic Gate With Stored Variable Setting," *RCA Review*, Vol. XVI, p. 303, June, 1955.

linear setting of the transfluxors by means of the two crossed electrode grids.

The switching of the grid is external to the mosaic but incorporated into the panel by means of vertical and horizontal magnetic-core shift registers. Only a single, relatively thin cable connects the panel to the receiver and power supply circuitry. This panel has 1200 picture elements, a contrast of 10, an output of two foot-lamberts, and television scanning rates. It is capable of line-scan television-type picture reproduction, and can also store a picture indefinitely. At the present time, the complexity and large power requirements of solid-state picture reproducers of this type are such that commercial exploitation is not feasible, and practical uses are to be expected only in large-area displays which require half-tone storage.

#### LOGIC NETWORKS AND COMPUTER COMPONENTS\*

Optoelectronic components for image-transducing and image-storing devices have been discussed. Such components detect, transmit, store and reproduce information without intentionally altering the intelligence to be communicated. Reliability and accuracy of the transmitted signals and messages are the measures of performance. In the following sections, components which process, reduce, and digest incoming information are considered. Their output is a more or less complex function of their input. Such functional components are commonly found in data handling and processing machines, sometimes called computers. Because they are capable of carrying out functions of formal logic, these machines are also called logic machines and their component networks logic networks.

Since optoelectronic computer components and systems are a relatively new concept it is helpful to try to determine their position relative to other computer components and systems. An abbreviated computer system chronology is shown in Figure 14.

The impetus to contemporary computer technology came from the invention of the electronic flip-flop. It terminated the mechanical era and introduced the internal degree of freedom of electronic devices as the configurational valve to replace electromechanical relays in electronic network topology. More recently, it has been shown that a large number of solid-state phenomena, such as magnetic, superconductive,

---

\* Portions of this and the succeeding sections were first presented at the "May 1958 AIEE-IRE Philadelphia Symposium on Components for Computers of the Future."

and thermoelectric, may dispossess the thermionic valve from its position. Hysteretic ferrite cores are just one of many examples.

The immediate future represents another transitional stage. This time the information carrier, which thus far has been the electron exclusively, is being replaced by photons, phonons, spins, and the like. The configurational network is no longer composed solely of conductive paths forming a circuit; magnetic flux branches, optical flux links, and other nonelectrical nets compete for the information carrying and processing function. In such advanced functional solid-state devices, the spatial configuration of their chemico-physical make-up takes on as much importance as the electronic flow pattern. Thus space topology, fundamental to mechanical devices, is making a comeback.

STAGES OF COMPUTER TECHNOLOGY		
STAGE	SYSTEMS	DEVICE
MECHANICAL	TRANSLATIONAL	ABACUS
	ROTATIONAL	PASCAL'S ADDER
	ELECTRO-MECHANICAL MORSE RELAY	
ELECTRONIC	ELECTRONIC FLIP-FLOP	ECCLES-JORDAN
	HYSTERETIC MATERIALS	FERRITE CORES
	OPTO-ELECTRONIC	
OPTICAL	{ ?	

Fig. 14—Evolutionary stages of computer technology.

In the following sections, the discussion is limited to just one of these solid-state systems—the optoelectronic one. The others are analogous as has been pointed out in a recent publication.<sup>33</sup> A diagrammatic comparison of electromechanical, electro-optical, and optoelectronic relays is seen in Figure 15. The first two use electron information carriers, and mechanical or optical coupling, respectively. The third uses photons as information carriers and electrons for coupling.

#### FUNCTIONAL COMPONENTS

Figure 16 shows an optoelectronic triple inclusive “OR-gate” network. Any of the three photon signals, A, B, or C, incident on three parallel photoconductors or on a single photoconductor will produce a photon output from the electroluminor in series with the photocon-

<sup>33</sup> E. E. Loebner, U. S. Patent 2,970,001 (1959).

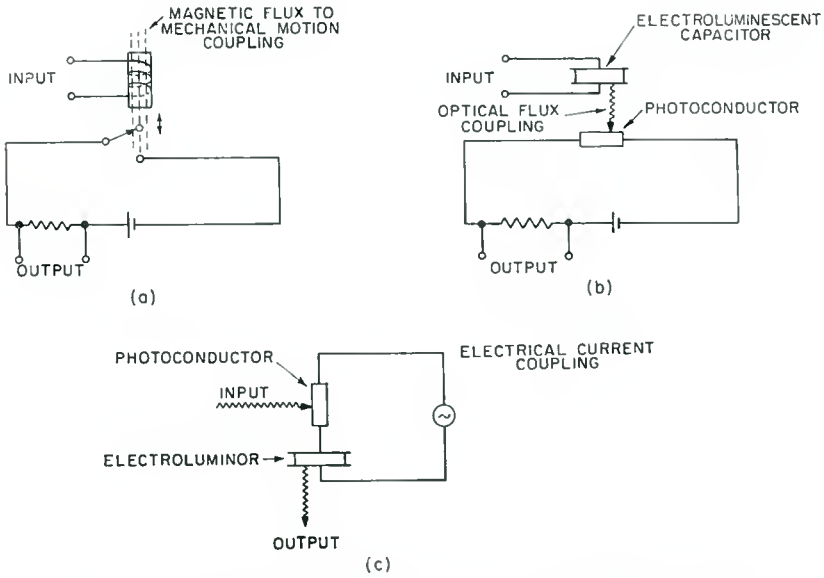


Fig. 15—Schematic of three relays: (a) electromechanical, (b) electro-optical, (c) optoelectronic.

ductors. This principle has been used in the design of the first optoelectronic shift register<sup>22</sup> in which individual photoconductors can be exposed to light from two light sources. A triple “AND-gate” network is seen in Figure 17. Only the simultaneous incidence of photon signals A, B, and C on the three series photoconductors will produce a photon output from the electro-luminescent in series with them. Figure 18 shows how optoelectronic logic nets may be cascaded both optically and elec-

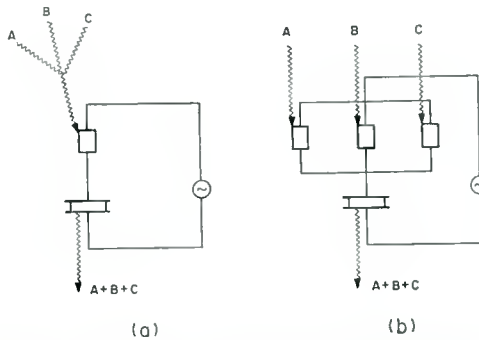


Fig. 16—Schematic of triple “inclusive-OR-gate” networks (a) using a single photoconductor and (b) using three electrically parallel photoconductors.

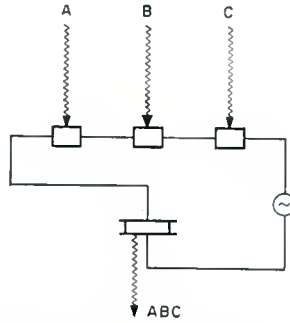


Fig. 17—Schematic of triple "AND-gate" network.

trically. Multiple cascades in diode logic nets present difficulties because of the required bias applied to diodes. These difficulties are absent in optoelectronic logic nets. Figure 19 shows an optoelectronic tree composed of fourteen photoconductors and eight electroluminors. The inputs are photon fluxes or (exclusively)  $\bar{A}$ , and B or (exclusively)  $\bar{B}$ , and C or (exclusively)  $\bar{C}$ . The eight possible photon outputs, each from one electroluminor at a time, are indicated in the drawing. Figure 20 shows the schematic of an optoelectronic inverter or inhibitor or negator. The presence of a photon flux A precludes photon output  $\bar{A}$ , while the absence of A produces  $\bar{A}$ . Figure 21 contains six binary double-input logic elements together with their respective truth tables. The top left element represents a nonconjunction, i.e., no output for the coincidence of A and B but an output for the absence of either or both. The nonconjunction is a negation of the conjunction or "AND". The top middle element represents the negation of the disjunction.

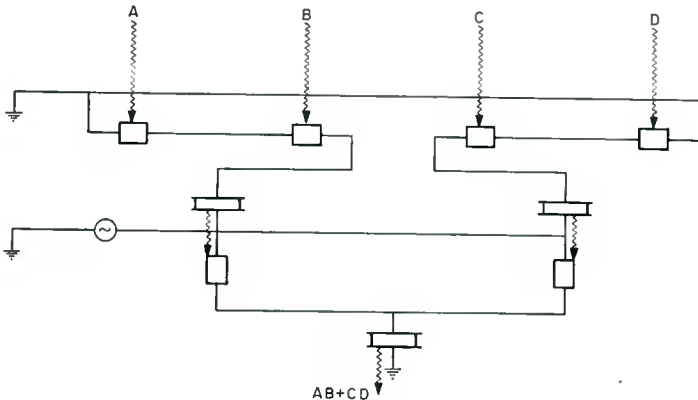


Fig. 18—Schematic of an optically cascaded decision network.

It has an output only in the absence of both A and B. The top right network represents the exclusive "OR". It provides an output if either A or B is present but not both. The bottom left element provides an output only if A is present and B is absent. It is a negation of the logic implication  $A \supset B$ . The last two elements never have an output, whatever the inputs. They represent "CONTRADICTIONS." These

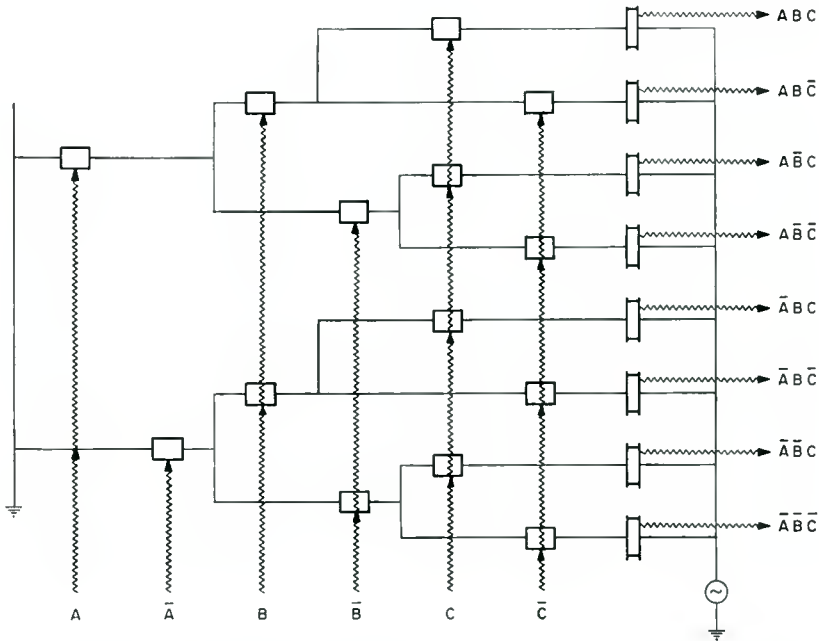


Fig. 19—Schematic of an optoelectronic tree or binary decoding network.

cases are by no means trivial, since in self-organizing systems based on stochastic processes it is of importance that photoconductor-electroluminescent configurational variations provide a great many logic functions, including that of no transfer or isolation.

Ghandi<sup>34</sup> reported recently that the recovery time of optoelectronic circuits can be shortened appreciably by the incorporation of a balancing arrangement first introduced by Tomlinson.<sup>35</sup>

<sup>34</sup> S. K. Ghandi, "Photoelectronic Circuit Applications," *Proc. I.R.E.*, Vol. 47, p. 4, January, 1959.

<sup>35</sup> T. B. Tomlinson, "Principles of the Light Amplifier and Allied Devices," *Jour. British I.R.E.*, Vol. 17, p. 141, 1957.

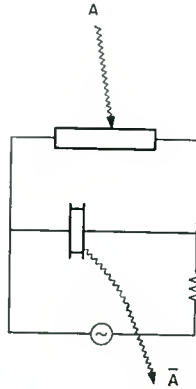


Fig. 20—Schematic of an optoelectronic inverter.

Applications of optoelectronic networks are manifold. One of the most pressing current problems is alphanumeric character display or output in response to the binary code language used in a computer. Not so long ago Westinghouse researchers reported work in this area.<sup>36,37</sup> These systems employ photoconductor-controlled electrolumi-

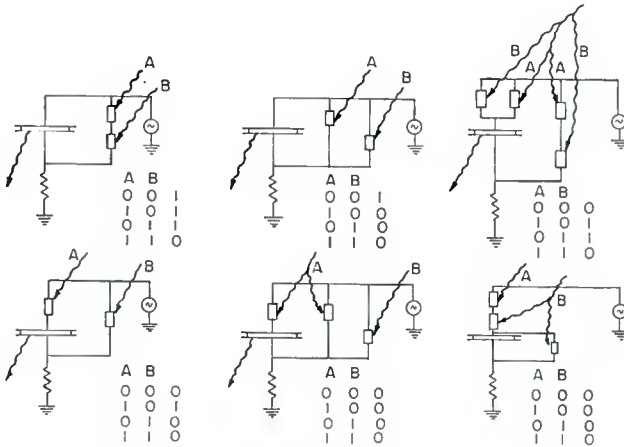


Fig. 21—Schematics and truth tables of six binary double-input single-output logic networks. From left to right, the upper row contains a “non-conjunction,” an “inverse disjunction” and “exclusive OR;” the lower row contains an inverse of implication  $A \supset B$  and two contradiction networks.

<sup>36</sup> E. A. Sack, “An Electroluminescent Digital Indicator With Elpak Translation Logic,” *AIEE Transactions*, Part I—Communications and Electronics, Vol. 77, p. 113, March, 1958.

<sup>37</sup> R. C. Lyman, C. I. Jones and A. Leger, “Remotely Controlled Electroluminescent Totalizing Display,” *Proceedings of the 1958 National Electronics Conference*, Chicago, Ill.

nescent segments from which the alphanumeric characters are synthesized. However, the accompanying switching circuitry is conventional. Quite recently the author described a proposed design of an all optoelectronic number display with storage and binary decoding.<sup>33</sup> Such a device would consist of two photoconductive layers sandwiched among three electroluminescent layers. The output of the device is in the form of an electroluminescent number display similar to the previous ones.<sup>36</sup> However, there are only four binary input signal leads, one set and reset lead, and two power leads, all this in a volume not much greater than that necessary for the display alone.

Another future application will be in character recognition or encoding functions. Various optoelectronic logic decision networks are being studied concurrently. Figure 22 shows the proposed luminous

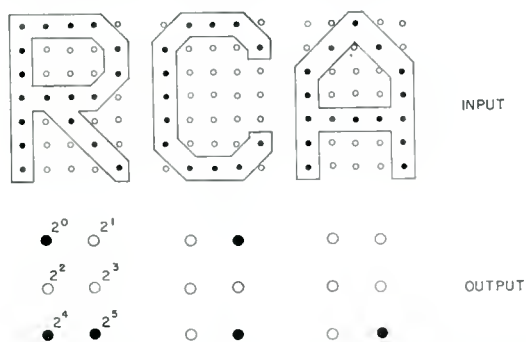


Fig. 22—Luminous input and output patterns of a proposed cognitron.

input and output patterns of a cognitron, i.e., a deterministic cognitive system based on information-retrieval principles. The input arrives in the form of stylized, size- and shape-corrected characters registered onto seven-by-five matrices of optical receptors. There may be hundreds of such matrices on one cognitron panel. The output appears on two-by-three matrices in the form of the binary code used by the RCA 501 computer. Each of these corresponds to one seven-by-five matrix. Even with the relatively slow response of photoconductors, the cognitron approach might increase the present rate of character processing by several orders of magnitude.

#### SHIFT REGISTERS

A shift register is an important component of modern digital computers. It normally is composed of a series of stages, each capable of

<sup>33</sup> E. E. Loebner, "Solid-State Opto-Electronics," *Jour. Electrochem. Soc.*, Vol. 106, p. 59C, March, 1959.

storing or registering a number, most commonly a binary number. Upon an external signal command, referred to either as a transfer or clocking signal, each register stage passes on its number to the succeeding stage. This clears the first stage for the "read-in" of new information and forces a "read-out" at the last stage. Some registers are reversible, i.e., they can be shifted in either of the two directions. Some registers have so-called parallel read-out, i.e., they can also provide an output at once from each stage rather than being limited to sequential or serial read-out.

An optoelectronic shift register was described four years ago.<sup>22</sup> It has two stages per bit of stored information. Each consists of one electroluminor and four photoconductors. Three parallel photoconductors are in series with the electroluminor and one is in shunt. The read-in is optical and occurs at the first stage only. Clocking is optical and there are two clocks. The output is optical and can be read in sequence or in parallel. Each of the three parallel photoconductors has half sensitivity, which makes the operation of the device critical. Trigger of the transferee stage occurs through the coincidence of priming by the transferor stage and of optical clocking. The extinction of the transferor stage is also accomplished by the same clocking pulse. This requires a higher switching rate for the trigger function.

Another shift register, due to Tomlinson,<sup>35</sup> employs an electroluminor-photoconductor series pair per stage in a two stage per bit design. The stages are arranged in two electrically independent series, but optically coupled in a zig-zag fashion. This shift register uses optical priming and two electrical clocks. Although structurally simpler, this system poses a reliability problem due to the necessary timing of the electrical switching. An improvement has been reported by Bray.<sup>39</sup> It is accomplished through the introduction of a third series of stages. This design also enables a reversible operation.

An improvement of the original design was described recently.<sup>40</sup> It eliminates one of the parallel photoconductors and extinguishes the transferor stage by optical feedback from the transferee stage. This same principle was also employed by Reis<sup>41</sup> in a shift register that employs two series rather than parallel photoconductors and uses electrical pulse clocking.

A relatively different shift register design<sup>21,33</sup> is one which uses

---

<sup>39</sup> T. E. Bray, "An Electro-Optical Shift Register," *Digest of the Solid State Circuit Conference*, Philadelphia, Pa., pp. 32-33, February, 1959.

<sup>40</sup> E. E. Loebner, U. S. Patent 2,895,054 (1959).

<sup>41</sup> C. S. Reis, U. S. Patent 2,900,522 (1959).

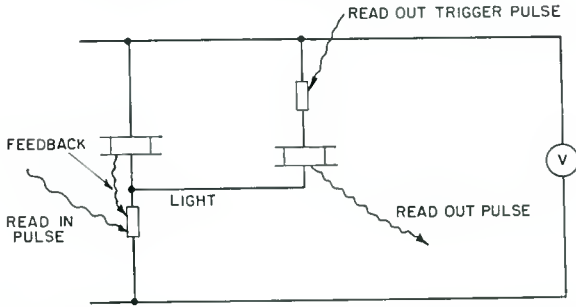


Fig. 23—Schematic of a single stage of an optical-sensing shift register.

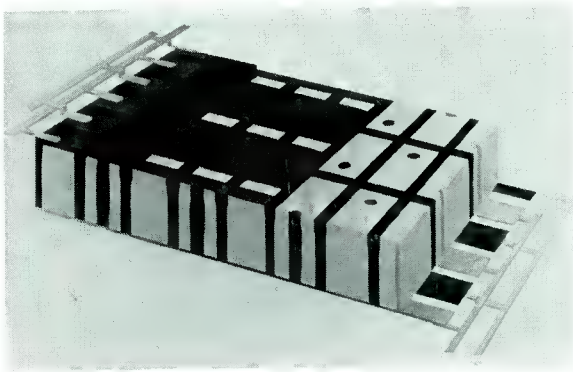


Fig. 24—Cross-sectional diagram of a proposed Fotoform structure of an array of three optically clocked parallel read-out shift registers.

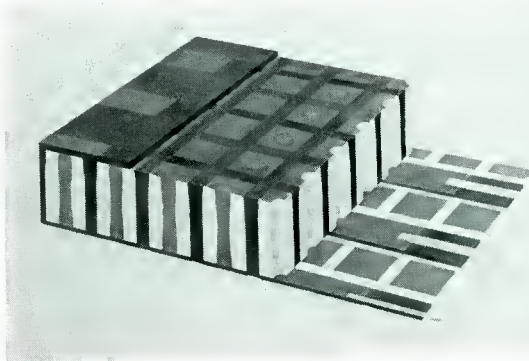


Fig. 25—Cross-sectional diagram of a proposed Fotoform structure of an array of three optically clocked parallel read-out shift registers.

a destructive readout of the register stage shown in Figure 23. Such a transferor stage is self-extinguishing and provides a read-out signal which can be intercepted by the transferee stage.

Proposed three-dimensional structures for a bank of shift registers with electrical and optical clocking, respectively, are seen in Figures 24 and 25. Basically, the same techniques are employed as in the early storage light intensifiers except that the photoducts, photoconductors, electroluminors, and electrodes appear in more complex patterns.

#### IMAGE-PROCESSING PANELS AND SYSTEMS

The various functional optoelectronic components<sup>22,34-37</sup> have been discussed as has the existing image transmission, conversion, and storage technology; it is suggested that their synthesis will lead to novel picture-processing panels and computer systems. Such photo-handling of pictorial data could provide decision networks which geometrically process in parallel many alphanumeric symbols. The output of such devices can appear either in conventional machine code or in synthesized and stylized displays which would not overload a human input channel.

Let us consider a planar mosaic of image elements. For conceptual simplicity they have been arranged into a rectangular matrix. The space between the image elements is available for incorporation of logic components whose inputs come from the primary image elements and whose output represents the processed primary image. These intraplanar logic components could provide any of the numerous logic functions discussed above, their combinations, or other functions not specifically mentioned. In Figure 26, a design of a vertical and horizontal intramultiplication panel is shown. The intrapanel directionality can be obtained through the use of color codes. Thus, a quadruple grid of color transmission filter bands is formed in the pattern indicated in Figure 26. These are to replace the dark mesh of the previously discussed panel-storage image intensifiers and panel shift-register banks. The image input of the panel is incident through the compartments containing the hatched squares. Since the letters R G B Y indicate red, green, blue, and yellow transmission filters, the primary polychromatic image elements will feed red light to the left, green light to the right, blue light down and yellow light up. The compartments between the neighboring primary image elements contain logic elements of the conjunction between up-down and left-right. Only if blue from above and yellow from below is incident, will there be an output from the vertically inbetween elements, and, similarly, only green from left and simultaneously red from right will produce

an output from the horizontally interposed logic elements. These can be powered separately or together. The output can be obtained directly, testing for vertical and horizontal connectivity of the input image, or can be further handled by intraprocessing. Thus, if, for instance, the vertical intra-elements have a green output and the horizontal intra-elements have a blue output and if we place in the lower-right diagonal empty space an inclusive "OR" circuit responsive to green and blue inputs, the output of this circuit will indicate the absence of a lower or right edge or both at the associated primary image element. If the "AND" logic is replaced in this panel by the negative implications (i.e., presence of blue, absence of yellow and presence of green

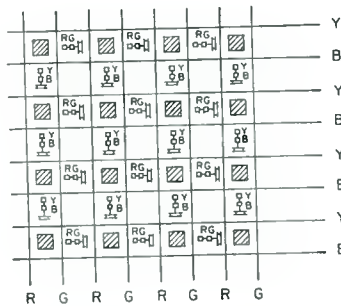


Fig. 26—Schematic of a vertical and horizontal intramultiplication panel design. Such panels perform nearest neighbor logic in the two directions.

and absence of red), these will indicate the presence of figure edges at the bottom and at the right respectively. And if we further cascade using an "AND" instead of the previously considered "OR" in the empty space, the read-out will indicate lower right corners of all figures in the primary image. It is thus clear that the incorporation of intra-panel logic provides a powerful image-processing tool.

As the second example, consider the same grid as in Figure 27, but now at each image element shown, consider the color-code directional distributor of Figure 28. Only one in four of the main storage pairs receives an input light pulse. The color code photoconductor-electroluminor pairs are as follows: green-yellow, red-blue, blue-green, and yellow-red. This gives rise to a two-dimensional planar shift register.\* Upon receipt of a train of color light pulses, the total image will translate a number of lattice spacings equal to one half the number of pulses. The color of the pulse determines the direction of translation.

\* Work on two-dimensional optoelectronic planar shift registers is being currently sponsored by the Cambridge Air Force Research Center.

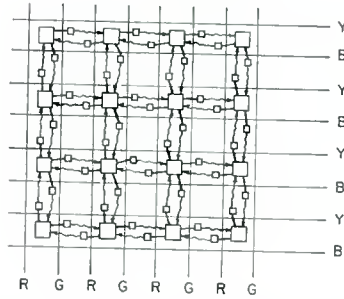


Fig. 27—Schematic of a two-dimensional planar shift register.

In addition to various intra-panel processings,<sup>21</sup> numerous inter-panel processings can be incorporated by cascading images or component images in depth from panel to panel. It is clear that a sufficient number of interconnected intra-logic panels will lead to a novel type of spatially functional computer. It can be shown that this new computer concept does resemble in many ways the type of computer organization almost concurrently proposed by Unger.<sup>42</sup>

It is worthwhile to consider the implications of this new concept to the current organization of information processing. The present type of organization is shown as part A at the top of Figure 29. It consists of serial processing through single input memory processing, control, and output units. The organization of image-data-handling machines of the type described above calls for parallel processing,

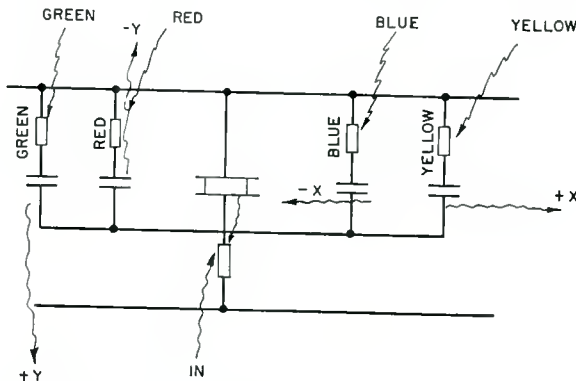


Fig. 28—Diagram of a color-coded four-directional sensing distributor.

<sup>42</sup> S. H. Unger, "A Computer Oriented Toward Spatial Problems," *Proc. I.R.E.*, Vol. 46, p. 1744, October, 1958.

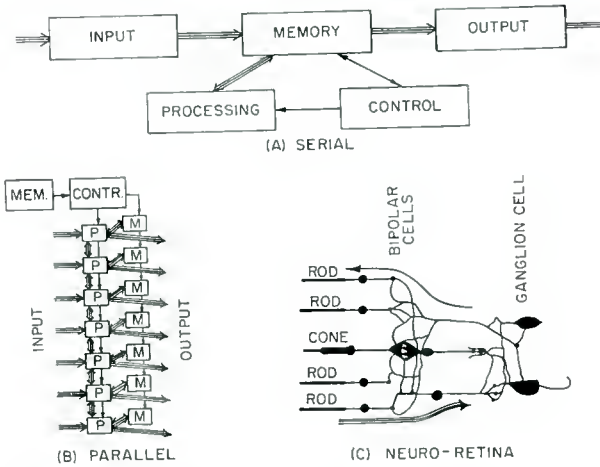


Fig. 29—Schematic of organization of information or data processing. (a) Conventional in series, (b) proposed for parallel or planar processing, (c) biological in neuro-retinas.

shown in the lower left of Figure 29 as part B. Structurally, parallel processing resembles the organization of the neuro-retina (see part C of Figure 29) which is also a parallel processing network.<sup>43</sup>

To show that the resemblance to neuron-like elements is not purely external, a photo-threshold logic network is indicated in Figure 30.

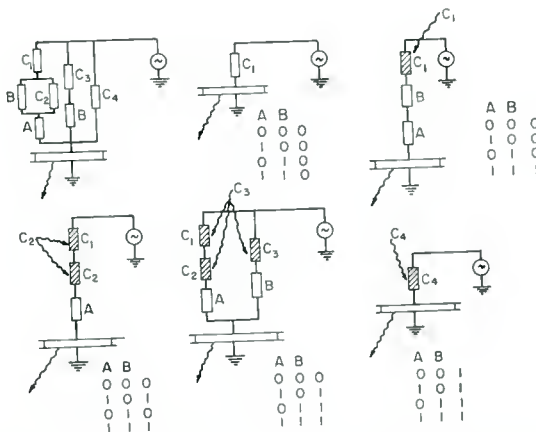


Fig. 30—Schematics and truth tables of logically flexible photo-threshold networks.

<sup>43</sup> H. B. Barlow, "Summation and Inhibition in The Frog's Retina," *Jour. Physiol.*, Vol. 119, p. 69, January, 1953.

The two inputs are A B or, let us say, blue- and yellow-sensitive photoconductors, while the C's are red-sensitive photoconductors of graded sensitivity from high for  $C_1$  to low for  $C_4$ . The five logic functions of "CONTRADICTION", "AND", "A" (irrespective of B), "OR", and "TAUTOLOGY" follow the McCulloch rules.

Thus future data-handling systems will resemble more and more neural networks of the kind found in biological organs. The retina of the frog<sup>44</sup> provides a good example. It has a built-in decision network to respond only to inputs which are characteristic of photo-signals received from a fly moving in the frog's proximity. Built-in specificities to various image inputs might help to advance not only particular data-retrieval technologies, but more generally, intelligence coding, language transformation, and automation of thought processes.

### CONCLUSIONS

Solid-state optoelectronics concerns the use and control of numerous relations among optical and electronic phenomena in solids. These phenomena, in which photons and electrons interact with each other in many ways, can be used to generate, convert, and modulate power, or to detect, transmit, process, and display signals. Although most of the optoelectronic phenomena have been known for a great many years, it is only recently that their technological exploitation has begun to accelerate. A growing semiconductor technology has resulted in a more concerted effort in research and development of electroluminescent and photoelectric devices. These devices have been discussed in order of increasing complexity.

The simplest class of optoelectronic devices consists of converters. One of the earliest optoelectronic converters is the photovoltaic cell. In the past only a qualitative detector of radiation, this device promises to become quite useful in conversion of solar power. Very recently new photovoltaic effects, which might extend the utility of photovoltaic converters, were discovered in disordered crystals.

An electroluminescent cell is not only formally but also operationally the conjugate of the photovoltaic converter; an interchange of the input and output power is possible on the very same device. Both devices incorporate a solid-state structure known to be characteristic of rectifiers. The electroluminescent converter is undergoing a develop-

---

<sup>44</sup> W. S. McCulloch, "Stability of Biological Systems," paper #11, *Proceedings of the Symposium on Homeostatic Mechanics*, Brookhaven Symposia in Biology (1957); "Apathe Tyche of Neuron Nets—The Lucky Reckoners," paper 4-3, *Transactions of the Symposium on the Mechanization of Thought Processes*, National Physical Laboratory, Teddington, England, November, 1958.

ment in two areas — as a radiant power source and as an electric-to-radiant signal transducer. In the former case improvements of its operating characteristics, i.e., efficiency, output level and life expectancy, are being sought; in the latter case new applications in controls, automation, instrumentation and displays are being found.

A more complex class of optoelectronic devices consists of modulators. Many of these are capable of power gain and quantum yield greater than unity. Photoconductor devices are the oldest and best known of the various modulators. The passage of current through them is modulated by the amount and spectral composition of incident radiation. Devices in which the radiation modulates electroluminescent power conversion have been called photoelectroluminescent devices, while devices with electrical modulation of a photon to photon conversion process have been referred to as electrophotoluminescent. Electrical modulation of electrofluorescent power conversion has also been reported in germanium. Thus far, only the photoconductor has achieved industrial prominence.

The third level of complexity is attained by an electrical association between an electroluminescent cell and some modulator such as a photoconductor, transfluxor, or transpolarizer, and the arraying of these cells into large-area display panels. Such panel devices are potential contenders for the place of the thus far dominant cathode-ray tubes in special large-area applications. Many problems remain unsolved, although many image-intensifying, converting, storing, and reproducing panel devices have been built.

A fourth level of complexity is found in optoelectronic logic nets and computer components, which, in spite of their present sluggishness, offer the advantages of small size, weight, power consumption, and cost. Parallel and series electric and optic associations of conjugate optoelectronic transducers are used to design image-processing panels such as planar shift registers, logic matrices, and code converters.

The highest level of complexity is exemplified by optoelectronic devices of the future, which may consist of many-layered optically coupled stacks of the planar devices described above. Alphanumeric character encoding and decoding devices or picture-analyzing and abstracting data-handling equipment are some of the possible future applications of solid-state optoelectronics. The logic organization of such devices will most likely tend to resemble more and more that of biological neural networks, such as the neuro-retina in vertebrates. Logic flexibility can be incorporated into optoelectronic networks using the threshold of photoresponsivity.

# OPTICAL FEEDBACK TYPE STORAGE LIGHT INTENSIFIERS\*

BY

H. O. HOOK

RCA Laboratories,  
Princeton, N. J.

*Summary*—Three designs of storage light intensifiers were evaluated by building samples. One design uses a Fotoform glass structure to support the photoconductor and electroluminor and to provide optical isolation of cells. Another uses a transparent (glass or plastic) multiple pedestal structure to provide light paths through the photoconductor and support the active materials. The photoconductor itself provides the optical isolation. The third design uses a flat glass plate as a support, the active materials and optical isolation being built up in layer fashion. Devices of the last type worked best. Typical operation provided optical trigger of 0.1 foot-candle second, half-hour storage and 0.1 second erasure in a 12 inch square panel with 250,000 storage cells. With suitable operating conditions, half-tone pictures could be displayed for one minute or longer.

## INTRODUCTION

SEVERAL DESIGNS have been suggested for storage light intensifiers which use positive optical feedback to cause elements of an intensifier to remain on once they are triggered by an input light signal.<sup>1-4</sup> Unless the feedback light is confined to the photoconductive element controlling the electroluminescent element, adjacent cells may be triggered, and spreading results. Several structure designs of differing complexity were tested as optical-feedback storage light intensifiers. In general, the simpler the construction the better the results.

## PERFORATED PHOTODUCT STRUCTURE

In one design, the photoconductor is placed in perforations in a

---

\* Manuscript received October 8, 1959.

<sup>1</sup> E. E. Loebner, "Opto-Electronic Devices and Networks," *Proc. I.R.E.*, Vol. 43, p. 1897, December, 1955.

<sup>2</sup> G. Diemer, H. A. Klasens, and J. G. van Santen, "Solid State Image Intensifiers," *Philips Research Report*, Vol. 10, p. 401, December, 1955.

<sup>3</sup> D. B. Barker and F. W. Quelle, "Solid State Storage Display Panel." Presented at *Electron Devices Meeting*, Washington, D. C., October 25, 1956.

<sup>4</sup> E. E. Loebner, H. O. Hook, and D. C. Darling, "Design of Storage Light Intensifier Panels," Presented at *Electron Devices Meeting*, Washington, D. C., November 1, 1957.

transparent plate (photoduct). A Fotoform<sup>†</sup> glass processed to provide the structure illustrated in Figure 1 was used for this evaluation. Figure 2 is an artist's rendition of the way in which the storage light intensifier is completed. After photoconductor material is placed in the holes, an electroluminescent layer is sprayed on the side having

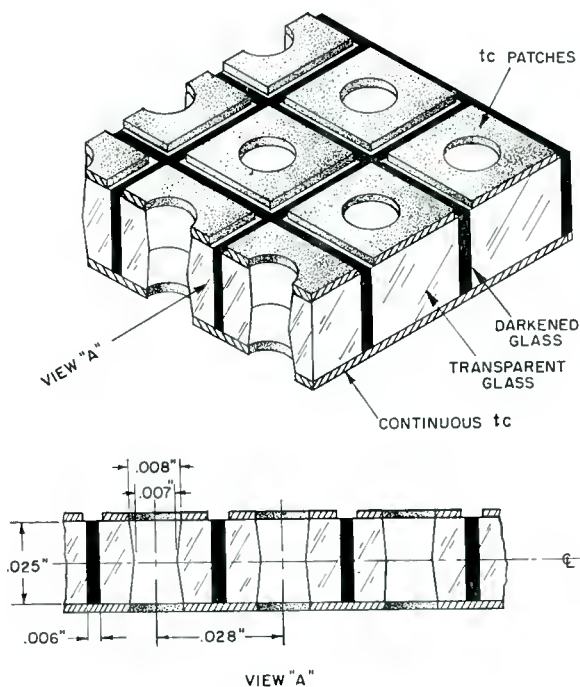


Fig. 1—Perforated photoduct structure.

patches of transparent conductor. A semi-transparent layer of evaporated gold is applied over the electroluminescent layer to complete the device. Figure 3 illustrates the results obtained on a device of this type containing approximately 4800 elements in a surface area 2 inches square.

#### PEDESTAL PHOTODUCT STRUCTURES

Another structure considered for making storage light intensifiers is illustrated in Figure 4. In this structure, the photoduct consists of a transparent or translucent pedestal surrounded by photoconductor,

<sup>†</sup> Registered trade mark.

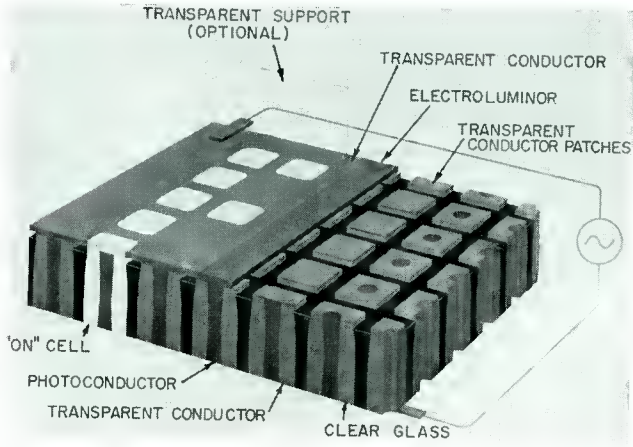
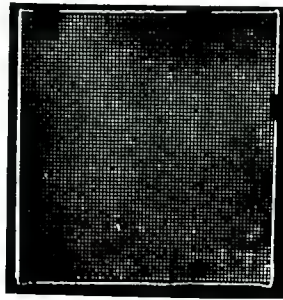


Fig. 2—Perforated-photoduct-structure storage light intensifier.



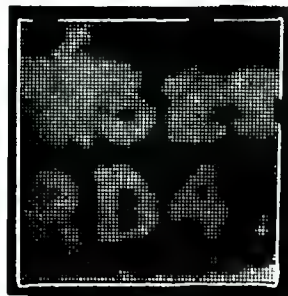
(a)

STORED PATTERN - UNIFORM INPUT



(b)

STORED PATTERN - FIGURE INPUT



(c)

STORED FIGURE PATTERN  
AFTER 1 MINUTE

Fig. 3—Perforated-photoduct storage light intensifier in operation.

rather than a pedestal of photoconductor surrounded by a photoconductor as in the previous structure. The pedestal is generally translucent plastic, although glass has also been used. The electrode at the input on the lower side in Figure 4 is a metal mesh under the photoconductor. A black insulator layer is placed in recesses in the photoconductor, and patches of transparent conductor are applied over the top of each transparent pedestal and the surrounding photoconductor. Over this is applied an electroluminescent layer and a semitransparent output coating of metal paint or evaporated metal.

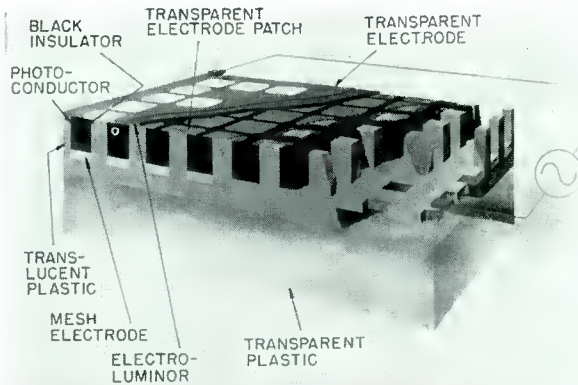


Fig. 4—Plastic-pedestal-structure storage light intensifier.

In this type of structure, the photoconductor is the first material to be applied. Since the photoconductor is very sensitive to operations performed on it after application, it was very difficult to complete a structure that would operate satisfactorily. Both insertion of the black material and application of the electroluminescent layer seemed to damage the photoconductor. Also, there was interaction of the plastic structures with the photoconductor binder solvents. Although plastic structure-photoconductor binder solvent combinations were found in which this problem was minimized, really satisfactory results were not obtained.

Ultrasonic machining and grinding were tried for producing panels with a limited number of pedestals. Neither of these techniques seems applicable to very large area panels and so were used only as means for producing small panels of a few elements for evaluation of the structure itself. Fairly satisfactory arrays of four by four pedestals were made by grinding glass with rubber-base wheels.

A laminated mold which was fairly easy to construct was designed, and quite satisfactory vinyl plastic pedestal structures were molded from it. These flexible structures must be cemented to a rigid base for ease of fabrication. A satisfactory method of cementing the structures to the base was found by using a vinyl cement to attach the flexible vinyl structures to a rigid acrylic sheet. The cement was applied in a thin line at the point where the structures were being joined as they were run between rubber rollers similar to a washing-machine wringer. A fast-setting cement was used so that the structures were essentially set as they came through the rollers.

One of the most persistent difficulties in making successful devices from the pedestal structures was that of providing suitable conductor patches at the interlayer between the photoconductor and the electroluminescent layer. Evaporated gold was the best material tried, although limited success was achieved with conductive paints. Microscopic examination showed that although semitransparent conducting paint films could be obtained in relatively large areas, its application in patches on the tops of the pedestals usually resulted in conducting circles or conducting patches with isolated islands. These patches did not provide sufficiently continuous conduction for satisfactory feedback operation.

### *Layer-Type Structures*

By far the simplest structures to fabricate are those in which the active materials are put on in successive layers, preferably with the electroluminescent layer being applied before the photoconductor layer and the photoconductor layer being applied as near the end of the assembly process as possible. Most of the layer-type structures make use of subdivision of the electroluminescent layer for dividing the structure into cells.

One structure of this type, termed the dimpled electroluminor structure, is illustrated in Figure 5. This structure performed as a bistable light intensifier; because of the thin photoconductor used, however, the contrast between the cells which were off and those which were on was low—about 2 to 1. Also, the fabrication of the dimpled glass was somewhat difficult and did not seem to lend itself easily to large size panels.

Another type of layer structure, shown in Figure 6, uses a black mesh to divide the electroluminescent layer into cells.<sup>5</sup> These devices

---

<sup>5</sup> A slightly more complex structure with similar performance has been described by B. Kazan, "A Feedback Light-Amplifier Panel for Picture Storage," *Proc. I.R.E.*, Vol. 47, p. 12, January, 1959.

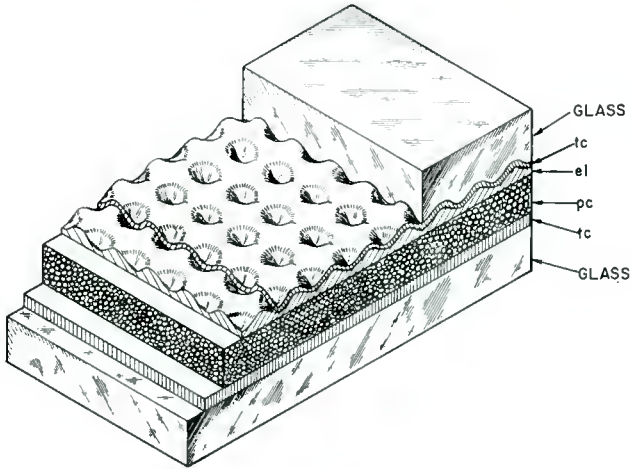


Fig. 5—Dimpled electroluminor-type storage light intensifier.

are made by silk screening the black mesh onto a transparent conductive coating on a sheet of glass chosen to be flat and with parallel surfaces to make subsequent machining operations easier. After the black mesh is cured, a layer of electroluminescent powder in an epoxy binder is spread into the mesh openings by means of a "doctor" blade. After curing the electroluminescent layer, the photoconductor layer is

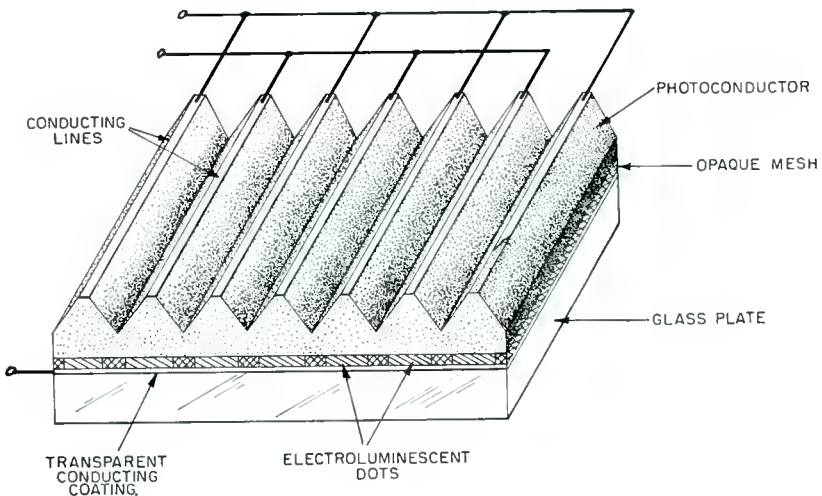
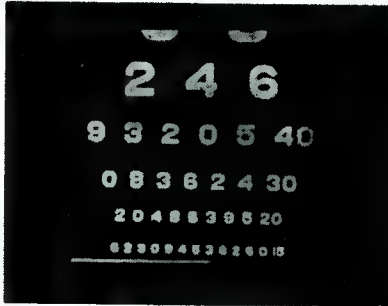
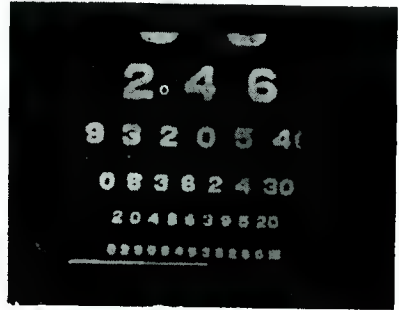


Fig. 6—Layer type storage light amplifier.

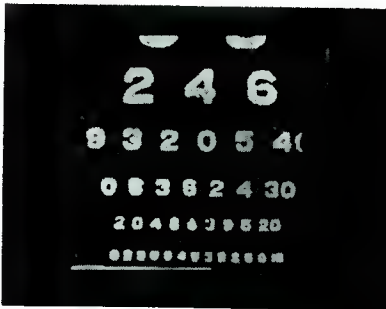
spread on, also by the use of a doctor blade. Silver paint is sprayed on top of the photoconductor until the conductivity is about 1 ohm per square. Grooves are machined into the photoconductor layer both to expose the photoconductor to the input light and to permit an interdigitated input electrode structure which allows the use of direct-current bias which may be reversed for erasing.



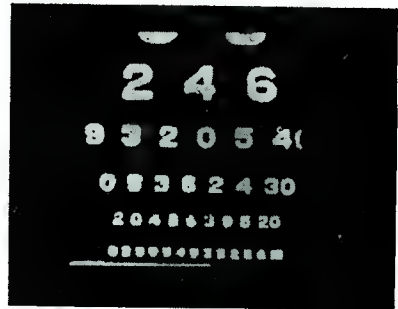
(a) IMMEDIATELY



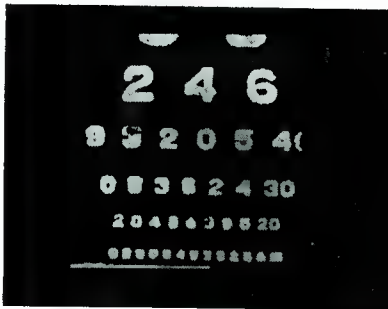
(b) 5 MINUTES



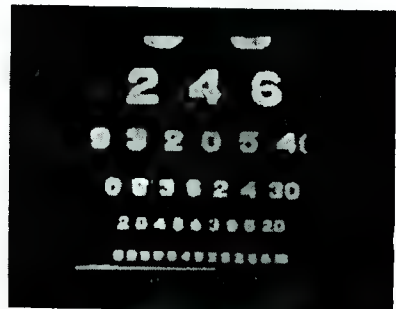
(c) 10 MINUTES



(d) 15 MINUTES



(e) 20 MINUTES



(f) 30 MINUTES

Fig. 7—Stored numbers (layer type storage light intensifier).

Typically, these devices operate with approximately 150 volts a-c at 400 cycles and 150 volts d-c bias. By reversing the bias, the stored pattern may be erased in less than 0.1 second. The trigger sensitivity is of the order of one foot-candle second. The output brightness is of the order of 0.1 foot-lambert. Higher brightness can no doubt be obtained by using a lower amount of feedback which



Fig. 8—Slow-drift halftone picture.

would permit operation at higher voltages. Also, higher brightness can be obtained with very little sacrifice in input sensitivity by operating at higher frequencies; however, operation at higher frequencies requires a more expensive power supply and life may be shortened. Figure 7 is a photograph of stored numbers on a grooved layer-type storage light amplifier. The deterioration of the stored pattern is such that many of the letters are still visible after 30 minutes of operation.

#### QUASI-STABLE HALFTONE STORAGE (SLOW DRIFT)

When the layer-type structures described above are operated at a voltage such that the gain is a little less than that necessary for bi-stable operation, good half-tone storage can be obtained. This half-

tone storage depends on exciting the panel to several different levels which change very slowly because the feedback light tends to keep them illuminated. The decay, as observed on a side-by-side test of a standard light amplifier with no feedback and a light amplifier with feedback just less than that necessary to cause bi-stable operation, is slowed by a factor of 5 to 10.

Figure 8 is a photograph of a stored half-tone picture on a 6-inch panel having 40 elements per linear inch (over 50,000 total elements). This picture showed reasonable half-tones after one minute of storage. If the operating voltage was too high, the picture would slowly separate into fully "on" or fully "off" elements. By operating at a slightly lower voltage the whole picture could be made to decay slowly to all dark. The method of operation for half-tones can be chosen according to the desired result.

# A REVIEW OF "ELECTROFAX"† BEHAVIOR\*

BY

JAMES A. AMICK

RCA Laboratories,  
Princeton, N.J.

*Summary*—The physical, optical, and electrical properties of Electrofax layers are reviewed, with special emphasis on the physical model for Electrofax developed by Rose, Gerritsen, and Ruppel. The characteristics of the latent images which can be formed in an Electrofax layer are discussed, as are techniques which can be used to make these latent images visible.

## INTRODUCTION

THERE ARE two steps in the preparation of an Electrofax print.<sup>1</sup> First, a latent image is formed in or on a layer of insulating (large-band-gap) photoconductor. Second, the latent image is made visible by suitable development, such as by dusting with electroscopic powders or by plating techniques.

When the Electrofax technique was first discovered, many details of its operation were obscure. Since then, most of the unusual electrical properties of Electrofax layers have been traced to the striking differences that can be produced in photoconducting layers when the electrical contacts are changed from injecting to blocking. A physical model for Electrofax layers developed by Rose, Gerritsen, and Ruppel is especially helpful in interpreting and understanding Electrofax behavior, and much of the information included in this review is taken from their work. With recent additions, this model permits a clearer understanding of most of the processes involved in preparing Electrofax prints. It is the intent of this review to present a concise, coherent picture of Electrofax operation. Such a picture, it is hoped, will be of value to those interested in the physics of photoconduction as well as those associated directly with electrophotography.

---

† Registered trade mark.

\* Manuscript received October 15, 1959.

<sup>1</sup> For a general introduction to the Electrofax technique, the reader is referred to C. J. Young and H. G. Greig, "Electrofax—Direct Electrophotographic Printing on Paper," *RCA Review*, Vol. XV, p. 469, December, 1954.

## PHYSICAL PROPERTIES OF AN ELECTROFAX LAYER

An Electrofax layer is a mixture of two materials: a crystalline photoconductive powder, usually zinc oxide,\* which forms perhaps one half of the layer by volume and an insulating resin or "binder," usually a low-molecular-weight silicone. This mixture retains some of the characteristics of each of its components; it is photoconducting, white, matte-surfaced, and opaque because of the particulate zinc oxide and is soft, flexible and hydrophobic because of the silicone resin which holds the zinc oxide particles together. It is the blending of chemical, physical, and electrical properties of the two components which makes the layer especially useful in electrostatic photography. In practice, an Electrofax sheet consists of a 0.5-mil coating of this mixture on paper or some other suitable supporting conductor.

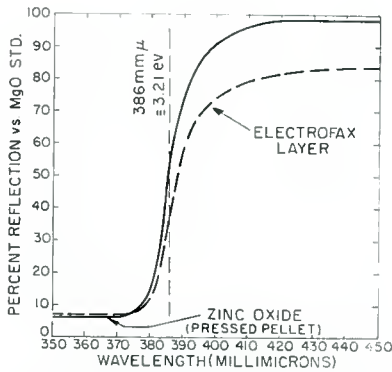


Fig. 1—Reflection from an Electrofax layer and from a zinc oxide pressed pellet as a function of wavelength.

Although highly reflecting for visible light, zinc oxide strongly absorbs ultraviolet radiation corresponding in energy to its band gap (Figure 1). The absorption coefficient of zinc oxide has been reported<sup>2,3</sup> as about  $3 \times 10^5 \text{ cm}^{-1}$ . Most of the incident band-gap radiation would thus be absorbed in a zinc oxide layer about 0.1 micron thick. However, about 10 per cent of the band-gap radiation incident on an Electrofax layer averaging 14 microns in thickness reaches the

\* The zinc oxide crystallites in an Electrofax layer are either acicular or are nearly isometric parallelepipeds about 0.05 to  $0.5\mu$  on an edge.

<sup>2</sup> E. Mollwo, "Electrical and Optical Properties of ZnO," *Photoconductivity Conference*, John Wiley & Sons, Inc., New York, N. Y., 1954, p. 509.

<sup>3</sup> G. Heiland, E. Mollwo and F. Stockmann, "Electronic Processes in Zinc Oxide," *Solid State Physics*, Vol. 8, Academic Press Inc., New York, N. Y., p. 268, 1959.

back surface of the layer. Apparently, the radiation travels through the transparent resin and is reflected at crystallite-resin interfaces.

#### ELECTRICAL PROPERTIES OF THE LAYERS

One of the most fruitful concepts advanced by Rose, Gerritsen, and Ruppel was that the Electrofax layer could be considered as a homogeneous semiconductor. In spite of the particulate nature of the zinc oxide powder, the crystallites are in electrical contact with one another and are not separated by any significant amount of insulating resin. Further, the crystallite size is less than the thickness of the barriers which can be formed in the layer. As a result, the distinction between the surface and the volume of individual crystallites is lost. The resin apparently serves the vital function of keeping moisture away from the crystallite surfaces. Aside from the dielectric constant and the optical absorption coefficient, the layer behaves electrically

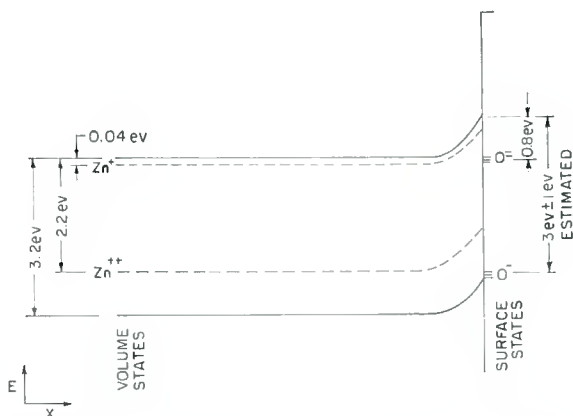


Fig. 2—Band picture for zinc oxide (after Morrison<sup>4</sup>).

and optically like pure zinc oxide, and the band picture for zinc oxide can be used as a good approximation to the band picture for an Electrofax layer.

A band picture for zinc oxide has been given by Morrison<sup>4</sup> and is reproduced in Figure 2. Microscopic crystals of zinc oxide are always observed to be n-type, presumably due to excess interstitial zinc donors. The rectifying properties of the Electrofax layers are also consistent with the assumption of n-type conductivity, both in the dark and under

<sup>4</sup>S. R. Morrison, "Surface Barrier Effects in Adsorption, Illustrated by Zinc Oxide," *Advances in Catalysis*, Vol. 7, Academic Press, Inc., New York, N. Y., p. 259, 1955.

illumination. In addition to the energy levels shown in Figure 2, there appears to be a continuous distribution of traps decreasing in density with increasing distance from the conduction band.

Measurements of the lifetime of electrons in the conduction band of the layer give values of about  $10^{-5}$  second;<sup>5</sup> holes have extremely short lifetimes.<sup>6</sup> Consequently, the behavior of an Electrofax layer is described in terms of a one-carrier model in which electrons, the majority carriers, play the significant role. Furthermore, because of the large band gap in zinc oxide, thermal generation of carriers across the band gap may be neglected at room temperature.

#### LIGHT ADAPTATION

When zinc oxide, or an Electrofax layer, absorbs band-gap radiation, hole-electron pairs are created near the surface. The holes have a very short lifetime and are permanently trapped near the site of their formation. Electrons have a very long lifetime in the conduction band, about  $10^{-5}$  second, before they recombine with a hole and are permanently lost. Instead of remaining in the conduction band for  $10^{-5}$  second and then disappearing, however, the electrons fall rapidly into shallow traps lying near the conduction band and in thermal equilibrium with it. Recombination of the electrons resident in the shallow traps with the bound holes is negligible, since they are physically separated. Thus, the electrons return to the conduction band again and again until recombination with the bound holes finally occurs. Rose, Gerritsen, and Ruppel<sup>5,6</sup> give an estimate of the density of these shallow traps as  $10^{14}/\text{cm}^3 (kT)^{-1}$  at 0.8 eV below the conduction band.\* They also estimate that only 1 in  $10^9$  of the electrons remains in the conduction band after an exposure, the majority being located in the shallow traps. The presence of these traps consequently increases the time required to reach electrical equilibrium by a factor of  $10^9$  and accounts for the very slow return of a light-adapted layer to the dark-adapted state.

#### DARK ADAPTATION

In the dark, given sufficient time, the layer becomes highly insu-

---

<sup>5</sup> H. J. Gerritsen, W. Ruppel and A. Rose, "Photoleitfähigkeit von Zinkoxyd bei Ohmschen und Sperrenden Kontakten," *Helv. Physica Acta*, Vol. 30, p. 235, No. 4, 1957.

<sup>6</sup> H. J. Gerritsen, W. Ruppel and A. Rose, "Photoproperties of Zinc Oxide with Ohmic and Blocking Contacts," *Helv. Physica Acta*, Vol. 30, p. 504, No. 6, 1957.

\* Since the Fermi level in high-purity zinc oxide is about 0.8 volt below the conduction band in the dark-adapted state, these traps can still be considered shallow.

lating, reaching resistivities of  $10^{14}$  ohm cm or more.<sup>7</sup> The time constant for dark adaptation may be estimated by multiplying the lifetime of an electron in the conduction band by the ratio of the electrons in shallow traps to those in the conduction band. This product is about  $10^4$  seconds or about 3 hours. Time constants of  $\frac{1}{2}$  hour and greater have been observed for Electrofax layers, in agreement with this estimate (Figure 3).

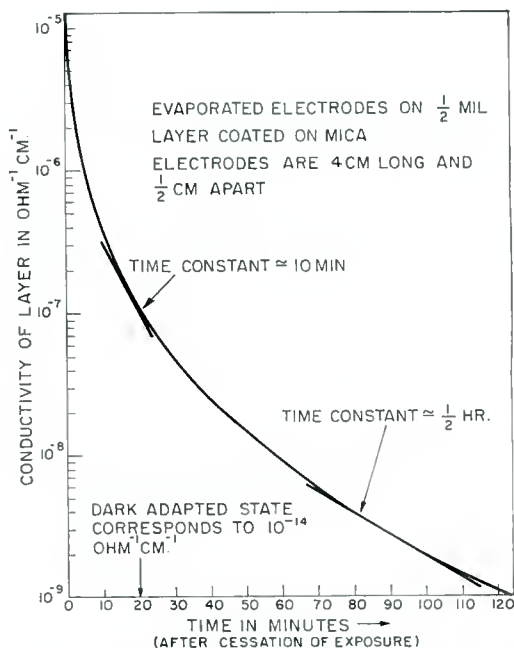


Fig. 3—Typical photoconductivity decay characteristic of an Electrofax layer.

The following is a probable mechanism by which dark adaptation occurs: Oxygen from the ambient is adsorbed on the surface of the n-type crystallites where it dissociates<sup>†</sup>, trapping electrons from the conduction band of the zinc oxide in tightly bound, localized states.

<sup>7</sup> W. Ruppel, H. J. Gerritsen and A. Rose, "An Approach to Intrinsic Zinc Oxide," *Helv. Physica Acta*, Vol. 30, p. 495, No. 6, 1957.

<sup>†</sup> The dissociation energy for an oxygen molecule (Sidgwick<sup>8</sup>) is about 4.95 ev. From Figure 2, about 3 ev is available for each oxygen atom which traps an electron from the conduction band. There is thus more than enough energy to permit the oxygen to dissociate.

<sup>8</sup> N. V. Sidgwick, *The Chemical Elements and Their Compounds*, Vol. II, Oxford Clarendon Press, London, England, p. 858, 1952.

Since the crystallites are small, the surface to volume ratio is large. Therefore, the number of sites on the surface which can accommodate oxygen atoms is large compared with the number of electrons available from the bulk of the crystallites. As more oxygen is adsorbed, the barrier height for successive electrons rises (Figure 4) until the rate at which electrons cross the barrier becomes negligible or until the interior is in thermal equilibrium with the oxygen ions on the surface. By this time, the density of mobile electrons throughout the volume of the crystallites has decreased, and the resistivity of the layer corresponds to the dark steady-state value,  $10^{14}$  ohm cm, as stated previously.

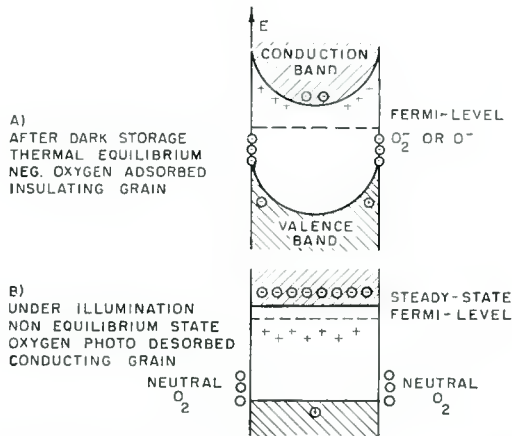


Fig. 4—Zinc oxide powder particle of  $10^{-5}$  cm diameter (a) dark adapted and (b) light adapted (after Ruppel, Gerritsen and Rose<sup>7</sup>).

Dark adaptation may be hastened by exposing the layer to infrared radiation. The radiation presumably increases the number of electrons in the conduction band of the zinc oxide by exciting them from the shallow traps. As a consequence, the ratio of the density of electrons in the shallow traps to that in the conduction band decreases and the dark decay time is correspondingly shortened.

#### NEGATIVE CORONA CHARGING

Corona charging of a layer is accomplished with a corona wand and a 6000-volt d-c power supply.<sup>1</sup> Fine wires in the wand are maintained 6000 volts negative with respect to ground, while the surrounding shield and the metal ground plate on which the layer is charged are at ground potential (Figure 5). When the potential is applied to the wand, a discharge occurs producing ions in the vicinity of the fine

wires. Negative ions are accelerated toward the shield or the metal ground plate and, when an Electrofax sheet is interposed, land on the surface of the sensitive layer. As the density of ions on the front surface increases, positive charges pile up on or near the paper-layer interface to maintain the Electrofax sheet nearly neutral as a whole. The potential across the layer continues to rise until breakdown occurs.\* When the corona is turned off, the potential drops rapidly

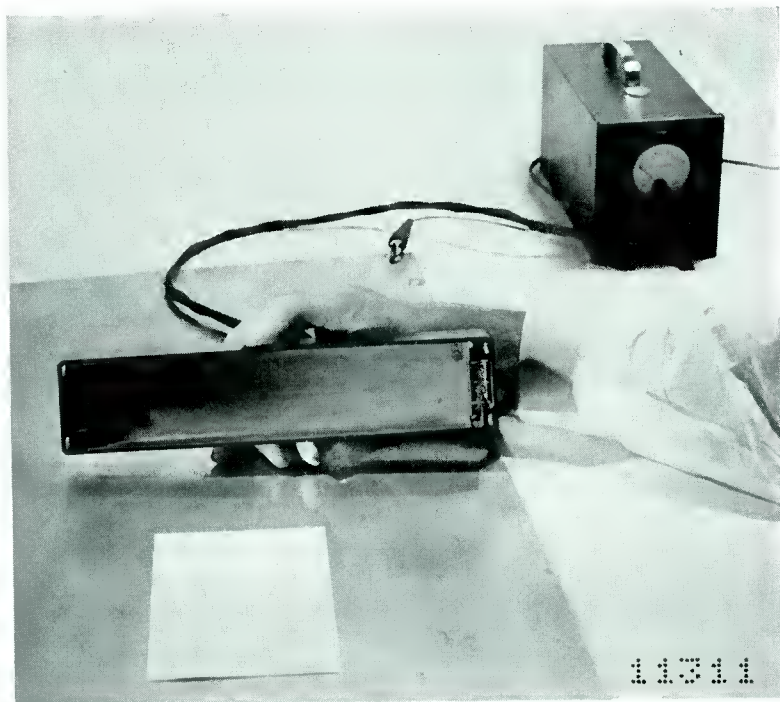


Fig. 5—Apparatus for corona charging of Electrofax layers. Note fine wires in corona wand.

for a short time but becomes stable within about 45 seconds after the cessation of charging.<sup>9</sup> From this time on, the decay constant for the potential across the layer varies from a few minutes to several hours

\* The potential which can be measured across different Electrofax layers of the same thickness after corona charging is observed to depend on the oxide from which the layer is prepared.<sup>9</sup> In particular, the density of ionizable volume charge and the critical field at the surface which corresponds to the onset of breakdown, determine the potential across the layer.

<sup>9</sup> J. A. Amick, "A Volume-Charge Capacitor Model for 'Electrofax' Layers," *RCA Review*, Vol. XX, p. 770, December, 1959.

depending on such external variables as the humidity and the temperature.<sup>‡</sup> This long time constant indicates a high resistivity for the layer and demonstrates that the corona ions bound to the surface form a blocking contact to the conduction band of the layer.

That the charging step involves the deposition of oxygen ions is strongly suggested by experiments in which the ambient during charging was altered. When layers were exposed to a corona discharge in helium or in nitrogen, no resultant potential across the layer could be detected. When corona-charged in pure oxygen, the layers behaved as if they had been charged in air.

During corona charging, the electrons are brought to the surface in the form of negative oxygen ions and are not required to cross the surface barrier as in dark adaptation. The only limit to the height of the barrier at the surface is the value at which breakdown, probably tunneling, begins. The charging of the surface by the negative corona may be viewed as back biasing a p-n junction. In the back-biased condition, current flow is small\* and the potential drop across the junction is therefore maintained for long periods of time.

Because the ions form a blocking contact to the surface, mobile electrons in the volume, whether from donors or from previous light absorption, are exhausted from the bulk of the layer during charging and are not replaced. The corona charging process thus removes the effects of previous light exposure and forcibly returns the layer to a high-resistivity (dark-adapted) condition.<sup>7</sup> Since the lifetime of the electrons in this process is limited to their transit time through the layer, the layer returns to a dark-adapted state in a time much shorter than that required for normal dark adaptation. In particular, the lifetime of a free electron has been reduced from the value of  $10^{-5}$  second, as measured with ohmic contacts, to approximately  $10^{-9}$  second, the estimated time required for a free electron to traverse the layer. The dark-adaptation time should be reduced by the same factor, namely  $10^{-4}$ . Thus, a previously light-adapted layer can be rendered insulating in a few seconds by corona charging, while unaided dark adaptation requires several hours. Even with dark-adapted Electrofax layers, the corona charging step removes residual shallow-trapped electrons and increases the resistivity of the layer; values of  $10^{16}$  to  $10^{17}$  ohm cm

---

‡ The long time constant for dark decay is also critically dependent on the band gap of the photoconductor. If this band gap is much less than about 1 ev, thermal generation of carriers across the gap will shorten the dark decay to one second or less, making the layer unsuitable for normal Electrofax processing.

\* For an ideal blocking contact and in the absence of thermal generation of hole-electron pairs, the current should be strictly zero.

have been estimated from the dark relaxation time of the corona-charged layers.<sup>5</sup>

### POSITIVE CORONA CHARGING

In contrast to the results obtained with a negative corona, positive corona charging of a *light-adapted* Electrofax layer is usually unsatisfactory because the potential decays in times almost too short to measure. This behavior may be ascribed to biasing the p-n junction at the surface in the forward direction. Normal characteristics of a forward-biased junction are large current densities and short time constants for the decay of an impressed potential. Thus, the forcible return of a light-adapted layer to the dark-adapted state, which is so characteristic of negative corona charging, does not occur when a positive corona is used. If the layers are thoroughly dark adapted, they can be charged with a positive corona, but the potentials retained are smaller and the time constants for decay are shorter than for negatively charged layers.

### INJECTING AND BLOCKING CONTACTS

As noted above, the oxygen ions form a blocking (non-injecting) contact to the conduction band of the layer. With this blocking contact, the time constant for reaching an electrical steady state is a few seconds. Furthermore, the quantum yield is limited to unity since each photon creates one electron which can be transferred from near the front surface to the back surface. Once it reaches the back surface it combines with a positive charge and the process is complete. The paper support used with normal Electrofax layers also forms a rectifying contact to the layer; although the paper readily accepts electrons from the layer, it apparently is incapable of injecting electrons into the layer. Moisture probably provides the small amount of conductivity observed in the paper. However, negative ions, such as  $\text{OH}^-$ , should bind electrons so tightly that injection into the conduction band of the layer does not occur.<sup>7</sup>

When contacts to the surface are made by metals, quite different phenomena are observed.<sup>3</sup> Metal powders, such as nickel, aluminum, iron, and zinc, and evaporated metal electrodes are capable of injecting electrons into the conduction band of the layer as well as extracting electrons from the conduction band if any are present, but these contacts do not act as hole injectors (Figure 6). The photoconductive response time is increased to several hours at low lights when metal contacts are used, as shown in Figure 3, and secondary photoconduc-

tive gains of  $10^4$  are observed. This behavior is expected whenever ohmic, or injecting, contacts are made to the layer. Electrons produced by illumination travel easily through the layer under the influence of an external field. When they reach the paper-layer interface, additional electrons are injected at the front surface to maintain space-charge neutrality. In this way, each photon may result in the passage of  $10^4$  electrons through the layer, this being the number of transits which an electron may make during its lifetime.

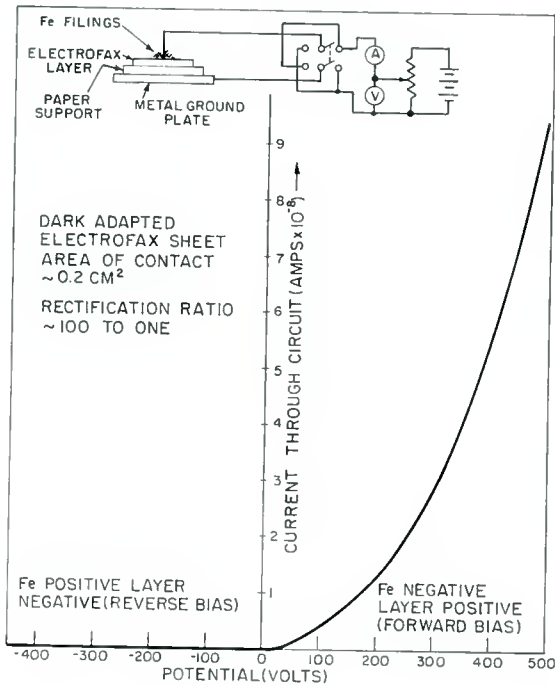


Fig. 6—Voltage-current characteristics for an Electrofax-iron filing contact.

In summary, blocking contacts cause zinc oxide layers to assume the character of the highly insulating and photoconductively insensitive layers of amorphous selenium, since the lifetime of a carrier is limited to its transit time through the layer. Ohmic contacts, on the other hand, permit the high intrinsic sensitivity of the zinc oxide layers to be observed, much as in the well known sensitive layers of cadmium sulfide and cadmium selenide.

FORMATION OF THE LATENT IMAGE

There are two types of latent images which can be formed with an Electrofax layer, the "latent electron image" and the "latent electrostatic image." The latent *electron* image (Figure 7), which may also be called a latent conductivity image, is produced by normal exposure of a dark-adapted layer. Following the exposure, most of the electrons produced by light are present in shallow traps near the site at which they were formed, being electrostatically attracted to the trapped positive holes. By applying an appropriate external field, those few electrons present in the conduction band may be extracted from the layer. As they leave, the electrons in the shallow traps are thermally

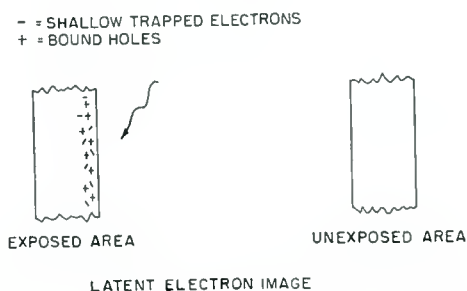


Fig. 7—Cross sections of exposed and unexposed Electrofax layers showing the latent electron image.

excited into the conduction band from which, in turn, they may also be extracted. These "available" electrons which form the latent image are the same electrons originally produced by the absorption of light, and the time constant for the decay of this latent image is simply the dark-adaptation time constant for the layer (normally a few hours). Since the latent image is made up of excited electrons and bound holes within the zinc oxide crystallites, it is not affected by water immersion.

A latent *electrostatic* image is easily formed on a corona-charged layer (Figure 8). In the nonilluminated areas, the potential difference across the layer corresponds to that after corona charging; in the illuminated areas, the potential difference across the layer is decreased by the motion of electrons from the front surface to the layer-support interface. The holes may remain in bound states near the negative oxygen ions or they may neutralize the oxygen ions which then desorb from the surface.

After a normal exposure,\* about 30 seconds elapses before the

\* About  $10^{12}$  band gap photons/cm<sup>2</sup> (see reference (9)).

potential across the layer reaches a new stationary value.<sup>9</sup> The time constant (time for decay to  $1/e$  of its stationary value) is a few seconds and is much greater than the  $10^{-9}$  second transit time of the electrons because of the shallow traps. Measurements of the rise time of photoconductivity in Electrofax layers<sup>7</sup> indicate that an electron falls into a shallow trap before it travels  $1/10$  of the way through the layer. Thus, nearly all of the electrons are trapped several times during their passage through the layer. By multiplying the density ratio of the electrons in shallow traps to those in the conduction band by the transit time of a free electron, a response time of about 1 second is obtained, in fair agreement with the observed time constant.

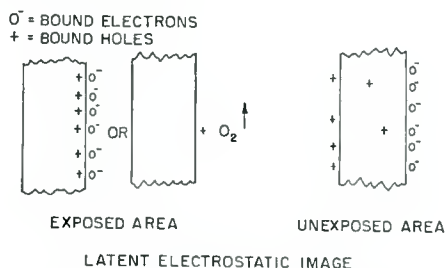


Fig. 8—Cross sections of exposed and unexposed Electrofax layers showing the latent electrostatic image.

The separation of charges in the nonilluminated areas represents stored energy which can be used for subsequent development. The characteristic decay time for this latent image is the dark-relaxation time for the layer, which is normally several hours. If the layer is immersed in water, however, the layer discharges almost immediately and the latent image is destroyed. Since, in forming the latent image, the electrons produced by light are used immediately to reduce the potential across the layer, they are no longer “available” at the time of development.

#### DEVELOPMENT

Development of an image depends on distinguishing, in some manner, those areas which were exposed to light, and thus possess or possessed mobile electrons, from those which were not. Techniques are known which can be used to develop either type of latent image.

##### *Latent Electron Image*

Development of the latent electron image requires the application of an external field which supplies the energy required for the develop-

ment. Figure 9 illustrates a technique invented by A. Rose<sup>10</sup> in which metal powder is sprinkled over the surface. A potential is then applied between the powder and the ground plate on which the Electrofax sheet lies. When the powder is positive and the ground plate negative, available electrons are extracted from the layer and neutralize the metal powder which subsequently falls off. In regions where no electrons are available, the charged powder is bound to the layer by electrostatic forces and the image becomes visible. This development

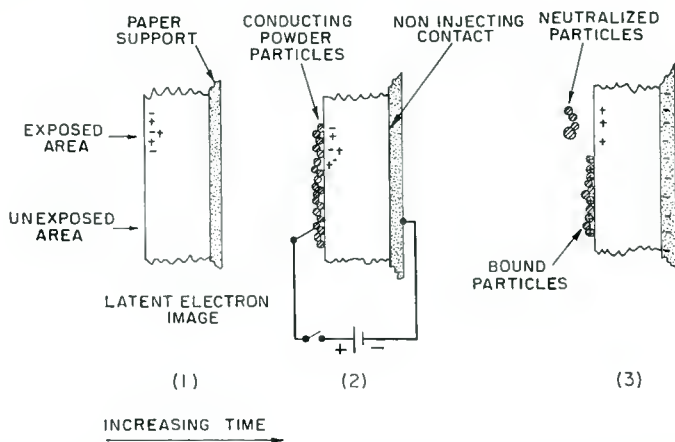


Fig. 9—Sequence of steps used in developing a latent electron image.

makes use of the blocking contact made by the paper support to the layer. Because this contact is incapable of injecting significant numbers of electrons, neutralization of the powder occurs only where light-produced carriers are available. As a result of this blocking contact, the quantum gain is limited to unity. This development produces a direct-positive print, i.e., no reversal occurs during development.

A second technique which may be used to detect the mobile electrons is the electrodeposition of metal ions from a solution. A potential is applied between the back of the layer and a solution containing, for example, silver ions, the solution being made positive. Wherever mobile electrons are available, silver is electrodeposited onto the surface, darkening it. In areas containing no mobile electrons, no silver is deposited. Quantum gains of  $10^4$  have been observed for this type of development when a metal contact is made to the back of the layer, since, in this direction of current flow, the metal contact is injecting.

<sup>10</sup> A. Rose, private communication.

This technique, of course, gives reversal prints rather than direct positives.

It should be noted that in the first technique only the surface of the layer need be photoconducting, while in the second, the entire thickness of the layer must be made photoconducting.

### *Latent Electrostatic Image*

Development of a latent electrostatic image can be carried out with a mixture of iron filings and a suitable electroscopic powder<sup>1</sup> (Figure 10). Iron filings, as described earlier, have the ability to inject electrons into the conduction band of the layer, and certain developing

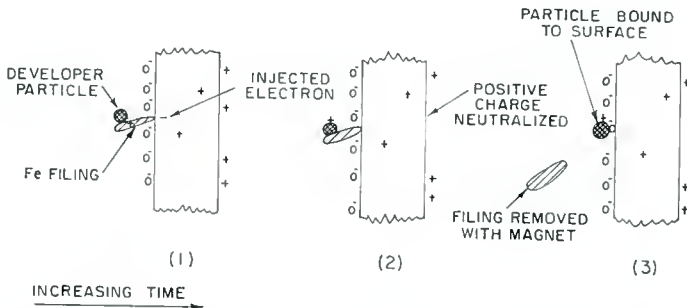


Fig. 10—Sequence of steps used in developing a latent electrostatic image.

powders become positively charged when brought into contact with iron filings. The sequence of steps in the development of an image can then be visualized as follows. Some developer particles donate electrons to the iron filings and become triboelectrically positively charged. The iron filings, meanwhile, are in contact with the conduction band of the layer. These injected electrons are subject to the fields present in the layer and, in the unexposed areas, travel to the layer-support interface, neutralizing positive charges. In effect, the positive charges at the layer-support interface have been transferred to developer particles which are then attracted and bound to the negative surface charges in the nonilluminated areas.

This transfer of positive charges from the layer-support interface to the developer particles will continue as long as the total energy decreases as a result of the transfer. This condition is approximately met if the distance between a positive charge and its corresponding negative charge decreases during the transfer; originally, the positive charge and its corresponding negative charge were separated by the thickness of the layer, about 14 microns. After the transfer, the charge is located on the surface of the developer particle which is a

few microns in diameter. Depending on the roughness of the Electrofax surface and the developer particle surface, the separation between the positive charge on the developer particle and the negative charge on the surface may now be 0.1 to 1 micron. In the exposed areas, the separation between the bound holes (created by exposure) and the corresponding negative surface charges is about 0.1 micron because of the large absorption coefficient of zinc oxide for band-gap radiation. In these areas, there is clearly no decrease in the total energy of the system when a positive charge is transferred to a developer particle. Therefore, very little developer is bound to the surface in the exposed areas. The print produced by this development is a direct positive.

Reversal prints may be prepared by using a triboelectrically negative developing powder with the iron filings. This reversal may be qualitatively described as follows. As before, the iron filings in the *unexposed* area of the latent image inject electrons and become positively charged. As these remaining filings are brushed across the surface, any shallow-trapped electrons in the *exposed* areas are extracted. This step transfers the positive charge from the iron filings to the *exposed* areas of the surface. The negatively charged developing powder is repelled by the negative oxygen ions on the unexposed areas and attracted by the immobile positive charges in the exposed areas, thus forming a visible image. An alternative explanation would be that the negatively charged developing powder is repelled from the unexposed surface areas by the oxygen ions and attracted to the neutral exposed areas by image forces.

In any powder development of the latent electrostatic image, the developer powder must effectively form a blocking contact to the charges on the surface. Otherwise, the powder would be neutralized by the surface charges and would then no longer adhere.

#### DYE SENSITIZATION

The sensitivity of Electrofax layers to normally available light sources can be greatly "increased" by the addition of certain organic dyes to the layer.<sup>11</sup> The amount of dye required amounts to at most a few monolayers. If too much dye is added, the sensitivity of the layer passes through a maximum and then decreases.<sup>11</sup> Experimental measurements of the sensitivity of dyed layers, when used with corona charging, show that the quantum gain is still limited to unity. Apparently, the dye molecule, after absorbing a photon of visible light, injects an electron into the conduction band of a zinc oxide crystallite.

<sup>11</sup> E. Giaimo and H. G. Greig, private communication.

This electron now behaves as if it had been created by an ultraviolet photon within the crystallite itself. The increase in sensitivity obtained by adding the dye is thus due solely to the extended spectral response of the layer, as shown in Figure 11.

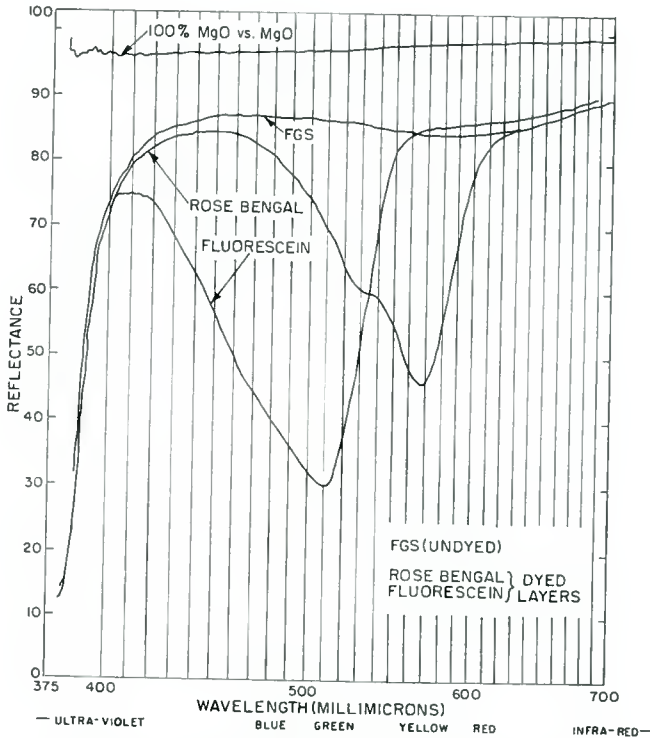


Fig. 11—Reflection of Electrofax layers as a function of wavelength showing the increased absorption of dyed layers.

## SUMMARY

### *Latent Electrostatic Image*

1. A dark-adapted or a light-adapted Electrofax layer is charged with negative oxygen ions from a corona discharge. After charging, a potential of about 500 volts is retained across the layer because of the blocking contact formed by the oxygen ions.
2. Illumination of the layer creates hole-electron pairs close to the surface. The holes are immediately trapped, but the electrons move to the back of the layer and neutralize positive charges there. This results in a decrease in the potential across the layer in the illuminated areas, producing a latent electrostatic image.

3. During development, the energy stored across the layer in the nonilluminated areas is used. Electrons are injected into the front surface of the layer by iron filings. These electrons travel to the back of the layer and neutralize positive charges. The iron transfers its positive charge to the developer powder particles which then are electrostatically bound to the uncompensated negative oxygen ions on the surface.

*Latent Electron Image or Latent Conductivity Image*

1. A thoroughly dark-adapted Electrofax layer is exposed to illumination. The electrons which are produced are quickly trapped in shallow traps but are still "available," forming a latent electron image.

2. When an external field is applied across the layer, these electrons can be extracted from the layer in the illuminated areas and used to neutralize a charged conducting powder which is then released from the surface. In the dark-adapted, nonilluminated regions, the charged powder is not neutralized and remains bound to the surface, forming a visible image.

Addition of a suitable dye to the layer increases its sensitivity by extending its spectral response into the visible region.

ACKNOWLEDGMENT

For extremely helpful and valuable discussions, I would like to thank A. Rose, H. J. Gerritsen, W. Ruppel, H. G. Greig, C. J. Young, and E. Giaino. Special thanks are due H. G. Greig who kindly supplied the materials for the work reported here, and to A. Rose for his critical reading and revision of the manuscript.

# A VOLUME-CHARGE CAPACITOR MODEL FOR "ELECTROFAX"† LAYERS\*

BY

JAMES A. AMICK

RCA Laboratories,  
Princeton, N. J.

*Summary*—Observed nonlinearities of the light discharge curves for Electrofax layers are ascribed to ionizable centers uniformly distributed throughout the volume of the dark-adapted layer. When the layers are corona charged, the centers are emptied leaving uncompensated positive charges within the layer. As a result, the charging-discharging characteristics of Electrofax layers are not the same as those for a simple capacitor. By determining the density of ionizable centers present in different Electrofax layers, light-discharge curves can be calculated which agree well with the experimentally observed curves.

## INTRODUCTION

THE ELECTROPHOTOGRAPHIC technique, in which zinc oxide powder embedded in a resin matrix is the photosensitive material, was discovered by Young and Greig<sup>1</sup> and has been given the name "Electrofax." While studying the electrical properties of thin layers of this material, Gerritsen, Ruppel, and Rose<sup>2</sup> observed that, at potentials less than 200 volts across the layer, the discharging of the layer by incident light was a nonlinear function of light exposure.

It has now been found that the degree of nonlinearity depends on the zinc oxide powder from which the layer is prepared. By fitting the observed discharge curves to a simple model, it is possible to calculate, for a given layer, a density of volume-distributed, shallow-trapped charge which characterizes that layer. The same model should also prove useful in understanding the electrical characteristics of layers consisting of a relatively pure, large-band-gap semiconductor embedded in an insulating matrix, whenever blocking contacts are employed.

---

† Registered trade mark.

\* Manuscript received October 15, 1959.

<sup>1</sup> C. J. Young and H. G. Greig, "Electrofax—Direct Electrophotographic Printing on Paper," *RCA Review*, Vol. XV, p. 469, December, 1954.

<sup>2</sup> H. J. Gerritsen, W. Ruppel, and A. Rose, "Photoleitfähigkeit von Zink-oxyd bei Ohmschen und Sperrrenden Kontakten," *Helv. Physica Acta.*, Vol. 30, p. 235, No. 4, 1957.

## EXPERIMENTAL MATERIALS

The Electrofax layers on which measurements were made contain zinc oxide crystalline powders<sup>‡</sup> in which the size of the average particle ranges from about 0.1  $\mu$  to about 10  $\mu$ . Although no special precautions were taken, the thickness of the sensitive layers was substantially constant at  $\frac{1}{2}$  mil for all of the layers studied. The only known difference between layers was in the zinc oxide powders used, all of which were selected from commercially available samples. The layers, coated on paper, were dark adapted for at least 48 hours in total darkness before beginning the measurements.

For convenience, the layers are identified with code letters descriptive of the zinc oxide used in them. A list of these code letters, which usually follow the manufacturer's practice, is given in Table I.

Table I—Source and Identification of Zinc Oxide Crystalline Powders Used in Electrofax Layers

<i>Identification</i>	<i>Name</i>	<i>Source</i>
WXAV-1	Mallinckrodt Analytical Reagent WXAV-1	Mallinckrodt Chemical Works, New York, N. Y.
WYEB	Mallinckrodt Analytical Reagent WYEB	Mallinckrodt Chemical Works, New York, N. Y.
FGS	Florence Green Seal	New Jersey Zinc Company Palmerton, Pa.
Fisher Wet	Eimer and Amend, Wet Process	Eimer and Amend Co. Division of Fisher Scientific Co., New York 14, N. Y.
EP USP	Eagle Picher US Pharmacopoeia	Eagle Picher Sales Co. Philadelphia, Pa.
G. F. Smith	G. F. Smith	G. F. Smith Chemical Co. 60 E. 42nd St., New York, N. Y.
B + A Wet	Baker and Adamson Wet Process	Baker and Adamson, General Chemical Division 40 Rector St., New York, N. Y.
CE-8099-3	CE-8099-3	New Jersey Zinc Company Palmerton, Pa.
AZO-33	AZO-ZZZ-33	American Zinc Sales Co. New York, N. Y.

## INSTRUMENTATION

The instruments used are shown in a typical test setup in Figure 1. Since the charge density on the surface of a charged sensitive layer is no greater than about  $10^{12}$  per  $\text{cm}^2$ , measurements of potential must be made with a high-impedance voltmeter. For this purpose, the

<sup>‡</sup> The Electrofax layers were prepared as described in U. S. Patent 2,857,271 (October 21, 1958), example 1.

Keithley model 200 electrometer with a 100:1 voltage divider was found satisfactory. With this divider, the electrometer has an input impedance of  $10^{12}$  ohms and measures potentials up to 2000 volts.

A 2×2 inch glass probe having a transparent conductive coating was connected to the input terminal of the electrometer with a 6-inch length of self-supporting, plastic-insulated flexible wire. Near the

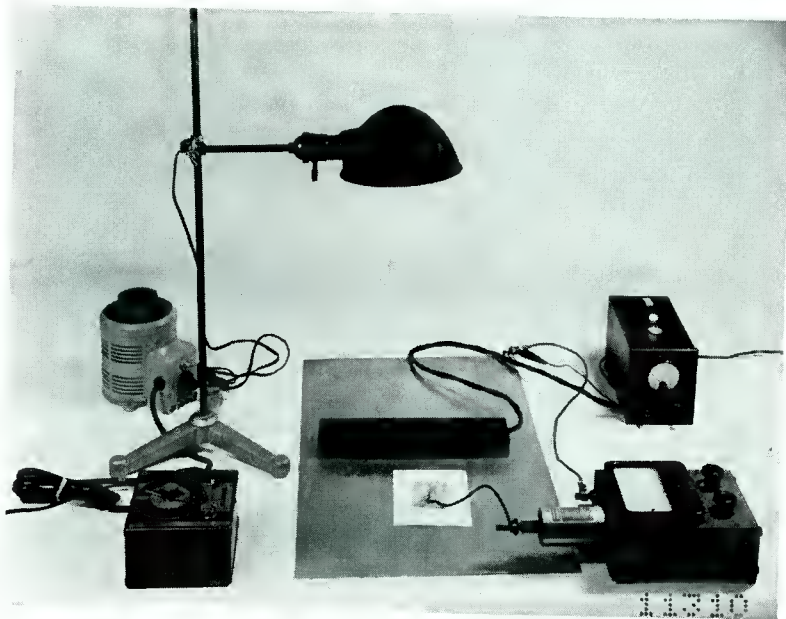


Fig. 1—Apparatus used in determining the discharge characteristics of Electrofax layers. Upper right—power supply for corona charger; lower right—electrometer; upper left—variac; lower left—timer; top—tungsten lamp in reflecting housing; center—metal ground plate, corona wand, Electrofax sheet, and electrometer probe.

probe end of the wire, a short length of Scotch\* tape was fastened which served as a handle for moving the probe about. To minimize charge transfer between the Electrofax surface and the probe during a measurement, the conducting surface of the probe was covered with a piece of loosely knit nylon mesh cut from a nylon glove.

A corona charging unit,<sup>1,3,4</sup> consisting of a power supply and a corona wand, was used to charge the layers. The fine wires in the

\* Registered trade mark.

<sup>3</sup>M. L. Sugarman, *Proceedings of the Conference of the Seventh Annual Meeting, Technical Association of the Graphic Arts*, May, 1955.

<sup>4</sup>J. A. Amick, "A Review of Electrofax Behavior," *RCA Review*, Vol. XX, p. 753, December, 1959.

wand were connected to the negative terminal of the 6000-volt d-c supply; the outer shield of the wand and the metal ground plate were connected to the positive terminal.

A tungsten lamp in a reflecting housing provided a convenient light source. The intensity and duration of the light are easily controlled with a Variac\*\* and a timer. Although the light is not monochromatic, zinc oxide absorbs strongly only light of wavelengths shorter than 3800 Å, and the effects produced by unfiltered tungsten light are similar to those obtained using monochromatic radiation. The light source was calibrated against a vacuum photocell which had previously been calibrated against a primary standard.

#### TECHNIQUE AND MEASUREMENTS

An Electrofax sheet is placed on the metal ground plate, sensitive surface upward, and negatively corona charged. The sheet is now lifted from the ground plate to reduce stray fields across the paper-metal interface as much as possible. After replacement of the sheet on the ground plate, the probe is gently placed, conducting side down, on the surface of the layer. Within about 2 seconds, the needle of the electrometer rises to a maximum value, hovers there for about 5 seconds, and then begins slowly to fall back owing to the leakage resistance of the electrometer. This maximum potential is recorded as the potential across the layer. Successive measurements show that the potential is reproducible only to about 10 per cent and depends slightly on the height from which the probe is dropped onto the surface.

The potential was first recorded for each layer as a function of elapsed time in the dark following corona charging (Figure 2). From these measurements it was determined that, after a 45-second interval, the potential across an Electrofax layer remains nearly constant with time. A waiting period of at least 45 seconds following corona charging was therefore provided in all subsequent experiments to allow for any rapid initial dark decay.\*†

The nine coatings represented in Figure 2 were chosen because the

---

\*\* Registered trade mark.

\* The initial rapid decay is probably due to a tunneling process that limits the field at the surface of the layer to about  $5 \times 10^5$  volts per cm, as described below. Since tunneling current is an extremely steep function of the field, it rapidly becomes negligible as the field decreases.

† Dark measurements were first carried out in total darkness except for a dim red safelight used to read the electrometer. It was verified subsequently that the yellow safelights used in normal handling of Electrofax materials did not alter the dark decay appreciably. Therefore, in later experiments, these yellow lamps (GE 100-watt insect repellent lamps) were used.

potential drop across them, following corona charging, spanned the entire range of potentials observed for layers of this thickness. Differences in this potential are attributed to differences in the oxide powders used to prepare the layers.

The discharging of the (corona charged) layers by incident light was studied by measuring the potential across a charged layer, removing the probe from its surface, exposing the surface to a uniform flash of light of about 5 seconds duration, and monitoring the change

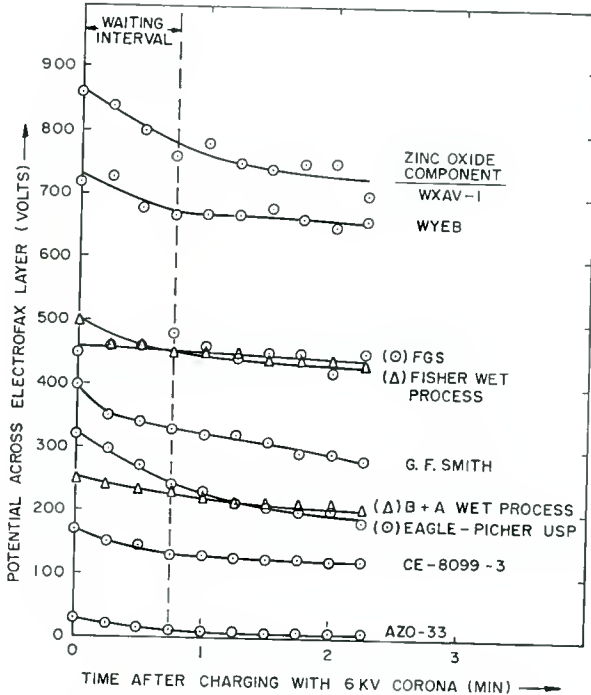


Fig. 2—Dark decay curves for corona charged Electrofax layers.

in potential across the layer with time. A second light pulse could then be provided and the resulting change in potential determined as before.

The result of exposing fully charged Electrofax layers to a single light pulse is shown in Figure 3 where, for clarity, only five of the Electrofax layers are represented. The first minute, for each curve, represents the dark decay waiting period. At the end of this period, the surface was exposed to a single 5-second light pulse providing  $5 \times 10^{11}$  band-gap photons per  $\text{cm}^2$  at the layer surface. As soon as practicable (approximately five seconds later) the potential was measured, and then remeasured at 15-second intervals. From Figure 3 it

may be seen that, following an exposure, a steady state is not established immediately. A tail in the discharge characteristic is visible for intervals up to 30 seconds following the termination of the exposure. Because of this slow response it is imperative, when determining the effects of exposure on charged Electrofax layers, to divide the incident light into pulses and to wait for attainment of a steady state after each pulse.

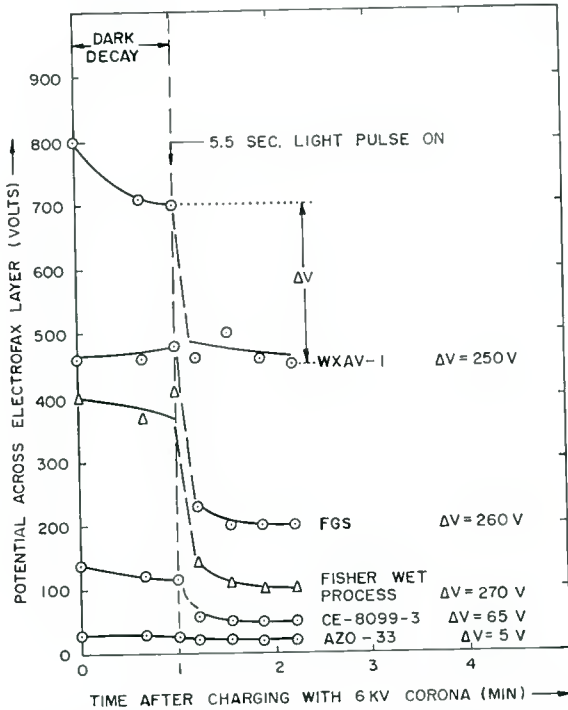


Fig. 3—Discharge characteristics of Electrofax layers with a single light pulse containing  $5 \times 10^{11}$  photons/cm<sup>2</sup>.

Complete discharge characteristics for the nine different Electrofax layers were obtained by this technique and are shown in Figure 4. Each light pulse contained  $1.06 \times 10^{11}$  photons of band-gap radiation per cm<sup>2</sup> at the Electrofax surface, and had a duration of 5 seconds. With this smaller exposure, the potential drop for each pulse is less, permitting a larger number of points to be obtained for the discharge curve. The steady-state potential across each layer, following an exposure, was measured 30 seconds after termination of the exposure.

Those Electrofax layers having a high potential following corona charging exhibit a linear discharge characteristic until the potential

across the layer drops to about 100 volts. Below this value, the discharge is no longer linear with incident light. Those layers having a low potential following corona charging show only the nonlinear discharge characteristic. This nonlinear behavior was not anticipated on the basis of the early models used to describe Electrofax.

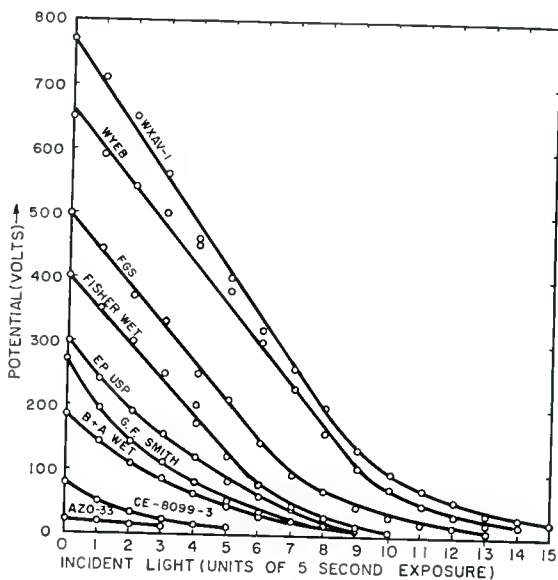


Fig. 4—Light-discharge characteristics of Electrofax layers. Standard layer thickness is  $14.5 \times 10^{-4}$  cm, and each 5-second light pulse provides  $1.06 \times 10^{11}$  photons/cm<sup>2</sup> at the Electrofax surface.

#### EARLY MODELS FOR ELECTROFAX

The Electrofax layer was originally pictured as a uniform homogeneous dielectric. Charging of the layer in the dark was regarded simply as the charging of an insulator, the metal ground plate or the paper support forming one contact and the corona discharge forming the other.

Gerritsen, Ruppel, and Rose developed a more refined model in which the layer was visualized as a homogeneous semiconductor having a well defined band gap equal to that of zinc oxide. A bulk resistivity<sup>5</sup> of  $10^{16}$  ohm cm, and a quantum yield of nearly unity<sup>2,6</sup> were meas-

<sup>5</sup> W. Ruppel, H. J. Gerritsen and A. Rose, "An Approach to Intrinsic Zinc Oxide," *Helv. Physica Acta.*, Vol. 30, p. 495, No. 6, 1957.

<sup>6</sup> H. J. Gerritsen, W. Ruppel and A. Rose, "Photoproperties of Zinc Oxide with Ohmic and Blocking Contacts," *Helv. Physica Acta.*, Vol. 30, p. 504, No. 6, 1957.

ured for "standard" or FGS layers. Both observations suggested strongly that the ions deposited on the Electrofax surface during corona charging formed a blocking contact to the layer.<sup>2</sup> Charges were postulated to lie entirely on the surfaces of the layer, negative ions at the air-layer interface and positive charges at the paper-layer interface (Figure 5). By shining band-gap radiation onto the sensitive surface, hole-electron pairs are created in a very shallow region near the surface; the absorption coefficient of zinc oxide for band-gap radiation<sup>7</sup> is about  $3 \times 10^5$  per cm.

The electron-hole pairs formed by the exposure are promptly separated, the electrons moving through the conduction band of the layer toward the positive (layer-paper) interface. The long time intervals required to reach a steady state after an exposure are ascribed to repeated trapping of the electrons during their transit. Because of these traps, the photoconductive response time is increased from the value  $10^{-9}$  second, calculated from  $\tau = L^2/\mu V$ , to a few seconds.<sup>4,8</sup>

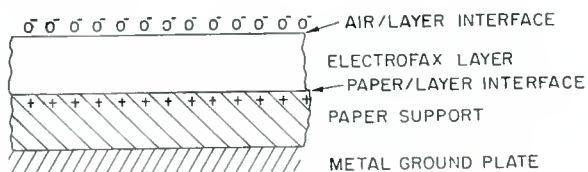


Fig. 5—Cross section of a charged Electrofax layer.

A maximum quantum yield of unity is predicted from this model since the net result of each photon is the transfer of one electron, and only one, from very near the negative (air-layer) interface to the positive (paper-layer) interface; the blocking character of the negative charge on the surface prevents the injection of electrons to replace those which move out of the layer. A linear light-discharge characteristic is also predicted. The layer should behave like a charged, fixed capacitor, each light pulse transferring the same number of charges from one plate to the other.

#### VOLUME-CHARGE CAPACITOR MODEL

With the addition of two hypotheses, the model described above may be modified to conform more exactly to the observed discharge

<sup>7</sup> E. Mollwo, "Electrical and Optical Properties of ZnO," *Photoconductivity Conference*, John Wiley & Sons, Inc., New York, N. Y., 1954, p. 509.

<sup>8</sup> A. Rose, "Photoconductivity in Insulators," *RCA Review*, Vol. XII, p. 303, September, 1951; "An Outline of Some Photoconductive Processes," *RCA Review*, Vol. XII, p. 362, September, 1951.

characteristics. The first hypothesis is that a uniform density of ionizable centers exists throughout the volume of the layer. As before, the layer is regarded as a homogeneous semiconductor having a definite band gap and well-defined valence and conduction bands. The ionizable centers are presumed to be in thermal equilibrium with the conduction band in the layer. During corona charging, the electrons from these centers are forced to the back, and then out through the paper-layer interface. This process leaves immobile positive charges within the layer. The first electrons to leave are those which come from centers near the air-layer interface (Figure 6a). When these

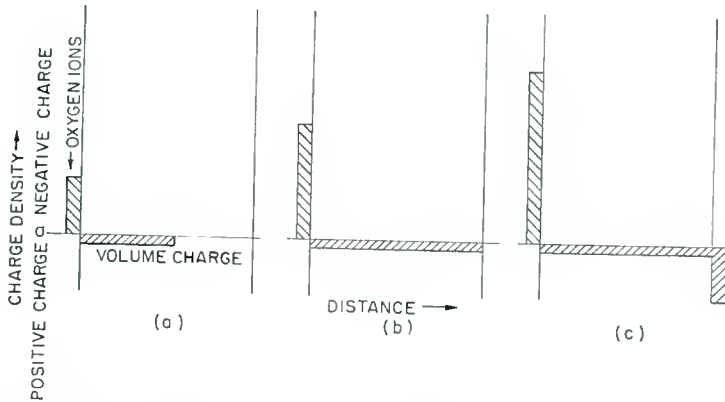


Fig. 6—Density of oxygen ions on an Electrofax surface and the location of the compensating charges (a) at start of corona charging, (b) at intermediate stage of corona charging, and (c) when completely corona charged.

centers are exhausted, those deeper in the bulk are emptied (Figure 6b). When all of the bulk centers have been ionized, positive charge piles up on the paper-layer interface to compensate any additional negative ions deposited on the front surface (Figure 6c). Discharge is presumed to occur in the inverse fashion, the positive charges at the paper-layer interface being neutralized first. Volume centers are then refilled starting from the paper-layer interface.

To explain the differences in the potential across different Electrofax layers following corona charging, a second hypothesis is required. When the field at the front surface (air-layer interface) rises above a critical value, a nondestructive breakdown occurs which reduces the field back to the critical value. In normal use, Electrofax layers have potentials of less than about 800 volts across them after corona charging. Insulator sheets have been charged to potentials as high as 1500 volts with the same corona wand. From this it may be inferred that

a breakdown process in the layer, rather than the corona power supply, determines the potential across the layer after charging. Furthermore, breakdown processes such as tunneling are known to be field-dependent phenomena.

The critical field is reached when the charge deposited on the front surface reaches a value given by

$$E_{\text{crit}} = \frac{e}{\kappa \epsilon_0} n_{\sigma \text{crit}} \quad (\text{MKS units}) \quad (1)$$

where

$E_{\text{crit}}$  is the field at the onset of breakdown,

$e$  is the electronic charge,

$\kappa$  is the relative dielectric constant,

$\epsilon_0$  is the dielectric constant of free space,

$n_{\sigma \text{crit}}$  is the critical surface-charge density corresponding to the onset of breakdown.

The critical field should not depend strongly on small differences in the chemical composition of the layers. The second postulate may therefore be rephrased: The critical charge density on the front surface of all corona charged Electrofax layers should be the same.

Differences between Electrofax layers may be visualized as follows: If the density of ionizable charge in the volume is sufficiently small, the layer is quickly exhausted of mobile charge and the charging-discharging characteristics resemble those for a simple capacitor. If the density of ionizable charge is sufficiently great, the volume is not completely exhausted, even when the critical charge density has been reached at the air-layer interface. Consequently, the potential across such layers is lower and the charging-discharging characteristics are nonlinear over the entire range.

The characteristics expected for a given Electrofax layer are found by integrating Poisson's equation twice to give

$$V = \frac{1.81 \times 10^{-6}}{\kappa} \left( n_{\sigma} x - \frac{nx^2}{2} \right), \quad (2)$$

where

$V$  is the potential across the layer,

$n_{\sigma}$  is the density of negative charge on the air-layer interface (front surface) in number/cm<sup>2</sup>,

$n$  is the density of positive (ionizable) charge in the bulk in number/cm<sup>3</sup>,

$x$  is the distance measured from the front of the layer toward the back, in cm.

The characteristic curves may be divided into two parts corresponding to surface densities  $n_\sigma$  either less than or greater than the total available volume charge,  $na$ , where  $a$  is the thickness of the layer. When  $n_\sigma$  is less than  $na$ , the volume is not completely exhausted of ionizable charge. Charge neutrality of the layer as a whole requires that  $n_\sigma = nx$  and Equation (2) may be rewritten

$$V = \frac{1.81 \times 10^{-6} n_\sigma^2}{2\kappa n}. \quad (3)$$

When  $n_\sigma$  is greater than  $na$ , the volume is completely exhausted and the second term in the expression becomes a constant:

$$V = \frac{1.81 \times 10^{-6}}{\kappa} a \left( n_\sigma - \frac{na}{2} \right). \quad (4)$$

By applying the appropriate forms of Equations (3) and (4), discharge curves may be calculated for the Electrofax layers. It is first necessary to evaluate the constants  $a$ ,  $\kappa$ , and  $n_{\text{crit}}$  which are the same for all layers.  $a$  can be determined directly from the weight of the Electrofax layer per unit area, knowing its density. By this method, a thickness of  $14.5 \times 10^{-4}$  cm is obtained for the standard layers. Optical microscopy indicates that the layer is approximately  $12.5 \times 10^{-4}$  cm thick. The first value, which should be more precise, is used in subsequent calculations.

$\kappa$  may be determined from the linear portion of the discharge curves of Figure 4 using Equation (4). Except for the layer containing WXAV-1 oxide, the slope of the linear portion of the characteristic discharge curves is seen to be the same for all layers, as expected. From this slope, a dielectric constant of 4.66 is calculated. The quantum yield is assumed equal to unity for this calculation and the number of charges transferred from the front to the back surface is taken as the number of band-gap photons incident on the layer.

The value of  $n_{\text{crit}}$  can be found from the expression

$$V_{\text{crit}} = \frac{1.81 \times 10^{-6}}{\kappa} a n_{\text{crit}} - V'$$

where  $V_{\text{crit}}$  is the potential across a layer at the onset of breakdown, i.e.,

the potential retained across a layer after corona charging, and  $V'$  is the potential at which the discharge curve for a layer changes from linear to nonlinear ( $n_\sigma = na$ ).  $V'$  can be found by inspection from the discharge curve for the layer (Figure 4). Estimating  $V'$  as 180 volts and  $V_{\text{crit}}$  as 500 volts for the FGS layer, a value of  $n_{\sigma_{\text{crit}}}$  of  $1.21 \times 10^{12}$  per  $\text{cm}^2$  is obtained. This corresponds to a critical field of about  $5 \times 10^5$  volts per cm which is in the region of breakdown fields for insulators.

With these constants and knowing  $V_{\text{crit}}$ , the volume density of ionizable impurities,  $n$ , may now be calculated for each layer from the appropriate form of Equations (3) or (4). Values calculated in this way are listed in column I of Table II. By plotting  $V$  as a function of  $n_\sigma^2$  for the nonlinear portion of the discharge curves of Figure 4 and

Table II

Layer	Values of $n$ calculated from $V_{\text{crit}}$	Values of $n$ calculated from $\frac{\Delta V}{\Delta n_\sigma^2}$
WXAV-1	0 (see text)	insufficient
WYEB	$0.83 \times 10^{14}$	square law region
FGS	$4.5 \times 10^{14}$	$5.5 \times 10^{14}$
Fisher Wet	$6.9 \times 10^{14}$	$7.8 \times 10^{14}$
EP USP	$9.5 \times 10^{14}$	$9.3 \times 10^{14}$
G. F. Smith	$1.1 \times 10^{15}$	$1.1 \times 10^{15}$
B and A wet	$1.5 \times 10^{15}$	$1.6 \times 10^{15}$
CE-8099-3	$3.7 \times 10^{15}$	$3.1 \times 10^{15}$
AZO-33	$1.3 \times 10^{16}$	$1.3 \times 10^{16}$

using Equation (3), values of  $n$  may independently be calculated. Sample graphs of  $V$  versus  $n_\sigma^2$  are shown in Figure 7 and values of  $n$  calculated from these curves are given in column II of Table II. Agreement between the two sets of values is well within the experimental accuracy of the measurements. Points for the Fisher Wet Process zinc oxide layer have not been included since they nearly coincide with the values for the EP USP layer. The value for  $n$  of the FGS layer reported here is in good agreement with the value  $10^{14}$  per  $\text{cm}^3$  calculated by Gerritsen, Rose, and Ruppel<sup>6</sup> to explain the photoconductive response time observed for FGS layers.

Finally, using these values of  $n$ , complete discharge curves for the Electrofax layers may be calculated using the appropriate form of Equations (3) or (4). These curves are shown in Figure 8, in which the solid line represents the calculated curve and the points represent the experimental data of Figure 4. A special curve has been calculated

not warrant such attempts at present, the model might be modified by using a distribution of volume charge different from the step function assumed here. The requirement that the charge on the paper-layer interface be completely neutralized before the volume centers are refilled may also be too stringent.

This model has proven helpful in understanding the contrast characteristics of Electrofax prints prepared with the different layers.

#### ACKNOWLEDGMENT

For valuable and stimulating discussions about the model described here, the author would like to thank M. A. Lampert and A. Rose. The samples on which the measurements were made were supplied by H. G. Greig and C. J. Young. Finally, thanks are due to Mrs. J. Bacskai and to G. Gustavson for help in making the measurements.

# RCA TECHNICAL PAPERS†

Third Quarter, 1959

Any request for copies of papers listed herein should be addressed to the publication to which credited.

"Acoustoelectronic Auditorium," H. F. Olson, <i>Jour. Acous. Soc. Amer.</i> (July) .....	1959
"The Filling in of an Antenna Null by Off-Path Scattering on a Tropospheric Scatter Circuit," H. Staras, <i>Trans. I.R.E. PGAP</i> (July) .....	1959
"Low-Noise Tunnel-Diode Amplifier," K. K. N. Chang, <i>Proc. I.R.E.</i> (July) (Letter to the Editor) .....	1959
"A Method for Enhancing the Performance of Nonreciprocal Microwave Devices," B. A. Johnson, <i>Trans. I.R.E. PGMTT</i> (July) .....	1959
"Noise Level Reduction of 'Depressed' Freeways," M. Rettinger, <i>Noise Control</i> (July) .....	1959
"Sensitivity and Motion Capturing Ability of Television Camera Tubes," R. G. Neuhauser, <i>Jour. S.M.P.T.E.</i> (July) .....	1959
"The Serviceman and Printed Circuits," D. H. Kunsman, <i>Signal</i> (July) .....	1959
"Taping a TV Program," J. L. Bernstein, <i>Radio-Electronics</i> (July) .....	1959
"Thermionic Converters," K. G. Hernqvist, <i>Nucleonics</i> (July) .....	1959
"Tunnel Diodes as High-Frequency Devices," H. S. Sommers, Jr., <i>Proc. I.R.E.</i> (July) .....	1959
"Bimolecular Electroluminescent Transitions in GaP," E. E. Loebner and E. W. Poor, Jr., <i>Phys. Rev. Letters</i> (July 1) .....	1959
"Studies of the Semiconducting Properties of the Compound CsAu," W. E. Spicer, A. H. Sommer, and J. G. White, <i>Phys. Rev.</i> (July 1) .....	1959
"Voltage Control of Magnetron Frequency," L. Cuccia, <i>Electronics</i> (July 10) .....	1959
"Displacement Thresholds in Semiconductors," J. J. Loferski and P. Rappaport, <i>Jour. Appl. Phys.</i> (August) .....	1959
"Electron-Bombardment Induced Recombination Centers in Germanium," J. J. Loferski and P. Rappaport, <i>Jour. Appl. Phys.</i> (August) .....	1959
"Microwave Parametric Subharmonic Oscillators for Digital Computing," F. Sterzer, <i>Proc. I.R.E.</i> (August) .....	1959
"Role of Powder Density in Dry-Pressed Ceramic Parts," W. C. Allen, T. F. Berry, and W. A. Hassett, <i>The American Ceramic Society Bulletin</i> (August) .....	1959
"Selection of Air Filters for Electronic Equipment," T. G. Nessler, <i>Electrical Manufacturing</i> (August) .....	1959
"On Supplementing Human Faculties," R. E. Mueller, <i>Science</i> (August 7) (Letter to the Editor) .....	1959

† Report all corrections or additions to RCA Review, RCA Laboratories, Princeton, N. J.

- "Delineation of Junctions in Semiconductors by Electroscopic Powers," J. A. Amick and B. Goldstein, *Jour. Appl. Phys.* (September) (Letter to the Editor) ..... 1959
- "Determination of Lead-Wire Inductances in Miniature Tubes," W. A. Harris and R. N. Peterson, *RCA Review* (September) ..... 1959
- "Electronic Hardware," L. H. Henschel, *Electronic Industries* (September) ..... 1959
- "Fast Microwave Logic Circuits," D. J. Blattner and F. Sterzer, *Trans. I.R.E. PGEC* (September) ..... 1959
- "An Industrial Dynamic Approach to the Management of Research and Development," A. Katz, *Trans. I.R.E. PGEM* (September) ..... 1959
- "Infrared Photoemission," G. A. Morton, *Proc. I.R.E.* (September) ..... 1959
- "An Infrared Pickup Tube," G. A. Morton and S. V. Forgue, *Proc. I.R.E.* (September) ..... 1959
- "Investigation of the Electrochemical Characteristics of Organic Compounds—IV Quinone Compounds," R. Glicksman and C. K. Morehouse, *Jour. Electrochem. Soc.* (September) ..... 1959
- "Latest Trends in TV Broadcast Antennas," H. E. Gihring, *Broadcast News* (September) ..... 1959
- "Long-distance V.H.F. Reception," J. E. Le B. Terry, *Wireless World* (September) (Letter to the Editor) ..... 1959
- "Magnetic Dual-Dubbing Reproducer," C. E. Hittle, *Jour. S.M.P.T.E.* (September) ..... 1959
- "Medium-Power L- and S-Band Electrostatically Focused Traveling-Wave Tubes," D. J. Blattner, F. E. Vaccaro, C. L. Cuccia, and W. C. Johnson, *RCA Review* (September) ..... 1959
- "New 25-KW High-Band Television Transmitter," D. R. Mason, *Broadcast News* (September) ..... 1959
- "Nonlaminar Flow in Magnetically Focused Electron Beams from Magnetically Shielded Guns," T. W. Johnston, *Jour. Appl. Phys.* (September) (Letter to the Editor) ..... 1959
- "Parametric Phase-Locked Oscillator—Characteristics and Applications to Digital Systems," L. S. Onyshkevych, W. F. Kosonocky, and A. W. Lo, *Trans. I.R.E. PGEC* (September) ..... 1959
- "Pattern Synthesis," G. H. Brown, *Broadcast News* (September) .. 1959
- "Pattern Synthesis—Simplified Methods of Array Design to Obtain a Desired Directive Pattern," G. H. Brown, *RCA Review* (September) ..... 1959
- "Performance of 'Low-Plate Potential' Tube Types at Mobile-Communications Frequencies," (Abstract) R. J. Nelson and C. Gonzalez, *Trans. I.R.E. PGVC* (September) ..... 1959
- "The Photovoltaic Effect and Its Utilization," P. Rappaport, *RCA Review* (September) ..... 1959
- "Portable Envelope-Delay Measuring Equipment," J. C. Chiabrande, *Broadcast News* (September) ..... 1959
- "A Post-Geneva Review of Controlled Thermonuclear Fusion," E. W. Herold, *Trans. I.R.E. PGNS* (September) ..... 1959
- "Production of Fine Patterns by Evaporation," S. Gray and P. K. Weimer, *RCA Review* (September) ..... 1959
- "A Progress Report on Video-Tape Standardization," A. H. Lind, *Jour. S.M.P.T.E.* (September) ..... 1959
- "Real-Time Data Transmission System," C. R. Scott and W. H. Butler, *Trans. I.R.E. PGCS* (September) ..... 1959

“Relationship between Signal-to-Noise Ratio and Threshold of Response of Infrared Photoconductors Limited by Generation-Recombination Noise,” W. E. Spicer, *Jour. Appl. Phys.* (September) ..... 1959

“Satellites Extend Canadian Television Coverage,” B. R. Machum, *Broadcast News* (September) ..... 1959

“Semiconductor Parametric Diodes in Microwave Computers,” J. Hili- brand, C. W. Mueller, C. F. Stocker, and R. D. Gold, *Trans. I.R.E. PGEC* (September) ..... 1959

“Spectrum-Selection Automatic Frequency Control for Ultra-Short- Pulse Signaling Systems,” H. Kihn and R. J. Klensch, *RCA Review* (September) ..... 1959

“Transient Cross Modulation in the Detection of Asymmetric-Side- band Signals,” T. Murakami and R. W. Sonnenfeldt, *RCA Review* (September) ..... 1959

“Voltage Sensitivity of Local Oscillators,” W. Y. Pan, *RCA Review* (September) ..... 1959

“Photoconductivity of Gallium Selenide Crystals,” R. H. Bube and E. L. Lind, *Phys. Rev.* (September 1) ..... 1959

“Variational Approach to Deviations from Ohm’s Law,” I. Adawi, *Phys. Rev.* (September 1) ..... 1959

“Low-Distortion Transistor Monitor Amplifier,” H. J. Paz, *Electronics* (September 11) ..... 1959

“Transistorizing Automobile Broadcast Receivers,” R. A. Santilli and C. F. Wheatley, *Electronics* (September 18) ..... 1959

“Electrical Properties of p-Type InP,” M. Glicksman and K. Weiser, *Journal of the Physics and Chemistry of Solids*, Vol. 10, No. 4, pp. 337-340, Pergamon Press, N. Y. .... 1959

“An Industrial Dynamic Approach to the Management of Research and Development,” A. Katz, *I.R.E. Wescon Convention Record, Part 8, Instrumentation, Medical Electronics, Nuclear Science, Engineering Management* ..... 1959

“Miniaturized Low-Noise Traveling-Wave Tubes for Airborne Appli- cations,” C. L. Cuccia, H. Wolkstein, and J. Napoleon, *I.R.E. Wescon Convention Record* ..... 1959

“Nondestructive Measurement of Tensile and Compressive Stresses,” R. A. Shahbender, *I.R.E. Wescon Convention Record, Part 6, Component Parts, Industrial Electronics, Production Tech- niques, Reliability and Quality Control, Ultrasonics Engi- neering* ..... 1959

“Photoconductivity in Indium Sulfide Powders and Crystals,” R. H. Bube and W. H. McCarroll, *Journal of the Physics and Chem- istry of Solids*, Vol. 10, No. 4, pp. 333-335, Pergamon Press, N. Y. .... 1959

## AUTHORS



JAMES A. AMICK received the A.B. degree in chemistry from Princeton University in 1949, and the M.A. and Ph.D. degrees in physical chemistry from the same institution in 1951 and 1952. From February, 1949 to September, 1950 he was a fellow at the Brookhaven National Laboratories, Upton, Long Island. After a post-doctoral year at Princeton, he joined the staff of the RCA Laboratories where he engaged in research on X-ray diffraction and electron microscopy and, in 1954, became associated with research on Electrofax. In 1956-1957 he spent six months at the Zurich Laboratory of the Electrofax group. Dr. Amick is a member of Sigma Xi, the American Chemical Society, the New York Society of Electron Microscopists, and the American Crystallographic Association.

LUCIAN A. BARTON received the B.A. Degree in Chemistry from Rutgers University in 1957 and is presently doing graduate work at the Rutgers Graduate School of Chemistry. From 1946 to 1951 he attended courses in Chemical Engineering at the Polytechnic Institute of Turin in Italy. He came to this country at the end of 1951. In 1952 he was employed by the Thiokol Chemical Corporation, and in 1955 joined RCA Laboratories in Princeton where he is working on photoconductors. Mr. Barton is a Senior Member of the American Chemical Society.



RICHARD H. BUBE received the Sc.B. degree from Brown University in 1946 and the Ph.D. degree in Physics from Princeton University in 1950. Since 1948 he has been associated with RCA Laboratories at Princeton, N.J., currently in the Physical and Chemical Research Laboratory, where he is engaged primarily in research on luminescence and photoconductivity of solids. Dr. Bube is a Fellow of the American Physical Society, and a Member of Sigma Xi and the American Scientific Affiliation.

R. W. CHRISTENSEN served in the U. S. Navy from 1942 to 1946, and again from 1951 to 1952. From 1947 to 1950 he was a student at the University of Miami, where he received the B.S. degree in Physics. From 1950 to 1951 he did graduate work at New York University, and he is presently continuing his graduate work at Franklin and Marshall College. He joined the RCA Electron Tube Division in Lancaster, Pa., in 1952. His interest has been in the field of solid-state devices, and he has been responsible for the design of several photoconductive and photovoltaic cells which have proved very successful and are now in commercial production. Mr. Christensen is a member of the Institute of Radio Engineers.





EDWARD FISCHER served in the U. S. Navy as an Electronic Technician from 1944 to 1946; from 1946 to 1952 he was a student at Kansas State College, where he received both the B.S. and the M.S. degrees in Electrical Engineering. He joined the RCA Electron Tube Division in Lancaster, Pa., in 1952, and has since worked on the design and application of storage tubes and multiplier phototubes. Mr. Fischer is a member of Phi Kappa Phi, Sigma Tau, Eta Kappa Nu, Kappa Mu Epsilon, and the Institute of Radio Engineers.

C. P. HADLEY did his undergraduate and early graduate work in Physics at Dartmouth College prior to 1944. From 1944 to 1946, he served as Radar Officer in the U. S. Navy. In 1946 he resumed his graduate work at the Massachusetts Institute of Technology, and in 1950 received the Ph.D. degree. His field of specialization was solid-state physics. He joined the RCA Electron Tube Division in Lancaster, Pa., in 1950, and since then his interest has been in thermionic emitters and in the energy-level structure of electronically active solids. Dr. Hadley is Secretary of the Photosensitive Devices Committee of the Joint Electron Tube Engineering Council (JTC-4). He is a member of Sigma Pi Sigma, Phi Beta Kappa, and Sigma Xi.



WILLIAM E. HARTY received the B.S. degree in chemistry at Rutgers University in 1949 and the Ph.D. degree in chemistry at the University of California in 1953. His graduate work was in the field of chemical kinetics. He joined RCA Laboratories in July, 1953, and is now with the Physical and Chemical Research Laboratory, engaged in preparation and research on materials useful as infrared photoconductors. Dr. Harty is a member of Phi Beta Kappa, Sigma Xi, and the American Physical Society.

HARVEY O. HOOK received the B.A. degree with Chemistry major from Elon College in 1947, the B.E.E. degree from North Carolina State College in 1949, and the M.S.E.E. degree from North Carolina State College in 1950. Since 1950 he has been with RCA Laboratories Division. Mr. Hook is a Senior Member of the Institute of Radio Engineers and an Associate Member of Sigma Xi.



SIMON LARACH received the B.S. degree from the City College of New York, and the A.M. and Ph.D. degrees from Princeton University, and is now Head of Photo-electronic, Magnetic and Dielectric Research at RCA Laboratories. He served as electronics officer in the Air Corps from 1943 to 1946. In this capacity, he was associated with the Cruft Laboratory of Harvard University and the M.I.T. radar school, joining RCA Laboratories in 1946. He received a citation from the Office of Scientific Research and Development in 1946. Dr. Larach is

a member of the American Physical Society, American Chemical Society, Electrochemical Society, and Sigma Xi.

M. A. LAMPERT (*see RCA Review*, Vol. XX, No. 1, March 1959, p. 186.)



EGON E. LOEBNER received the professional degree of Mechanical Engineering at the Second State Higher Industrial School, Plzeň, Czechoslovakia in 1945 and the B.S. and Ph.D. degrees in Physics in 1950 and 1955, respectively, from the University of Buffalo. From 1952 to 1955 he was employed by Sylvania Electric Products Inc. Since 1955 he has been engaged in applied solid state physics research at RCA Laboratories, Princeton, N.J. Dr. Loebner is a member of the American Physical Society, Sigma Xi, the American Association for the

Advancement of Science, a senior member of the Institute of Radio Engineers and a Fellow of the Physical Society. He serves on the New Jersey Commission for Radiation Protection.

GEORGE A. MORTON received the B.S. degree in electrical engineering in 1926, the M.S. degree in electrical engineering in 1928, and the Ph.D. degree in physics in 1932, all from the Massachusetts Institute of Technology. From 1933 to 1941 he was a research engineer at the RCA Manufacturing Company in Camden, N.J., and from 1942 to 1946 he was a member of the technical staff of RCA Laboratories in Princeton, N.J. In 1946, on leave of absence from RCA, he was employed as a nuclear physicist at the U. S. Atomic Energy Commission in Oak Ridge, Tenn. In 1947 he returned to RCA Laboratories at Princeton as a member of the technical staff, and from 1955 to the present time he has been Associate Director of the Physical and Chemical Research Laboratory.



He has contributed in the fields of infrared, scintillation counting, television, and electronics and has many publications in these fields. He is also co-author of several volumes on television and electron optics. During World War II and after, he served as a member of the National Defense Research Committee, AAF Scientific Advisory Board, and the Infrared Panel of the Research and Development Board.

Dr. Morton is a Fellow of the Institute of Radio Engineers and the American Physical Society and a member of Sigma Xi, American Association for the Advancement of Science, and American Institute of Electrical Engineers.



FREDERICK H. NICOLL received the B.Sc. degree in Physics from Saskatchewan University, Canada, in 1929 and the M.Sc. degree in 1931. He held an 1851 Exhibition Scholarship to Cambridge University, England for three years research and received the Ph.D. degree from that university in 1934. He was a research physicist with Electric and Musical Industries, Ltd. in London from 1934 to 1939. From 1939 to 1941 he was with the RCA Victor Division at Camden, N. J. as a research engineer. Since 1942 he has been with the RCA Laboratories in Princeton, N. J. engaged in research on cathode-ray

tubes and electron optics and, more recently, photoconduction and electroluminescence. Dr. Nicoll is a Senior Member of the Institute of Radio Engineers and a Member of the American Physical Society and of Sigma Xi.

R. W. PETER (*see RCA Review*, Vol. XX, No. 1, March 1959, p. 187.)

A. ROSE (*see RCA Review*, Vol. XX, No. 1, March 1959, p. 187.)

WOLFGANG RUPPEL attended the University of Karlsruhe from 1947 to 1951 and the University of Grenoble from 1951 to 1952. He received the doctor's degree from Braunschweig in 1955. Dr. Ruppel joined Laboratories RCA, Ltd., Zurich, Switzerland, in 1955 and since then has worked on the physics of Electrofax and insulators. During the period from April to October 1959 he was at RCA Laboratories, Princeton.



photoconductors.

Dr. Schultz is a member of the American Chemical Society, the American Association for the Advancement of Science, Phi Beta Kappa, and Sigma Xi.

ROSS E. SHRADER received the B.A. degree from the University of Pennsylvania in 1928 and the Ph.D. degree from Cornell University in 1936. After a short period with the Shell Oil Company as a seismologist, he returned to Cornell as a research associate. In 1939 he joined the RCA Victor Division, Camden, N.J. In 1942 he transferred to RCA Laboratories where he is currently engaged in research concerned with the physics of the solid state, particularly in the field of luminescence. Dr. Shrader is a member of the American Physical Society, and has had many technical papers published.



R. W. SMITH (*see RCA Review*, Vol. XX, No. 1, March 1959, p. 188.)

# RCA REVIEW

*a technical journal*

RADIO AND ELECTRONICS  
RESEARCH • ENGINEERING

---

## INDEX

---

VOLUME XX

---

### TABLE OF CONTENTS

---

#### March

	PAGE
Nonlinear-Capacitance Amplifiers .....	3
L. S. NERGAARD	
The Exponential Gun — A Low-Noise Gun for Traveling-Wave-Tube Amplifiers .....	18
A. L. EICHENBAUM AND R. W. PETER	
Gain-Bandwidth Product for Photoconductors .....	57
A. ROSE AND M. A. LAMPERT	
Properties of Deep Traps Derived from Space-Charge-Current Flow and Photoconductive Decay .....	69
R. W. SMITH	
Gains, Response Times, and Trap Distributions in Powder Photoconductors .....	79
H. B. DEVORE	
Magnetics for Computers — A Survey of the State of the Art .....	92
J. A. RAJCHMAN	
Unified Representation of Junction Transistor Transient Response ...	136
A. HAREL AND J. F. CASHEN	
The Megacoder — A High-Speed, Large-Capacity Microminiature Decoder for Selective Communication .....	153
H. KIHN AND W. E. BARNETTE	

#### June

Thermionic Emitters .....	191
L. S. NERGAARD	
Analysis of a Four-Terminal Parametric Amplifier .....	205
K. K. N. CHANG	
Surface-Immune Transistor Structure .....	222
H. NELSON	

	PAGE
Semiconductor Diodes in Parametric Subharmonic Oscillators .....	229
J. HILIBRAND AND W. R. BEAM	
The Propagation of Perturbations along Magnetically Focused Electron Beams .....	254
F. PASCHKE	
Stabilization of Transistor Gain over Wide Temperature Ranges ....	284
R. A. SCHMELTZER	
Quality-Control Determinations of the Screen Persistence of Color Picture Tubes .....	293
J. M. FORMAN AND G. P. KIRKPATRICK	
Microwave Propagation over Rough Surfaces .....	308
M. P. BACHYNSKI	
The Effect of Several Variables on Phosphor-Dot Size in Color Picture Tubes .....	336
N. R. GOLDSTEIN	
Reduction of Co-Channel Interference by Precise Frequency Control of Television Picture Carriers .....	349
W. L. BEHREND	
<b>September</b>	
The Photovoltaic Effect and Its Utilization .....	373
P. RAPPAPORT	
Pattern Synthesis—Simplified Methods of Array Design to Obtain a Desired Directive Pattern .....	398
G. H. BROWN	
Production of Fine Patterns by Evaporation .....	413
S. GRAY AND P. K. WEIMER	
Medium-Power L- and S-Band Electrostatically Focused Traveling- Wave Tubes .....	426
D. J. BLATTNER, F. E. VACCARO, C. L. CUCCI, AND W. C. JOHNSON	
An Analysis of Parametric Amplification in Periodically Loaded Transmission Lines .....	442
G. H. HEILMEIER	
Transient Cross Modulation in the Detection of Asymmetric-Sideband Signals .....	455
T. MURAKAMI AND R. W. SONNENFELDT	
Voltage Sensitivity of Local Oscillators .....	473
W. Y. PAN	
Determination of Lead-Wire Inductances in Miniature Tubes .....	485
W. A. HARRIS AND R. N. PETERSON	
Spectrum-Selection Automatic Frequency Control for Ultra-Short- Pulse Signaling Systems .....	499
H. KIHN AND R. J. KLENSCH	
<b>December</b>	
R. W. PETER	
Electroluminescence of Polycrystallites .....	532
S. LARACH AND R. W. SHRADER	

	PAGE
Amick, J. A.—“A Review of Electrofax Behavior” .....	Dec. 753
“A Volume-Charge Capacitor Model for Electrofax Layers” .....	Dec. 770
Bachynski, M. P.—“Microwave Propagation over Rough Surfaces” .....	June 308
Barnette, W. E. (Coauthor)—“The Megacoder—A High-Speed, Large-Capacity Microminiature Decoder for Selective Communication” .....	Mar. 153
Barton, L. A. (Coauthor)—“The Achievement of Maximum Photoconductivity Performance in Cadmium Sulfide Crystals” .....	Dec. 564
Beam, W. R. (Coauthor)—“Semiconductor Diodes in Parametric Subharmonic Oscillators” .....	June 229
Behrend, W. L.—“Reduction of Co-Channel Interference by Precise Frequency Control of Television Picture Carriers” .....	June 349
Blattner, D. J. (Coauthor)—“Medium-Power L- and S-Band Electrostatically Focused Traveling-Wave Tubes” .....	Sept. 426
Brown, G. H.—“Pattern Synthesis—Simplified Methods of Array Design to Obtain a Desired Directive Pattern” ...	Sept. 398
The Achievement of Maximum Photoconductivity Performance in Cadmium Sulfide Crystals .....	564
R. H. BUBE AND L. A. BARTON	
Infrared Photoconductive Detectors Using Impurity-Activated Germanium-Silicon Alloys .....	599
G. A. MORTON, M. L. SCHULTZ AND W. E. HARTY	
Sintered Cadmium Sulfide Photoconductive Cells .....	635
C. P. HADLEY AND E. FISCHER	
Role of Space-Charge Currents in Light Amplifiers .....	648
A. ROSE AND R. H. BUBE	
Properties of a Single-Element Light Amplifier Using Sintered Cadmium Selenide Photoconductive Material .....	658
F. H. NICOLL	
Solid-State Image Intensifier Under Dynamic Operation .....	670
C. P. HADLEY AND R. W. CHRISTENSEN	
A Simplified Theory of Two-Carrier Space-Charge-Limited Current Flow in Solids .....	682
M. A. LAMPERT	
CdS Analog Diode and Triode .....	702
W. RUPPEL AND R. W. SMITH	
Solid-State Optoelectronics .....	715
E. E. LOEBNER	
Optical Feedback Type Storage Light Intensifiers .....	744
H. O. HOOK	
A Review of Electrofax Behavior .....	753
J. A. AMICK	
A Volume-Charge Capacitor Model for Electrofax Layers .....	770
J. A. AMICK	

## AUTHORS, VOLUME XX

	ISSUE	PAGE
Bube, R. H. (Coauthor)—“The Achievement of Maximum Photoconductivity Performance in Cadmium Sulfide Crystals”	Dec.	564
(Coauthor)—“Role of Space-Charge Currents in Light Amplifiers”	Dec.	648
Cashen, J. F. (Coauthor)—“Unified Representation of Junction Transistor Transient Response”	Mar.	136
Chang, K. K. N.—“Analysis of a Four-Terminal Parametric Amplifier”	June	205
Christensen, R. W. (Coauthor)—“Solid-State Image Intensifier Under Dynamic Operation”	Dec.	670
Cuccia, C. L. (Coauthor)—“Medium-Power L- and S-Band Electrostatically Focused Traveling-Wave Tubes”	Sept.	426
DeVore, H. B.—“Gains, Response Times, and Trap Distributions in Powder Photoconductors”	Mar.	79
Eichenbaum, A. L. (Coauthor)—“The Exponential Gun — A Low-Noise Gun for Traveling-Wave-Tube Amplifiers”	Mar.	18
Fischer, E. (Coauthor)—“Sintered Cadmium Sulfide Photoconductive Cells”	Dec.	635
Forman, J. M. (Coauthor)—“Quality-Control Determinations of the Screen Persistence of Color Picture Tubes”	June	293
Goldstein, N. R.—“The Effect of Several Variables on Phosphor-Dot Size in Color Picture Tubes”	June	336
Gray, S. (Coauthor)—“Production of Fine Patterns by Evaporation”	Sept.	413
Hadley, C. P. (Coauthor)—“Sintered Cadmium Sulfide Photoconductive Cells”	Dec.	635
(Coauthor)—“Solid-State Image Intensifier Under Dynamic Operation”	Dec.	670
Harel, A. (Coauthor)—“Unified Representation of Junction Transistor Transient Response”	Mar.	136
Harris, W. A. (Coauthor)—“Determination of Lead-Wire Inductances in Miniature Tubes”	Sept.	485
Harty, W. E. (Coauthor)—“Infrared Photoconductive Detectors Using Impurity-Activated Germanium-Silicon Alloys”	Dec.	599
Heilmeier, G. H.—“An Analysis of Parametric Amplification in Periodically Loaded Transmission Lines”	Sept.	442
Hilibrand, J. (Coauthor)—“Semiconductor Diodes in Parametric Subharmonic Oscillators”	June	229
Hook, H. O.—“Optical Feedback Type Storage Light Intensifiers”	Dec.	744
Johnson, W. C. (Coauthor)—“Medium-Power L- and S-Band Electrostatically Focused Traveling-Wave Tubes”	Sept.	426
Kihn, H. (Coauthor)—“The Megacoder — A High-Speed, Large-Capacity Microminiature Decoder for Selective Communication”	Mar.	153
(Coauthor)—“Spectrum-Selection Automatic Frequency Control for Ultra-Short-Pulse Signaling Systems”	Sept.	499
Kirkpatrick, G. P. (Coauthor)—“Quality-Control Determinations of the Screen Persistence of Color Picture Tubes”	June	293
Klensch, R. J. (Coauthor)—“Spectrum-Selection Automatic Frequency Control for Ultra-Short-Pulse Signaling Systems”	Sept.	499
Lampert, M. A. (Coauthor)—“Gain-Bandwidth Product for Photoconductors”	Mar.	57
“A Simplified Theory of Two-Carrier Space-Charge-Limited Current Flow in Solids”	Dec.	682
Larach, S. (Coauthor)—“Electroluminescence of Polycrystallites”	Dec.	532
Loebner, E. E.—“Solid-State Optoelectronics”	Dec.	715
Morton, G. A. (Coauthor)—“Infrared Photoconductive Detectors Using Impurity-Activated Germanium-Silicon Alloys”	Dec.	599

## AUTHORS, VOLUME XX

	ISSUE	PAGE
Murakami, T. (Coauthor)—“Transient Cross Modulation in the Detection of Asymmetric-Sideband Signals” . . . . .	Sept.	455
Nelson, H.—“Surface-Immune Transistor Structure” . . . . .	June	222
Nergaard, L. S.—“Nonlinear-Capacitance Amplifiers” . . . . .	Mar.	3
“Thermionic Emitters” . . . . .	June	191
Nicoll, F. H.—“Properties of a Single-Element Light Amplifier Using Sintered Cadmium Selenide Photoconductive Material” . . . . .	Dec.	658
Pan, W. Y.—“Voltage Sensitivity of Local Oscillators” . . . . .	Sept.	473
Paschke, F.—“The Propagation of Perturbations along Magnetically Focused Electron Beams” . . . . .	June	254
Peter, R. W. (Coauthor)—“The Exponential Gun — A Low-Noise Gun for Traveling-Wave-Tube Amplifiers” . . . . .	Mar.	18
Peterson, R. N. (Coauthor)—“Determination of Lead-Wire Inductances in Miniature Tubes” . . . . .	Sept.	485
Rajchman, J. A.—“Magnetics for Computers — A Survey of the State of the Art” . . . . .	Mar.	92
Rappaport, P.—“The Photovoltaic Effect and Its Utilization” . . . . .	Sept.	373
Rose, A. (Coauthor)—“Gain-Bandwidth Product for Photoconductors” . . . . .	Mar.	57
(Coauthor)—“Role of Space-Charge Currents in Light Amplifiers” . . . . .	Dec.	648
Ruppel, W. (Coauthor)—“CdS Analog Diode and Triode” . . . . .	Dec.	702
Schmeltzer, R. A.—“Stabilization of Transistor Gain over Wide Temperature Ranges” . . . . .	June	284
Schultz, M. L. (Coauthor)—“Infrared Photoconductive Detectors Using Impurity-Activated Germanium-Silicon Alloys” . . . . .	Dec.	599
Shrader, R. W. (Coauthor)—“Electroluminescence of Polycrystallites” . . . . .	Dec.	532
Sonnenfeldt, R. W. (Coauthor)—“Transient Cross Modulation in the Detection of Asymmetric-Sideband Signals” . . . . .	Sept.	455
Smith, R. W. (Coauthor)—“Properties of Deep Traps Derived from Space-Charge-Current Flow and Photoconductive Decay” . . . . .	Mar.	69
“CdS Analog Diode and Triode” . . . . .	Dec.	702
Vaccaro, F. E. (Coauthor)—“Medium-Power L- and S-Band Electrostatically Focused Traveling-Wave Tubes” . . . . .	Sept.	426
Weimer, P. K. (Coauthor)—“Production of Fine Patterns by Evaporation” . . . . .	Sept.	413







